European Commission
Research Programme of the Research Fund for Coal and Steel

INNOSEIS

Valorization of innovative anti-seismic devices

WORK PACKAGE 4 – DELIVERABLE 4.1

Volume on case studies for low-rise buildings

Coordinator:

National Technical University of Athens - NTUA, Greece

Beneficiaries:

Universitatea Politehnica Timisoara - UPT, Romania

Politecnico di Milano - POLIMI, Italy

Universita Degli Studi di Napoli Federico II - UNINA, Italy

Universita di Pisa - UNIPI, Italy

Rheinisch-Westfaelische Technische Hochschule Aachen - RWTH, Germany

Instituto Superior Tecnico - IST, Portugal

Universitet po Architektura Stroitelstvo i Geodezija - UACEG, Bulgaria

Universiteit Hasselt - UHasselt, Belgium

Maurer Sohne Engineering GmbH & CO KG - MSE, Germany

Convention Europeenne de la Construction Metallique ASBL - ECCS, Belgium

Grant Agreement Number: 709434

05/03/2017

AUTHORS:

POLITECNICO DI MILANO (POLIMI)
Department of Architecture, Built Environment and Construction Engineering
Piazza Leonardo da Vinci, 32, 20133 Milan, Italy
Chapters 2, 6
Authors: Carlo Andrea Castiglioni, Amin Alavi

HASSELT UNIVERSITY
Construction Engineering Research Group
Campus Diepenbeek, Agoralaan building H, BE3590 Diepenbeek, Belgium
Chapter 3
Authors: Jose Henriques, Herve Degee

RHEINISCH-WESTFAELISCHE TECHNISCHE HOCHSCHULE AACHEN (RWTH)
Institute of Steel Construction
52074 Aachen, Germany
Chapter 4
Authors: Benno Hoffmeister, Marius Pinkawa

NATIONAL TECHNICAL UNIVERSITY OF ATHENS (NTUA)
Institute of Steel Structures
15780 Athens, Greece
Chapter 5
Authors: Ioannis Vayas, Pavlos Thanopoulos, Panagiotis Tsarpalis

INSTITUTO SUPERIOR TÉCNICO (IST)
Department of Civil Engineering, Architecture and Georesources
Av. Rovisco Pais, 1049-001 Lisbon, Portugal
Chapter 7
Authors: Luís Calado, Jorge M. Proença, João Sio

POLITEHNICA UNIVERSITY OF TIMISOARA (UPT)
Department of Steel Structures and Structural Mechanics
Ioan Curea Street, no.1, Timisoara, Romania
Chapters 8, 9
Authors of Chapter 8: Adriana Chesoan, Aurel Stratan, Dan Dubina
Authors of Chapter 9: Calin Neagu, Florea Dinu, Dan Dubina

UNIVERSITET PO ARCHITEKTURA STROITELSTVO I GEODEZIJA (UACEG)
Department of Steel and Timber Structures
1 Hr. Smirnenski blvd. 1046 Sofia, Bulgaria
Chapter 10
Authors: Tzvetan Georgiev, Dimo Zhelev, Lora Raycheva, Nikolaj Rangelov

UNIVERSITY OF PISA (UNIPI)
Department of Civil and Industrial Engineering
56122 Pisa, Italy
Chapter 11
Authors: Walter Salvatore, Francesco Morelli, Andrea Piscini

MAURER SOHNE ENGINEERING GMBH & CO. KG (MSE)
Frankfurter Ring 193
80807 Munich, Germany
Chapters 12, 13
Authors of Chapter 12: Emanuele Gandelli, Christiane Butz
Authors of Chapter 13: Emanuele Gandelli, Valentina Renzi, Christiane Butz

CONTENTS

1 INTRODUCTION

This Volume presents twelve elaborated case studies demonstrating implementation of innovative seismic systems and devices in earthquake-resistant structural design. They have been developed within the activities of the European disseminating project INNOSEIS by eight academic and one industrial parthners. The Volume illustrates conceptual planning, analysis based on code adopted methods, design and detailing for practical applications of specific joints and connections.

The case studies are based on the specific recommendations presented in “Volume with pre-normative design guidelines for innovative devices” where supplementary clauses of EN 1998-1 are formulated and are in compliance with the design philosify and metodology of EN 1998-1, 2004.

Almost all working examples have been developed on a provisory design project for a new two-storey office building that will be built in hign seismicity area.

The example of section 9 deals with four storey building because of specificity of the system. The device of section 13 is not applicable for low rise buildings, that is why the design is not elaborated. The case study in section 2 combines two systems so it is a proper example for impelemnattion of more novelties in one design project.

2 INERD PIN CONNECTIONS

2.1 GENERAL INFORMATION

In this current chapter, the combination of two innovative systems in the low-rise case study building which are so called FUSEIS Bolted Beam Splices and INERD Pin Connections will be presented.

2.1.1 Introduction

In the frame of the European Research Programs “Dissipative devices for seismic resistant steel frames” RFSR-CT-2008-00032 (Acronym: FUSEIS) and “Two Innovations for Earthquake Resistant Design” (Acronym: INERD) under contract number 7210-PR-316, two innovative dissipative systems, named FUSEIS2 and INERD^{TM} pin connections were introduced and relevant design guides developed. Current report presents the low rise case study (2-storey) equipped with both FUSEIS bolted beam splices and INERD pin connections, as well as it introduces the design procedures for steel and composite buildings in which the systems are used as seismic resistant systems.
The case study elaborated comprises the conceptual design, modelling and analysis by linear response spectrum analysis methods (RSA), detailed design of main dissipative and non-dissipative members and basic structural detailing of some connections.

2.1.2 Description of the building

2.1.2.1 Geometry and general assumptions

An archetype configurations which are vertically regular and square-plan, have been selected. The building considered as a general office (class-B) and it is designed according to EN1993-1 [1] /EN1998-1 [2] and to the specific design guideline of the dissipative system [3].
A common plan view has been selected for the building. The number of bays in both direction is 3 with a span length of equal to 8m. The height of each story is sat to be 4m. The building consists of a steel-concrete composite moment resisting frame in the Y direction and concentrically braced steel frame in X direction. Bolted beam splices are included in the structure at the end of the all beams in Y direction, (FUSEIS bolted beam splice) [4], while the INERD^{TM} [5] pin connections are equipped at the end of all steel bracing elements in X direction. The concentric bracing system is located to accommodate the columns around their weak axis bending and the FUSEIS bolted beam splices are located in the direction along which the column are placed with strong axes bending. Diaphragms are assumed rigid, thus neglecting membrane (in-plane) deformations.

2.1.2.2 Material

2.1.2.2.1 Non-dissipative zones

The materials used in the three buildings are given below:

- Structural steel: S355
- Concrete: C25/30
- Steel sheeting: Fe320
- Reinforcing steel: B500C

2.1.2.2.2 Dissipative zones

During the earthquake, it is expected that the dissipative zones yield before other zones i.e., non-dissipative zones, hence, according to EC 1998-1, the yield strength $f_{y,max}$ of the dissipative zones must be satisfied by Eq. (2.1).

$$f_{y,max} \leq 1{,}1 \gamma_{ov} f_y \qquad \textbf{Eq. (2.1)}$$

where

γ_{ov} is the overstrength factor, the recommended value is 1.25

f_y is the nominal yield strength of the steel

2.1.2.3 Loads and load combinations

A summary of the applied loads is given in the following; and Table 2.1 represents the coefficients for the various load combinations.

- Dead Loads:

  2.75 kN/m² composite slab + steel sheeting

- Superimposed Loads:

  Services, ceiling, raised floor: 0.70 kN/m² for intermediate floors
  1.00 kN/m² for top floor
  Perimeter walls 4.00 kN/m

- Live Loads:

  Offices (Class B): 3.00 kN/m²
  Movable partitions 0.80 kN/m²
  Total live load: 3.80 kN/m²
  Snow load to be ignored

- Seismic Load:

  Importance factor: $\gamma_I = 1.0$

Peak ground acceleration: $\alpha_{gR} = 0.20 \cdot g$
Ground Type C – Type 1 spectrum:
S =1.15 TB = 0.20 sec TC = 0.60 sec TD = 2.00 sec
Lower bound factor: β = 0.2
Vertical ground acceleration to be ignored.
Behaviour factor q= 4

Table 2.1 Coefficients for the various load combinations

Coefficient	Value
γ_G	1.35
γ_Q	1.50
Ψ_2 Office (Class B)	0.30
Ψ_2 Roof	0.00
φ Correlated floors	0.80
φ Roof	1.00

The seismic masses are calculated according to Eq. (2.2) and presented in Table 2.2.

$$\sum_{j>1} \boldsymbol{G_{k,j}} + \sum_{i>1} \boldsymbol{\Psi_{2,i} \cdot \varphi_i \cdot Q_{k,i}} \qquad \textbf{Eq. (2.2)}$$

Table 2.2: Quantification of seismic masses

Seismic mass floor 1		**317.52 t**
Concrete and metal deck self-weight + Composite IPE and HEA + IPE500 (Gk1,1)	(2.75*24.0*24.0+73.01+59.63+85.717)/9.81	183.73 t
Utilities, ceiling, floor finishing (Gk2,1)	0.70*24.0*24.0/9.81	41.10 t
Perimeter walls (Gk3,1)	4*4*24/9.81	39.14 t
Partitions (Qk1,1)	0.8*0.3*0.8*24*24/9.81	11.27 t
Imposed loads (Qk2,1)	0.8*0.3*3.0*24*24/9.81	42.28 t
Seismic mass floor 2 (roof)		**242.44 t**
Concrete and metal deck self-weight + Composite IPE and HEA + IPE500 (Gk1,2)	(2.75*24.0*24.0+73.01+59.63+85.717)/9.81	183.73 t
Utilities, ceiling, floor finishing (Gk2,2)	1.00*24.0*24.0/9.81	58.72 t

Imposed loads (Qk,1)	0*1*24.0*24.0*3/9.81	0.00 t
Columns and CBF mass		**27.22 t**
Total		**587.18 t**

2.2 SEISMIC ANALYSIS

2.2.1 Simulation

A building with both FUSEIS bolted beam splice and INERD pin connections may be simulated with a linear-elastic model by appropriate beam elements. The simulation has done based on the design rules which are intended to ensure that yielding, will take place in the fuse prior to any yielding or failure elsewhere. Therefore, the design of buildings with FUSEIS bolted beam splice and INERD pin connections is based on the assumption that the fuses are able to dissipate energy by the formation of plastic bending mechanisms.
The modelling of the buildings were performed by means of the finite element program SAP2000. All beams and columns were simulated as beam elements, while no-section shell elements were used for the distribution of the load's area. Figure 2.1 shows the schematic view of the building under the consideration.

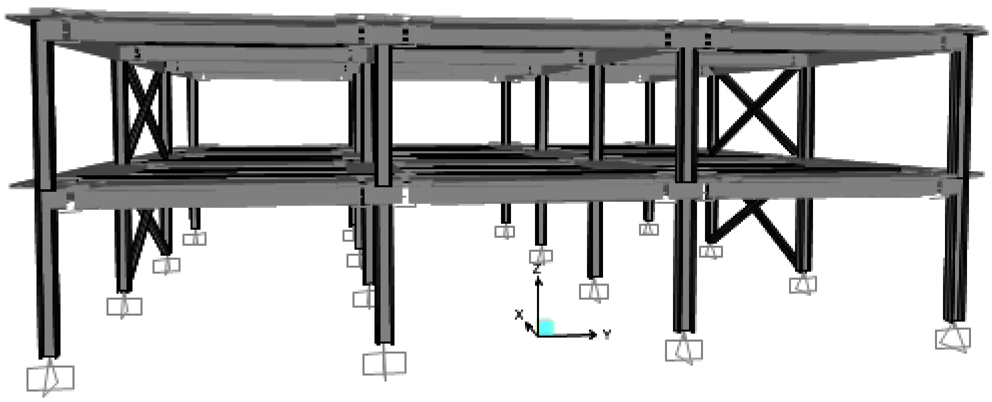

Figure 2.1 Schematic View of the Building Under the Consideration

2.2.2 Seismic design situation

Since, the building is recognized as regular in plan and in height. Hence, theoretically the center of masses and the center of rigidity are coincide. according to EC 1998-1:2004 [2], to account for uncertainties in the location of masses and thus for the rotational component of the seismic motion, additional accidental mass eccentricity of 5% in both directions are considered. To account for the torsional effects, the story seismic forces in both main directions were calculated based on the lateral force method of EC 1998-1: 2004 [2]. The final seismic design situation accounting for accidental torsional effects was derived by Eq. (2.3) and Eq. (2.4).

$$E = E_x + 0.3E_y \pm T \qquad \text{Eq. (2.3)}$$

$$E = 0.3E_x + E_y \pm T \qquad \text{Eq. (2.4)}$$

Where:

T is considered as $T_x + T_y$;

T_x and T_y are accidental torsional effects of applied story seismic force with eccentricity of 5% in X and Y direction, respectively;

E_x and E_y are results of analysis without accidental torsion by applying RSA in X and Y direction, respectively.

The seismic combination is calculated according to Eq. (2.5).

$$\sum_{j>1} G_{k,j} + \sum_{i>1} \psi_2 \times Q_{k,i} + E \qquad \text{Eq. (2.5)}$$

where:

$G_{k,j}$ is the gravity load effects in seismic design situation;

$Q_{k,i}$ is the movable load effects in seismic design situation;

ψ_2 is given in Table 2.1;

E is the effect of the seismic action including accidental torsional effects.

2.2.3 Response Spectrum Analysis

The response spectrum analysis which permits the multiple modes of response of a building to be taken into account in the frequency domain is considered in design scenario. In this kind of analysis, the response of a structure defined as a combination of many modes that in a vibrating string correspond to the harmonics. For each mode, a response is read from the design spectrum, based on the modal frequency and the modal mass then, they are combined to provide an estimate of the total response of the structure by calculating the magnitude of forces in all directions. The combination method used in this research is square root of the sum of the squares (SRSS).

The first, second and third natural modes of vibrations are presented in Figure 2.2. They correspond to the X and Y translational and the torsional mode, in that order. The results from the analysis are summarized in Table 2.3. The table indicates that 2 more translational modes were needed to activate the modal mass participation more than 90% of the total mass In Y-direction.

Table 2.3: Modal mass participating ratio and periods of vibration

Mode no.	Translation	Period [s]	Mass participating in X-direction (%)	Mass participating in Y-direction (%)
1	X	0.88	96	0.00
2	Y	0.61	0.00	89
3	TORSION	0.52	0.00	0.00
4	X	0.30	4	0.00
5	Y	0.19	0.00	11
Sum of mass participating			100	100

Mode I	Mode II	Mode III
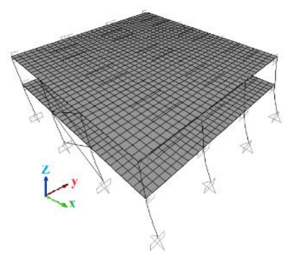	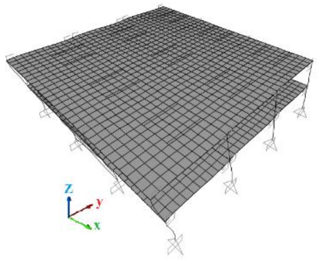	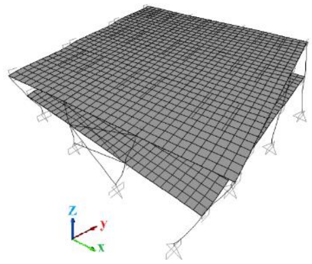
Translation in X	Translation in Y	Torsional

Figure 2.2 Natural fundamental vibration

2.3 DESIGN SUMMARY

2.3.1 Design of building without dissipative elements

2.3.1.1 Design Process

In the building design process, the cross-sections of the relevant structural elements should be first pre-designed for the same building but without any dissipative elements i.e. Bolted Beam Splice and INERD pin connection, considering the relevant limit states. The bolted beam splices then should be included at the all beam ends that belong to the MRF system. While INERD pin connection should be included at the ends of all bracing in the CBF system.

2.3.1.2 Simulation

The analysis and design of the building, was performed by means of the finite element program SAP2000. The composite slabs were designed by the program SymDeck Designer, which takes into account construction phases both for the ultimate and serviceability limit states. Columns are designed as steel members, with their section varying depending on the floor.
For all floors IPE450 has been chosen for primary composite beams. Secondary beams are composite and simply supported with steel profile HEA200. Construction phases were critical for the design of these beams, so temporary supports need to be placed in order to reduce both bending deformation and section size. Slabs are composite for all floors. They have been designed and

checked according to the requirements of EuroCode 4 [6] for all possible situations and no temporary supports are needed during construction phases.
Figure 2.3 shows the plan view of the case study.
Figure 2.4 and Figure 2.5 represent the archetype structure and elevation view of the examined case study in Y-direction and X-direction, respectively. Finally, Figure 2.6 represents the Schematic representation of the composite slab. The thickness of the steel sheet is 0.80mm and the longitudinal reinforcement is Ø8/100. The steel beam is assumed to be connected to the concrete slab with the full shear transfer.

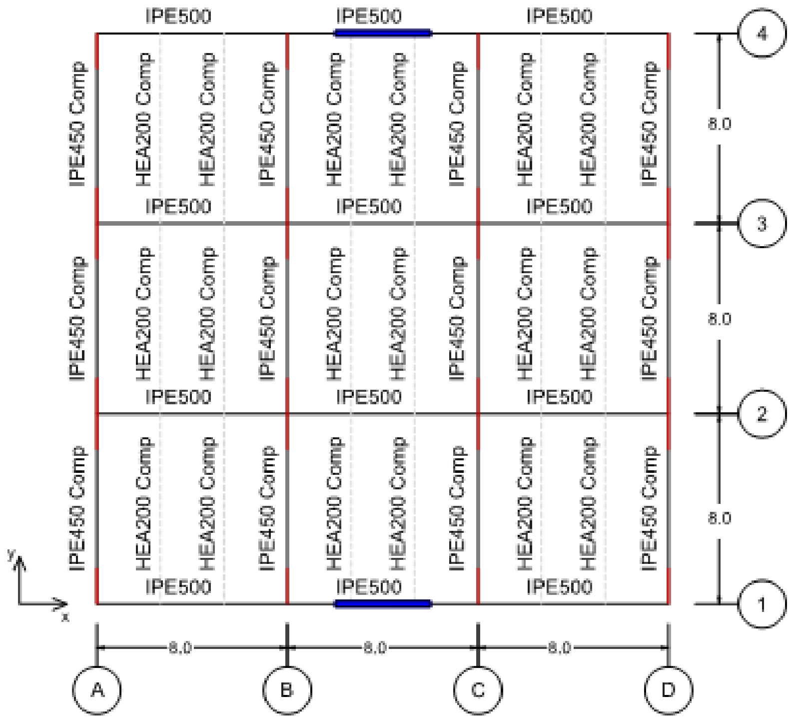

Figure 2.3 Plan view of the case study building

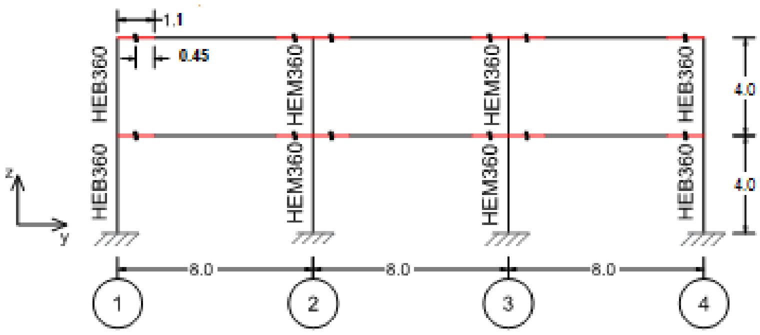

Figure 2.4 Side view of the case study building in Y-direction

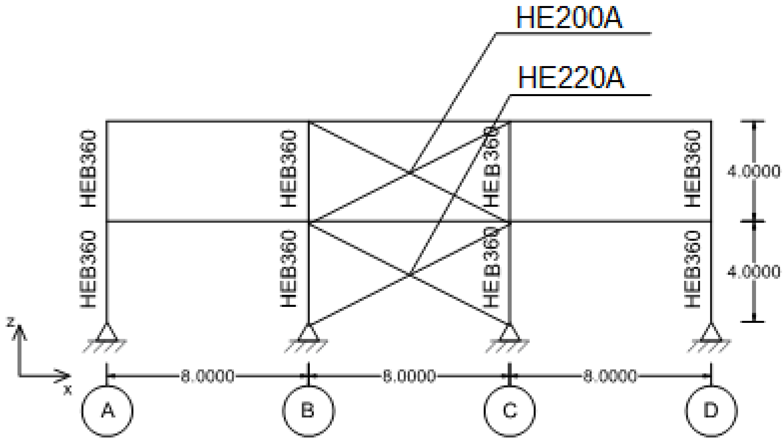

Figure 2.5 Side view of the case study building in X-direction

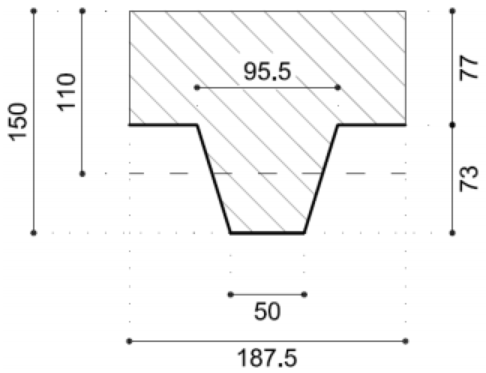

Figure 2.6 Schematic representation of the composite slab

2.3.2 Design of buildings with FUSEIS bolted beam splices

To design a building equipped with FUSEIS bolted beam splices, different steps should be carried out.

After designing the conventional building without dissipative elements and verification of all codified requirements according to EC 1993-1-1: 2005 [7] and EC 1998-1: 2004 [2]. At the end of this step, the cross sections of the steel columns and the composite steel-concrete beams are selected. Using a response spectrum reduced to the elastic one by behaviour factor assumed (in first iteration) according to EC8, seismic response spectrum analysis (RSA) on the building is performed and the bending moment M_{Ed} at the ends of the beams are identified. These values are taken as reference for the performance required to the dissipative beam splices in terms of moment resistance ($M_{Ed} \approx M_{y,\ fuse}$). In fact, in the building subjected to the design seismic actions (ULS), the exploitation of the post-elastic resources of the dissipative and reparable joints is to be guaranteed. It is worth noting that the distribution of the bending moment associated to seismic actions is not uniform along the different floors, resulting that the beams of lower stories are more stressed than the ones of the upper levels. This observation leads to assume several reference resistance thresholds of beam splices for multi-storey buildings. Therefore, the final layout of the structure should be characterized by increasing beam splice dimensions for lower beam levels in order to activate a global collapse mechanism and avoid the onset of brittle soft-storey mechanisms.

2.3.2.1 Design of Bolted Beam Splices

Generally, two main parameters of the joints govern the verification results: the bending moment resistance and the initial elastic stiffness of the FUSEIS beam splices.

Once it is clear the moment resistance and the stiffness level required to verify the structure, the geometrical properties of beam splices have been finalized.

The area of flange plate is calculated referring to the hogging moment resistance required (230 kNm).

The level arm z is calculated from the center of rotation in the middle of the rebars and the flange plate

$$z = h_a + h_p + \frac{h_c}{2} = 450mm + 73mm + \frac{77}{2}mm = 561.5\,mm$$

$$A_{f,fuse} = \frac{M^-_{Rd,fuse}}{f_{yd}\ z} = \frac{150x\ 10^6\ Nmm}{\frac{235}{1.15}\ \frac{N}{mm2}\ x\ 561.5\ mm} = 1307\ mm2$$

Fixing the width of the flange plate equal to 170 mm, slightly lower than the flange width of the steel beam IPE450 (190 mm); the thickness of the plate is obtained.

$$t_{f,fuse} = \frac{1307\ mm2}{170\ mm} = 7.7\ mm$$

Therefore, a thickness of 8 mm is selected. The web plates of the bolted beam splice are designed to resist shear forces only. According to the capacity design principles, the maximum shear forces that could possibly be developed on the beam ends depend on the resistant capacities of the beams. Table 2.4 shows Dimension of the flange and web plates

Table 2.4: Dimension of the flange plates

Storey	Flange Plate (mm)	Web Plate (mm)
1-2	170x8	170x6

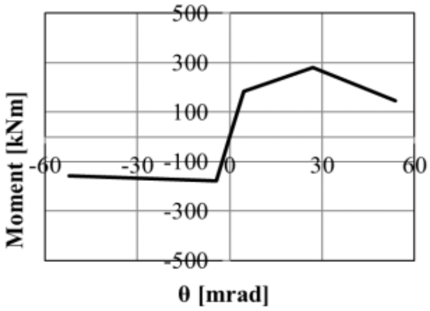

Figure 2.7 Beam Splices Hysteresis Rule in Terms of Moment-Rotation

The free buckling length is calculated for the beam splices.

$$L_0 = \frac{2\sqrt{2}\,M_p}{Af_y\sqrt{\varepsilon}} = \frac{2\sqrt{2}\,x\,\left(\frac{1}{4}\right) x\ 170\ mm\ x\ 8\ mm^2\ x\ 235\ N/mm2}{8\ mm\ x\ 170\ mm\ x\ 235\ N/mm2\ x\ \sqrt{0.002}} = 126\ mm$$

Therefore, a free buckling length equal to 130 mm is applied for all beam splice joints.

In order to design the rebars, to optimize the solution, an iterative procedure should be conducted, aiming at obtaining a lower amount of rebar quantity. The following values were estimated. One should notice that only the rebars positioned within the effective width of the slab will account for the bending resistance.

Table 2.5: Area of longitudinal rebars in the beam splices

	A, upper rebar (mm^2)	**A, lower rebar (mm^2)**
Beam Splice	6000	3000

The bolts are designed with grade 8.8 M16 having 90mm long so that the shear stresses are transferred through the unthreaded portion of the bolt's body. 2 washers can be employed on the bolts body.

2.3.3 Design of building with INERD pin connection

Braced frames with pin INERD-connections may be designed according to the general rules of EC 1998-1:2004 [2] and EC1993-1-1:2005 [7], duly modified in order to consider that energy dissipation is taking place in the pin connections and not in the tension braces.

The INERD pin connections designed according to Table 2.6 to ensure the more efficient response of the connections, all the geometric requirements given in Table 2.6 are satisfied.

The pin dimensions are 45 x 55 mm, S 235. The clear distance between external and internal eye-bars is equal to a = 70 mm.

2.3.3.1 Verification of the brace dimensions

$$N_{Ed} = 393{,}4\ kN \leq\ N_{b,Rd} = 403{,}9\ kN$$

$N_{b,Rd}$ buckling resistance of the diagonal

2.3.3.2 Verification of the pin dimensions

2.3.3.2.1 Verification of design yield strength of the pin connection ($P_{y,Rd}$)

$$P_{y,Rd} = \frac{P_{y,Rk}}{\Upsilon_{Mser}} \geq N_{E,ser} \qquad \text{Eq. (2.6)}$$

Where $P_{y,Rk}$ is the yield strength of the connection can be calculated by the following formula;

$$P_{y,Rk} = \frac{2.M_P}{({}^{a}/_{1.1})} \qquad \text{Eq. (2.7)}$$

$$M_p = W_{pl}.f_y \qquad \text{Eq. (2.8)}$$

$$W_p = bh^2/12 \qquad \text{Eq. (2.9)}$$

Where

f_y is the yield stress of pin
M_p is the plastic moment of pin cross section
W_{pl} is the plastic modulus of pin cross section
h is the pin height
b is the pin width
Υ_{Mser} is the partial safety factor of resistance (=1,0)
$N_{E,ser}$ is the design force of the diagonal at the damage limitation state can be evaluated by the following criteria

$$N_{E,ser} = \frac{Ned}{\nu} \qquad \text{Eq. (2.10)}$$

N_{Ed} is the design force of the diagonal
ν is the reduction factor which takes into account the lower return period of the seismic action associated with the damage limitation requirement equal to 2.5.

$$N_{E,ser} = \frac{394kN}{2.5}$$

$$P_{y,Rd} = \frac{P_{y,Rk}}{\Upsilon_{Mser}} = 205 \geq N_{E,ser} = 157kN$$

2.3.3.2.2 Verification of deformation capacity of the pin connection (δ_{lim})

$$\delta_{lim} = 0.8a \geq \frac{D.H.cos\varphi}{2} \quad \text{Eq. (2.11)}$$

a is the clear distance between internal and external eye-bars
D is the lateral drift ratio
H is the storey height
φ is the angle of inclination of the diagonal

$$a \geq \frac{D.H.cos\varphi}{2 * 0.8} = 53.6mm$$

2.3.3.2.3 Verification of design ultimate strength of the pin connection ($P_{u,Rd}$)

$$P_{u,Rd} = \frac{P_{u,Rk}}{\Upsilon_{M0}} \geq N_{Ed} \quad \text{Eq. (2.12)}$$

Where
$P_{u,Rk}$ ultimate strength of the connection

$$P_{u,Rk} = \frac{4.M_P}{(^a/_{1.1})} \quad \text{Eq. (2.13)}$$

Υ_{M0} partial safety factor of resistance (=1,0)

$$P_{u,Rd} = 411kN \geq 394kN$$

2.3.3.3 Verification of eye-bars dimensions

The thicknesses of the eye bars shall additionally verify the following requirements:

Table 2.6 Geometric requirements for INERD pin connections

Shape of the pin cross section	$h \leq b \leq 2 \cdot h$
Minimum distance between plates	$a \geq h$
Thickness of external plates:	$t_{ext} \geq 0.75 \cdot h$
Thickness of internal plates:	$t_{int} \geq 0.5 \cdot t_{ext}$ for two plates $t_{int} \geq t_{ext}$ for one plate
Basic dimensions of an INERD pin connection: *b* the width of the pin *h* the height of the pin t_{ext} the thickness of the external plate t_{int} the thickness of the internal plate *a* the clear distance between the internal and external plates	

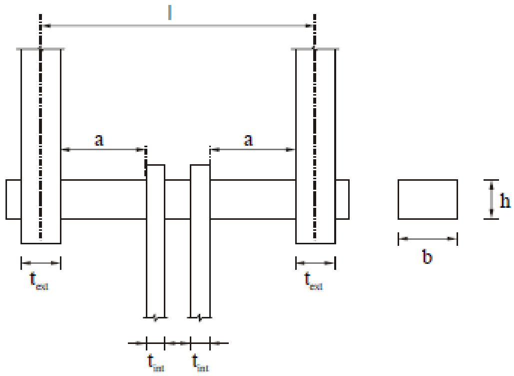

Figure 2.8 INERD pin connection geometry

According to the above mention requirements the dimension of eye bars are chosen as follows:

T_{ext} = 36mm

T_{ext} = 18mm

Steel quality of the eye-bars designed to be equal than that of the pin = S235.

2.3.3.3.1 Verification of gross sectional failure

The connection element verified for the capacity design as follows:

$$P_{Ed} \leq N_{t,Rd} \quad \text{Eq. (2.14)}$$

Where

P_{Ed} is the capacity design force calculated by the following equation

$$P_{Ed} = 1.3 * P_{Rd} \quad \text{Eq. (2.15)}$$

$$N_{t,Rd} = A.f_y/\Upsilon_{M1} \quad \text{Eq. (2.16)}$$

$$535\ kN \leq 2075\ kN$$

2.4 VERIFICATION OF CODIFIED LIMITS FOR THE ENTIRE BUILDING

2.4.1 Damage limitation – limitation of inter-story drift

Assuming that the building has ductile non-structural elements, the verifications is:

$$d_r \cdot v \leq 0.0075h = 0.0075 \cdot 4 = 30\ mm \quad \text{Eq. (2.17)}$$

where $v = 0.5$ is the reduction factor according to EC 1998-1:2004 §4.4.3.2 (1) [2], h is the story height and d_r is the design inter-story drift. Table 2.7 includes the results from the analysis of each story.

Table 2.7: Check of the lower bound for the horizontal design spectrum

X-Direction			Y-Direction		
Story	1	2	**Story**	1	2
$d_{r,max}$ **[m]**	0.0151	0.0167	$d_{r,max}$ **[m]**	0.0408	0.0507
$d_{r,max} \cdot v$ **[m]**	0.0083	0.0076	$d_{r,max} \cdot v$ **[m]**	0.0254	0.0240
≤ 0.030 [m]	Ok	OK	**≤ 0.030 [m]**	Ok	OK

where $d_{r,max}$ is the maximum design inter-story drift value within each directional earthquake combination, obtained by the production of the elastic inter-story drift and the behavior factor.

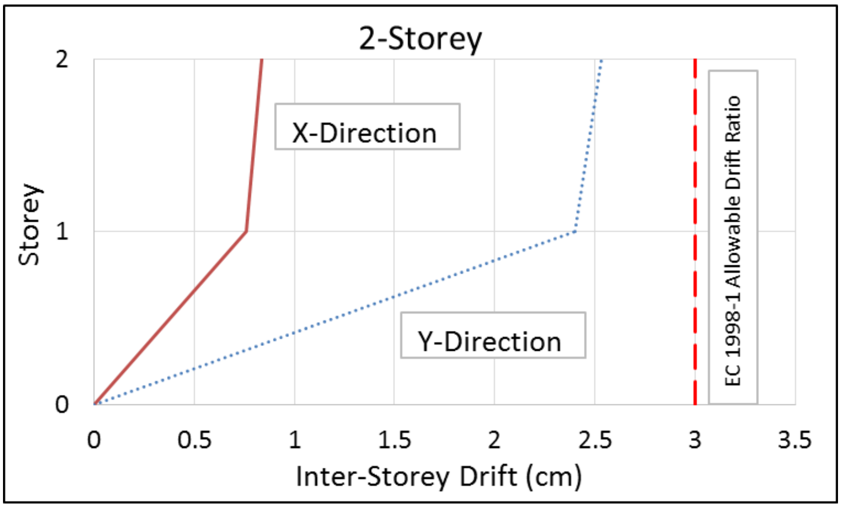

Figure 2.9 Inter-Storey drift

2.4.2 *Second order effects*

The sensitivity to second order effects is estimated by the inter-story drift sensitivity coefficient θ given by Eq. (2.18), where P_{tot} and V_{tot} are the total gravity load at and above the story considered in the seismic design situation and the total seismic story shear at the story under consideration, respectively. Second-order effects (P-Δ effects) need not be taken into account if the following condition is fulfilled in all storeys:

$$\theta = \frac{P_{tot} \cdot d_r}{V_{tot} \cdot h} \leq 0.1 \qquad \text{Eq. (2.18)}$$

Table 2.8 gives the calculated values of θ for directional earthquake combination X and Y, respectively.

Table 2.8: 2nd order effects

X-Direction			Y-Direction		
Story	1	2	**Story**	1	2
$d_{r,}$ /h [m]	0.0019	0.0021	**$d_{r,}$ /h[m]**	0.0060	0.0063
P_{tot} [kN]	1944.8	909.9	**P_{tot} [kN]**	1843.5	868.7
V [kN]	190.9	256.8	**V [kN]**	556.5	326.9
ϴ [rad]	0.019 < 0.1	0.007 < 0.1	**ϴ [rad]**	0.020< 0.1	0.017 < 0.1

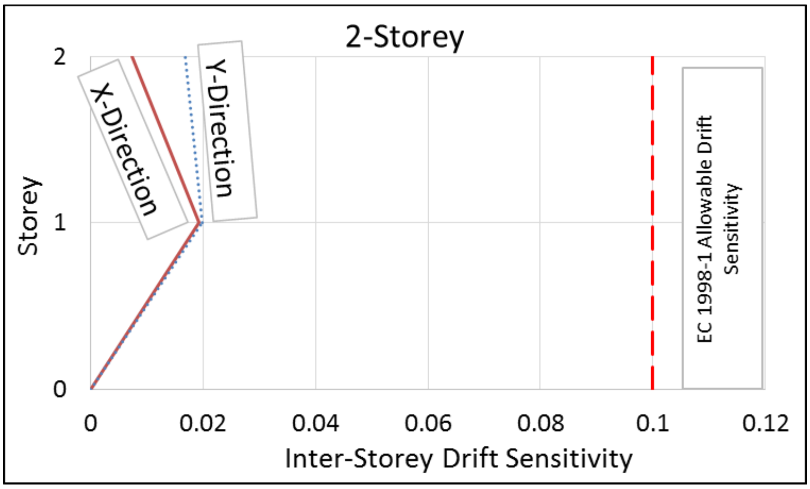

Figure 2.10 Drift sensitivity

2.4.3 Soft Storey Constraint

Since, in multi-storey buildings formation of a soft storey plastic mechanism shall be prevented, as such a mechanism might entail excessive local ductility demands in the columns of the soft storey.

Hence, the following condition should be satisfied at all joints of primary or secondary beams with primary columns:

$$\sum M_{RC} \geq 1.3 \sum M_{Rb} \qquad \text{Eq. (2.19)}$$

Where

ΣM_{Rc} is the sum of the design values of the moments of resistance of the columns framing the joint.

ΣM_{Rb} is the sum of the design values of the moments of resistance of the beams framing the joint.

Table 2.9 Soft Storey Checking

Storey	ΣM_{Rc}		ΣM_{Rb}		Condition
	Interior	Exterior	Interior	Exterior	
1	2x2453 kN.m	2x1296 kN.m	2x117 kN.m	1117 kN.m	OK
2	2x2453 kN.m	2x1296 kN.m	2x117 kN.m	1117 kN.m	OK

Note that, 2 denotes the number of columns or beams in the relevant direction.

2.5 STRUCTURAL DETAILING

The following Figures describe the structural detailing for FUSEIS Bolted Beam Splices and INERD Pin Connections.

2.5.1 FUSEIS Bolted Beam Splices

Figure 2.11 shows the overall detailing of the FUSEIS system followed by section A-A and section B-B in

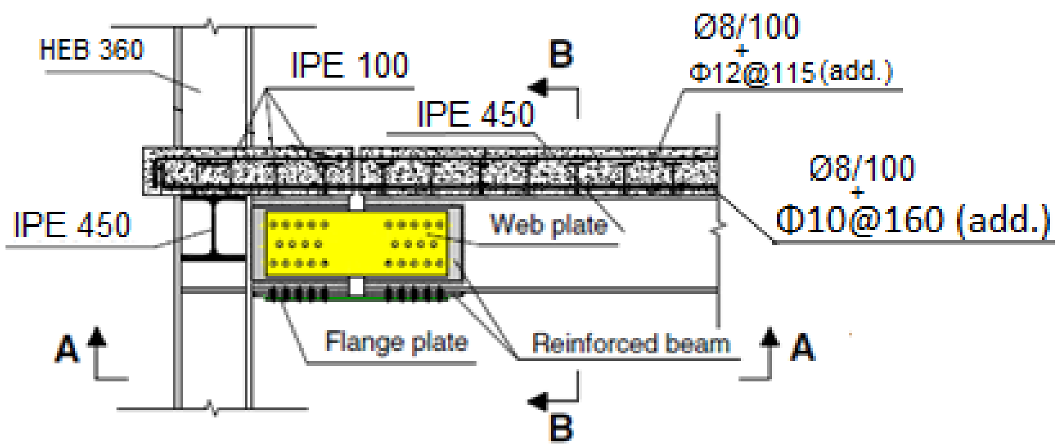

Figure 2.11 Overall Detailing of the FUSEIS System

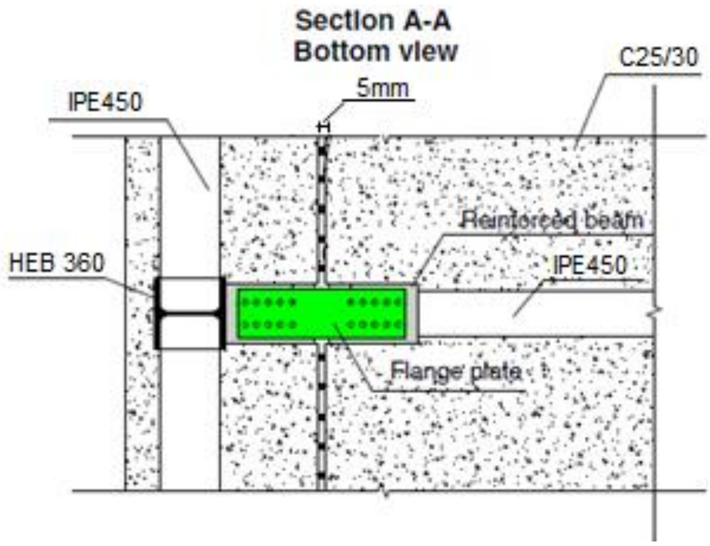

Figure 2.12 Section A-A, Bottom View

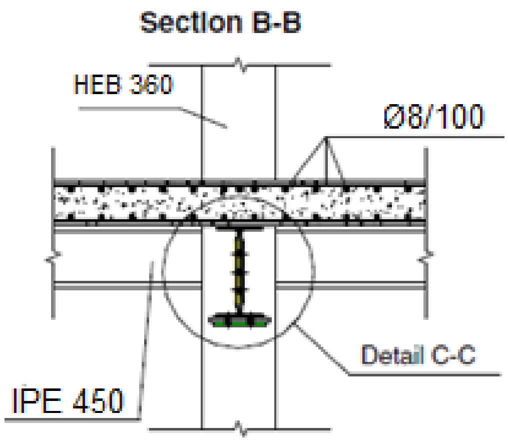

Figure 2.13 Section B-B, Front View

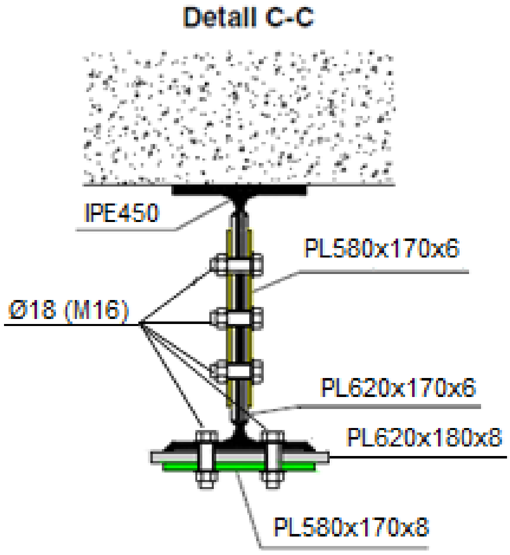

Figure 2.14 Detail C-C, FUSEIS and Additional Plates

Figure 2.15 and Figure 2.16 display the typical web and flange plate, respectively.

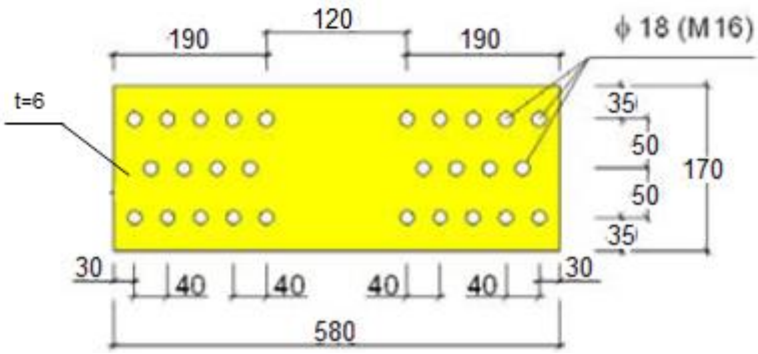

Figure 2.15 Typical Web Plate

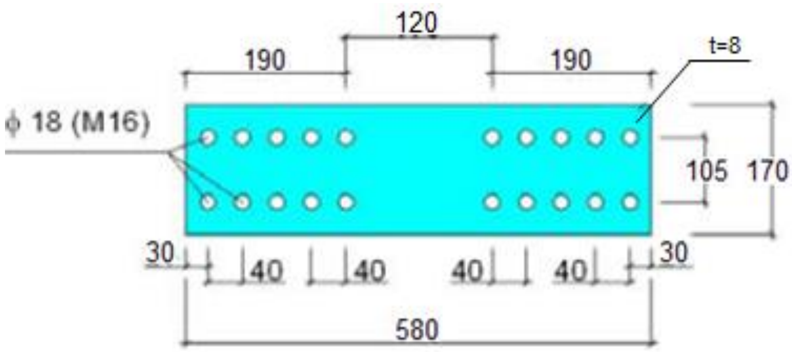

Figure 2.16 Typical Flange Plate

2.5.2 INERD Pin Connections

Figure 2.17 reperesents the overal view of inerd pin connections followed by detail A-A, Figure 2.18, and detail B-B, Figure 2.19.

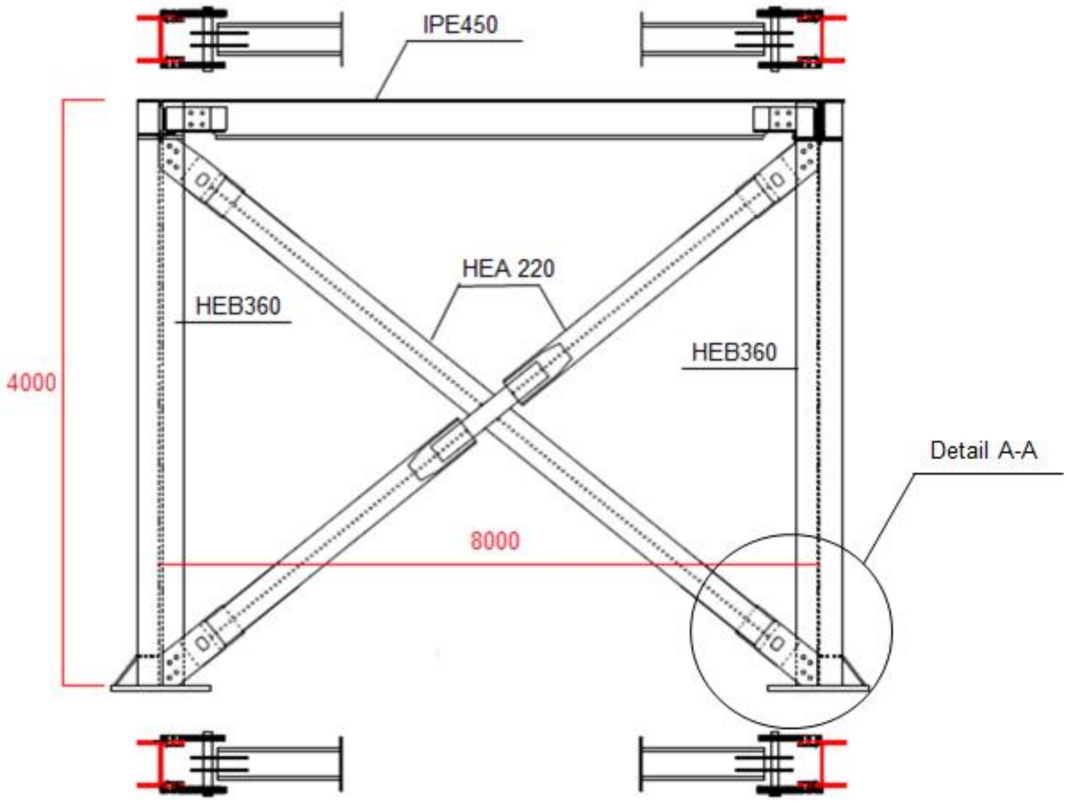

Figure 2.17 Overal View of INERD Pin Connections

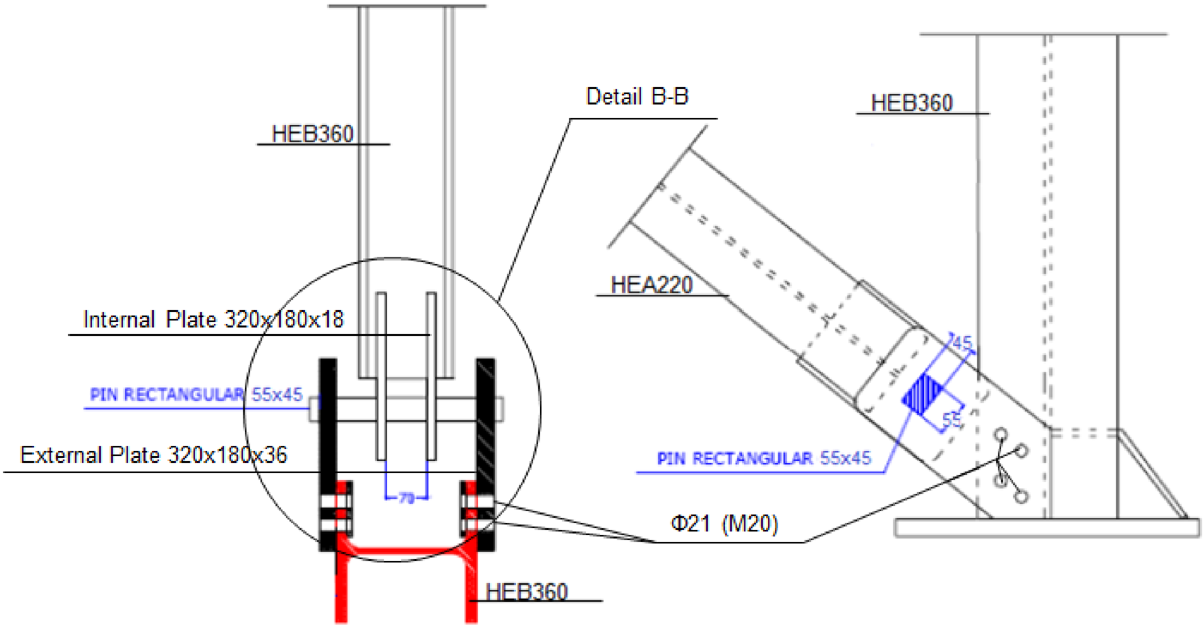

Figure 2.18 Detail A-A

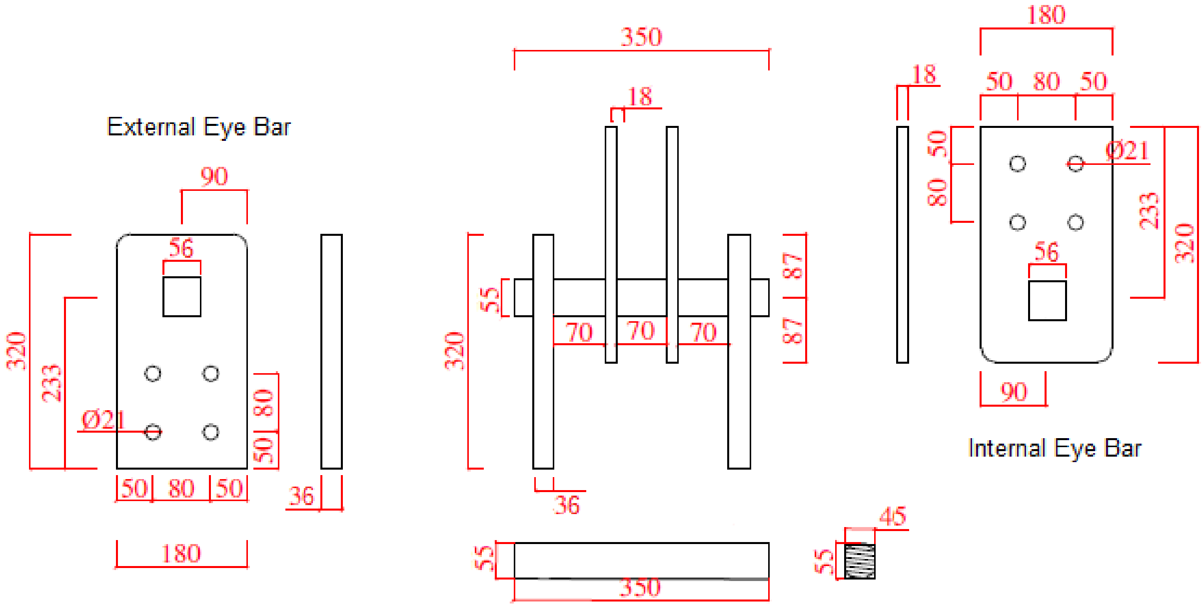

Figure 2.19 Detail B-B

2.6 REFERENCES

[1] "EN 1993-1-1: Eurocode 3: Design of Steel Structures. Part 1-1: General Rules and Rules for Buildings," 2005.

[2] *EC 1998-1: 2004 Design of Structures for Earthquake Resistance-part 1: General rules, seismic actions and rules for buildings*. British Standards, 2004.

[3] *INNOSEIS Project RFCS-02-2015, Valorization of Innovative Anti-Seismic Devices, DESIGN GUIDLINES, Deliverable 3.2*. ECCS, 2017.

[4] C. Castiglioni, A. Drei, A. Kanyilmaz, L. Calado, and I. Vayas, "Numerical and Experimental Results of Project FUSEIS (Seismic Resistant Composite Steel Frames)," 2012.

[5] A. Plumier, C. Doneux, C. Castiglioni, and J. Brescianini, *Two INnovations for Earthquake Resistant Design: The INERD Project.* 2006.

[6] "EC 1994-1-1:2004; Eurocode 4: Design of Composite Steel and Concrete Structures-Part 1-1: General rules and rules for buildings," *Eur. Stand.*, 2004.

[7] *EC 1993-1-1: 2005; Design of steel structures —Part 1-1: General rules and rules for buildings*. 2005.

3 CBF- U-PLATE INERD CONNECTION

3.1 GENERAL

3.1.1 Introduction

This case study refers to the seismic design of new two-storey steel office building. It aims at demonstration of implementation of the Concentrically Braced Frames with U-Device developed within the INERD research project (U-PLATE INERD CONNECTION). The case study elaborated refers to conceptual design, modelling and analysis by linear response spectrum analysis methods (RSA), detailed design of main dissipative and non-dissipative members and basic structural detailing of U-PLATE INERD CONNECTION. The design of members and connections is performed according to [1, 2].

3.1.2 Description of building

3.1.2.1 Geometry and general assumptions

The case study deals with a two-storey frame building with three 8m bays in both directions. The gravity frames are composed of beams and columns, located at each structural axis. The beam-to-column joints and column bases are assumed as pinned. The horizontal resisting systems consist of concentric braces. The U-PLATE INERD CONNECTION is used to perform the connection between braces and columns. Due to the limited resistance and stiffness of these connections, in the present case study 4 braces for each orthogonal direction are considered, as illustrated in Figure 3.1. However, the number of braces in each direction is case dependent and the designer should choose accordingly.

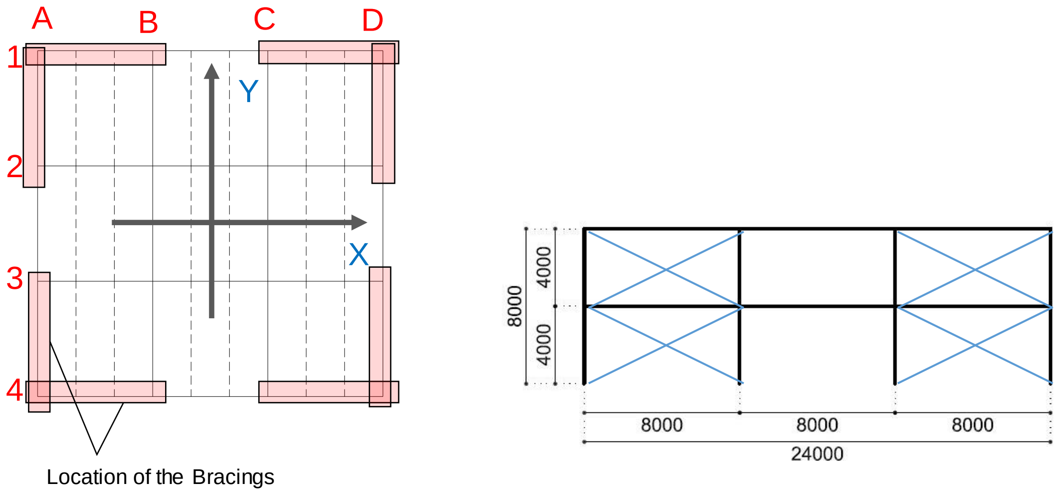

Figure 3.1: Floor plan and elevation

Hot rolled HEB profiles for columns and IPE profiles [3] for floor beams are used for all gravity frames. Both floor slabs (first floor and roof) are designed with steel beams and concrete deck. Composite action with the concrete slab is not considered. However, dowels connecting main and secondary beams to the concrete deck are used to provide structural integration and floor diaphragm action. Diaphragms are assumed rigid, thus neglecting membrane (in-plane) deformations.

The braces consist in hot rolled profiles HEA connected to the columns by means of U-PLATE INERD CONNECTION. The latter consist of one bent U-shaped thick plates (Figure 3.2) and are the dissipative elements of the structure.

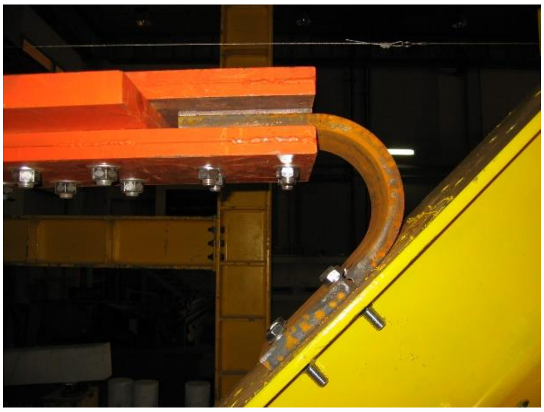

Figure 3.2: U-PLATE INERD CONNECTION

3.1.2.2 Materials

At this stage, no model is available for the design of U-PLATE INERD CONNECTION; therefore, the design is based on the results of the experimental tests performed within the research project INERD [4]. In these experimental tests, steel grade S355 was used for the U-PLATE INERD CONNECTIONS.

Both, braces and gravity frames are designed assuming S355 steel grade. Floor slabs are designed as composite slabs combining steel deck 1mm thickness, concrete C25/30 and reinforcing steel B500B are assumed. The composite slab design is not part of the present report.

3.1.2.3 Loads and load combinations

Table 3.1 summarizes the adopted gravity loads and seismic action parameters. Top floor loads are adopted as accessible roof. It is assumed that snow load intensity is less than the imposed roof load and the altitude of construction site is below 1000 meters. Consequently, the snow load is excluded from the seismic design situation.

Table 3.1: Loads and actions

Vertical loads	
Concrete and metal deck self-weight	2.75 kN/m^2
Utilities, ceiling, floor or roof finishing: – First floors – Roof	 0.70 kN/m^2 1.00 kN/m^2
Facades: Perimeter wall (not considered in the roof).	4.00 kN/m
Partitions, only at first floor	0.80 kN/m^2
Imposed loads 1st floor (category B): Imposed loads roof (category I → B):	3.00 kN/m^2 3.00 kN/m^2
Seismic action	
Design response spectrum for elastic analysis Reference peak ground acceleration Importance class II (Ordinary building) Ground type Behaviour factor *q* Damping ratio Factors for storey occupancy Factors for rood occupancy Seismic combination coefficient First floor Roof	Type 1 $a_{g,R} = 0.24g$ $\gamma_I = 1.0$ B (T_B = 0.15 s, T_C = 0.50 s) 3.0 5% φ = 0.80 φ = 1.00 $\psi_2 = 0.30$, $\psi_E = 0.24$ $\psi_2 = 0.30$, $\psi_E = 0.30$

The seismic masses are calculated according to Eq. (3.1) and presented in Table 3.2.

$$\sum_{j>1} G_{k,j} + \sum_{i>1} \psi_{E,i} . Q_{k,i} \qquad \text{Eq. (3.1)}$$

Table 3.2: Seismic masses

Seismic mass floor 1 = 295.3 t	
Concrete and metal deck self-weight – ($G_{k1,1}$)	2.75x24.0x24.0/9.81 = 161.5 t
Utilities, ceiling, floor finishing – ($G_{k2,1}$)	0.70x24.0x24.0/9.81 = 41.1 t
Facades – ($G_{k3,1}$)	4.0x4.0x24.0/9.81 = 39.1 t
Imposed loads – ($Q_{k1,1}$). Ψ_E	3.0x24.0x24.0x0.24/9.81= 42.3 t
Partitions – ($Q_{k1,2}$). Ψ_E	0.8x24.0x24.0x0.24/9.81= 11.3 t
Seismic mass roof = 273 t	
Concrete and metal deck self-weight – ($G_{k1,2}$)	2.75x24.0x24.0/9.81 = 161.5 t
Utilities, ceiling, floor finishing – ($G_{k2,2}$)	1.00x24.0x24.0/9.81 = 58.7 t
Imposed loads – ($Q_{k,2}$). Ψ_E	3x24.0x24.0x0.3/9.81= 52.8 t
Steel skeleton seismic mass = 52.7 t	

Seismic masses for the building are summarized in Table 3.3.

Table 3.3: Seismic masses per floor

Floor 1 mass = 295.3 t	Roof mass = 273 t	Skeleton mass = 52.7 t
Total seismic mass = 621.0 t		

3.2 BASIC AND NON-SEISMIC DESIGN

3.2.1 Selection of the U-PLATE INERD CONNECTION

As mentioned before, up to the this stage no model exist for the design of the U-PLATE INERD CONNECTION and therefore, the selection of the device geometric and material properties have to be based on the experimental tests of the INERD project [4]. Given the flexibility of these connections, the design should be iterative in order to incorporate the connections stiffness in the determination of the fundamental mode and of the seismic forces. These approach is given in detail in the next chapter (§3.3).

The U-PLATE INERD CONNECTION proposed within the project may have two different configurations, as depicted in Figure 3.3. The difference consists in the position of the U-Plate and consequently on the loading configuration (parallel to the U or Perpendicular to the U). Moreover, the following parameters of U plate may be varied: the bend radius, the width (B), the thickness, and the type of steel. Figure 3.4 illustrates these parameters.

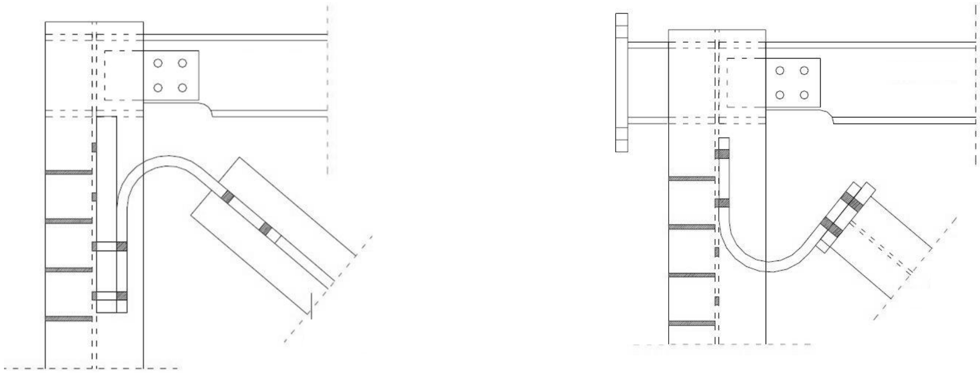

a) Load parallel to U-Connection b) Load perpendicular to U-Connection

Figure 3.3: U-PLATE INERD CONNECTION position and loading typology [4]

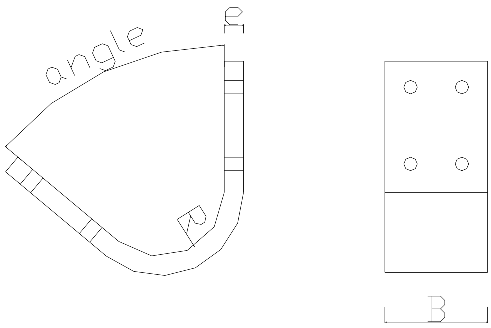

Figure 3.4: Geometric parameters for design of the U-PLATE [4]

3.2.2 Simulation of the U-PLATE INERD CONNECTION

A structural linear elastic model can be developed in any commercial available design software. In the present case study, plane CBF (Figure 3.5) was used in the analysis and modelled in the homemade software FinelG [5]. CBF members are designed and modelled as follows:

- Columns are continuous and pin-connected to the bases;
- Beams are pin-connected to the column;
- Braces are pin-connected to the columns;
- Floors are not modelled; floor loads are applied on the beams.

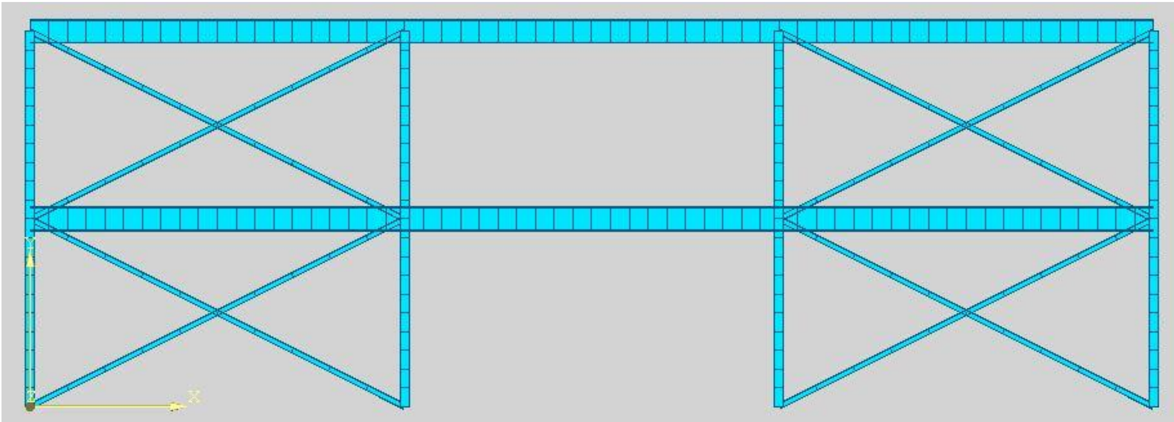

Figure 3.5: FE two-dimensional model

In what concerns the U-PLATE INERD CONNECTION, in a linear elastic model the simplest modelling technique consists in axial elastic spring (Figure 3.6). This spring is used in the connection between the braces and the columns. Because, the design of these connection is iterative, the initial stiffness can be assumed as rigid, in the first calculation. Then, with the selection of the U-PLATE INERD CONNECTION, the model should be improved with the connection axial stiffness. This procedure is further detailed in the next chapter.

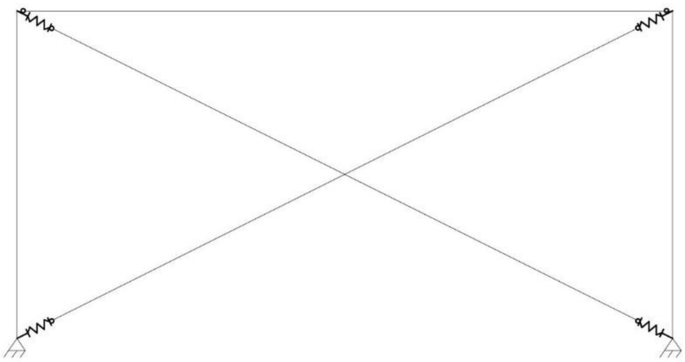

Figure 3.6: Simulation of the U-PLATE INERD CONNECTION in structural model

The current case study was developed by centreline-to-centreline (CL-to-CL) model. It is quick and easy to be defined, since the axis geometry of the frame is known at the beginning of the design process.

3.2.3 Design for static combinations

The design for the static loads, comprising permanent loads and variable loads (imposed loads), is performed previously to the seismic design. In CBF, except for the columns and beams participating in bracing systems, columns and beams are design for gravity loads. In the present case study, is assumed that the seismic design situation governs the design so that wind and snow load are neglected. These considerations are taken into account in the design for static combinations presented hereafter. In what concerns the columns and beams participating in bracing system, these are first design for the static combination and later verified in the seismic design situation.

3.2.3.1 Ultimate limit state results

The ultimate limit state load combination that governs the gravity members design is calculated according to Eq. (3.2).

$$\sum_{j>1} 1.35.G_{k,j} + \sum_{i>1} 1.5.Q_{k,i} \qquad \text{Eq. (3.2)}$$

3.2.3.2 Member design

The results from the member design are presented in Table 3.4. As a simplification, it was assumed that all columns are equal (same profile). This is an assumption that may vary from designer/contractor to designer/contractor. In an weight optimized design, corner, edge and internal columns could be differentiated. However, in some situations homogeneity of structural response (e.g. similar connections) and production, all columns are assumed equal. In what respects the beams, these were differentiated according to the direction, remember Figure 3.1, as the loads on the beams varied significantly. In the design verifications according to [2] the following was considered:

- Columns buckling calculated assuming bracings effective (non-sway frame);
- Beams LTB disregarded as the beams are simply supported and the floor slab is assumed to stabilize the upper flange (compression flange).

Table 3.4: Verification of gravity members

Member	Section	Steel grade	N_{Ed} (kN)	$M_{y,Ed}$ (kNm)	$M_{z,Ed}$ (kNm)	Ratio
Secondary beam (Direction Y)	IPE360	S355	-	239	-	0.838
Main beam (Direction X)	IPE500	S355	-	647	-	0.986
Columns	HEB200	S355	-1302	-	-	0.902

3.2.3.3 Serviceability limit state checks

Table 3.5: Verification of member's deflection

Member	Section	Deflection	type	Adopted limit
Secondary beam (Direction Y)	IPE360	1/312	floor	1/300
Main beam (Direction X)	IPE500	1/339	floor	1/300

3.3 SEISMIC ANALYSIS

3.3.1 Seismic design situation

The building is recognized as regular in plan and in height conforming with the criteria in §4.1 of the EN 1998-1 [1]. Thus, the analysis was performed using planar models, one for each main direction. As the structure is perfectly symmetric only the accidental eccentricity (0,05L) is taken into account for the global torsion of the structure and the consequent amplification of the horizontal forces.
The seismic mass results from the gravity actions on the building and is quantified from the following combination of actions Eq. (3.3).

$$\sum G_{k,j} \text{"}+\text{"} \sum \Psi_{E,i}\, Q_{k,i} \qquad \text{Eq. (3.3)}$$

where:
$G_{k,j}$ are the gravity load effects in seismic design situation;
$\Psi_{E,i}$ is the combination factor for variable load effect in seismic design situation;
$Q_{k,1}$ is the imposed load effects in seismic design situation;

3.3.2 Response Spectrum Analysis

As referred above, the flexibility of the U-PLATE INERD CONNECTION is significant and therefore, its behaviour influences the dynamic response of the structure. In order to select the connections to be used, it is necessary to estimate the loads on the connections and this depends on the estimation of the seismic forces. For this reason, an iterative procedure is necessary. Thus, the first estimation of the structure fundamental mode of vibration is performed using approximation given by Eq. (3.4) as prescribed in §4.3.3 of the EN 1998-1 [1]. Then, the design pseudo acceleration and the base shear are determined using Eq. (3.5) to Eq. (3.7). In Table 3.6 are summarized the results of these calculations.

$$T_1 = C_t H^{2/3} \qquad \text{Eq. (3.4)}$$

with

$C_t = 0{,}05$

$$a_g = \gamma_I a_{gR} \qquad \text{Eq. (3.5)}$$

$$T_B \le T \le T_C\colon S_d(T) = a_g S \frac{2{,}5}{q} \qquad \text{Eq. (3.6)}$$

$$F_b = S_d(T_1) m \lambda \qquad \text{Eq. (3.7)}$$

Table 3.6: Estimation of the base shear – 1st iteration

H [m]	C_t	T_1 [s]	a_g [m/s2]	S_d (T_1) [m/s^2]	λ	F_b [kN]
8,00	0,05	0,24	2,35	1,96	0,85	1035,70

The distribution of the seismic loads through the bracing systems is performed assuming equal lateral stiffness of all braced frames. Consequently, an uniform distribution of the base shear was considered amongst these frames. As referred above, the accidental eccentricity (0,05L) was taken into account for the global torsion of the structure. In Table 3.7 are given the forces per braced frame. Because the structure plan is a square and the brace frames are equally positioned in relation to the geometric centre, the distributed forces are equal in both directions.

Table 3.7: Distribution of seismic forces per braced frame

Frame	F_b [kN]	X [m]	L [m]	δ	F_b' [kN]
1	517,90	12	24	1,05	543,80
4					
A					
D					

The distribution of the masses per story is performed based on the mass of each story and the height of the story to the ground, as expressed in Eq. (3.8). In Table 3.8 are given the forces per story.

$$F_i = F_b' \frac{z_i m_i}{\sum z_j m_j} \qquad \text{Eq. (3.8)}$$

Table 3.8: Distribution of the seismic forces per story

Storey	z_i [m]	m*z_i [ton.m]	F_i [kN]
1	4	1287	190,00
2	8	2395	353,80
	Σm*z_i	3682	

Then, with the seismic forces per story, the forces on each brace and correspondingly on the U-PLATE INERD CONNECTIONS can be estimated. The selection of the connection configuration is made based on force on the brace and on the results of the experimental tests realized within the INERD project [5]. Subsequently, the connection elastic stiffness is known and can be introduced in the calculation of the fundamental mode. From this step, the calculations of the latter are performed using numerical plane models, as illustrated in Figure 3.5. The detail selection and design of the members is given in the next chapter. It should be remarked, that the connection behaviour in Tension and in Compression differs. As an simplification, the stiffness of the connection was assumed equal for both loading cases, and the mean value from the test results was used.

The selection of the U-Connection configuration has an important constraint which is the angle between the column and the brace. As currently no design model is available for the U-Connection, this constrain limits significantly the selection of the connection configuration. In the present case, this angle is about 63^{o}. Given the variability of the connection resistance with this angle, observed in the experimental tests of the INERD project, the connection properties cannot disregard the angle between column and brace. Accordingly, from the available configurations only one connection fits this practical requirement. It should be noted another conception could be considered adapting this angle through the reduction of the bracing system span and adding additional columns to the braced frames. It the case of several configurations are available, the described iterative procedure can be applied.

Hence, in the present case no iterative procedure to find the optimal solution was performed. Using the selected connection mechanical properties the braces profiles were determined. Then, using the actual bracings and U-Plate connection axial stiffness, the fundamental period of the frame was determined. In Table 3.9 are summarized the results of the calculation of the seismic forces using the EN 1998-1-1 [1] equation for estimation of the fundamental period and the seismic forces resulting from the fundamental period using the numerical model. These results show the importance of an accurate estimate of the fundamental period. The force ($N_{Ed,Brace}$) presented in Table 3.9 is the force in 1 brace, and consequently, the force used to design the U-PLATE INERD CONNECTION.

Table 3.9: Results of the iterative response spectrum analysis

Iteration	T_1 [s]	F_b [kN]	Storey	$F_{E,i}$ [kN]	$N_{Ed,Brace}$ [kN]	Comment
0	0,24	1035,7	1	190,0	152,0	Design criteria NOT OK. Insufficient connection resistance.
			2	353,8	98,9	
1	0,82	616,1	1	113,0	90,4	Design criteria OK.
			2	210,4	58,8	

3.4 DETAILED DESIGN

3.4.1 Design properties of the U-PLATE INERD CONNECTION

In Table 3.10 are summarized the properties of the U-Plate connections tested within the INERD project [4]. These properties were used in the design and in the response spectrum analysis described above. As referred before, the connection behaviour differs if the load applied is compression or tension. Thus, in Table 3.10 an $F_{y,min}$ and $F_{y,max}$ are given. The first was used to select the connection configuration, and the second was used in the design of the non-dissipative members. These two values represent the limit of elasticity of the connection. The connection initial stiffness ($K_{ini,con}$) given is the average value between the connection initial stiffness in compression and in tension. The geometric configuration of each connection can be checked in [6].

Table 3.10: U-PLATE INERD CONNECTION mechanical properties [4]

Connection ID	$\alpha_{Column\text{-}Brace}$ [^{o}]	$F_{y,min}$ [kN]	$F_{y,max}$ [kN]	$K_{ini,con}$ [kN/m]
Mola 2	45	98,0	133,0	9973,2
Mola 3	50	90,0	144,0	12825,8
Mola 4	50	153,0	217,0	16101,3
Mola 5	50	114,0	172,0	14908,7
Mola 6	30	63,0	96,0	5798,6
Mola 7	45	75,0	111,0	8577,1
Mola 8	50	77,8	130,0	6368,3
Mola 9	60	127,8	238,9	16812,0
Mola 10	51	127,8	260,0	15221,6
Mola 11	45	146,7	257,8	20915,8
Mola 12	51	205,6	390,0	22523,6

For the present case study, given the limitation on the column-brace angle, the final solution for the connections has only one option and is the following:

- 1st floor: Mola 9
- 2nd floor: Mola 9

3.4.2 Damage limitation – limitation of interstorey drift

Assuming that the building has ductile non-structural elements the verification is:

$$d_r.v \leq 0.0075h = 0.0075.4000 = 30.0\,\text{mm}, \qquad \text{Eq. (3.9)}$$

Where $v = 0.5$ is the reduction factor according to §4.4.3.2 (1) of [1], h is the story height and d_r is the design interstorey drift. Table 3.11 includes the results from the analysis for each of the stories.

Table 3.11: Limitation of interstorey drift

Storey	**1**	**2**
$d_{e,top}$ (mm)	14,0	23,0
$d_{e,bottom}$ (mm)	0,0	14,0
$d_r = (d_{e,top} - d_{e,\,bottom})\,q$ (mm)	42,0	27,0
$d_r\,v$	21,0 < 30.0	13,5 < 30.0

3.4.3 Second order effects

The sensitivity to second order (P–Δ) effects is estimated by the interstorey drift sensitivity coefficient θ given by Eq. (3.10), where P_{tot} and V_{tot} are the total gravity load at and above the storey considered in the seismic design situation and total seismic storey shear, respectively, at the storey under consideration. The calculated values of θ are listed in Table 3.12. The values given in the table are for each braced frame.

$$\theta = P_{tot}d_r / V_{tot}h \qquad \text{Eq. (3.10)}$$

Table 3.12: 2nd order effects

Storey	**1**	**2**
$d_r = (d_{e,top} - d_{e,\,bottom})\,q$ (mm)	42,0	27,0
P_{tot} / V_{tot}	3046 / 324	1469 / 210
h (mm)	4000	4000
θ	0,099 < 0,1	0,047 < 0,1

The values of θ for both storeys are less than 0.1, therefore second-order effects may be neglected.

3.4.4 Final verification of dissipative U-PLATE INERD CONNECTION

Table 3.13 summarizes the final design check of the connection and the corresponding overstrength factor Ω. The latter was calculated using Eq. (3.11). The value of $F_{y,max}$ was used in order to assure that the brace buckling does not occur.

$$\Omega = \frac{F_{y,max}}{N_{Ed,Brace}} \qquad \text{Eq. (3.11)}$$

Table 3.13: Verification of U-PLATE INERD CONNECTION

Storey	Connection ID	$N_{Ed,Brace}$ (kN)	$F_{y,min}$ (kN)	$F_{y,max}$ (kN)	Ω
1	Mola 9	90,4	127,8	238,9	2,64
2	Mola 9	58,8	127,8	238,9	4,07

REMARK: The solution proposed in this case study does not respect the homogeneity criteria given in §6.7.3 (8) of the EN 1998-1-1 [1]. This is due to the limitation on the connection configurations available for the present case study and consequently an optimization of the connection was not performed. In this situation, one the following procedure should be used: i) accept the value and verify by Push-over analysis that soft-storey does not occurs; ii) develop a new configuration to optimize the solution to be adopted for the 2nd level (at this stage, without a design model, testing of this configuration is required).

3.4.5 Capacity design of non-dissipative members

The columns shall be verified to resist design forces obtained from Eq. (3.12). The results for column verifications are presented in Table 3.14. Note that only the edge and corner columns belong to bracing systems. Thus the results presented in the referred table consider the seismic design situation. For the internal columns, the design governing situation is for the gravity loads. The values presented in the table for the internal columns are for the gravity load design situation.

$$N_{col,Ed} = N_{Ed,G} + 1{,}1\gamma_{Ov}\Omega_{min}\left(N_{Ed,E}\right) \qquad \text{Eq. (3.12)}$$

Where:

γ_{ov}=1.00 is the material overstrength factor (test results were used in the design), $\Omega_{MIN} = 2{,}64$ as per Table 3.13.

Table 3.14: Column verification

Column	Column cross-section / Material	$N_{col,Ed}$	Utilization factor
Edge	*HEB 200 / S355*	-461	0,314
Corner	*HEB 200 / S355*	-302	0,238
Internal	*HEB 200 / S355*	-1302	0,902

The design of the beams shall be verified to resist design forces obtained from Eq. (3.13) to Eq. (3.15). The results for beams verifications are presented in Table 3.15.

$$N_{Beam,Ed} = N_{Ed,G} + 1{,}1\gamma_{Ov}\Omega_{min}\left(N_{Ed,E}\right) \quad \text{Eq. (3.13)}$$

$$M_{Beam,Ed} = M_{Ed,G} \quad \text{Eq. (3.14)}$$

$$V_{Beam,Ed} = V_{Ed,G} \quad \text{Eq. (3.15)}$$

Table 3.15: Beam verification

Beam	Beam cross-section / Material	$N_{Beam,Ed}$	$M_{Beam,Ed}$	Utilization factor
Main	*IPE 500 / S355*	-154,9	647,2	0,867
Secondary	*IPE 360 / S355*	-154,9	239,2	0,721

The bracings shall be verified to resist design forces obtained from Eq. (3.16). The results are presented in Table 3.16.

$$N_{Brace,Ed} = 1{,}1\gamma_{Ov}\Omega_{min}\left(N_{Ed,E}\right) \quad \text{Eq. (3.16)}$$

Table 3.16: Brace verification

Storey	Brace cross-section / Material	$N_{Brace,Ed}$	Utilization factor
1	*HEA 140 / S355*	-262,8	0.882

3.5 STRUCTURAL DETAILING

After fulfilment of all checks in §2.4, the U-PLATE INERD CONNECTIONS may be detailed. The detailed dimensions of the selected connection is presented in Figure 3.7

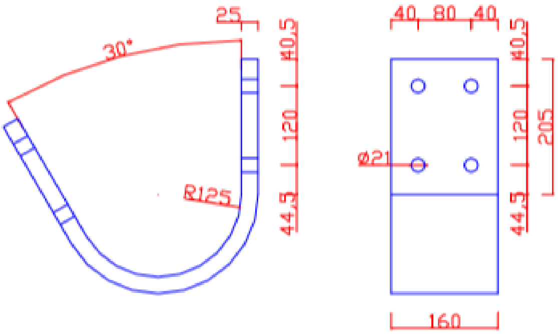

Figure 3.7: U-PLATE INERD CONNECTION (Mola 9) [4]

The braces are connected to the U-PLATE INERD CONNECTION by means of end-plate connection using fit bolts. The connection to the column is performed directly to the column web or flange, depending on the position of column (Figure 3.8).

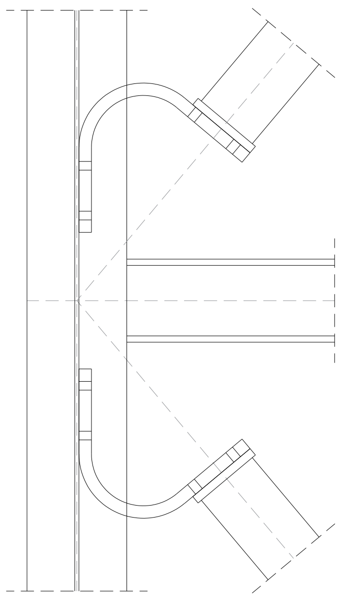

Figure 3.8: Double overlap connection between U-PLATE and Brace

3.6 REFERENCES

[1] Eurocode 8: Design of structures for earthquake resistance - Part 1: General rules, seismic actions and rules for buildings; EN 1998-1:2004.

[2] EN1993-1-1, Eurocode 3: Design of steel structures - Part 1-1: General rules and rules for buildings. Brussels: Comitee Europeen de Normalisation (CEN); 2005.

[3] Hot rolled products of structural steels – Part 2: Technical delivery conditions for non-alloy structural steels; EN 10025-2:2001.

[4] INERD (CEC Agreement No7210-PR-316) – Two innovations for Earthquake resistant design, The INERD project, 2001-2004.

[5] FINELG user's manual. Non-linear finite element analysis software. Version 9.3, July 2005.

[6] Georgiev Tzv., Zhelev D., Raycheva L., Rangelov N.," INNOSEIS - Valorization of innovative anti-seismic devices", WORK PACKAGE 1 – DELIVERABLE 1.1, Volume with information brochures for 12 innovative devices in English, European Commission Research Programme of the Research Fund for Coal and Steel, (Article in Press).

4 FUSEIS BEAM LINKS

4.1 GENERAL

4.1.1 Introduction

This report presents a case study applying the FUSEIS beam links as lateral load resisting system. The Eurocode framework as well the design guidelines have been applied for the design. After a general description of the case study it follows the general design with mentioning the most important design equations. The final design outcome for this specific structure is presented. Structural detailing solution is schematically sketched.

4.1.2 Description of building

4.1.2.1 Geometry and general assumptions

The case study considered herein is a low-rise office building with 2 storeys. The structural layout is regular both in plan and elevation. Dimensions are shown in Figure 4.1 and Figure 4.2. The storey height equals to 4 m. The number of bays in both directions is equal to 3, with an uniform bay width of 8 m. All buildings have composite slabs and secondary beams which transfer the loads to the main frames.

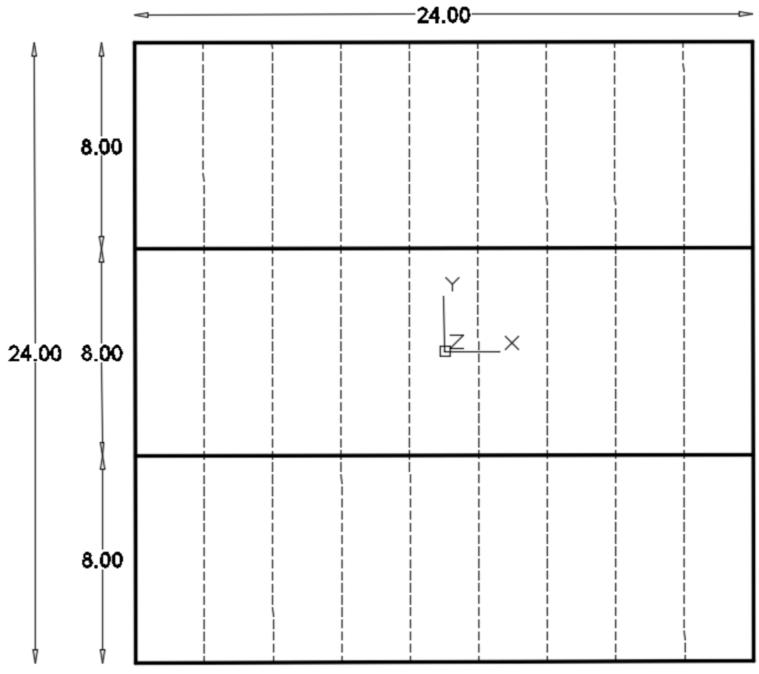

Figure 4.1: Floor plan of case study

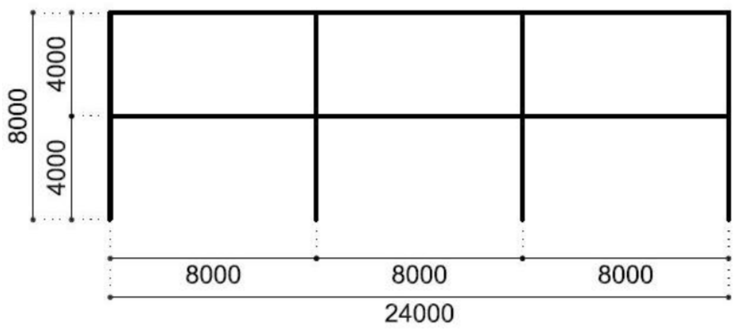

Figure 4.2: Side view of case study

4.1.2.2 Materials

Used materials – concrete and steel – are listed in Table 4.1. Standard C25/30 concrete has been used for the composite steel concrete slab. S355 steel has been used for almost all structural steel parts. Just for the FUSEIS beam links a lower steel grade of S235 has been used. This selection eases the capacity design and assures that the plastic hinge develops inside the FUSEIS beam link.

Table 4.1: Material properties

Concrete	C25/30, g = 25 kN/m3, E = 31 000 Mpa
Reinforcement	B500C
Structural steel	S235: Dissipative elements (FUSEIS beam links) S355: Non dissipative elements (beams and columns)

4.1.2.3 Loads and load combinations

The case study has been designed for vertical loads according to Eurocode 1, 3 and 4. Dead loads, superimposed loads and live loads have been considered as listed in Table 4.2.

Table 4.3 summarizes the main assumptions for seismic loading conditions. Wind loads have been neglected assuming the seismic loads to be governing the lateral load resisting frame design.

Table 4.2: Vertical loads

Dead loads	
Composite slab + steel sheeting	2.75 kN/m²
Superimposed loads	
... for intermediate floors	0.70 kN/m²
... for top floor	1.00 kN/m²

Perimeter walls	4.00 kN/m
Live loads	
Offices (Class B):	3.00 kN/m²
Movable partitions	0.80 kN/m²

Table 4.3: Seismic loads

Elastic response spectrum	Type 1
Peak ground acceleration	a_{gR} = 0.20g
Importance class II	γ_I = 1.0 (Ordinary buildings)
Ground type	B (T_B = 0.15 s, T_C = 0.50 s)
Behavior factor q	5
Damping ratio	5 %
Factors of operating loads for seismic comb.	φ = 1.00 (roof), φ = 0.80 (stories with correlated occupancies)
Seismic combination coefficient for the quasi-permanent value of variable actions	ψ_2 = 0.30

Table 4.4 summarizes all relevant load cases and load combinations which have been considered for the design of the case study.

Table 4.4: Load cases and combinations used for the design of the case study.

Load cases	
Load case LC1	Dead loads (including 1.1 ∗ self weight)
LC2	Live loads
LC3, 4, ...	Seismic equivalent loads per relevant mode
Load combinations	
LCOMB1	1.35 ∗ LC1 + 1.5 ∗ LC2
LCOMB2	LC1 + 0.3 ∗ LC2
LCOMB3	LC1 + 0.24 ∗ LC2
LCOMB4	Envelope of seismic loads in X-direction
LCOMB5	Envelope of seismic loads in Y-direction
LCOMB6	Envelope of seismic loads in both X- and Y-direction
LCOMB7	1.0 ∗ LC1 + 0.3 ∗ LC2 + 1.0 ∗ LCOMB6

4.2 ANALYSIS AND DIMENSIONING

4.2.1 Simulation

The software RSTAB 8 has been used for the design of the case study. This software is widely spread in German design offices. The main advantages are, besides the highly user friendly workflow, the possibility of automatically combining loads according to Eurocode 1, checking for all relevant design equations contained in Eurocode 3, as well as conducting multi modal response spectrum analysis according to Eurocode 8.

Cross section selection for all steel members was assisted by the automatic design checks of RSTAB 8. Design equations which are not incorporated in automatic checks in the software, as e.g. Eurocode inter storey drift criteria, have been checked manually. Hereby an Excel work sheet has been developed, where the verification could be done automatically. RSTAB 8 allows to export the model and results into such an Excel worksheet.

Design for vertical loads has been conducted by the National Technical University of Athens (NTUA). The composite slabs were designed separately with the program SymDeck Designer, a software provided by the manufacturer, which takes into account construction phases both for the ultimate and serviceability limit states.

As the structural layout can be classified as regular both in plan and elevation, a planar model may be used applying the lateral force linear-elastic analysis according to Eurocode 8. However the full 3D model has been used for the design presented in this report.

One FUSEIS beam link system has been applied for each lateral frame, as shown in Figure 4.3 (see also Figure 4.4 and Figure 4.5). The layout is choosen such, that torsional rigidity of the 3D-building is optimally achieved.

All girders and columns have been modelled as beam elements. The composite slabs are assumed to act as rigid diaphragm, what has been modelled by using rigid stiffening beams in each floor.

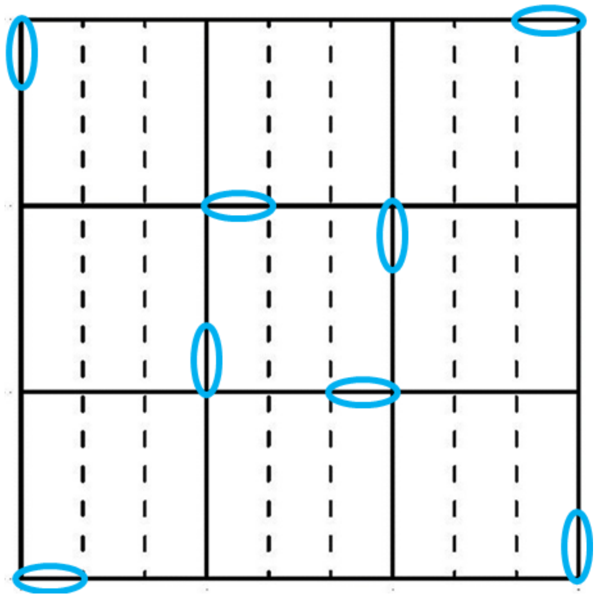

Figure 4.3: Positioning of FUSEIS beam link systems

4.2.2 Design for static and seismic combinations

4.2.2.1 Ultimate limit state results

Design checks according to Eurocode 3 have been automatically conducted by RSTAB. Cross section demand checks as well as stability failure (local and global buckling) have been considered. Profiles have been optimized until all design requirements have been fulfilled. Table 4.5 shows the final profiles for each structural member. While the gravity load bearing frame is solely determined by vertical loads the FUSEIS beam link system is governed by the horizontal seismic loads. Moreover maximum demand to capacity ratios taken into account the most critical load combination as well as design equation are listed in Table 4.5.

Table 4.5: Final cross sections and

Structural member	Profile	Exploitation
FUSEIS beam link system		
Column	HEB 300	0.45
Beam links storey 1	HEA 220	0.81
Beam links storey 2	HEA 200	0.48
Gravity load bearing frame		
Column	HEB 200	0.37
Pimary girder	IPE 500	0.90
Secondary girder	HEA 200	0.98

It should be mentioned that the profiles have been choosen not only on the base of Eurocode 3 verifications, but also due to the requirements contained in Eurocode 8 regarding strength, stiffness and capacity design. These requirements are listed in Section 4.3.3 of this document. Especially inter-storey drift limitations govern the design of the FUSEIS beam link system. Moreover, dissipative elements, and thus the FUSEIS beam links, need to satisfy demands of cross sectional class I, according to Eurocode 3.

4.2.2.2 Design outcome

The final design outcome is illustrated in Figure 4.4 and Figure 4.5. Final cross sections have been already listed in Table 4.5. The design of the FUSEIS beam link system is shown in Figure 4.6. 5 Fuseis beam links have been used per storey, resulting in a distance of 80 cm between the centre lines of each beam link. In order to account for increased storey shear and to optimize the design, a slightly stronger cross section has been used at the lower floor, compared to the upper one. The distance between the column centre lines was chosen to 210 cm.
Dynamic behaviour of the designed building is completely described by its first transversal mode in both directions. More than 95% of mass are participating in each of these modes. The first fundamental mode has a period of 0.30 seconds (global sway mode in X-direction) while the second is almost identical with 0.31 seconds (global sway mode in Y-direction).

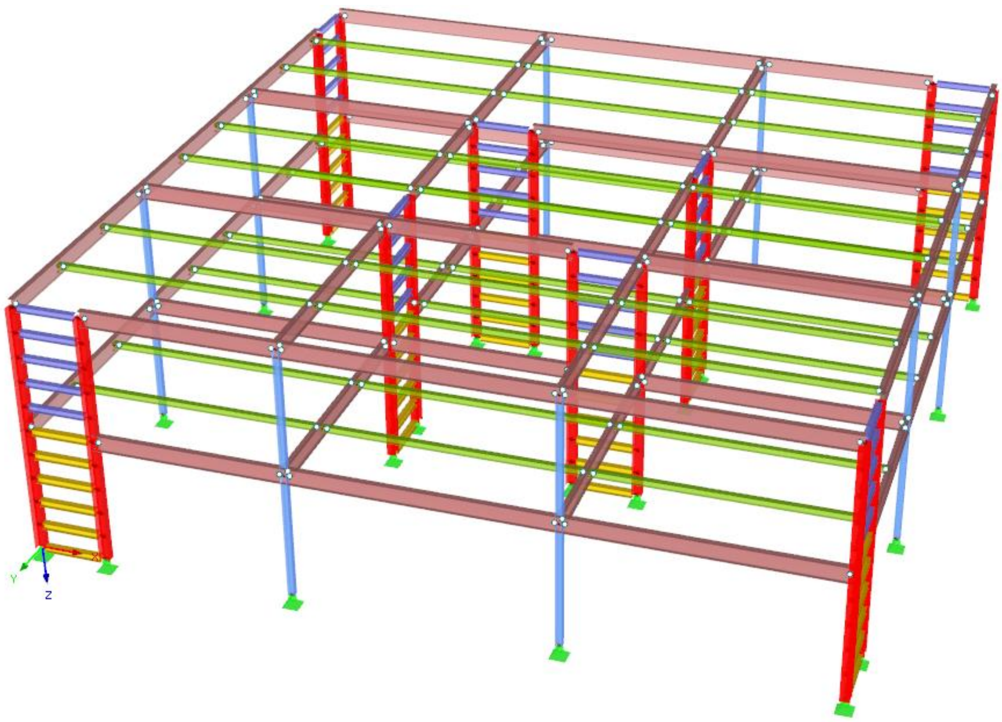

Figure 4.4: Isometric view of low-rise building

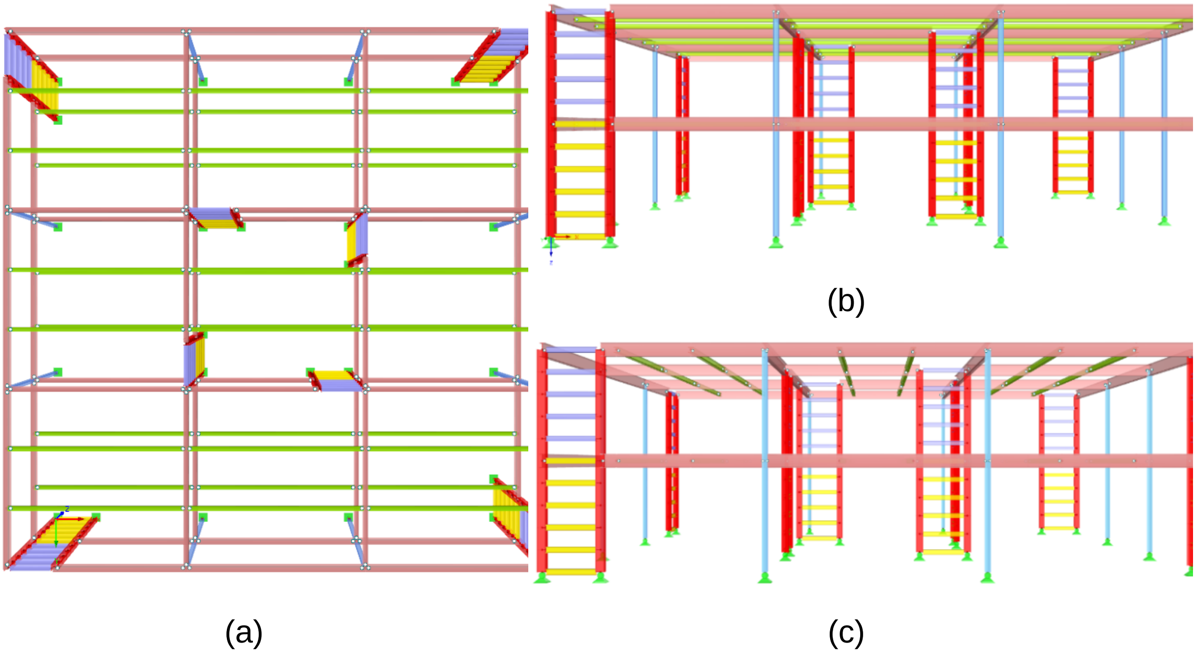

Figure 4.5: Low-rise building: (a) upper view, (b) side view in X-direction and (c) side view in Y-direction

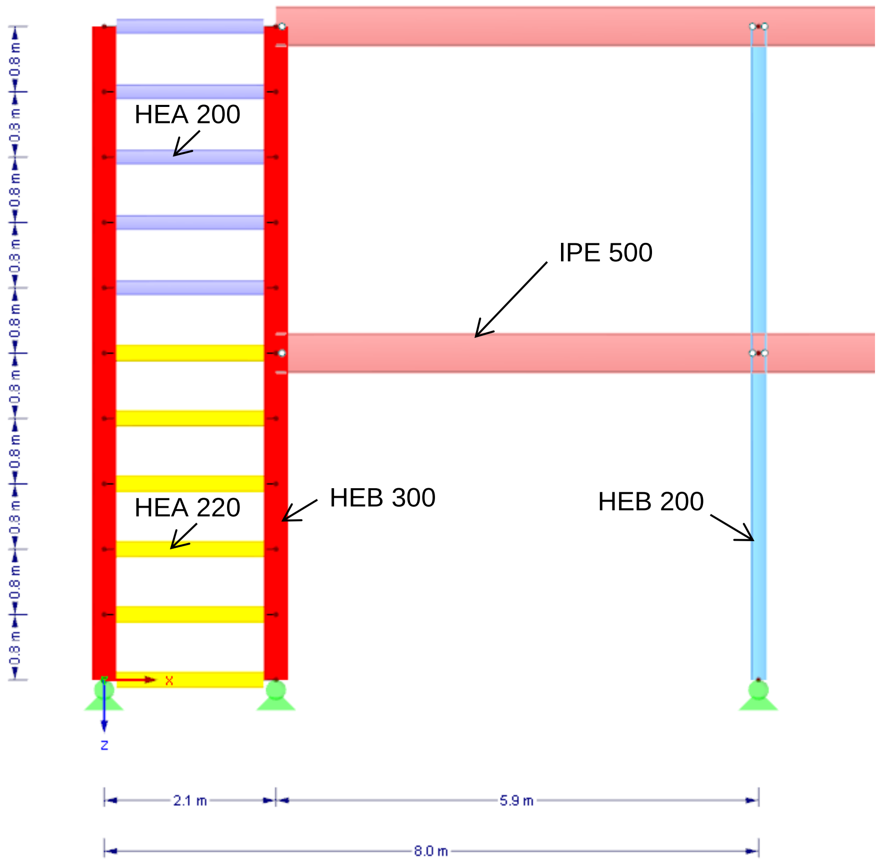

Figure 4.6: Design of FUSEIS beam link system.

4.3 DETAILED DESIGN

4.3.1 Limitation of interstorey drift – Damage limitation

The criterion in accordance to section 4.4.3.2 of Eurocode 8-1 to limit damage for non-structural elements was verified. The following equation needs to be fulfilled.

$$\boldsymbol{d_r \cdot v \leq \{0.005; 0.0075; 0.01\} \cdot h} \qquad \text{Eq. (4.1)}$$

Since the building is assigned to importance class I, the reduction factor $\boldsymbol{v}$ is equal to 0.5 (4.4.3.2 (2) Eurocode 8-1). It is assumed that ductile non-structural elements are present in the building, thus according to Table 4.6 the limit value is equal to 0.0075.

Table 4.6: Interstorey drift limits for damage limitation of non-structural elements

Non-structural element characteristics	**Limit value**
Brittle elements	0.0050
Ductile elements	0.0075
Without or with non-interfering elements	0.0100

The design interstorey drift d_r is calculated by multiplying the interstorey drift d_e obtained from the linear elastic analysis with the choosen value of the behaviour factor q, according to section 4.3.4 of Eurocode 8-1. This interstorey drift must be lower than the allowed one, which equals to 0.0075 * 4000 mm / 0.5 = 60 mm. As can be seen in Table 4.7 and
Table 4.8 respectively, this requirement is fulfilled in both directions. However, the inter-storey drift limitation was governing design and forced to choose a stiffer FUSEIS beam link system.

Table 4.7: Verification of interstorey drift limit – SLS – X-direction

Storey #	$\boldsymbol{d_e}$ **[mm]**	$\boldsymbol{d_r}$ **[mm]**	$\boldsymbol{d_{r,lim}}$ **[mm]**	**Ratio** $\boldsymbol{d_r/d_{r,lim}}$
1	10.6	53	60	0.88
2	5.5	27.5	60	0.46

Table 4.8: Verification of interstorey drift limit – SLS – Y-direction

Storey #	$\boldsymbol{d_e}$ **[mm]**	$\boldsymbol{d_r}$ **[mm]**	$\boldsymbol{d_{r,lim}}$ **[mm]**	**Ratio** $\boldsymbol{d_r/d_{r,lim}}$
1	11.5	57.5	60	0.96
2	8.3	41.5	60	0.69

4.3.2 Limitation of interstorey drift – P-delta effects (ULS)

According to section 4.4.2.2 of Eurocode 8-1 the second order coefficient calculated according to Eq. (4.2) must be checked. Second-order effects need not to be taken into account if it is higher than 0.1 and it shall not exceed 0.3.

$$\boldsymbol{\theta} = \frac{\boldsymbol{P_{tot}} \cdot \boldsymbol{d_r}}{\boldsymbol{V_{tot}} \cdot \boldsymbol{h}} \qquad \text{Eq. (4.2)}$$

The evaluated sensitivity coefficients are calculated in Table 4.9 and
Table 4.10 for both directions. As can be seen for all cases the coefficient is smaller than 0.1, thus second-order effects would not be needed to taken into account.

Table 4.9: Verification of interstorey drift limit – ULS – X-direction

Storey #	$\boldsymbol{d_{r,x}}$ **[mm]**	$\boldsymbol{P_{tot}}$ **[kN]**	$\boldsymbol{V_{tot}}$ **[kN]**	$\boldsymbol{\theta}$
1	53	5 788	1 036	0.074
2	27.5	2 539	614	0.028

Table 4.10: Verification of interstorey drift limit – ULS – Y-direction

Storey #	$\boldsymbol{d_{r,y}}$ **[mm]**	$\boldsymbol{P_{tot}}$ **[kN]**	$\boldsymbol{V_{tot}}$ **[kN]**	$\boldsymbol{\theta}$
1	57.5	5 788	1 019	0.082
2	41.5	2 539	567	0.046

4.3.3 Design of dissipative devices

The horizontal beams in the FUSEIS beam link system are the primary dissipative zones where the energy dissipation capability is mainly located. Reduced beam sections (RBS) are recommended to clearly define the dissipative zones. Reduced beam sections (RBS) were designed according to EN 1998-3, see Figure 4.7. Geometrical boundary conditions are given in Eq. (4.3).

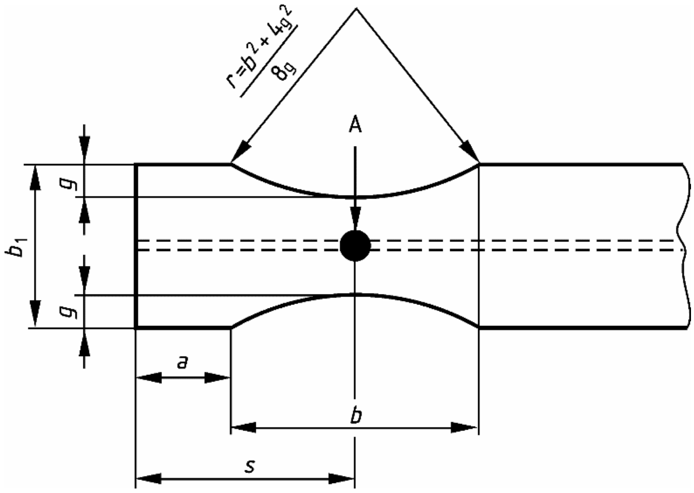

Figure 4.7: Geometrical characteristics of reduced beam section

$$a = 0.6 \cdot b_f$$
$$b = 0.75 \cdot d_b$$
$$g = 0.20 \cdot b_f \; to \; 0.25 \cdot b_f \qquad \text{Eq. (4.3)}$$

With

$$b_f = beam\ width$$
$$d_b = beam\ height$$

Due to the fact that beams can be modelled in RSTAB conveniently by directly choosing profiles from a library, e.g. HEA sections, and moreover that automatic design checks and profile optimization is based on these libraries, the original profiles were used - not taking into consideration the reduced beam section (RBS) explicitly. Instead, the yield strength of the FUSEIS beam link has been modified according to Eq. (4.4). With this modified yield strength RSTAB calculates internally beam section properties, representing the reduced beam section (RBS), which are then used for the design checks. The influence of reduced stiffness was not taken into account, as it showed to be of negligible influence.

$$f_{y,mod} = \frac{W_{pl,RBS} * f_y}{W_{pl}} \qquad \text{Eq. (4.4)}$$

With

$$W_{pl,RBS} = W_{pl} - 2 * g * t_f * (d_b - t_f)$$

4.3.4 Capacity design of non-dissipative members

4.3.4.1 Strong column weak beam criterion

According to 4.4.2.3 Eurocode 8-1 the plastic hinge must develop in the beam. The column must be capacity designed according to Eq. (4.5).

$$\sum M_{Rc} \geq 1.3 \cdot \sum M_{Rb} \qquad \text{Eq. (4.5)}$$

The regular primary and secondary beams bearing the gravity loads are not intended to take part in the lateral force resisting system. Thus, they are pinned or partly-fixed to the columns so that Eq. (4.5) is fulfilled easily. For the FUSEIS beam links Eq. (4.5) is already taken into account during the design of the reduced beam sections (RBS). The verification of the ends of FUSEIS beam links at top or bottom of the system is listed in the following Table 4.11.

Table 4.11: Verification of strong column weak beam principle

Storey #	M_{Rc} [kNm]	M_{Rb} [kNm]	$1.3 \cdot M_{Rb}$ [kNm]	$Ratio$ $1.3 \cdot M_{Rb}/M_{Rc}$
1	663 (HEB 300)	134 (HEA 220)	174	0.26
2	663 (HEB 300)	101 (HEA 200)	131	0.20

4.3.5 Lateral torsional buckling

Lateral torsional buckling of the girders and beams are prevented by stabilisation due to the concrete plate, which is connected with the members by headed studs. Overstrength of dissipative members due to the concrete plate has to be prevented by detailing of the connection joint. Lateral torsional buckling of FUSEIS beam links is assumed to be irrelevant, due to their short lengths.

4.3.6 FUSEIS columns

Columns shall be verified in compression whereby the force demands are to be calculated as follows (6.6.3 Eurocode 8-1):

$$N_{Ed} = N_{Ed,G} + 1.1 \cdot \gamma_{ov} \cdot \Omega \cdot N_{Ed,E} \quad \text{Eq. (4.6) (a)}$$

$$M_{Ed} = M_{Ed,G} + 1.1 \cdot \gamma_{ov} \cdot \Omega \cdot M_{Ed,E} \quad \text{(b)}$$

$$V_{Ed} = V_{Ed,G} + 1.1 \cdot \gamma_{ov} \cdot \Omega \cdot V_{Ed,E} \quad \text{(c)}$$

The factor Ω is calculated by the utilization rate of all beams in which dissipative zones are located:

$$\Omega = \min(\Omega_i)\,; \quad \Omega_i = {M_{pl,Rd,i}}/{M_{Ed,i}} \quad \text{Eq. (4.7)}$$

Demand to capacity ratios for axial and shear force as well as bending moments for FUSEIS strong columns are listed in the following tables.

Table 4.12: Demand capacity ratios for FUSEIS strong columns – Axial force

N_{Ed} [kN]	$N_{pl,Rd}$ [kN]	$N_{Ed}/N_{pl,Rd}$
1 632	5 191	0.31

Table 4.13: Demand capacity ratios for FUSEIS strong columns – Shear force

	V_{Ed} [kN]	$V_{pl,Rd}$ [kN]	$V_{Ed}/V_{pl,Rd}$
Strong axis	210	2 354	0.09
Weak axis	36	973	0.04

Table 4.14: Demand capacity ratios for FUSEIS strong columns – Bending moment

	M_{Ed} [kNm]	$M_{pl,Rd}$ [kNm]	$M_{Ed}/M_{pl,Rd}$
Strong axis	333	647	0.51
Weak axis	69	300	0.23

4.3.7 FUSEIS beam links

To prevent that full plastic moment resistance and rotation capacity at plastic hinges at the beam links are not decreased by compression and shear forces, the following Equations shall be fulfilled (6.6.2 Eurocode 8-1):

$$\frac{M_{Ed}}{M_{pl,Rd}} \leq 1,0; \quad \frac{N_{Ed}}{N_{pl,Rd}} \leq 0.15; \quad \frac{V_{Ed}}{V_{pl,Rd}} \leq 0.5 \qquad \text{Eq. (4.8)}$$

The shear force shall be calculated as follows:

$$V_{Ed} = V_{Ed,G} + V_{Ed,M} \quad \text{with} \quad V_{Ed,M} = {}^{2 \cdot M_{pl,Rd}}/_{L} \qquad \text{Eq. (4.9)}$$

Demand to capacity ratios for axial and shear force as well as bending moments for FUSEIS beam links are shown in the following tables. As the shear force ratio is larger than 0.5, interaction has been taken into account for calculating the plastic resistance of the beam sections.

Table 4.15: Demand capacity ratios for FUSEIS beam links – Axial force

Storey #	N_{Ed} [kN]	$N_{pl,Rd}$ [kN]	$N_{Ed}/N_{pl,Rd}$
1	61	1 000	0.06
2	52	841	0.09

Table 4.16: Demand capacity ratios for FUSEIS beam links – Shear force

Storey #	V_{Ed} [kN]	$V_{pl,Rd}$ [kN]	$V_{Ed}/V_{pl,Rd}$
1	110	185	0.59
2	85	163	0.52

Table 4.17: Demand capacity ratios for FUSEIS beam links – Bending moment

Storey #	M_{Ed} [kNm]	$M_{pl,Rd}$ [kNm]	$M_{Ed}/M_{pl,Rd}$
1	71	85	0.84
2	8	67	0.27

4.3.8 Shear panel verification

The shear panel of the FUSEIS strong columns needs to be verified by the following Eq. (4.**10**).

$$\boldsymbol{V_{wp,Ed} < V_{wp,Rd}} \qquad \text{Eq. (4.10)}$$

$$\boldsymbol{V_{wp,Ed} = \frac{M_{b1,Ed} + M_{b2,Ed}}{z}}$$

$$\boldsymbol{V_{wp,Rd} = 0,9 * V_{pl,Rd}}$$

Demand to capacity ratios for the shear panel of the FUSIES strong column are shown in .Table 4.18: Demand capacity ratios for FUSEIS strong columns – Shear panel verification

Table 4.18: Demand capacity ratios for FUSEIS strong columns – Shear panel verification

Storey #	$\boldsymbol{V_{wp,Ed}}$ **[kN]**	$\boldsymbol{V_{wp,Rd}}$ **[kN]**	$\boldsymbol{V_{Ed}/V_{pl,Rd}}$
1	444	875	0.51
2	373	875	0.43

4.3.9 Seismic link classification

Design and detailing rules for frames with eccentric bracings seismic links are discussed within 6.8.1 Eurocode 8-1. The FUSEIS beam links can also be considered as seismic links. Seismic links are classified into three categories:

- short links, which dissipate energy by yielding essentially in shear
- intermediate links, in which the plastic mechanism involves bending and shear
- long links, which dissipate energy by yielding essentially in bending

$$\boldsymbol{M_{p,link} = f_y * b * t_f * (h - t_f)} \qquad \text{Eq. (4.11)}$$

$$\boldsymbol{V_{p,link} = \frac{f_y}{\sqrt{3}} * t_w * (h - t_f)} \qquad \text{Eq. (4.12)}$$

Table 4.19: Classification of seismic links by its length

Short links	**Intermediate links**	**Long links**
$e_s = 1.6 \cdot M_{p,link}/V_{p,link}$	$e_s < e < e_L$	$e > e_L = 3.0 \cdot M_{p,link}/V_{p,link}$

The classification into short, intermediate or long links of the FUSEIS beam links is checked for informational issues. In the case study design considered herein, the beam links are to be classified into intermediate links.

4.4 STRUCTURAL DETAILING

The FUSEIS beam link to FUSEIS strong column joint is formed as rigid to enable the Vierendeel girder behaviour. Joints are capacity designed according to Eurocode 3 and Eurocode 8 with sufficient overstrength, to assure plastification only occurring in the FUSEIS beam links. Bolted end-plate connections which enable an easy mounting and replacement of the beam links should be used. Such a connection is schematically shown in Figure 4.8.

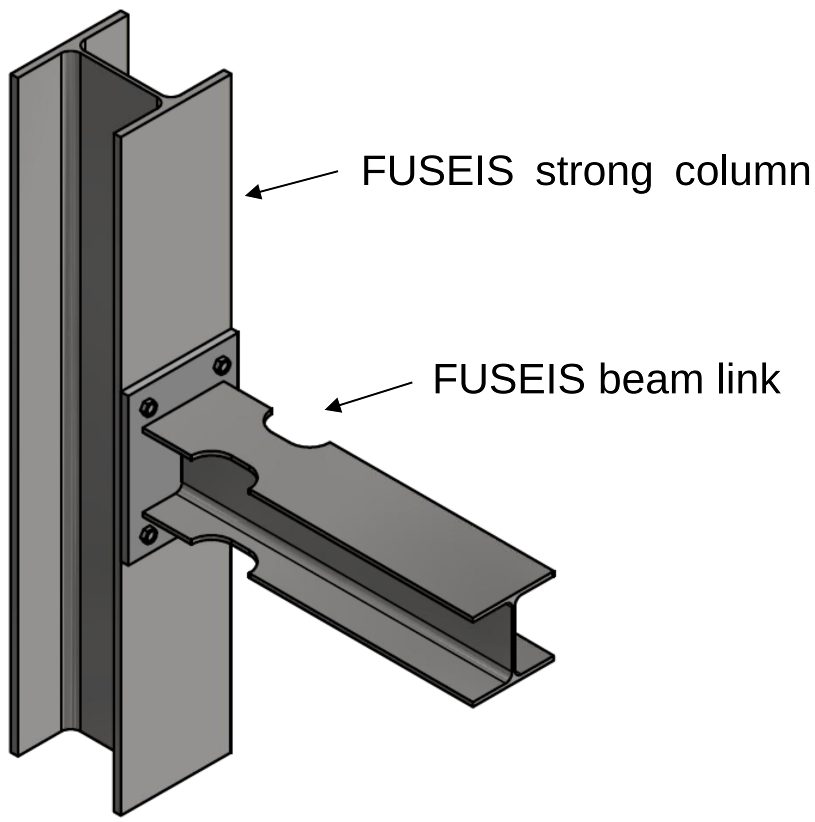

Figure 4.8: FUSEIS beam link system with bolted end-plate connection.

An exemplary detailing solution of the complete FUSEIS beam link system for a two storey low-rise building is shown in Figure 4.9.

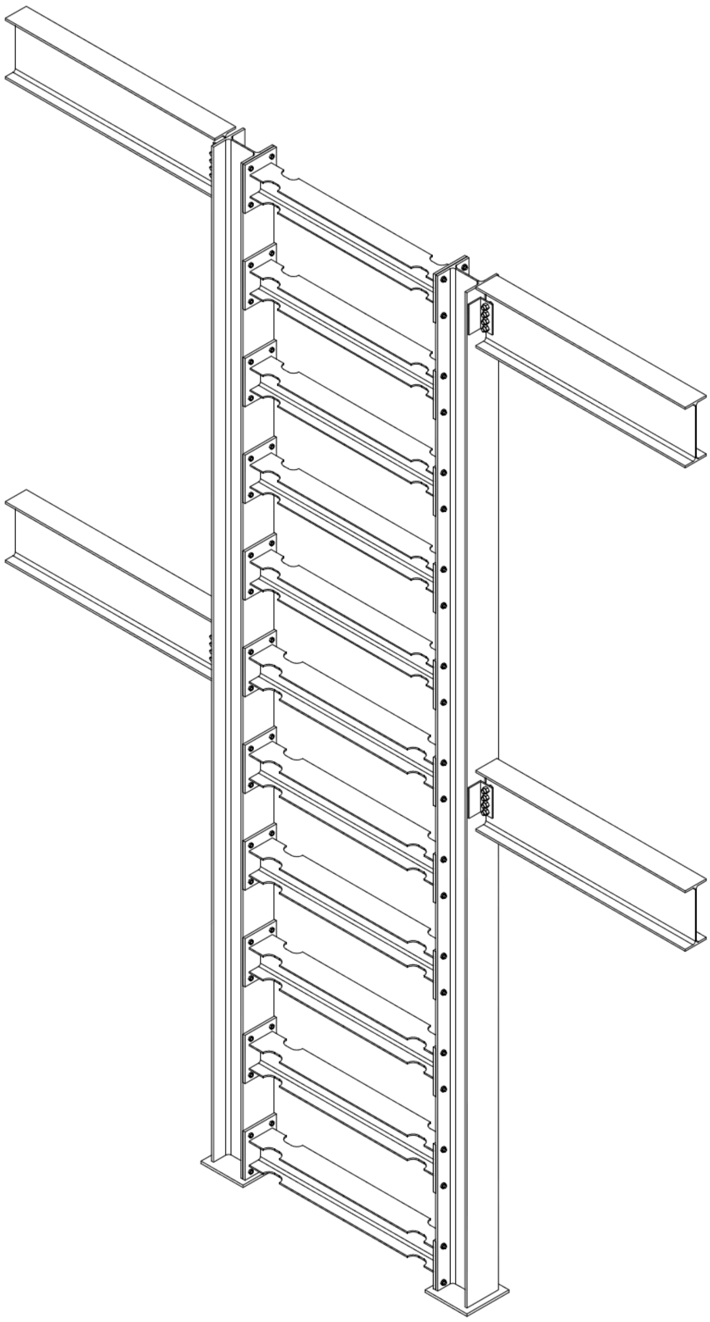

Figure 4.9: Schematical drawing of FUSEIS beam link system for two storey low-rise building.

4.5 CONCLUSIONS

This design example of a low-rise office building shows how effectively the FUSEIS beam link system can be applied as solely lateral force resisting system. Fulfilling all relevant design equations and limitations can easily be achieved. Moreover, the FUSEIS beam link system can be designed similar as a conventional Moment Resisting Frame (MRF), which is already well known in practical design.

4.6 REFERENCES

[1] Eurocode 0: Basis of structural design; EN 1990:2002 + A1:2005 + A1:2005/AC:2010.

[2] Eurocode 1: Actions on structures - Part 1-1: General actions - Densities, self-weight, imposed loads for buildings; EN 1991-1-1:2002 + AC2009.

[3] Eurocode 3: Design of steel structures - Part 1-1: General rules and rules for buildings; EN 1993-1-1:2005 + AC:2009.

[4] Eurocode 4: Design of composite steel and concrete structures - Part 1-1: General rules and rules for buildings; EN 1994-1-1:2004

[5] Eurocode 8: Design of structures for earthquake resistance - Part 1: General rules, seismic actions and rules for buildings; DIN EN 1998-1 + AC:2009, 2010.

[6] Eurocode 8: Design of structures for earthquake resistance - Part 3: Assessment and Retrofitting of buildings; EN 1998-3:2004.

[7] RSTAB 8, www.dlubal.com, 2017

5 FUSEIS PIN-LINK SYSTEM

5.1 GENERAL

5.1.1 Introduction

This case study refers to the detailed design of a 2-storey steel building incorporating the FUSEIS link system. A brief description of the FUSEIS pin link system is made in the beginning. Additional information about the system can be found in the document developed during the FUSEIS project [1], [2].

The design of the building was performed according to the provisions of the Eurocodes and the design guidelines presented within the INNOSEIS project

5.1.2 Description of the FUSEIS pin link system

The FUSEIS pin link system consists of a pair of strong columns rigidly connected by multiple links (Figure 5.1). The links consists of two receptacle beams connected through a short steel pin. The receptacle beams can have an H or hollow section and they are welded to the column flanges. The joint between the receptacles and the pins, is formed through an end plate on which the threaded section of the pin is screwed (Figure 5.2).

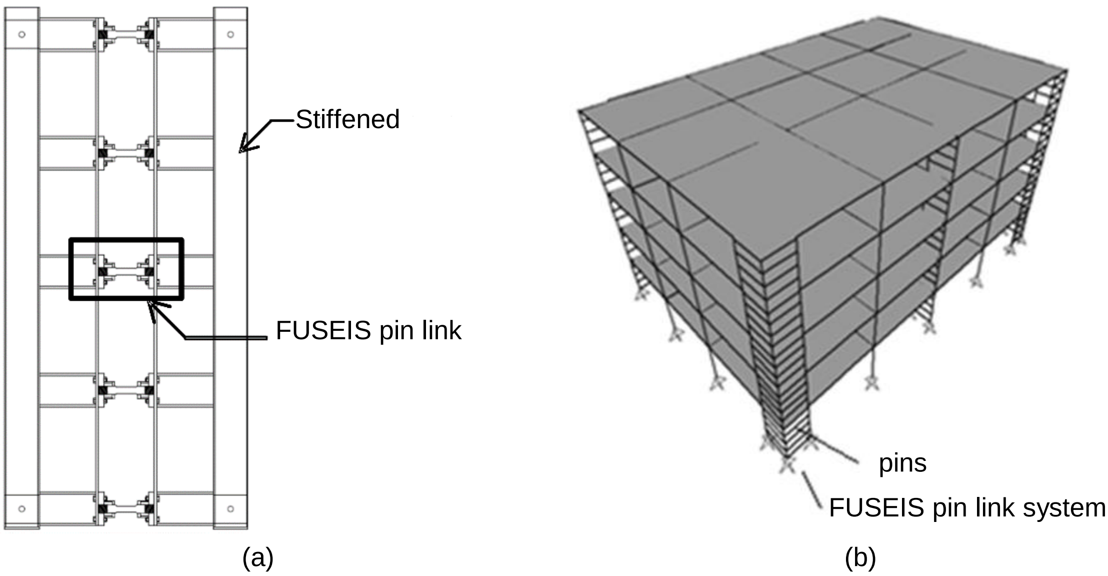

Figure 5.1: (a) FUSEIS pin link system configuration (b) Position of FUSEIS pin link system in a building

Under strong lateral forces, plastic hinges will form on the ends of the pins, thus dissipating a large amount of energy, while leaving the rest of the structure undamaged. The pin section is reduced in the middle part of the pin to ensure that plastification will take place away from the connection area. Repair works are easy, since they are restricted to the pins which are not generally subjected to vertical loads, as they are placed between floor levels.

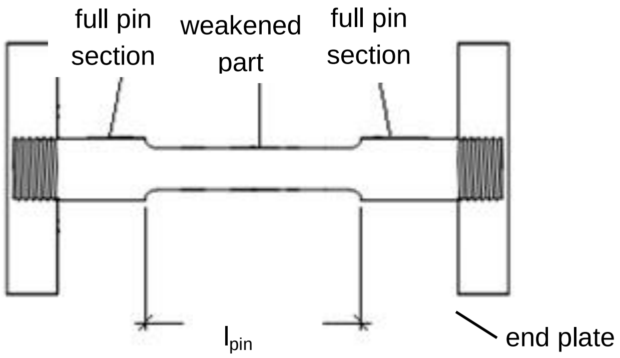

Figure 5.2: FUSEIS pin link

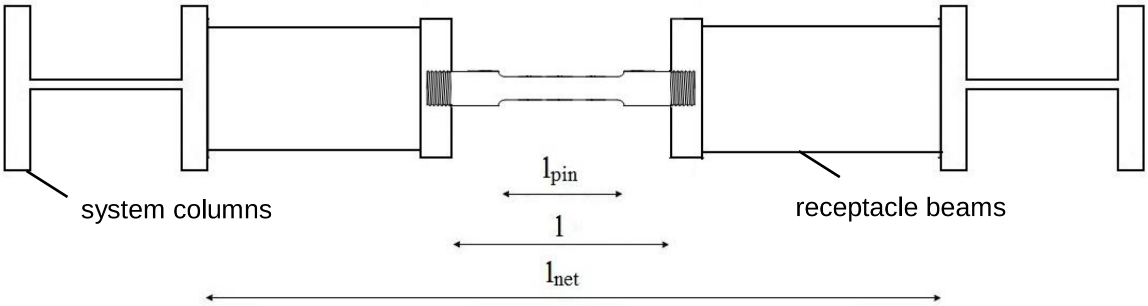

Figure 5.3: Typical plan view and dimensions of FUSEIS pin link system

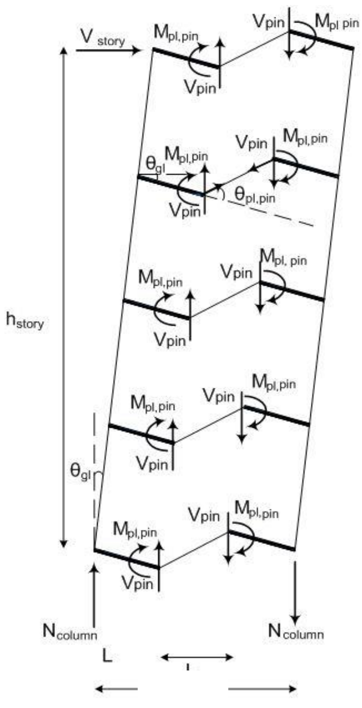

Figure 5.4: Vierendeel behaviour FUSEIS pin link system

Experimental investigations showed that the FUSEIS pin link system resists lateral loads as a vertical Vierendeel beam (Figure 5.4).

5.1.3 Geometry and general assumptions

The building is a 2-storey composite building, consisting of four frames with three 8m bays in each direction (Figure 5.5). All the connections of the frames are pinned and two FUSEIS pin link systems are applied on each of the external frames in order to provide the required lateral resistance. The non-system columns are H shaped (HEB type), the main and the secondary floor beams composed of steel beams with IPE and HEA sections respectively, both acting compositely with the concrete slab.

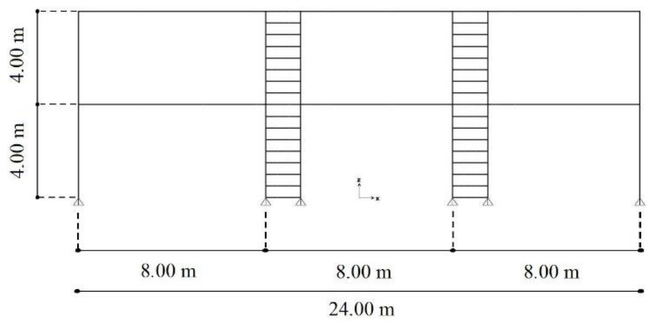

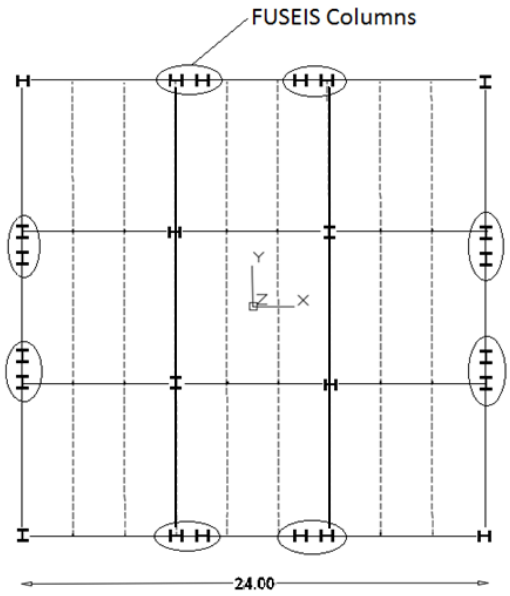

(a) Side view

(b) Plan view

Figure 5.5: Side and plan view of the building - FUSEIS systems position

Gravity and seismic loads are summarised in Table 5.1, according to EN 1991-1-1 [9]. The behaviour factor is equal to 3, as proposed by the design guidelines.

Table 5.1: Loading assumptions

Vertical loads	
dead loads (composite slab + steel sheeting)	2.75 kN/m²
superimposed loads for intermediate floors:	0.70 kN/m²
superimposed loads for top floor:	1.00 kN/m²
perimeter walls:	4.00 kN/m
total live load:	3.80 kN/m²:

Table 5.1 Loading assumptions (continued)

Design spectrum characteristics	
Elastic response spectra	Type 1
Peak ground acceleration	0.30g
Importance class II	$\gamma_I = 1.0$
Ground type	C
Behaviour factor	3
Seismic combination coefficient for the quasi-permanent value of variable actions	ψ_2=0.30

5.2 BASIC AND NON-SEISMIC DESIGN

5.2.1 Simulation

The modelling and design of the building, has been performed with the finite element software SAP2000v19 [6] The structural model is a linear-elastic model with beam elements, while no-section area elements were used for the correct distribution of the loads. The beam elements representing the FUSEIS pin links are divided into three parts with different cross sections in order to simulate the receptacle beams and the dissipative pin in the middle (Figure 5.7).

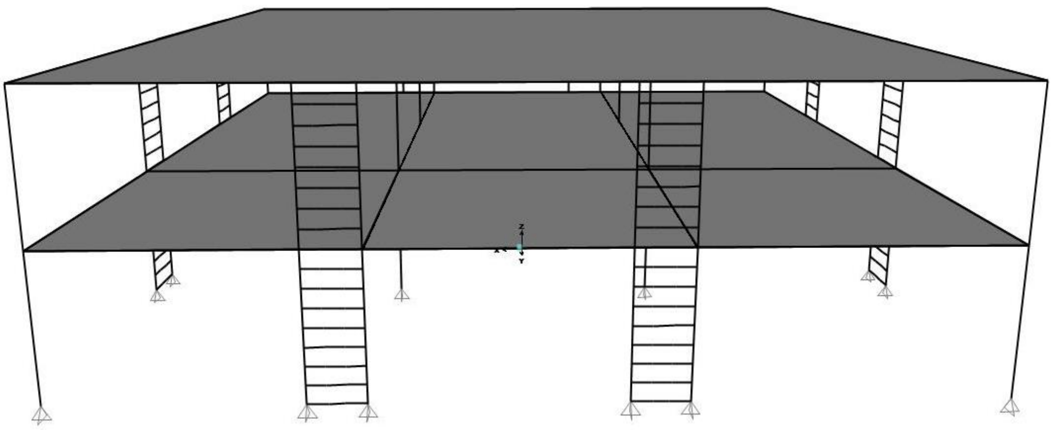

Figure 5.6: 3D view of the model in SAP2000

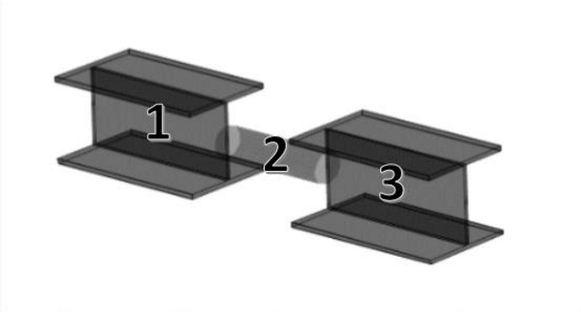

Figure 5.7: Simulation of FUSEIS pin link, division into three parts

5.2.2 Analysis and design

The columns and the beams of the main frame as well as the composite slabs, were designed both in the Ultimate Limit State (ULS) and the Serviceability Limit State (SLS) in accordance with the provisions of Eurocodes 3 and 4 [4], [8].

The profiles of all non-system members have been selected so that all the Eurocodes requirements are satisfied. When the programme automatic calculations were inadequate, e.g. for the design of the composite beams, hand calculations were used instead. The resulting cross section for the main beams was IPE500, for the secondary beams HEA200 and for the columns varied between HEB200 and HEB220. For the design of the secondary beams, construction phases were critical, so temporary supports should be placed to reduce both bending deformation and section size.

The slabs are composite for all floors and were designed with the program SymDeck Designer, a software provided by the manufacturer, which takes into account construction phases both for the ultimate and serviceability limit states. The materials used are Fe320 for the steel sheet, C25/30 for concrete and B500C for reinforcing steel. The thickness of the steel sheet is 0.80mm and the longitudinal reinforcement is Ø8/100.

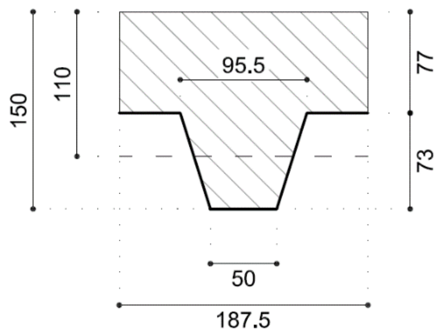

Figure 5.8: Composite slab section

Multi - Modal Response Spectrum Analysis was carried out, to calculate the lateral loads and deformations and to dimension the FUSEIS systems. The first 5 modes were used to activate more than 90% of the mass. The first and the second modes were translational while the third was rotational, with their eigen periods and shapes given in

Figure 5.9.

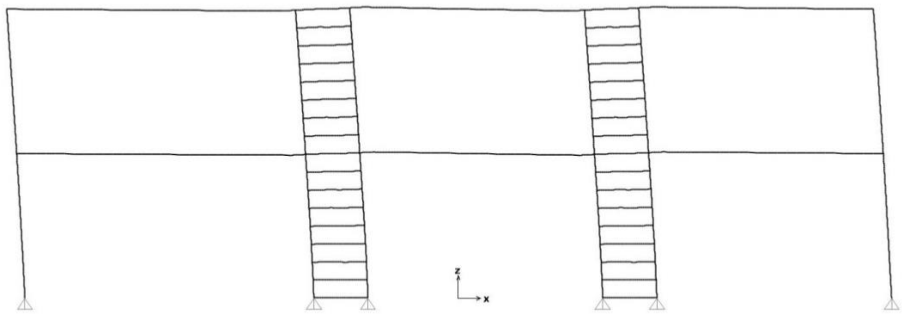

(a) 1st mode of vibration (T_1=0.62s)

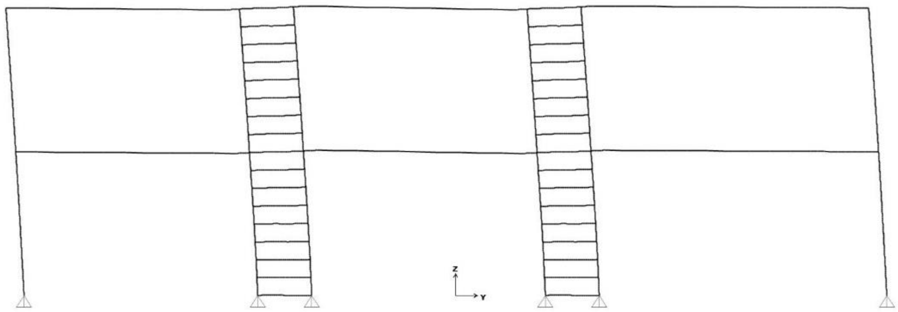

(b) 2nd mode of vibration (T_2=0.62s)

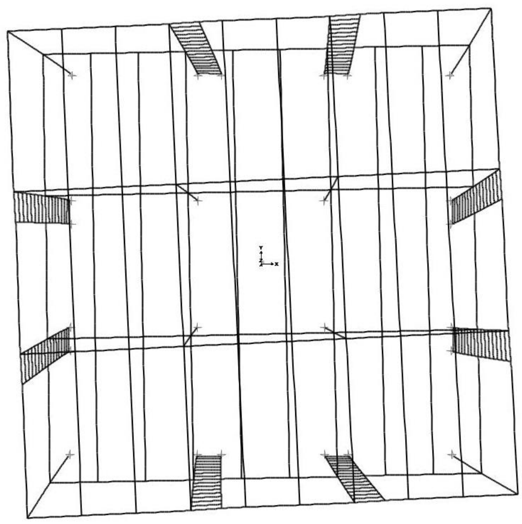

(c) 3rd mode of vibration (T_3=0.38s)

Figure 5.9: 1st, 2nd, 3rd mode shapes

The sections and configuration of the system were chosen after an iterative process. The FUSEIS systems consisted of a pair of strong columns (HEB300) at a central distance of 1.50m, the receptacle beams were HEA240, while nine links per storey were used, rigidly connected to the system columns. The dissipative

elements of the links have steel grade S235, while the receptacle beams are S275, which is lower than the rest of the structural members (S355).
Table 5.2 summarizes the cross sections of the FUSEIS systems, starting from the foundation level.

Table 5.2: Cross sections of FUSEIS pin system (starting from ground floor)

Number of links	Full diameter section	Reduced diameter section	FUSEIS columns section	FUSEIS receptacle beams
×9	Φ110	Φ90	HEB300	HEA240
×4	Φ100	Φ80	HEB300	HEA240
×4	Φ95	Φ75	HEB300	HEA240

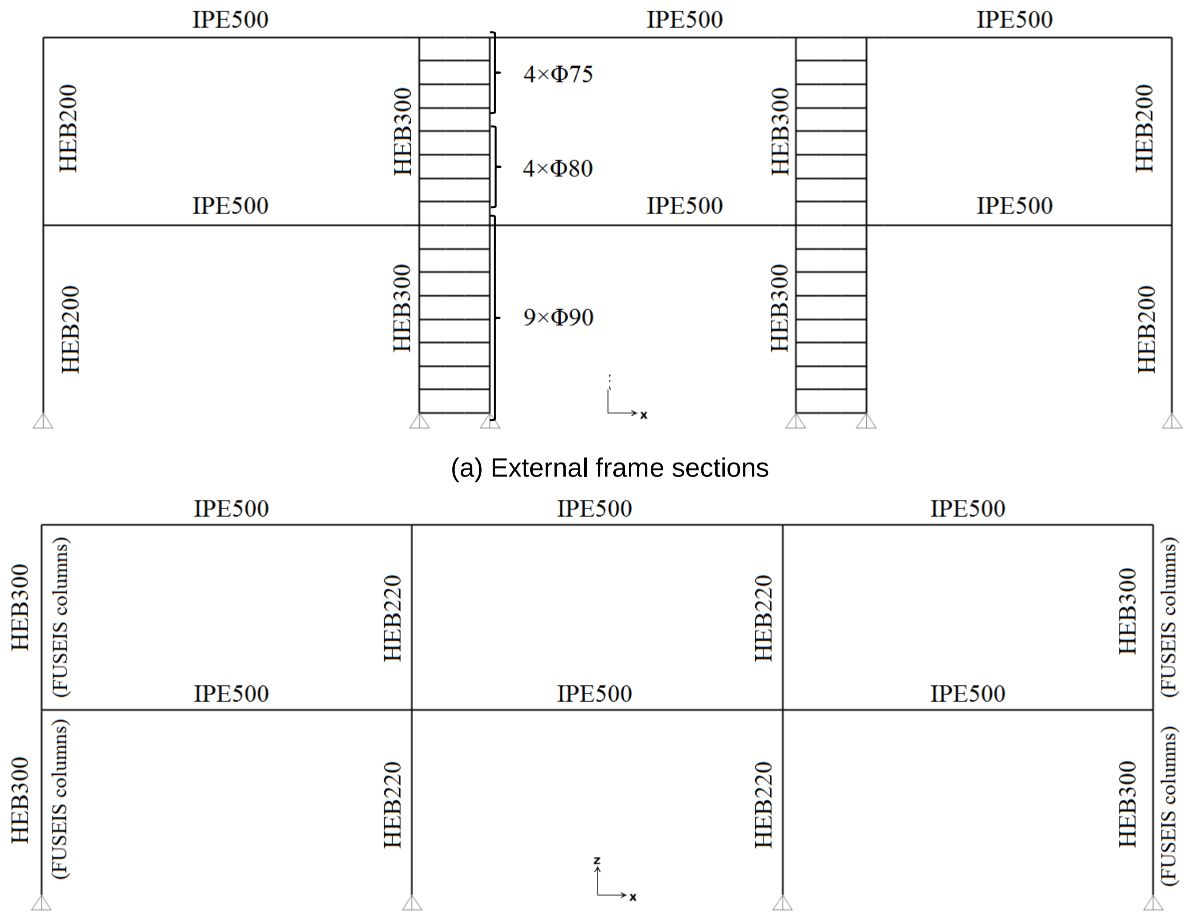

(a) External frame sections

(b) Internal frame sections
Figure 5.10: Cross sections of the building

In order to ensure the development of a bending mechanism at the RDS (reduced diameter section) positions, the length l_{pin} was taken larger than the one calculated from Eq. (5.1), i.e. 300mm.

$$l_{pin} \geq \frac{4 \times M_{pl,pin,Rd}}{V_{pl,pin,Rd}} = \frac{4 \times W_{pl,pin}}{A_v / \sqrt{3}} \qquad \text{Eq. (5.1)}$$

$M_{pl,\ pin,Rd}$ is the design plastic moment resistance of the weakened part of the pin
$V_{pl,\ pin,Rd}$ is the design shear resistance of the weakened part of the pin
l_{pin} is the length of the weakened part of the pin (Figure 5.3)
$W_{pl,\ pin}$ is the plastic section modulus of the weakened part of the pin

5.3 SEISMIC ANALYSIS

5.3.1 Seismic design

The conventional method for calculating the seismic loads is by applying Multi - Modal Response Spectrum Analysis, according to Eurocode 8 [3]. In each direction, the number of modes taken into consideration is such, that the sum of the effective modal mass is greater than the 90% of the total mass. In order for the inelastic deformations to be considered, a behaviour factor must be introduced. The design guidelines propose a maximum value of the behaviour factor q equal to 3 for the FUSEIS pin link system.

In order to control the overall stability of the structure and the design of the ductile and non-ductile members under seismic loads, the conditions of §5.3.2-5.3.50 should be fulfilled, according to the design guide. Because the structure has similar stiffness and behaviour in both directions, only the results of x-direction are presented.

5.3.2 Limitation of inter-storey drift

Considering that the building has ductile non-structural members, Eq. (5.2) must be fulfilled.

Table 5.3 shows the results of the analysis and in both cases the check is verified in all storeys.

$$d_r v \leq 0.0075h \qquad \text{Eq. (5.2)}$$

Table 5.3: Limitation of inter-storey drift

Case	Storey	u_x (mm)	d_{ex} (mm)	q^*d_{ex} (mm)	v^*d_{rx} (mm)	Check	0.0075h
1st	1st	19.7	19.7	59.1	29.6	≤	30
	2nd	39.7	20.0	60.0	30.0	≤	30
2nd	1st	16.4	16.4	49.2	24.6	≤	30
	4th	35.0	18.6	55.7	27.8	≤	30

5.3.3 Magnitude of 2nd order effects

The inter-storey drift coefficient θ may be calculated by a linear buckling analysis through the factor α_{cr}, the factor by which the design loading has to be increased to cause elastic instability in a global mode.
This check indicates whether the deformations of the structure are too big to ignore 2nd order effects. A linear buckling analysis was performed and the critical buckling factor α_{cr}, coefficient θ and checks derived from this analysis are presented in Table 5.4. According to EN1998-1 §4.4.2.2, when the inter-storey drift sensitivity coefficient θ, is limited to $\theta \leq 0.1$, 2nd order effects can be ignored.

Table 5.4: Magnitude of 2nd order effects

Case	α_{cr}	$\theta = q / \alpha_{cr}$	Check	limit	Seismic load multiplier
1st	47	0.064	≤	0.1	1.00

5.3.4 Dissipative elements verifications

The FUSEIS systems were designed based on the results of the most unfavourable seismic combination 1.0G+0.3Q+E. In order to ensure a uniform dissipative behaviour, the overstrength values Ω of the reduced sections were checked to differ less than 25%. A factor maxΩ/minΩ=1.18 was calculated. Table 5.5 to Table 5.8 summarize the results of all dissipative element verifications. As shown, the bending moment check was the most critical, with maximum utilization factor equal to 92.4%. Additionally, it was derived from the shear check, that no reduction of bending moment resistance was needed due to high shear force.

Table 5.5: Check of axial forces

Reduced diameter pins Φ(mm)	N_{Ed} (kN)	$N_{pl,pin,Rd}$ (kN)	$\frac{N_{Ed}}{N_{pl,pin,Rd}} \leq 0.15$
90	10.58	1495.01	0.007
80	18.12	1181.24	0.015
75	5.00	1038.20	0.005

Table 5.6: Check of shear forces

Reduced diameter pins Φ(mm)	$V_{CD,Ed}$ (kN)	$V_{pl,pin,Rd}$ (kN)	$\frac{V_{CD,Ed}}{V_{pl,RBS/pin,Rd}} \leq 0.5$
90	188.00	863.14	0.22
80	133.17	682.00	0.20
75	109.67	599.40	0.18

Table 5.7: Check of bending moments

Reduced diameter pins Φ(mm)	M_{Ed} (kNm)	$M_{pl,pin,Rd}$ (kNm)	$\frac{M_{Ed}}{M_{pl,pin,Rd}} \leq 1.00$
90	25.14	28.20	0.89
80	18.14	19.98	0.91
75	15.19	16.45	0.92

Considerably large rotations developed in FUSEIS pins during seismic excitation. Therefore, it is necessary to limit these rotations accordingly.

$$\theta_{pin} = \frac{L}{l_{pin}} \times \theta_{gl} \leq \theta_{ULS,pin} \qquad \text{Eq. (5.3)}$$

Where

L is the axial distance between the FUSEIS columns (Figure 5.4)

l_{pin} is the length of the weakened part of the pin (Figure 5.3)

θ_{gl} is the rotation of the FUSEIS system as shown in (Figure 5.4)

$\theta_{ULS,pin}$ is equal to 14%

The results in Table 5.8 show that all rotations are well below the limit value.

Table 5.8: Check of chord rotation

Storey number	θ_{pin} (mrad)	check	$\theta_{pl,pin}$ (mrad)
1	12.31	≤	140
2	13.92	≤	140

5.3.5 Non-dissipative elements verifications

The non-dissipative elements i.e. the system columns, the receptacle beams, the full section pins and their connections were capacity designed for increased internal forces.

5.3.5.1 System columns

The utilization factors of the system columns were calculated according to the provisions of EN1993-1-1 [4]. The increased forces were calculated according to the following equations:

$$N_{CD,Ed} = N_{Ed,G} + 1.1 \times \alpha \times \gamma_{ov} \times \Omega \times N_{Ed,E} \qquad \text{Eq. (5.4)}$$

$$M_{CD,Ed} = M_{Ed,G} + 1.1 \times \alpha \times \gamma_{ov} \times \Omega \times M_{Ed,E} \qquad \text{Eq. (5.5)}$$

$$V_{CD,Ed} = V_{Ed,G} + 1.1 \times \alpha \times \gamma_{ov} \times \Omega \times V_{Ed,E} \qquad \text{Eq. (5.6)}$$

where,

$N_{Ed,G}$, $M_{Ed,G}$, $V_{Ed,G}$ are the internal forces due to the non-seismic actions of the seismic combination

$N_{Ed,E}$, $M_{Ed,E}$, $V_{Ed,E}$ are the internal forces due to the seismic action

$\Omega = \min\Omega_i = \min\left\{\dfrac{M_{pl,RBS,pin,Rd,i}}{M_{Ed,i}}\right\}$ is the minimum overstrength factor

γ_{ov} is the material overstrength factor (suggested value 1.25)

α=1.5 is an additional factor only used for the FUSEIS pin link system, to ensure that pin links will yield first

In any case, the increment factor ($1.1\times\gamma_{ov}\times\Omega$ or $1.1\times\alpha\times\gamma_{ov}\times\Omega$) shall not exceed the behaviour factor q.

In Figure 5.11 the utilization factors of four FUSEIS columns is showed as resulted from the capacity design. The results are similar for the rest of the system columns. The utilization factors range from 57% to 100%.

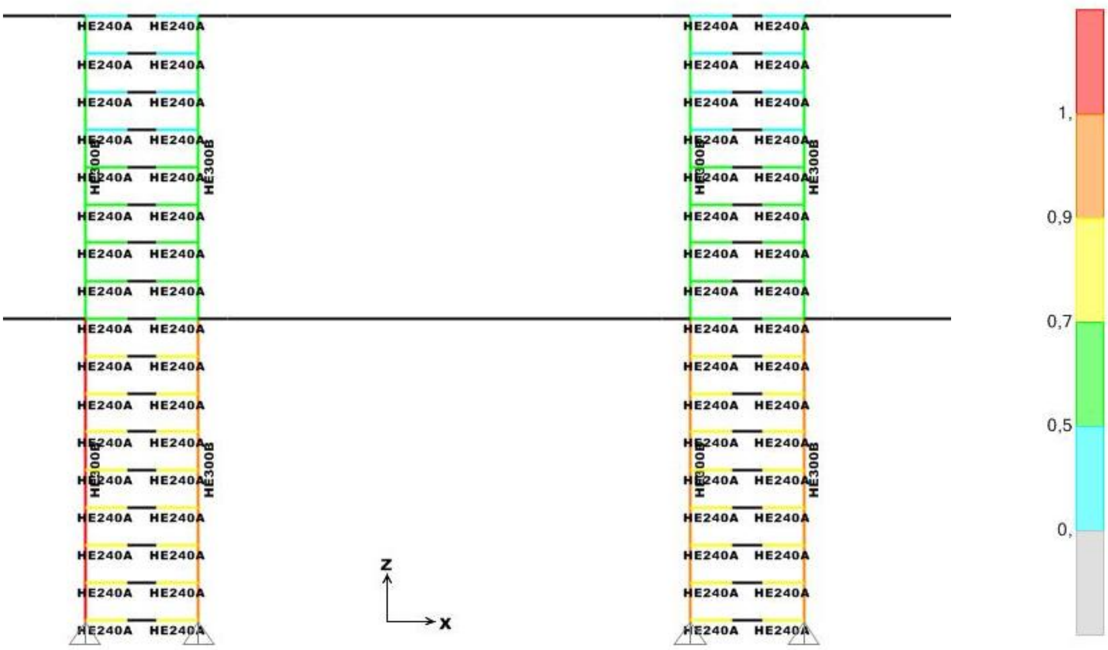

Figure 5.11: Utilization factors for FUSEIS columns

5.3.5.2 Full pin sections and receptacles

The moment resistance of the full pins sections was verified at the contact area with the face plates. The utilization factors for pin sections and receptacles are shown in Table 5.9.

a) Receptacle beams

The receptacle beams shall be capacity designed, to ensure that they will not yield prior to the reduced diameter section pin, according to Eq. (5.8):

$$\frac{M_{CD,Ed}}{M_{pl,rec,Rd}} \leq 1.0 \qquad \text{Eq. (5.7)}$$

$$M_{CD,Ed} = \frac{l_{net}}{l_{pin}} M_{pl,pin,Rd} \qquad \text{Eq. (5.8)}$$

where,

$M_{pl,\,pin,Rd}$ is the design plastic moment resistance of the weakened part of the pin

$M_{CD,Ed}$ is the capacity design bending moment

l_{net} is the total length of the link between the column flanges (Figure 5.3)

$M_{pl,rec,Rd}$ is the design bending moment resistance of the receptacle beam

b) Full pin section

To ensure that the full cross section of the pins will not yield prior to the reduced sections, the moment resistance of the full cross section shall be verified to be greater than the capacity design moment $M_{CD,Ed}$, calculated as shown in Eq. (5.9).

$$\frac{M_{CD,Ed}}{M_{pl,Rd}} \leq 1.0 \qquad \text{Eq. (5.9)}$$

$$M_{CD,Ed} = \frac{l}{l_{pin}} M_{pl,pin,Rd} \qquad \text{Eq. (5.10)}$$

where,

l for FUSEIS beam link system is the length between the face plates of the columns and for FUSEIS pin links is the length between the face plates of the receptacles (Figure 5.3)

$M_{pl,Rd}$ is the design bending moment resistance of the full beam/pin section

Table 5.9: Utilization factors of the full pin sections and receptacles

Full diameter pins Φ(mm)	$M_{CD,Ed}$ (kNm)	$M_{pl,Rd}$ (kNm)	$\frac{M_{CD,Ed}}{M_{pl,Rd}} \leq 1.00$
110	37.60	51.70	0.73
100	26.63	38.78	0.69
95	21.93	33.37	0.66
Receptacle HEA240	112.80	204.77	0.55

c) Connection between the FUSEIS links and the columns

The joints between the FUSEIS links and the system columns, are formed as fully welded. To ensure that these connections will have enough overstrength to yield after the plastification of the links, they are capacity designed according to Eq. (5.11) and Eq. (5.12) and the results for a typical connection are given in
Table 5.10.

$$M_{CD,con,Ed} = 1.1 \times \gamma_{ov} \frac{L_{net}}{l_{pin}} M_{pl,pin,Rd} \qquad \text{Eq. (5.11)}$$

$$V_{CD,con,Ed} = 1.1 \times \gamma_{ov} \frac{2 \times M_{pl,pin,Rd}}{l_{pin}} \qquad \text{Eq. (5.12)}$$

Table 5.10: Welded connection design

Design moment (kNm)	Design force (kN)	Stiffeners Thickness (mm)	Beam welds	Utilization factor
155	255	8	a_f=8mm a_w=5mm	0.84

5.4 STRUCTURAL DETAILING

After fulfilment of all checks the FUSEIS links may be detailed. Their final design is presented in Figure 5.13 and Figure 5.14. The lengths of each part of the FUSEIS links are the same along the height of the building. Only the diameter of the pin is variable, as shown in Table 5.2.

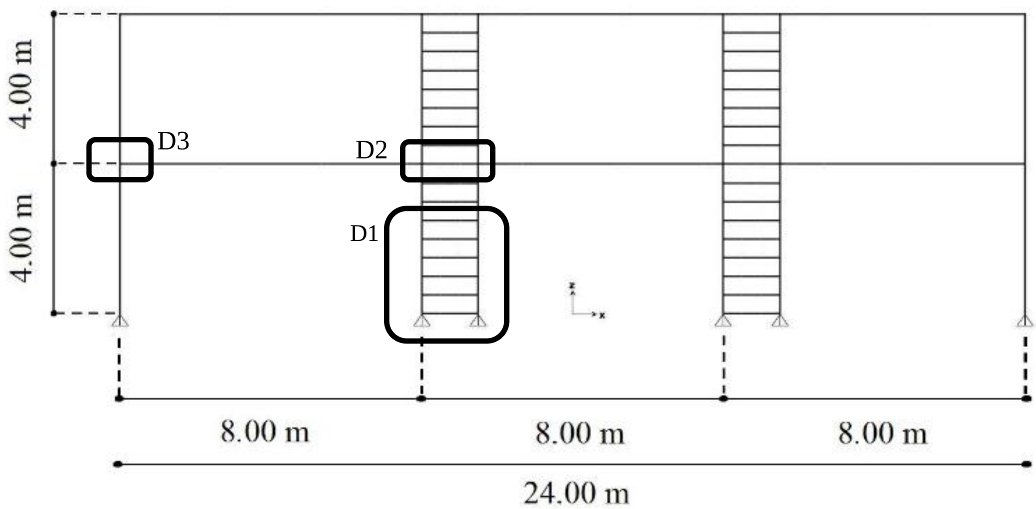

Figure 5.12: Side view of building

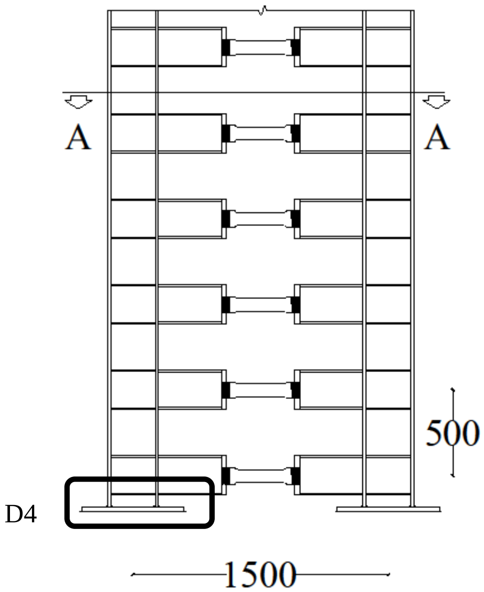

Figure 5.13: Detail D1

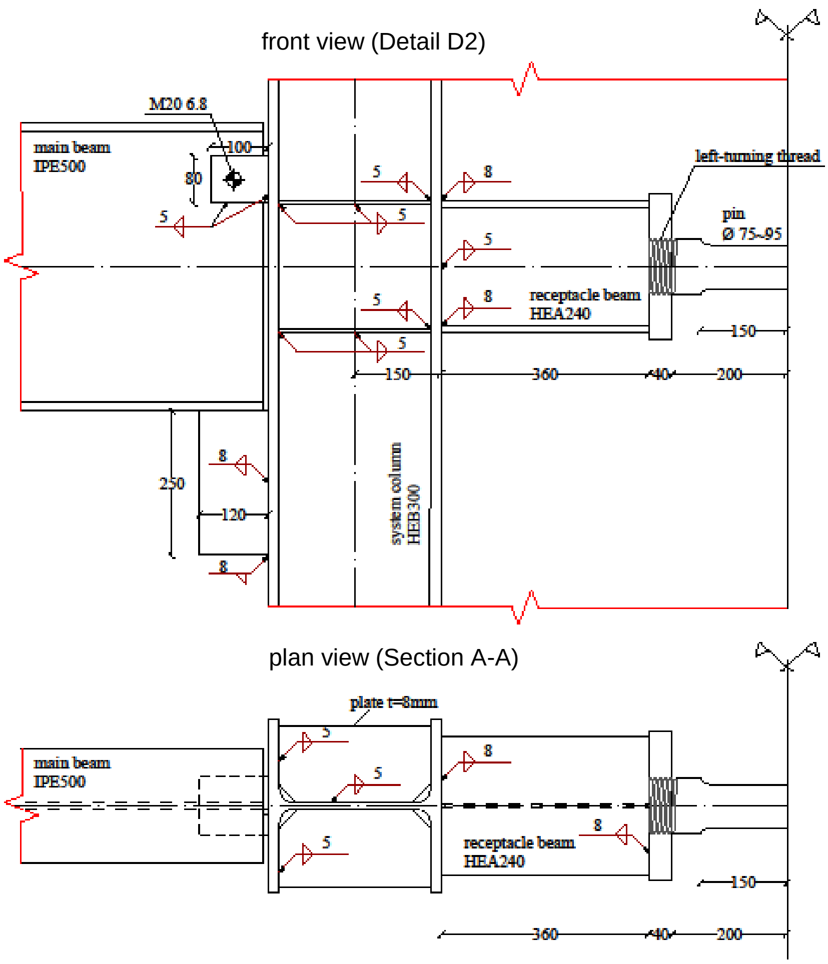

Figure 5.14: Side view and plan view of a typical FUSEIS horizontal link

front view (Detail D3)

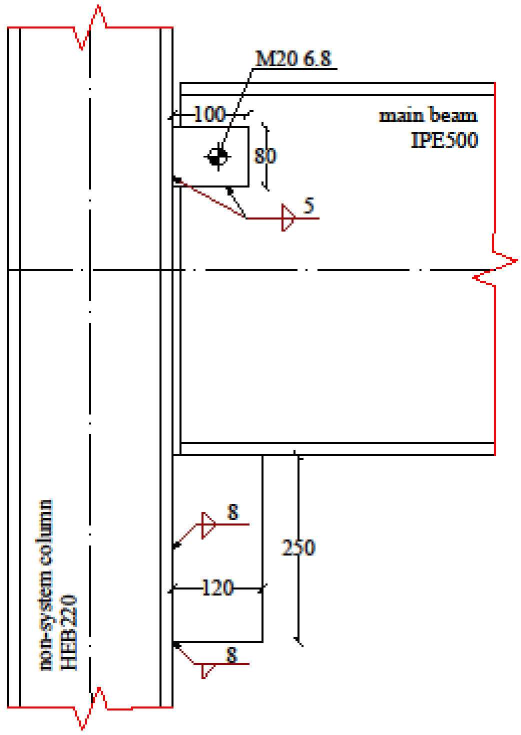

plan view (Detail D3)

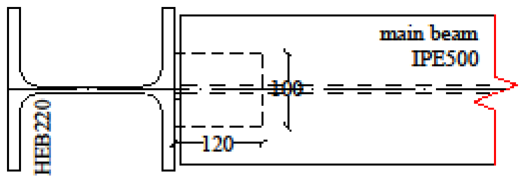

Figure 5.15: Beam to column connection of the main frame

The connection between the system column and the receptacle beams is a welded connection. In the simulation and design of the beam to column connection was performed in Robot 2016.

In Figure 5.16 the FUSEIS column base joint is shown which was formed as a pinned connection.

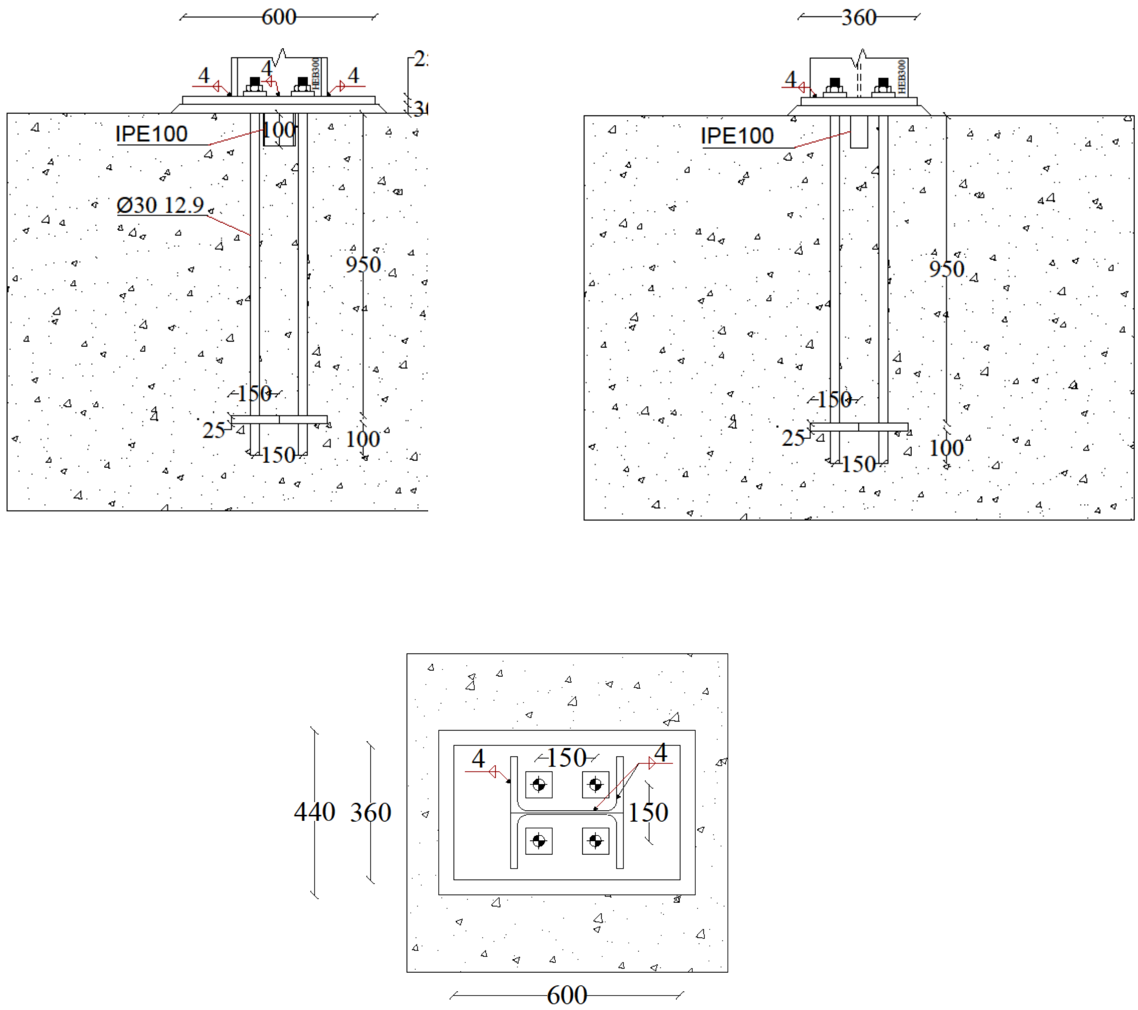

Figure 5.16: Detail D4 of foundation connection

5.5 REFERENCES

[1] Vayas, I., Karydakis, Ph., Dimakogianni, D., Dougka, G., Castiglioni, C. A., Kanyilmaz, A. et al. Dissipative devices for seismic resistant steel frames - The FUSEIS Project, Design Guide. Research Programme of the Research Fund for Coal and Steel 2012.

[2] I. Vayas, Ph. Karydakis, D. Dimakogianni, G. Dougka, Castiglioni, C. A., Kanyilmaz, A. et al. Dissipative devices for seismic-resistant steel frames (FUSEIS). Research Fund for Coal and Steel, European Commission; EU 25901 EN 2013.

[3] EN1998-1-1, Eurocode 8: Design of structures for earthquake resistance – Part 1-1: General rules, seismic actions and rules for buildings. Brussels: Comitee Europeen de Normalisation (CEN); 2003.

[4] EN1993-1-1, Eurocode 3: Design of steel structures - Part 1-1: General rules and rules for buildings. Brussels: Comitee Europeen de Normalisation (CEN); 2003.

[5] FEMA – 356: Prestandard and Commentary for the seismic rehabilitation of Buildings. Washington; 2000.

[6] SAP2000, CSI, Computers and Structures Inc., www.csiberkeley.com.
[7] EN1994-1-1: Eurocode 4: Design of composite steel and concrete structures. Part 1-1: General rules and rules for buildings. Brussels: Comité Européen de Normalisation (CEN); 2005.
[8] EN 1993-1-8: Eurocode 3: Design of steel structures. Part 1-8: Design of joints. Brussels: Comité Européen de Normalisation (CEN); 2004.
[9] EN1991-1-1, Eurocode 1: Actions on structures

6 BOLTED FUSEIS BEAM SPLICE

The case study which presents the implementation of dissipative bolted FUSEIS beam splices is elaborated in section 2. The report presents the low rise case study (2-storey) equipped with FUSEIS bolted beam splices and INERD pin connections in both main directions of the buildings. The reader is kindly invited to go back in the text and follow the case study there.

7 WELDED FUSEIS BEAM SPLICE

7.1 GENERAL

7.1.1 Introduction

This case study refers to the seismic design of new two-story composite concrete and steel office buildings. It aims to demonstrate the implementation of the welded FUSEIS beam splice. The elaborated case study comprises the conceptual design, modelling and analysis by linear response spectrum analysis methods (RSA), detailed design of main dissipative and non-dissipative members as well as basic structural detailing of welded beam splice.

7.1.2 Description of the building

7.1.2.1 Geometry, materials and general assumptions

The case study deals with a two-story frame building with three 8 m bays in both directions. The gravity frames are composed of beams and columns, located at each structural axis. Lateral forces are resisted by the moment resistant frames with welded FUSEIS beam splices (MRF-WFBS) in the Y direction and by conventional concentrically braced frames (CBF) in the X direction. In this respect, beam-to-column joints and column bases are assumed as fully fixed in the Y direction and nominally pinned in the X direction. The floor plan and elevation of the building are illustrated in Figure 7.1 to Figure 7.5. Figure 7.6 gives the dimensions assigned to the concrete slab. The elements and materials used herein are:

In the Y direction – MRF-WFBS

- IPE450 composite beams (S275 steel grade and C25/30, A500 NR concrete)
- HEA200 composite beams (S355 steel grade and C25/30, A500 NR concrete) – resist vertical loads only
- Columns with S355 steel grade (strong moment of inertia)

In the X direction – CBF

- IPE500 beams (S355 steel grade)
- Columns with S355 steel grade (weak moment of inertia)
- CBF bracings which are assumed to function in tension only (highlighted in blue in Figure 7.1 and Figure 7.4).

The welded FUSEIS beam splices are placed near the null moment sections defined by the gravity loading. The reinforced beam zone adjacent to the welded FUSEIS beam splices (red segments in Figure 7.1) consists in the reinforcement of the IPE450 composite beam with welded web and flange plates. Diaphragms are assumed rigid, thus neglecting membrane (in-plane) deformations.

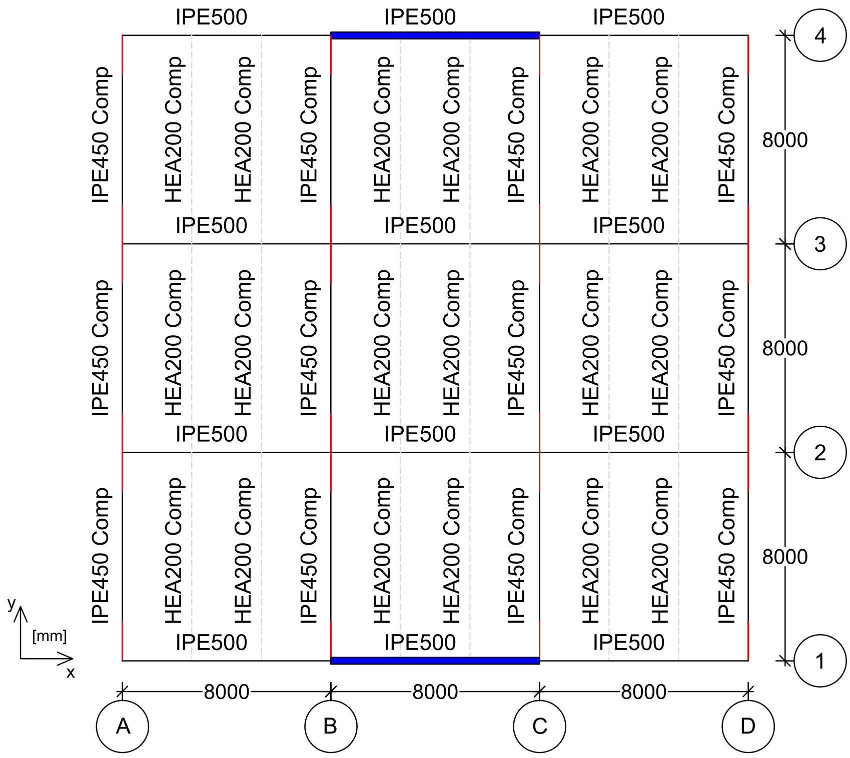

Figure 7.1: Plan view of the case study building

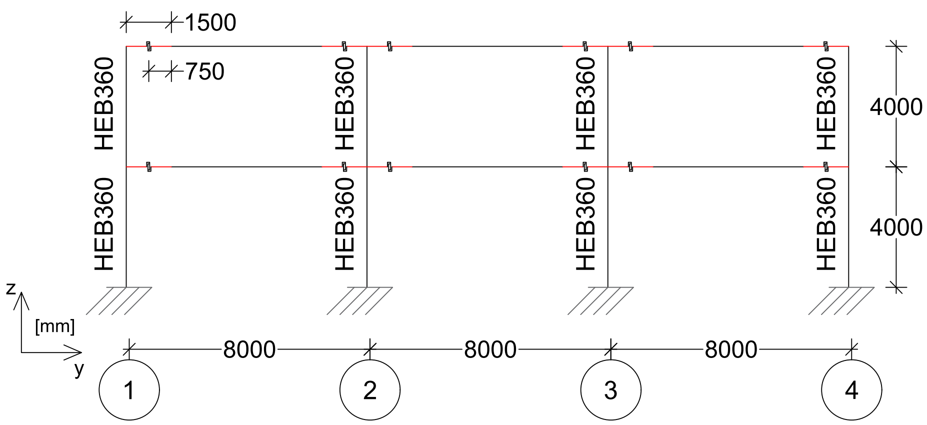

Figure 7.2: Exterior side view of the case study building (Y direction)

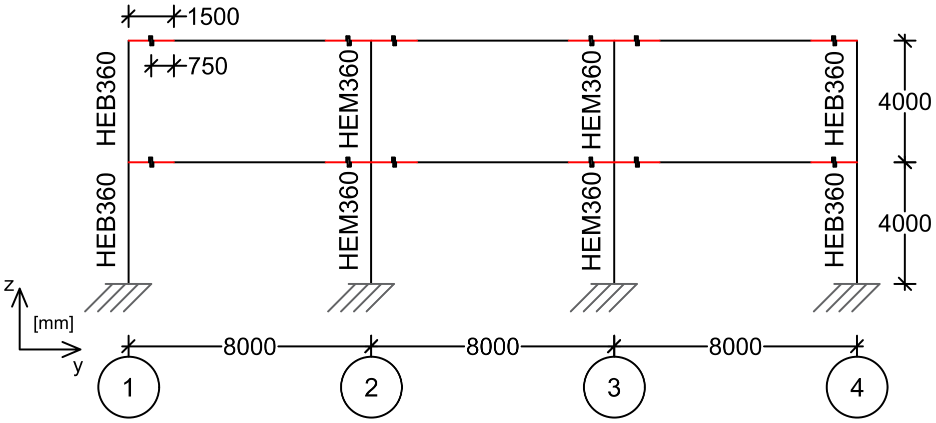

Figure 7.3: Interior side view of the case study building (Y direction)

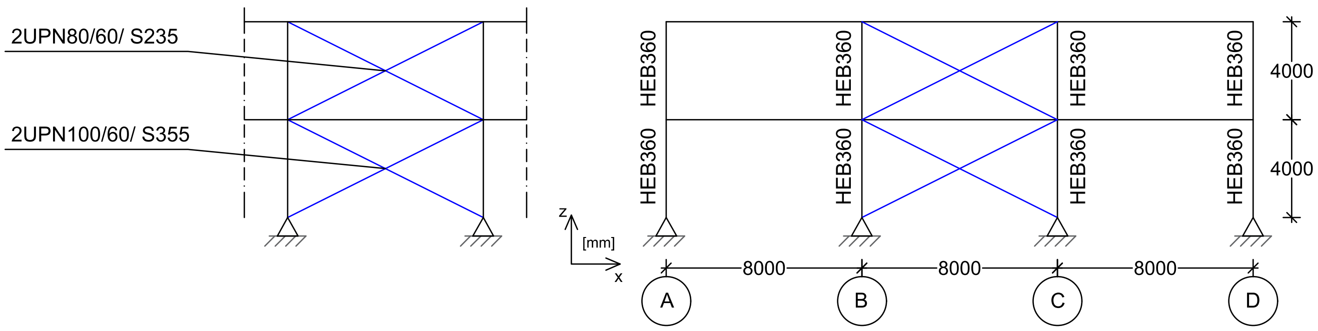

Figure 7.4: Exterior side view of the case study building (X direction)

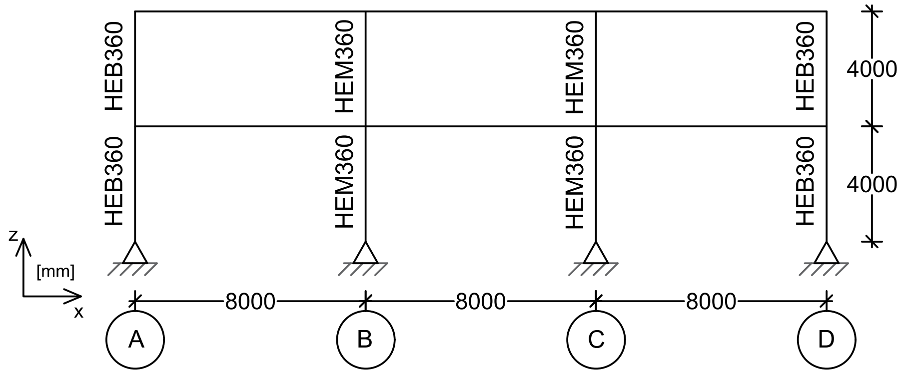

Figure 7.5: Interior side view of the case study building (X direction)

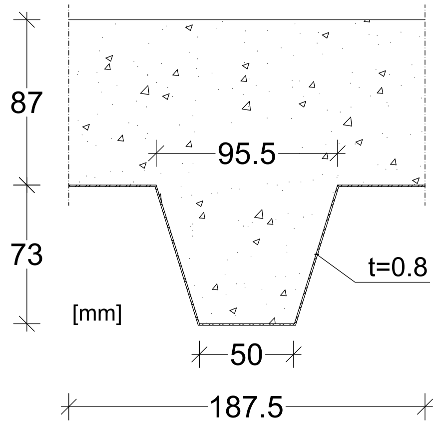

Figure 7.6: Representation of the composite slab (thickness of the profile steel sheet – 0.8 mm)

7.1.2.2 Loads and load combinations

The gravity loads and seismic action parameters are summarized in Table 7.1, whereas Table 7.2 presents the coefficients for the various load combinations.

Table 7.1: Quantification of the applied gravity loads and seismic action parameters

Vertical loads		
Load Class	Type of load	Value
Dead Load	Composite slab with profile sheeting	3.00 kN/m
Superimposed loads	Services, celling and raised floors	0.70/1.00 kN/m2[1]
	Perimeter walls	4.00 kN/m
Live loads	Office (Class B)	3.00 kN/m2[2]
	Movable partitions	0.80 kN/m2
Seismic action		
Importance factor (Class II)	γ_I=1.00	
Soil acceleration	agr=0.30g	
Soil type	C	
S_{max}	1.15	
T_B	0.20 sec	
T_C	0.60 sec	
T_D	2.00 sec	
Damping ratio	5%	
Behavior factor	4	

[1] 0.70 kN/m^2 for the first floor and 1.00 kN/m^2 for the roof

[2] The roof is considered as accessible and, according to the paragraph 6.3.4.1(2) of [1], this has the same live load value as the service floor.

Table 7.2: Coefficients used for the load combinations

Coefficient	Value
γ_G	1.35
γ_Q	1.50
Ψ_2 Office (Class B)	0.30
Ψ_2 Roof	0.00
φ Correlated floors	0.80
φ Roof	1.00

The seismic masses are calculated according to Eq. (7.1) and presented in Table 7.3.

$$\sum_{j>1} G_{k,j} + \sum_{i>1} \Psi_{2,i} \cdot \varphi_i \cdot Q_{k,i} \qquad \text{Eq. (7.1)}$$

Table 7.3: Quantification of seismic masses

Seismic mass floor 1		**332.20 t**
Concrete and metal deck self-weight + Composite IPE and HEA + IPE500 (Gk1,1)	(3.00*24.0*24.0+73.01+59.63+85.717)/9.81	198.41 t
Utilities, ceiling, floor finishing (Gk2,1)	0.70*24.0*24.0/9.81	41.10 t
Perimeter walls (Gk3,1)	4.00*4.00*24.00/9.81	39.14 t
Partitions (Qk1,1)	0.80*0.30*0.80*24.00*24.00/9.81	11.27 t
Imposed loads (Qk2,1)	0.80*0.30*3.00*24.00*24.00/9.81	42.28 t
Seismic mass floor 2 (roof)		**257.12 t**
Concrete and metal deck self-weight + Composite IPE and HEA + IPE500 (Gk1,2)	(3.00*24.00*24.00+73.01+59.63+85.717)/9.81	198.41 t
Utilities, ceiling, floor finishing (Gk2,2)	1.00*24.00*24.00/9.81	58.72 t
Imposed loads (Qk1,2)	0.00*1.00*24.00*24.00*3/9.81	0.00 t
Columns and CBF mass		**22.49 t**
Total		**611.81 t**

7.2 BASIC AND NON-SEISMIC DESIGN

7.2.1 Preliminary design of the welded FUSEIS beam splices and reinforcing zones

To assess the MRF-WFBS resistance to seismic action based on the linear response spectrum analysis, initial dimensions of the welded FUSEIS beam splice components must be defined. Following the recommendations in [2] and [3], the user shall begin with the preliminary design of the gravity members based on the ultimate and serviceability limit state criteria, assuming a building without welded FUSEIS beam splices. Then, subjecting the conventional structure to a linear response spectrum analysis the user acquires an initial idea of the building performance under earthquake loading, thus estimating approximately the acting moment that the welded FUSEIS beam splice will have to resist. Finally, all other components' preliminary dimensions may be subsequently derived. Table 7.4 presents the acting moment estimated based on the conventional structure and the dimensions chosen for the flange plate of the fuses. Table 7.5 gives the computed dimensions for the rest of the components.

Figure 7.7 indicates the location of the welded FUSEIS beam splice and the span of the reinforced beam cross section. Finally,

Figure 7.8 illustrates the definition of each dimension.

Table 7.4: Preliminary design of the flange plate of the fuses

Floor	$M_{Ed,est}$ [kNm]	Lever arm (z) [m]	$N_{f,est}$ [kN]	Flange plate dimensions (t_f*b_f) [mm^2]
1	123	0.567	217	170*8 (S235)
2	60	0.567	106	170*8 (S235)

where:

$M_{ed,est}$ Estimated design moment for the welded beam splices

$N_{f,est}=M_{Ed,est}/z$ Estimated design axial force for the flange plate of the fuse

Table 7.5: Dimensions adopted for the rest of the components

Component	Criteria	Assigned dimension	Material
Gap (g)	Approximately 10% of the beam cross-section height	50 mm	-
Free length (L_0)	Rotation capacity, buckling of the fuse flange plate	200 mm	-
Upper layer rebar (Φ_{up})	Must remain elastic, at least twice the mechanical area of the flange plate (i.e. $2*A_f*f_{sd}/f_{yd}$ where f_{sd}=235 MPa and f_{yd}=500 MPa)	12Φ16 mm	A500
Lower layer rebar (Φ_{low})	Must remain elastic	12Φ12 mm	A500
Web plate of the fuses (h_w*t_w)	Capacity design of the fuse resisting moment	2 plates of 170*8 mm^2	S235
Reinforcing flange plates ($b_{r,f}*t_{r,f}$)	Reinforced cross section must remain elastic	240*10 mm^2	S275
Reinforcing web plates ($h_{r,w}*t_{r,w}$)	Reinforced cross section must remain elastic	2 plates of 200*10 mm^2	S275
Beam	-	IPE450	S275

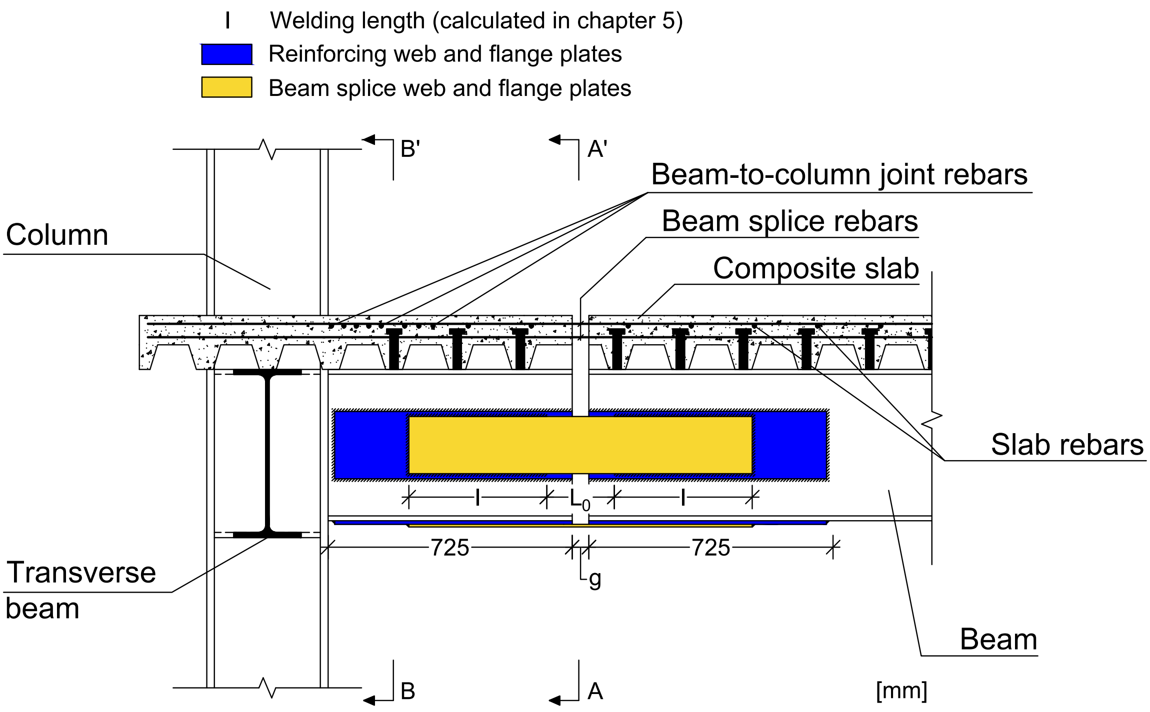

Figure 7.7: Location of the welded FUSEIS beam splice and span of the reinforced zone

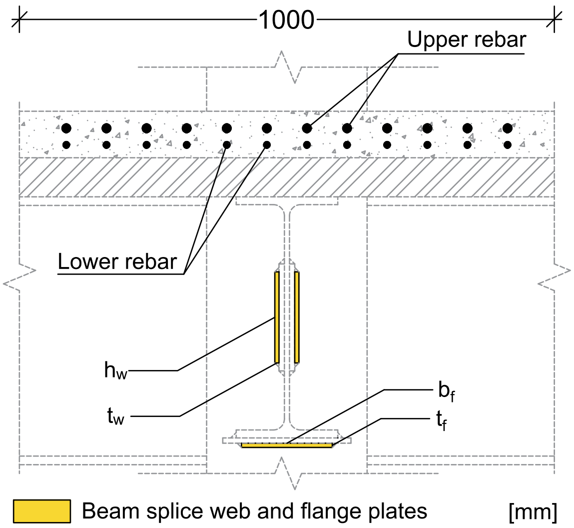

Cross section A-A'

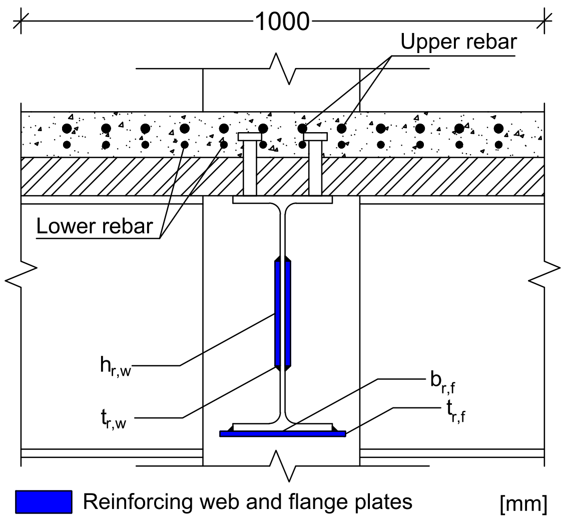

Cross section B-B'

Figure 7.8: Illustration of the dimensions of each component

7.2.2 Simulation

The building is modelled with frame type elements only, using the SAP2000 software [4]. The types of connections assigned for the beam-column joints and the base of the columns were already described in section 6.1.2.1. Diaphragm constraint is applied on each floor. The composite beams are modelled by means of the section designer command offered by SAP2000 [4]. The welded FUSEIS beam splices are simulated by plastic hinges or links with pivot hysteresis. The values for the yielding and ultimate moment and rotation were determined according to [2, 3]. Bracings are assumed to be tension-only. According to [5], braced systems should be modelled with one bracing only and not both diagonals which form the X cross. It should be noted that the equivalent number of bracings at each floor on each side of the structure shown below is equal to one, since one of them were assigned null axial stiffness for both tension and compression situations. These bracings were only applied to consider their mass.

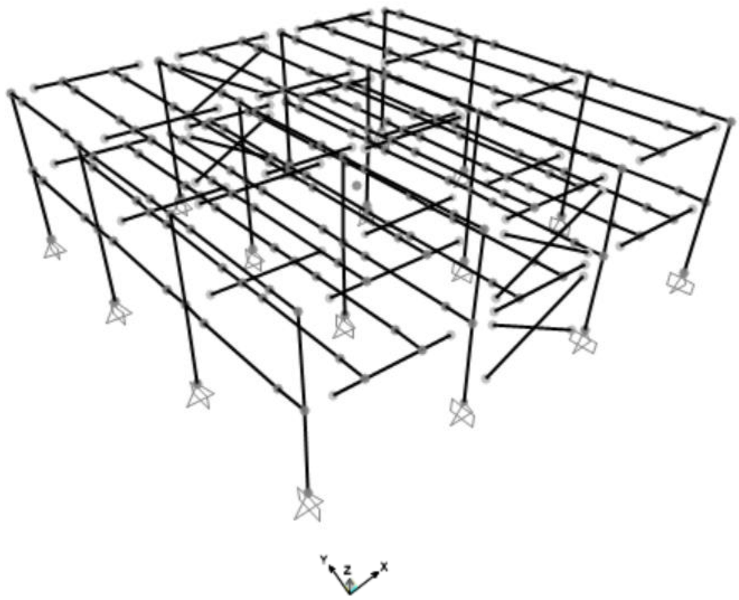

Figure 7.9: FE three-dimensional model

7.2.3 Design for static combinations

Given that the welded FUSEIS beam splices are placed strategically approximately at the null moment sections defined by gravity loads, these are in principle safety checked for static combinations. Nevertheless, this will be shown subsequently for demonstration purposes. Additionally, it is considered herein that the seismic design situation governs the design of the welded FUSEIS beam splices, therefore wind combination is not assessed.

7.2.3.1 *Ultimate limit state results*

The ultimate limit state load combination that governs the gravity members design is calculated according to Eq. (7.2).

$$\sum_{j>1} 1.35 \times G_{k,j} + \sum_{i>1} 1.5 \times Q_{k,i} \qquad \text{Eq. (7.2)}$$

The results from the member verification are presented in Table 7.6.

Table 7.6: Verification of gravity members (in kN and kNm)

<table>
<tr><th>Member</th><th>HEA composite</th><th>IPE composite</th><th>IPE500</th><th>Internal column</th><th>External column</th><th>Welded Beam Splice</th></tr>
<tr><td>Section</td><td>HEA200</td><td>IPE450</td><td>IPE500</td><td>HEM360</td><td>HEB360</td><td>-</td></tr>
<tr><td>Steel grade</td><td>S355</td><td>S275</td><td>S355</td><td>S355</td><td>S355</td><td>S235</td></tr>
<tr><td>M_{rd+}</td><td>382</td><td>918</td><td rowspan="2">779</td><td rowspan="2">-</td><td rowspan="2">-</td><td rowspan="2">163</td></tr>
<tr><td>M_{rd-}</td><td>184</td><td>*</td></tr>
<tr><td>N_{rd}</td><td>-</td><td>-</td><td>-</td><td>-11317</td><td>-6411</td><td>-</td></tr>
<tr><td>N_{ed}</td><td>-</td><td>-</td><td>-</td><td>-1463</td><td>-784</td><td>-</td></tr>
<tr><td>$M_{y,ed+}$</td><td>173</td><td>124</td><td rowspan="2">670</td><td rowspan="2">≈ 0</td><td rowspan="2">≈ 0</td><td rowspan="2">39</td></tr>
<tr><td>$M_{y,ed-}$</td><td>131</td><td>*</td></tr>
<tr><td>$M_{z,ed}$</td><td>-</td><td>-</td><td>-</td><td>≈ 0</td><td>≈ 0</td><td>-</td></tr>
<tr><td>Ratio+</td><td>0.45</td><td>0.14[a]</td><td rowspan="2">0.86</td><td rowspan="2">0.13[b]</td><td rowspan="2">0.12[c]</td><td rowspan="2">0.24[d]</td></tr>
<tr><td>Ratio-</td><td>0.71</td><td>*</td></tr>
</table>

[a, b, c] Section was designed to increase the global stiffness of the structure

[d] In elastic regime

* Negative moments are resisted by the reinforced cross section in IPE composite beams

7.2.3.2 *Serviceability limit state checks*

The serviceability limit state load combination is calculated according to Eq. (7.3).

$$\sum_{j>1} G_{k,j} + \sum_{i>1} \psi_0 \times Q_{k,i} \qquad \text{Eq. (7.3)}$$

The results from the member verification are presented in Table 7.7.

Table 7.7: Verification of member's deflection

Member	Displacement [m]	Deflection	Limit adopted	Ratio
HEA composite	17	1/476	1/250	0.52
IPE450 composite	2	1/4347	1/250	0.06
IPE500	28	1/288	1/250	0.87

7.3 SEISMIC ANALYSIS

7.3.1 Seismic design situation

The building is recognized as regular in plan and in height. Theoretically the center of masses and the center of rigidity coincide. To account for uncertainties in the location of masses and thus the rotational component of the seismic motion, additional accidental mass eccentricity (§4.3.3.3.3 [5]) with a value of 1200 mm (5% of 24000 mm) was introduced in both directions. The mass eccentricity effects were considered by defining two static load cases T_x and T_y, simulating rotation. To account for the torsional effects, the story seismic forces in both main directions were calculated based on the lateral force method (§4.3.3.2 [5]). The final seismic design situation accounting for accidental torsional effects was derived by Eq. (7.4) and Eq. (7.5).

$$E = E_x + 0.3E_y \pm T \qquad \text{Eq. (7.4)}$$

$$E = 0.3E_x + E_y \pm T \qquad \text{Eq. (7.5)}$$

where:

T is considered as $T_x + T_y$;

T_x and T_y are accidental torsional effects of applied story seismic force with eccentricity of 5% in X and Y direction, respectively;

E_x and E_y are the analysis results without accidental torsion by applying RSA in X and Y direction, respectively.

The seismic combination is calculated according to Eq. (7.6).

$$\sum_{j>1} G_{k,j} + \sum_{i>1} \psi_2 \times Q_{k,i} + E \qquad \text{Eq. (7.6)}$$

where:

$G_{k,j}$ are the gravity load effects in seismic design situation;
$Q_{k,i}$ are the movable load effects in seismic design situation;
ψ_2 is given in Table 7.2;
E is the effect of the seismic action including accidental torsional effects.

7.3.2 Response spectrum analysis

Multi-modal RSA was performed. The first, second and third natural modes of vibrations are presented in Figure 7.10 to Figure 7.12, respectively. They correspond to the X and Y translational and the torsional mode. The results from the analysis are summarized in Table 7.8. The table indicates that two more translational modes were needed to activate more than 90% of the total mass.

Table 7.8: Participating mass ratio and periods

Mode no.	Type	Period [s]	Participating mass in direction X	Participating mass in direction Y
1	X	0.561	0.925	0.000
2	Y	0.513	0.000	0.870
3	TORSION	0.369	0.000	0.000
4	X	0.214	0.075	0.000
5	Y	0.157	0.000	0.130
Sum of participating mass			0.999	0.999

According to [5] for a period higher than T_C the spectrum acceleration must be equal or greater than the lower bound. Since the first modes dominate the response, the check may be done with Eq. (7.7):

$$S_d(T) = \frac{V_{tot}}{P_{tot}} \geq \beta \cdot a_g \quad \text{Eq. (7.7)}$$

where $S_d(T)$ is the design spectrum acceleration, V_{tot} is the total base shear from the response spectrum analysis, P_{tot} is the total vertical load corresponding to the seismic design situation, a_g is the soil acceleration multiplied by the coefficient of importance (see Table 7.2) and $\beta = 0.2$ is the lower bound factor for the horizontal design spectrum. The checks presented in Table 7.9 and
Table 7.10 prove that there is no need to increase the base shear.

Table 7.9: Check of the lower bound for the horizontal design spectrum in the X direction

V_{tot} [kN]	P_{tot} [kN]	V_{tot}/P_{tot}	Lower Bound
1196	6007	0.199	0.060

Table 7.10: Check of the lower bound for the horizontal design spectrum in the Y direction

V_{tot} [kN]	P_{tot} [kN]	V_{tot}/P_{tot}	**Lower Bound**
1129	6007	0.188	0.060

Translation in X

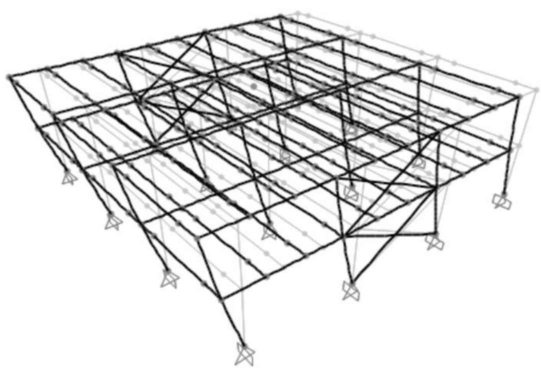

Figure 7.10: First mode of free vibration, $T_1 = 0.561$ s

Translation in Y

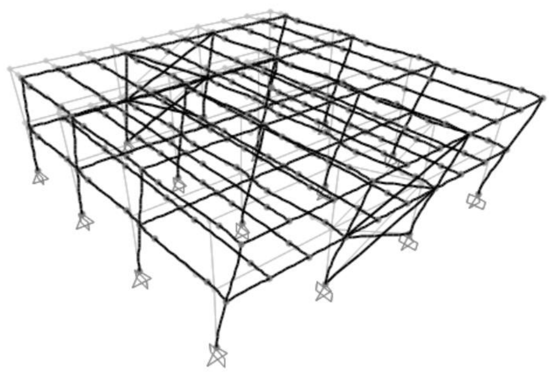

Figure 7.11: Second mode of free vibration, $T_2 = 0.513$ s

Torsional

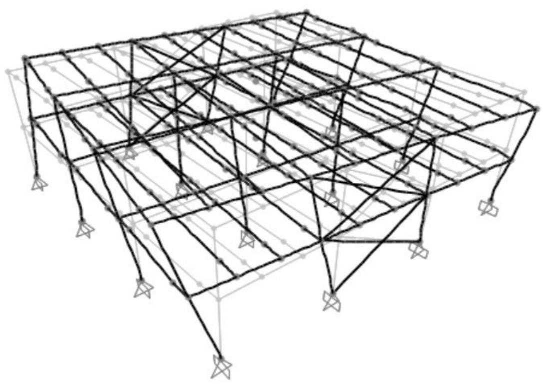

Figure 7.12: Third mode of free vibration, $T_3 = 0.369$ s

7.4 DETAILED DESIGN

7.4.1 Damage limitation – limitation of inter-story drift

Assuming that the building has ductile non-structural elements, the verifications is:

$$d_r \cdot v \leq 0.0075h = 0.0075 \cdot 4 = 0.030\ m \quad \text{Eq. (7.8)}$$

where $v = 0.5$ is the reduction factor according to §4.4.3.2 (1) of [5], h is the story height and d_r is the design inter-story drift. Table 7.11 includes the results from the analysis of each story.

Table 7.11: Inter-story drift verification

Earthquake in the X direction			Earthquake in the Y direction		
Story	1	2	**Story**	1	2
$\boldsymbol{d_{r,max}}$ **[m]**	0.048	0.037	$\boldsymbol{d_{r,max}}$ **[m]**	0.034	0.039
$\boldsymbol{d_{r,max} \cdot v}$ **[m]**	0.024	0.019	$\boldsymbol{d_{r,max} \cdot v}$ **[m]**	0.017	0.020
≤ 0.030?	True	True	**≤ 0.030?**	True	True

where $d_{r,max}$ is the maximum design inter-story drift value within each directional earthquake combination, obtained by the product between the elastic inter-story drift and the behavior factor.

7.4.2 Second order effects

The second order effects are considered by the inter-story drift sensitivity coefficient θ given by Eq. (7.9), where P_{tot} and V_{tot} are the total gravity load at and above the story considered in the seismic design situation and the total seismic story shear at the story under consideration, respectively. Table 7.12 gives the calculated values of θ for directional earthquake combination X and Y, respectively.

$$\theta = \frac{P_{tot} \cdot d_r}{V_{tot} \cdot h} \qquad \text{Eq. (7.9)}$$

Table 7.12: 2nd order effects

Earthquake in the X direction			Earthquake in the Y direction		
Story	1	2	**Story**	1	2
$\boldsymbol{d_{r,x}}$ **[m]**	0.047	0.036	$\boldsymbol{d_{r,x}}$ **[m]**	0.014	0.011
$\boldsymbol{d_{r,y}}$ **[m]**	0.010	0.012	$\boldsymbol{d_{r,y}}$ **[m]**	0.033	0.038
$\boldsymbol{P_{tot}}$ **[kN]**	6007	2634	$\boldsymbol{P_{tot}}$ **[kN]**	6007	2634
h [m]	4.000	4.000	**h [m]**	4.000	4.000
$\boldsymbol{V_x}$ **[kN]**	1197	749	$\boldsymbol{V_x}$ **[kN]**	360	226
$\boldsymbol{V_y}$ **[kN]**	340	220	$\boldsymbol{V_y}$ **[kN]**	1130	713
$\boldsymbol{\Theta_x}$ **[rad]**	0.059 < 0.100	0.031 < 0.100	$\boldsymbol{\Theta_x}$ **[rad]**	0.059 < 0.100	0.031 < 0.100
$\boldsymbol{\Theta_y}$ **[rad]**	0.043 < 0.100	0.034 < 0.100	$\boldsymbol{\Theta_y}$ **[rad]**	0.043 < 0.100	0.035 < 0.100

Since all θ values were below 0.1, second order effects may be disregarded.

7.4.3 Final verification of the welded FUSEIS beam splices

The bending moment, shear and axial resistances of the welded FUSEIS beam splice should fulfill §7.8.3 (2) and (7) of [3]. However, given the reduced design moment of the welded beam splices located on the roof floor as well as to ease the structural detailing, the same cross-section was considered for all the beam splices, resulting in the non-satisfaction of §7.8.3 (7) of [3]. Table 7.13 gives the moment verification of the welded FUSEIS beam splice and the check for the homogeneous dissipative behavior. Table 7.14 demonstrates the shear force verification.

The equations to satisfy §7.8.3 (2) of [3] are:

$$\frac{M_{ed}}{M_{FUSE,pl,rd}} \leq 1.00 \quad \text{Eq. (7.10)}$$

$$\frac{N_{ed}}{N_{FUSE,pl,rd}} \leq 0.15 \quad \text{Eq. (7.11)}$$

$$\frac{V_{ed}}{V_{FUSE,pl,rd}} \leq 0.50 \quad \text{Eq. (7.12)}$$

where:
$V_{Ed} = V_{Ed,G} + V_{Ed,M}$ with $V_{Ed,M}$ being the shear force obtained by capacity design;
M_{Ed} and N_{Ed} are the design moment and axial force;
$M_{FUSE,pl,Rd}$, $N_{FUSE,pl,Rd}$ and $V_{FUSE,pl,Rd}$ are the plastic moment, axial and shear resistance of the fuse, determined based on [2];

Table 7.13: Moment verification of the fuses and check for homogeneous dissipative behavior

Floor	**Fuse type [mm²]**	**M_{Ed} [kNm]**	**M_{Rd}- [kNm]**	**M_{Rd}+ [kNm]**	α^+	α^-	$\Omega = \frac{M_{FUSE,pl,Rd}}{M_{Ed}}$	$\frac{\max \Omega}{\min \Omega} \leq 1.25$
1	170*8	108	163	293	0.32	0.32	1.50	1.78
2	170*8	61	163	293	0.32	0.32	2.68	

where:
$\alpha = M_{FUSE,pl,Rd}/M_{beam,pl,Rd}$ and $\Omega = M_{FUSE,pl,Rd}/M_{Ed}$.

Table 7.14: Shear force verification of the fuses

Floor	**Fuse type [mm²]**	**V_{Ed} [kN]**	**V_{Rd} [kN]**	**Ratio**
1	170*8	112	369	0.30
2	170*8	107	369	0.29

7.4.4 *Final verification of the conventional bracings*

The verification of conventional bracings follows the design rules speculated in section 6.7 of [5]. Table 7.15 gives the normalized slenderness verification. Table 7.16 presents the axial force verification and the check for homogeneous dissipative behavior.

Table 7.15: Normalized slenderness verification

Floor	Bracing type	$L_{cr,y}$ [m]	$L_{cr,z}$ [m]	i_y [m]	i_z [m]	$1.30 < \bar{\lambda}_y < 2.00$	$1.30 < \bar{\lambda}_z < 2.00$
1	2UPN100/60/	4.472	8.944	0.039	0.068	1.50	1.72
2	2UPN80/60/	4.472	8.944	0.031	0.065	1.54	1.47

where:
$L_{cr,y}$ and $L_{cr,z}$ are the buckling length for the moment of inertia of the bracing along y (in-plane) and z direction (out-of-plane), respectively.
i_y and i_z are the radius of gyration for the moment of inertia of the bracing along y (in-plane) and z direction (out-of-plane), respectively;
$\bar{\lambda}_y$ and $\bar{\lambda}_z$ are the normalized slenderness for the moment of inertia of the bracing along y (in-plane) and z direction (out-of-plane), respectively;

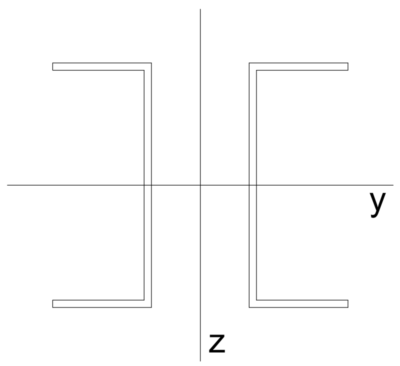

Figure 7.13: Schematic representation of the y and z axis

Table 7.16: Axial force verification of the bracings and check for homogeneous dissipative behavior (tension-only)

Floor	Bracing type	Steel	N_{pl} [kN]	N_{Ed} [kN]	Ratio	$\Omega = \frac{N_{pl}}{N_{Ed}}$	$\frac{\max \Omega}{\min \Omega} \leq 1.25$
1	2UNP100/60/	S355	959	717	0.97	1.34	1.16
2	2UNP80/60/	S235	517	450	0.87	1.15	

7.4.5 Capacity design of non-dissipative elements and members

The capacity design of non-dissipative elements and members (columns and reinforcing zones) should be done according to §7.8.3 (3) and (4) of [3]. The design forces are therefore obtained from Eq. (7.13) to Eq. (7.15).

$$N_{CD,Ed} = N_{Ed,G} + 1.1 \cdot \gamma_{ov} \cdot \Omega \cdot N_{\mathrm{Ed},E} \quad \text{Eq. (7.13)}$$

$$M_{CD,Ed} = M_{Ed,G} + 1.1 \cdot \gamma_{ov} \cdot \Omega \cdot M_{Ed,E} \quad \text{Eq. (7.14)}$$

$$V_{CD,Ed} = V_{Ed,G} + 1.1 \cdot \gamma_{ov} \cdot \Omega \cdot V_{Ed,E} \quad \text{Eq. (7.15)}$$

Table 7.17 present the verification of the reinforcing zone.

Table 7.17: Moment verifications of the reinforcing zone

Section	M_{Ed} [kNm]	M_y [kNm]	Ratio
Reinforcing zone (RZ)	165	822	0.20
Current beam section immediately after the RZ	83	657	0.13

where M_y is the yield moment.

Table 7.18 present the verification of the inner and outer governing columns of the welded FUSEIS beam splice moment resistant frames. Table 7.19 gives the CBF column verification.

Table 7.18: Safety check of conditional inner and outer columns of the MRF-WFBS

Column	Section	M_{Ed} [kNm]	V_{Ed} [kN]	N_{Ed} [kN]	Ratio
Inner	HEM360	674	235	656	0.38
Outer	HEB360	410	158	377	0.43

Table 7.19: Safety check of conditional column of the CBF

Column	Section	N_{Ed} [kN]	N_{pl} [kN]	Ratio
CBF	HEB360	1422	6411	0.22

7.5 STRUCTURAL DETAILING

The internal forces and moments transition from the flange and web fuse plates of the welded FUSEIS beam splice to the adjacent reinforcing zone is achieved by means of welds. These are designed such that the flange and web fuse plates mobilize their maximum resistance. Table 7.20 gives the design of the web plates' welds. Table 7.21 shows the safety check of the flange plate's welds. Lastly, Table 7.22 illustrates the verification of the reinforcing plates' welds, assuming the mobilization of the plates' maximum axial resistance.

Table 7.20: Design of the web fuse plates' weld thickness

l [mm]	V_{Ed} [kN]	M_{Ed} [kNm]	Weld thickness [mm]
410	185	63	5

Table 7.21: Verification of the flange fuse plate's weld thickness

l [mm]	N_{Ed} [kN]	$f_{w,Ed}$ [kN/m]	Weld thickness [mm]	$f_{w,rd}$ [kN/m]	Ratio
410	320	323	5	1039.23	0.31

Table 7.22: Verification of the reinforcing plates' weld thickness

Plate	N_{Ed} [kN]	$f_{w,Ed}$ [kN/m]	Weld thickness [mm]	$f_{w,Rd}$ [kN/m]	Ratio
Flange	660	423	7	1637	0.26
Web	550	353	7	1637	0.22

Shear connectors were designed to mobilize full connection at the positive critical moment section of the composite beams, which resulted in two Φ25 mm connectors ($f_u = 450\,MPa$, $h_{sc} = 120\,mm$) spaced by 187.5 mm along the composite beams. Design of current transverse rebar and concrete compression verifications were subsequently performed. The resulting rebar quantity is equal to Φ12//187.5 mm. The rebar near the beam-column joint were determined according to annex C of [5]. Table 7.23 presents the final dimensions adopted for the beam splices.

Table 7.23: Final beam splice dimensions

Fuse type		170*8
Applied at floor(s)	-	1-2
Fuse web plate S235	mm^2	2 plates of 170*8
Fuse flange plate S235	mm^2	170*8
Reinforcing web plate S275	mm^2	2 plates of 200*10
Reinforcing flange plate S275	mm^2	240*10
Welds: fuse web plate	mm	5
Welds: fuse flange plate	mm	5
Welds: fuse web and flange plate welding length (90)	mm	410
Welds: reinforcing web plate	mm	7
Welds: reinforcing flange plate	mm	7
Gap	mm	50
Free length	mm	200

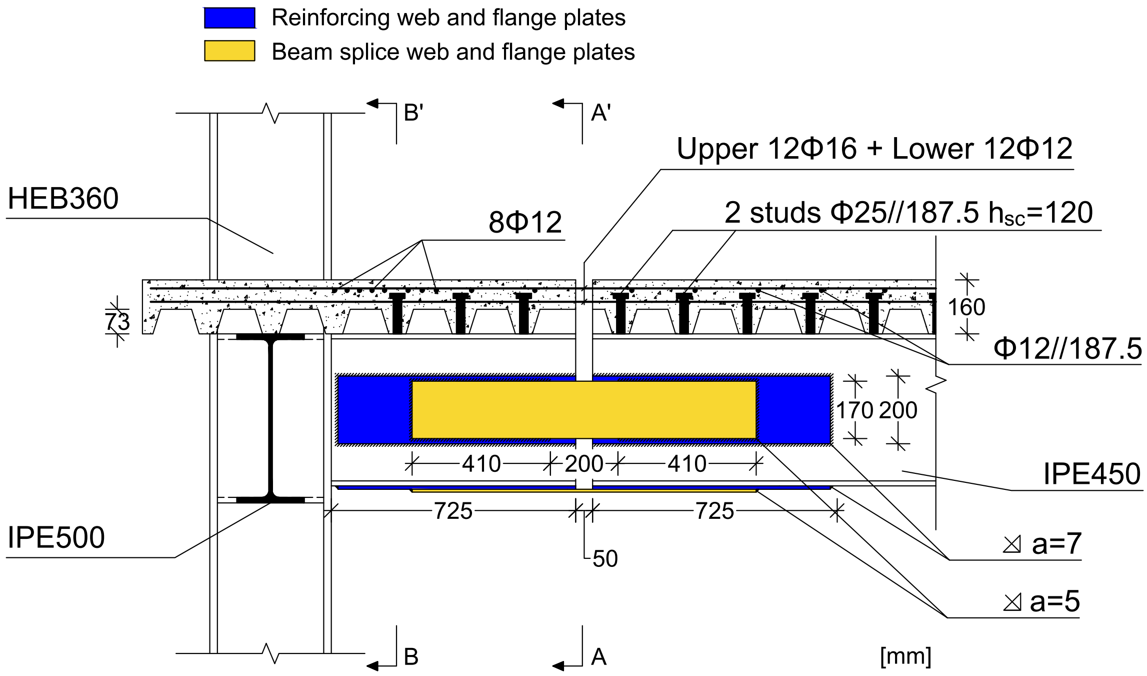

Figure 7.14 to Figure 7.17 presents the structural detailing of the beam splice.

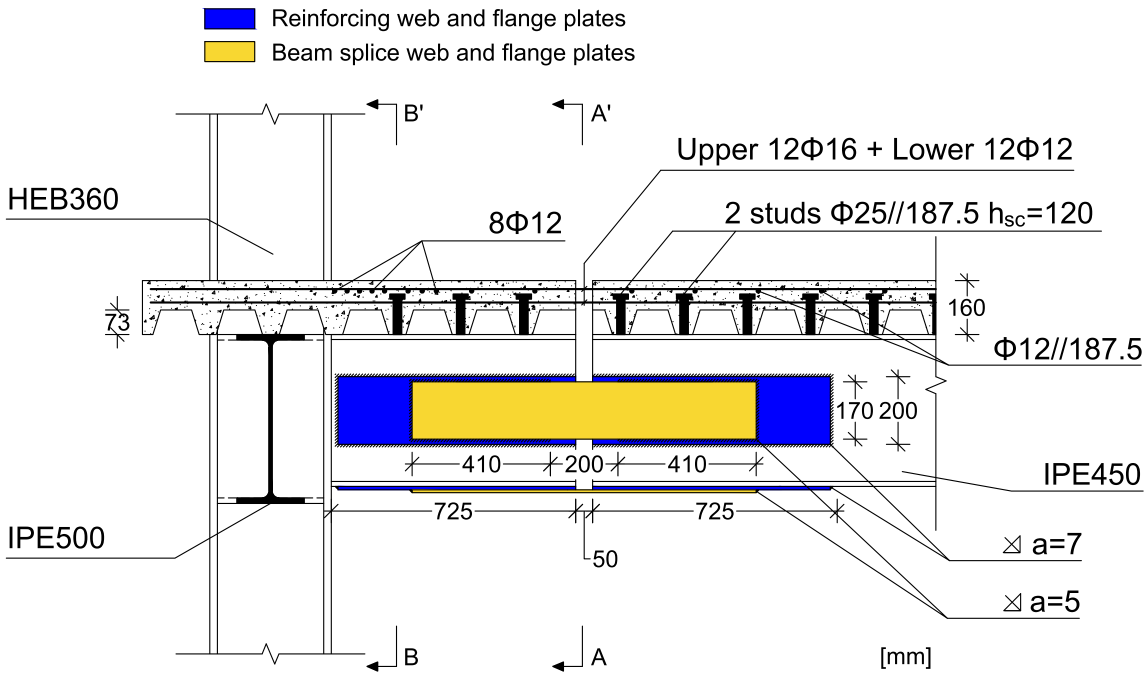

Figure 7.14: Structural detailing of the welded FUSEIS beam splice (side view)

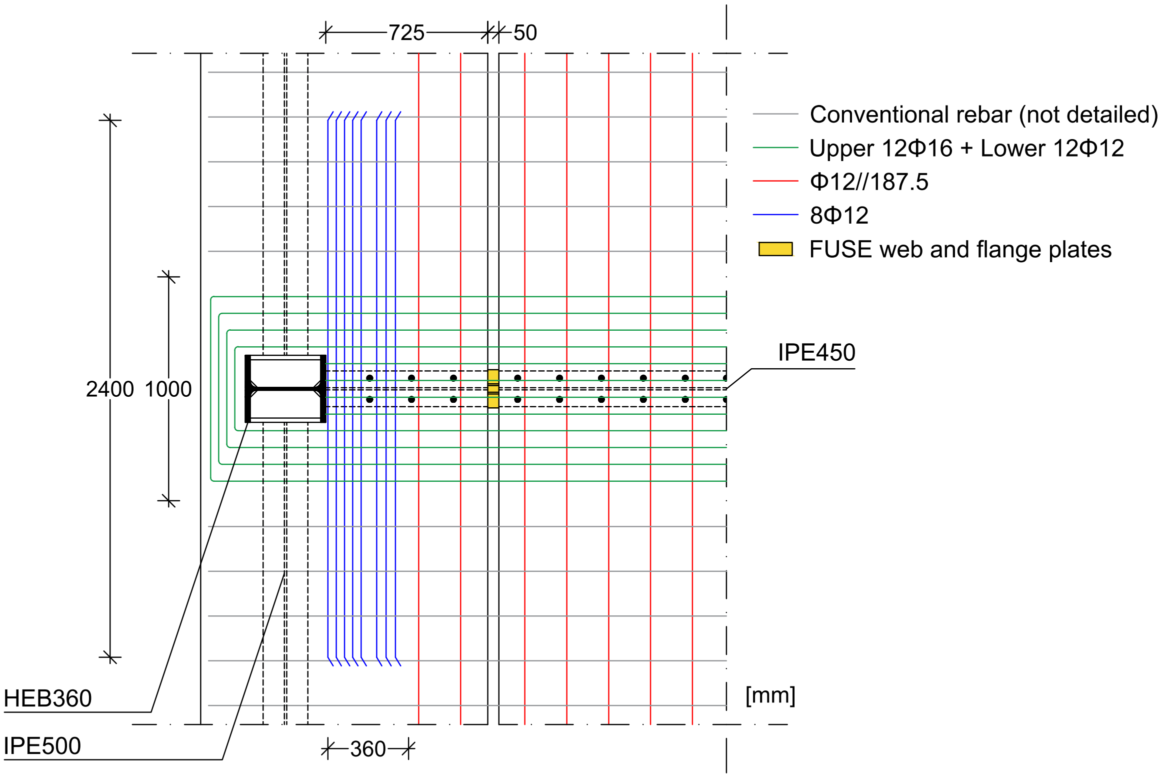

Figure 7.15: Structural detailing of the welded FUSEIS beam splice (top view)

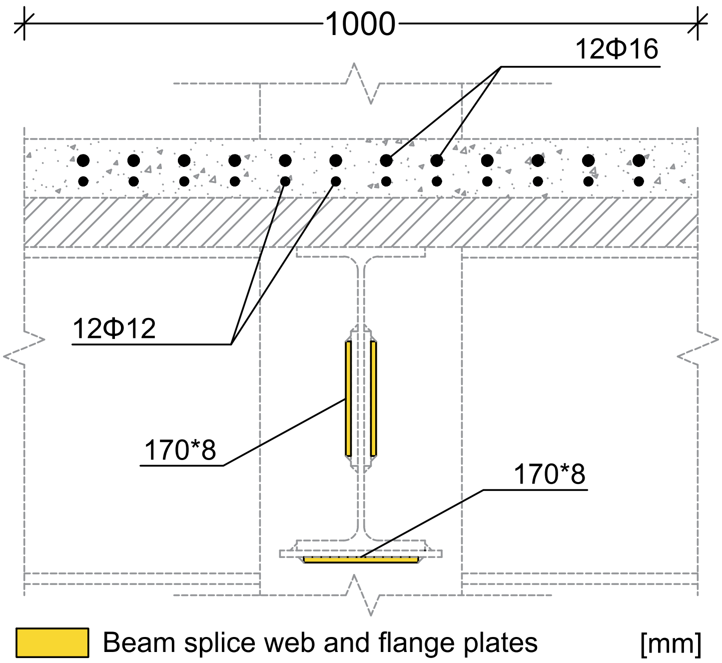

Figure 7.16: Cross section A-A’ from Eq. (7.14)

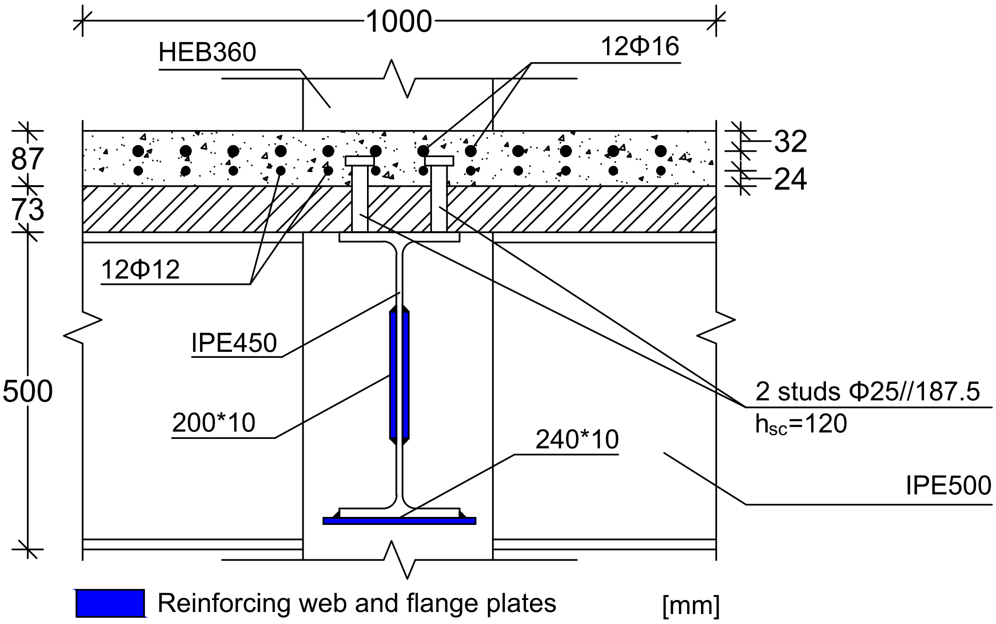

Figure 7.17: Cross section B-B' from Eq. (7.14)

7.6 REFERENCES

[1] EN1991-1-1, Eurocode 1: Actions on structures - Part 1-1: General actions - Densities, self-weight, imposed loads for buildings. Brussels: Comitee Europeen de Normalisation (CEN); 2002.

[2] Calado, L., Proença, J.M., Sio, J., "INNOSEIS – Valorization of innovative anti-seismic devices", WORK PACKAGE 1 – DELIVERABLE 1.1, Volume with information brochures for 12 innovative devices in English, European Commission Research Programme of the Research Fund for Coal and Steel, (Article in Press).

[3] Calado, L., Proença, J.M., Sio, J., "INNOSEIS – Valorization of innovative anti-seismic devices", WORK PACKAGE 3 – DELIVERABLE 3.2, Volume with pre-normative design guidelines for innovative devices, European Commission Research Programme of the Research Fund for Coal and Steel, (Article in Press).

[4] SAP2000, CSI, Computers and Structures Inc., www.csiberkeley.com.

[5] EN1998-1-1, Eurocode 8: Design of structures for earthquake resistance – Part 1-1: General rules, seismic actions and rules for buildings. Brussels: Comitee Europeen de Normalisation (CEN); 2003.

8 REPLACEABLE BOLTED LINKS

8.1 INTRODUCTION

Conventional seismic design philosophy is based on dissipative response, which implicitly accepts damage of the structure under the design earthquake and leads to significant economic losses. Repair of the structure is often impeded by the permanent (residual) drifts of the structure. In order to reduce the repair costs and downtime of a structure hit by an earthquake, and consequently obtain a more rational design approach in the context of sustainability, the concepts of removable dissipative members and re-centring capability of the structure are employed. These concepts are implemented in a dual structure, obtained by combining steel eccentrically braced frames (EBFs) with removable bolted links with moment resisting frames (MRFs). The bolted links are intended to provide the energy dissipation capacity and to be easily replaceable, while the more flexible MRFs would provide the necessary re-centring capability to the structure.

An experimental program was carried out at the European Laboratory for Structural Assessment (ELSA) of the Joint Research Centre (JRC) in Ispra, Italy, to validate the feasibility of the proposed solution through a pseudo-dynamic testing campaign of a full-scale three-story dual EBF structure [1]. This case study presents the conceptual design, modelling and analysis by linear response spectrum analysis methods [2-4] and basic structural detailing of the tested full-scale specimen.

8.2 DESCRIPTION OF BUILDING

8.2.1 Geometry and general assumptions

The prototype structure that was used to validate the proposed solution was a dual EBF structure in which the links from EBFs were conceived as removable (bolted links) dissipative elements because they were intended to provide the energy dissipation capacity and to be easily replaceable, while the more flexible MRFs provided the necessary re-centring capability to the structure. This structure has 3 spans of 6 meters and 5 bays of 6 meters, and 3 storeys of 3.5 meters each. The main lateral load resisting system is composed of eccentrically braced frames. Additionally, there are 4 moment resisting frames on transversal direction and 10 moment resisting frames on longitudinal direction, to assure the restoring forces after an earthquake (Figure 8.1). All interior frames are gravity loads resisting systems with pinned beams. The main features of the structure can be summarised as follows (Figure 8.2): columns realised from high strength steel; braces, beams and removable links realised from mild carbon steel; composite secondary beams; reinforced concrete floor cast in place on corrugated steel sheet.

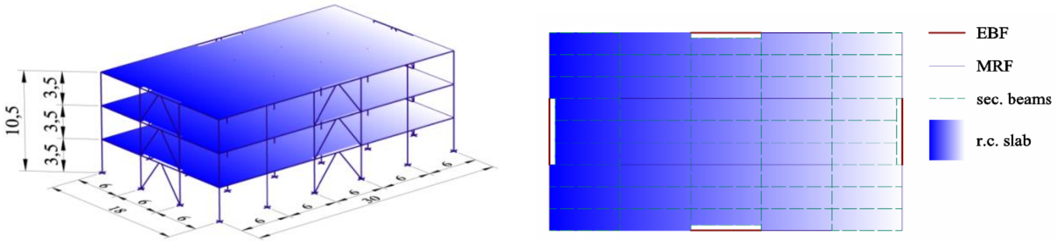

(a) (b)

Figure 8.1: 3D view (a) and plan layout (b) of the prototype structure.

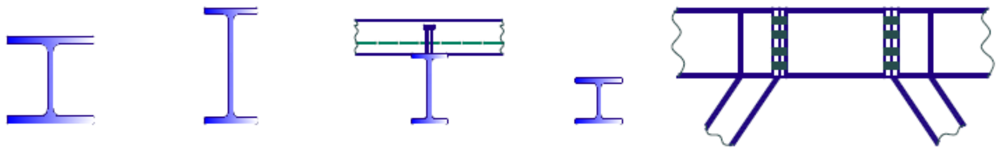

Steel column; high-strength steel	Steel main beams in MRFs; mild carbon steel	Composite steel concrete secondary beams; mild carbon steel	Steel braces; mild carbon steel	Bolted links; mild carbon steel

Figure 8.2: Typical structural members.

Considering that in the transversal direction of the prototype structure the lateral force resisting system is located on the perimeter frames only, and in order to reduce the cost of the experimental mock-up, the latter is composed of the two end frames only (Figure 8.3) with columns fixed at the base. It has 3 spans of 6 meters, 1 bay of 6 meters and 3 stories of 3.5 meters each. The lateral force resisting system is composed of two parallel dual EBFs + MRFs steel frames.

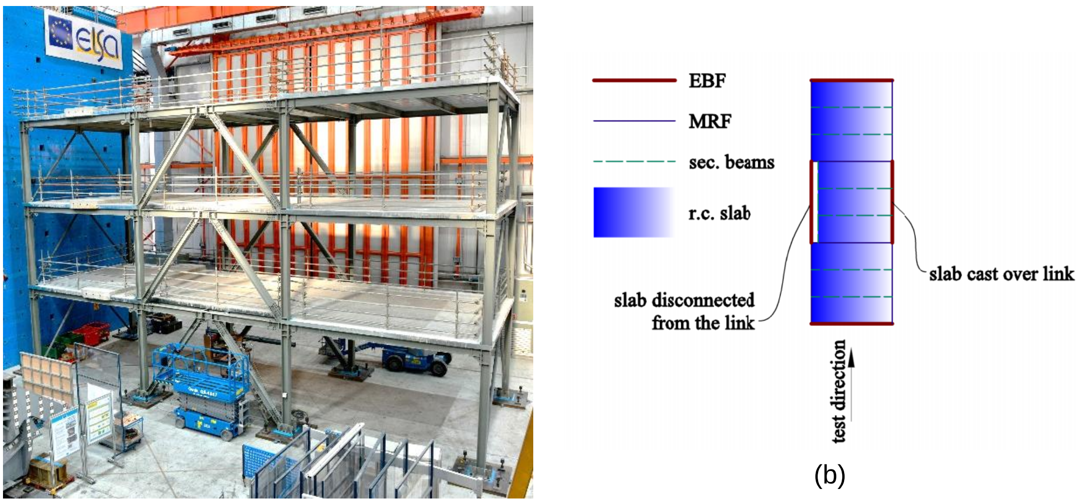

(a) (b)

Figure 8.3: 3D view (a) and plan layout (b) of the experimental mock-up.

8.2.2 Materials

Steel structural components were designed in S355 grade steel, with two exceptions (Figure 8.4). Grade S460 steel was used for columns, in order to obtain a larger capacity without increasing the stiffness. This approach helps promoting the capacity design rules. Links were designed from S235 steel grade (which was replaced during fabrication with equivalent DOMEX 240 YP B) mainly due to coping with available actuator capacities.

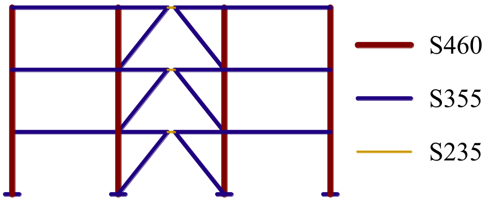

Figure 8.4: Specimen materials.

8.2.3 Loads

The permanent load G_k is composed of the dead weight of the structural elements $G_{k,1}$ and the dead weight of the floors $G_{k,2}$ that are reinforced concrete floors cast in place on corrugated steel sheet. The dead weight of the floors $G_{k,2}$ is computed according to EN1991 [5], tables from Annex A and the results are presented in Table 8.1.

Table 8.1: Dead weight of the floors

No.	Material	Thickness	Specific weight (kN/m^3)	Weight (kN/m^2)
1.	Finishing (tiles)	12 mm	20	0.24
2.	Mortar	9 mm	21	0.19
3.	Lightweight concrete	60 mm	14	0.84
4.	Thermal insulation (extruded polystyrene foam)	50 mm	0.35	0.018
5.	Concrete slab	120.22 mm	25	3.01
6.	Profiled Sheeting	-	-	0.1025
7.	Services and ceiling	-	-	0.50
				4.90

The live load Q_k is computed according to EN 1991 [5], table 6.2., Category B for current floors and Category I for the roof (office areas):

•$Q_{c,k}$ – applied live load for the current floors: 2.2 kN/m^2 (offices) + 0.8 kN/m^2 (partition walls) = 3.0 kN/m^2;

•$Q_{r,k}$ – applied live load for the roof: 3.0 kN/m^2;

Snow load was not considered because the structure was built inside ELSA facility, but if it is assumed that snow load intensity is less than the imposed roof load and the altitude of construction site is below 1000 meters, the snow load can be excluded from the seismic design situation.
The building was designed for stiff soil conditions (EN1998 [6] - Type 1 spectrum for soil type C), characterised by 0.19g peak ground acceleration. A behaviour factor q=4 was adopted for high ductility class (DCH).
To each of the two parallel frames were assigned the masses corresponding to half of the prototype structure, computed according to Eq. (8.1) and presented in Table 8.2.

$$\sum_{j>1} G_{k,j} + \sum_{i>1} \psi_{E,i} . Q_{k,i} \qquad \text{Eq. (8.1)}$$

Table 8.2: Seismic masses

Seismic mass assigned to each floor = 160 t	
Permanent loads	(4.9x18.0x15.0)/9.81 = 135 t
Live loads	0.30x(3.0x18.0x15.0)/9.81 = 25 t
Total seismic mass (without self-weight of structural elements) = 480 t	

8.3 MODELLING FOR LINEAR ELASTIC ANALYSIS

The modelling of the building was performed with the finite element software SeismoStruct [7]. Due to the fact that during testing of the experimental model the pseudo-dynamic procedure was applied on the south frame (with links disconnected from the slab), and the obtained displacements enforced on the north frame (with slab casted over links), a 2D numerical model of the south frame was used (Figure 8.5).

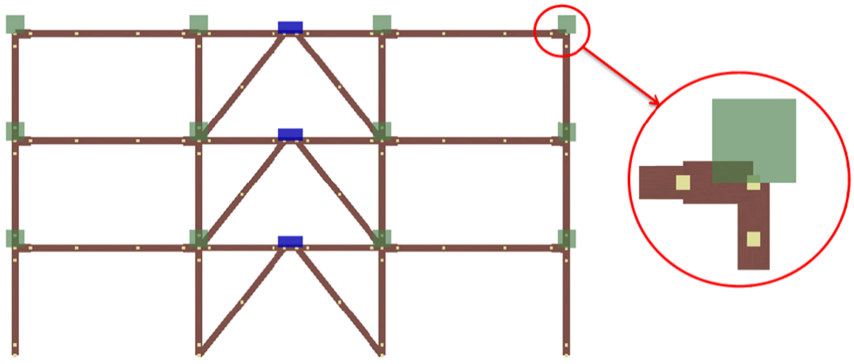

Figure 8.5: 2D numerical model of the specimen.

Force-based plastic hinge elements for beams and columns were used (plastic hinges being at the end of elastic haunches in the MRF beams). For braces, the physical theory model is used (two force based plastic hinge elements per brace; initial out-of-plane member imperfection). Bolted links were modelled using a force-based inelastic beam with two rotational springs at the end. The former was used in order to model the flexural stiffness of the link, while the latter were used in order to account for shear stiffness of the link, as well as rotational deformations and slip in the bolted connection (Figure 8.6). The rotational springs are modelled using multi-linear curve link elements that can simulate the deteriorating behaviour of strength, stiffness, and pinching.

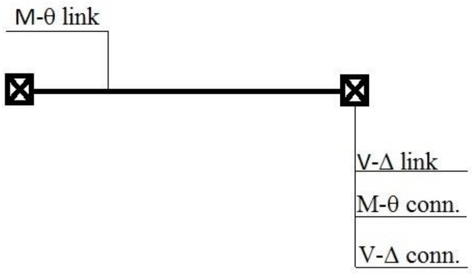

Figure 8.6 : Bolted link model.

The backbone curve used to define the multi-linear rotational springs is defined in Figure 8.7. The initial stiffness accounts for shear of the link (rotational deformations in the bolted connections were neglected due to bolts preloading), the ratio between the ultimate force and the yield force is 1.8 and the ultimate shear deformation γ_u=0.15 rad.

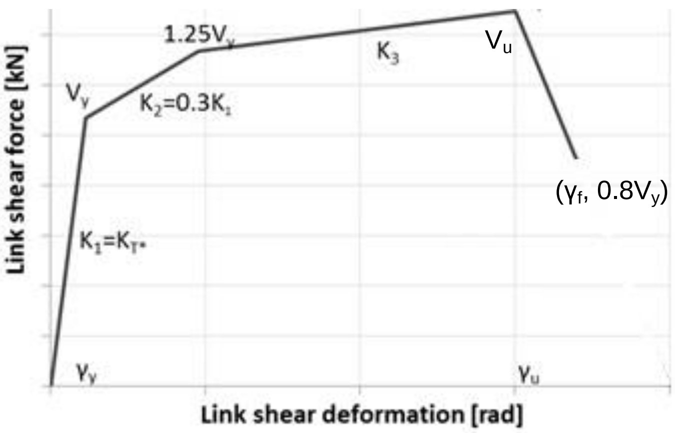

Figure 8.7: Multi-linear link element backbone curve

Rigid diaphragms were assigned at each level to account for the effect of reinforced concrete slabs. The structural masses (in tons) were assigned in the structural nodes.

8.4 PERSISTENT DESIGN SITUATION

8.4.1 Ultimate Limit State

MRFs were designed from fundamental Ultimate Limit State (ULS) load combination $1.35 \cdot G_k + 1.5 \cdot Q_k$. IPE240 sections were obtained for beams, HE240A sections for columns.

8.4.2 Serviceability Limit State

Beams deflections were checked from fundamental load combination $1.0 \cdot G_k + 1.0 \cdot Q_k$. They have deflections less than L/350 (17.14mm).

8.5 RESPONSE SPECTRUM ANALYSIS

Multi-modal response spectrum analysis was performed and the results are summarized in Table 8.3, presenting the modes that activated more than 90% of the mass.

Table 8.3: Participating mass ratio

Mode No	Eigen Period (s)	Participating mass ratio (%)	Total (%)
1	0.512	84.81	97.96
2	0.190	13.15	

8.6 GLOBAL IMPERFECTIONS AND 2ND ORDER EFFECTS

Global imperfections were considered in the structural analysis, according to EN1993-1-1 [8], through equivalent lateral forces, from combination $1.35 \cdot G_k + 1.5 \cdot Q_k$.

These forces were computed based on total gravitational loads and initial global imperfection ϕ, level by level, and because of the small value they were not taken into account further in design.

Second order effects were not accounted for in design because the inter-story drift sensitivity coefficient θ, computed according to EN1998-1-1 [6], found to be smaller than 0.1.

8.7 SEISMIC DESIGN

8.7.1 Ultimate Limit State - Dissipative elements design

Shear links are the dissipative elements of the system. They were designed from welded ($h \times b \times t_f \times t_w$) class 1 I-sections.

The links were designed as removable and replaceable (bolted). This was done by using a flush end-plate link-beam connection that was kept elastic. This means that the connection had a design shear force $V_{j,Ed}$ and bending moment $M_{j,Ed}$ corresponding to a fully yielded and strain hardened link, computed as follows:

$$V_{j,Ed} = \gamma_{sh}\gamma_{ov}V_{p,link} \quad \text{Eq. (8.2)}$$

$$M_{j,Ed} = \frac{V_{j,Ed}e}{2} \quad \text{Eq. (8.3)}$$

where γ_{ov} is 1.25 and γ_{sh} is adopted as 1.8 for DCH.

In order to achieve the connection over-strength, very short dissipative members were adopted (e=0.8$M_{p,link}$/$V_{p,link}$). Therefore, links had lengths of 0.4 m.

Links sections were obtained from the following governing seismic load combination: 1.0·G_k+0.3·Q_k+1.0·A_{Ed} (where A_{Ed} is seismic action) and are presented in the following tables:

Table 8.4: Links sections

Story	Link section	Ω_i	Min Ω_i	Ω
1	230x170x12x8	1.80	1.70	2.33
2	230x170x12x8	2.07		
3	230x120x12x4	1.70		

A homogeneous dissipative behavior was ensured between links (25%). The structural over-strength was computed as [6]:

$$\Omega = \gamma_{ov}\,\Omega_i \quad \text{Eq. (8.4)}$$

$$\Omega_i = \gamma_{sh}\frac{V_{p,link\,i}}{V_{Ed,i}} \quad \text{Eq. (8.5)}$$

8.7.2 Ultimate Limit State – Non - dissipative elements design

EBFs columns, braces and beams are the non-dissipative elements of the system and were designed from the seismic load combination that provides over-strength (Ω) to these elements with respect to dissipative ones: 1.0·G_k+0.3·Q_k+Ω·A_{Ed}. The sections are presented below:

Table 8.5: Elements sections

Element	Section	Height	Flange width	Flange thickness	Web thickness
Column	welded	230	240	12	8
EBF Beam	HE 240 A	230	240	12	8
Brace	HE 200 B	200	200	15	9

8.7.3 Limitation of inter-story drift

Considering that the building has ductile non-structural elements the following eq. is checked:

$$d_r \cdot v \leq 0.0075 \cdot h = 0.0075 \cdot 4000 = 30mm \qquad \text{Eq. (8.6)}$$

Where d_r is the design inter-storey drift, v=0.5 is a reduction factor on the design displacements due to the importance class of the building (ordinary buildings) and h is the story height. Table 8.6 includes the results of the analysis; the check is verified for all stories with values lower than the limit value 26.25mm.

Table 8.6: Limitation of inter-story drift

Story	Drift [mm]
1	18.00
2	19.37
3	14.64

8.7.4 Dual configurations

The duality of the structure was checked by verifying that the MRFs were able to resist at least 25% of the total seismic force [9-11]:

$$F_y^{MRF} \geq 0.25 \cdot (F_y^{MRF} + F_y^{EBF}) \qquad \text{Eq. (8.7)}$$

$$F_y^{EBF} = \frac{L}{H} V_{p,link} \qquad \text{Eq. (8.8)}$$

$$F_y^{MRF} = \frac{4M_{pl,b}}{H} \qquad \text{Eq. (8.9)}$$

where: F_y^{MRF} is the yield strength of MRF, F_y^{EBF} is the yield strength of EBF, L is the frame span, H is the frame story height, $V_{p,link}$ is the shear strength of the link and $M_{pl,b}$ is the beam plastic moment.

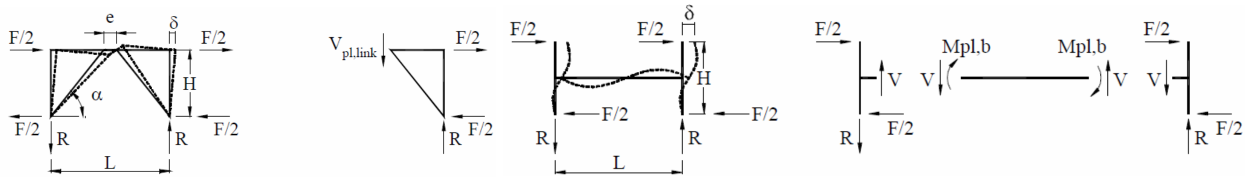

a) b)

Figure 8.8: Basic one-story a) EBF and b) MRF components [11].

The yield strength of the MRFs represents 27% for the first 2 levels and 42% for the 3rd one from the total yield strength of the system, the specimen being considered a dual structure.

8.7.5 Weak beam-strong column

The “weak beam-strong column” condition was checked and found to comply with recommendation given in EN 1998-1 [6]:

$$\sum M_{Rc} \geq 1.3 \sum M_{Rb} \qquad \text{Eq. (8.10)}$$

where: $\sum M_{Rc}$ is the sum of upper and lower columns moment resistance and $\sum M_{Rb}$ is the moment resistance of the MRF beam.

8.7.6 Re-centring verification

In order to verify the re-centering capability of eccentrically braced frames with removable links structures, it was checked that the ultimate displacement of the EBFs (δ_u^{EBF}) at ultimate limit state (ULS) (where the plastic deformation capacity of the link $\gamma_{\mathrm{pl,u}}$ is considered to be 0.11 rad) is smaller than the yield displacement of the MRFs (δ_y^{MRF}), meaning the yielding in MRFs is prevented up to the attainment of ultimate deformation capacity in the EBFs with removable links. This was done analytically, using formulas below [11]:

$$\delta_u^{EBF} = \delta_y^{EBF} + \delta_{pl}^{EBF} = \frac{F_y^{EBF}}{K^{EBF}} + \frac{e}{L \quad e} \quad H \quad \gamma_{pl,u} < \delta_y^{MRF} = \frac{F_y^{MRF}}{K^{MRF}} \qquad \text{Eq. (8.11)}$$

$$K^{EBF} = \frac{K_{link}^{EBF} \quad K_{br}^{EBF}}{K_{link}^{EBF} + K_{br}^{EBF}} \qquad \text{Eq. (8.12)}$$

$$K_{link}^{EBF} = \frac{L}{H^2} \quad (L \quad e) \quad \frac{G \quad A_s}{e} \qquad \text{Eq. (8.13)}$$

$$K_{br}^{EBF} = 2 \quad \frac{E \quad A}{l_{br}} \quad cos^2\alpha \qquad \text{Eq. (8.14)}$$

$$K^{MRF} = \frac{4}{H^2 \quad \dfrac{L}{6 \quad E \quad I_b} + \dfrac{H}{12 \quad E \quad I_c}} \qquad \text{Eq. (8.15)}$$

where δ_y^{EBF} is the yield displacement of the EBF, δ_{pl}^{EBF} is the plastic displacement of the EBF, K^{EBF} is the EBF stiffness, *e, L* and *H* are illustrated in Figure 8.8, $\gamma_{pl,u}$ is the plastic deformation capacity of the link, K^{MRF} is the MRFs stiffness, K_{link}^{EBF} is the link’s stiffness, K_{br}^{EBF} is the braces stiffness, *G* is the shear modulus, A_s is the link shear area, *E* is the Young's modulus, *A* is brace cross-section area, l_{br} is the brace length and α is the brace angle.

The analytical procedure was used as a pre-design of re-centering capability, being recommended for low-rise structures, where lateral deformation of the structure is dominated by a shear-type response.

Because using formulas is an approximate and simplified approach, nonlinear static and/or dynamic analyses are recommended for all structures in order to check the re-centering capability.

Table 8.7: Comparison of analytical and numerical predictions of storey displacements

	δ_u^{EBF}, mm	δ_y^{MRF}, mm	$\delta_y^{MRF}/\delta_u^{EBF}$
Analytical	29.4	54.6	1.86
Numerical	28,9	49.6	1.72

Table 8.7 presents a comparison of yield displacements in the MRFs and ultimate displacements in the EBF for the first storey, where largest demands are present. Acceptable agreement can be observed between analytical (formulas) and numerical (pushover analysis) results, observing a difference of only 8%.

8.7.7 Links removal

In what concerns the link removal and re-centering of frames, static nonlinear staged construction analysis from SAP2000 [12] was used. The steps of the analysis are the following: firstly the frame is loaded with gravitational forces and afterwards with lateral forces (until reaching ultimate deformation in links), then it is unloaded, secondly the links are removed story by story, starting from the first level to the top [13]. After the elimination of the last link, the structure comes back to its initial position (Figure 8.9) and new links may be introduced.

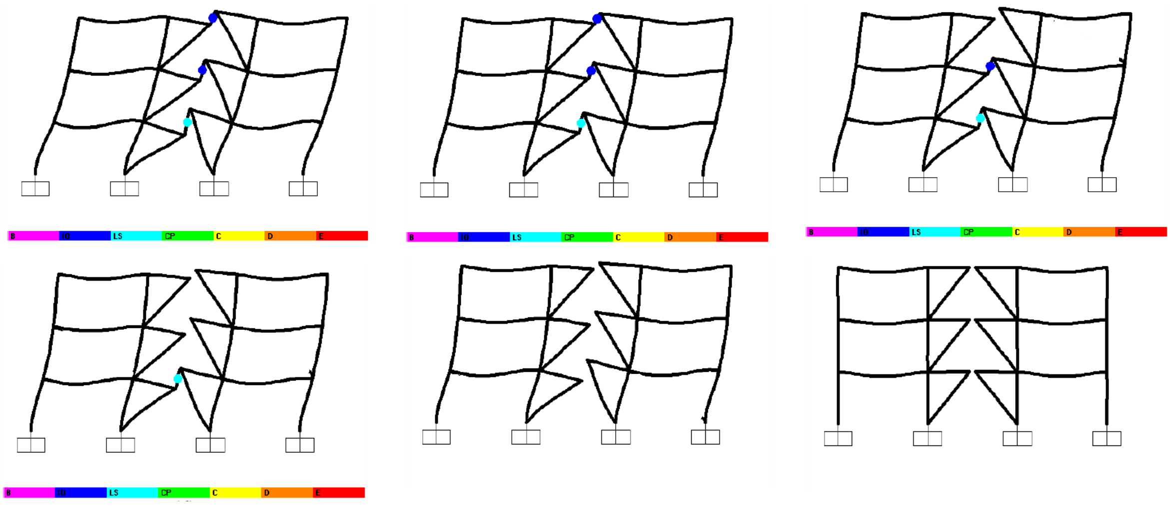

Figure 8.9: Links removal.

The technically easiest way to release the forces in links is by flame cutting the web and flanges of the link [14] if large permanent drifts occur or by unbolting otherwise, on a story by story basis [15].

8.8 STRUCTURAL DETAILING

This type of dual EBF frames can be conceived adopting different solutions of interaction between the removable link and the reinforced concrete slab. The floor layout of the presented structure was conceived in a manner that illustrates two different solutions (Figure 8.10). One of the two eccentrically braced frames was realised so that the beam containing the removable link is totally disconnected from the reinforced concrete slab (the south frame). This solution prevents any damage to the reinforced concrete slab. In the other EBF (the north frame) the beam containing removable links is connected to the slab in a conventional way. Some damage occurs in the reinforced concrete slab at the interface with the removable link, needing local repair after a strong earthquake.

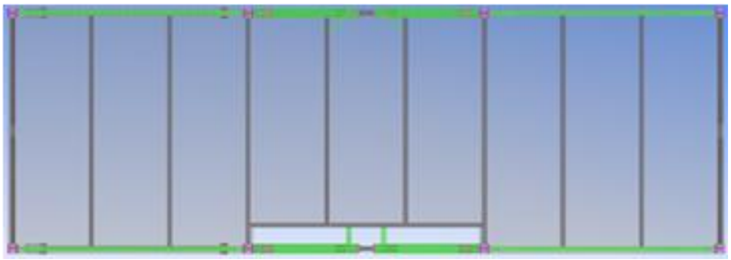

Figure 8.10: Floor layout

The reinforced concrete slab was designed as a one way slab, on the longitudinal direction. The 90 mm thickness slab is made from C25/30 concrete, reinforced with ϕ8/130 mm 610HD independent bars, cast over 0.8 mm thickness, 55 mm high, A55-P600 G5 corrugated steel sheeting used as formwork.
The ends of the links are fixed at the upper side by the slab, in the north frame, and at the lower side by L fly-braces and at both sides by L braces in the south frame (Figure 8.11).

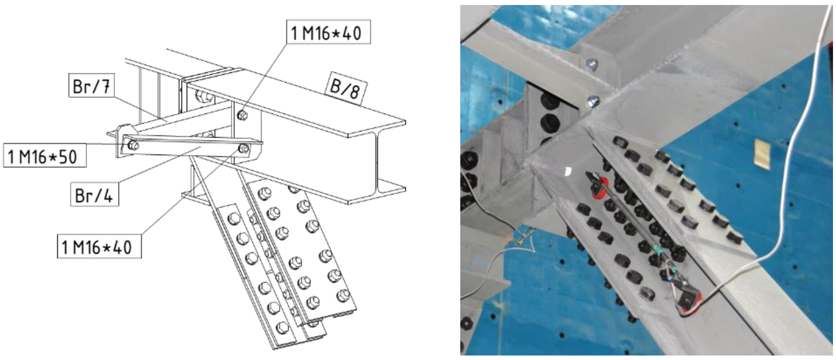

Figure 8.11: Link end braces

The secondary beams are pinned composite beams. Shear studs are present on the main beams, except the zones near the joints and over the links (Figure 8.12) and there is a 50 mm gap between the reinforced concrete slab and the steel columns, ensured by strips of polystyrene board in order to prevent transferring of forces between slab and columns (Figure 8.13).

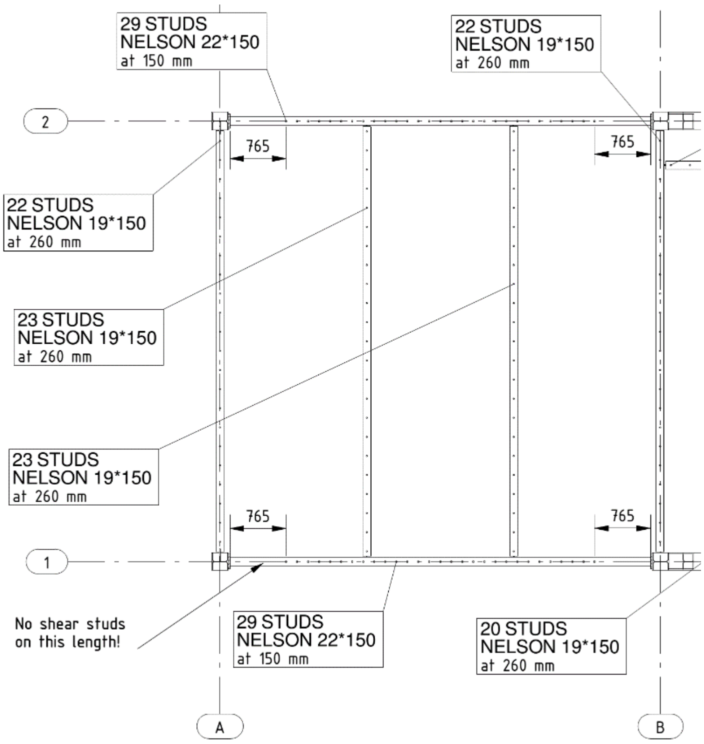

Figure 8.12: Shear studs arrangement

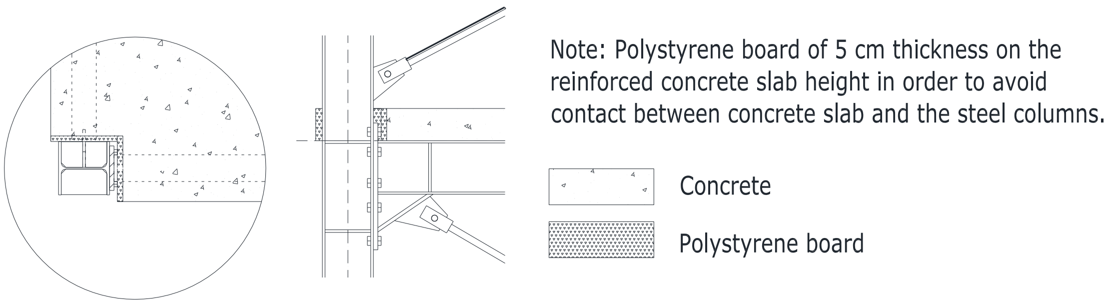

Figure 8.13: Details of gap between r.c. slab and steel columns

The extended full-strength end plate MRF beam to column connection (Figure 8.14), with haunch and M24 10.9 class bolts, was designed to resist efforts larger than the ones corresponding to the formation of plastic hinges at the ends of the beam.

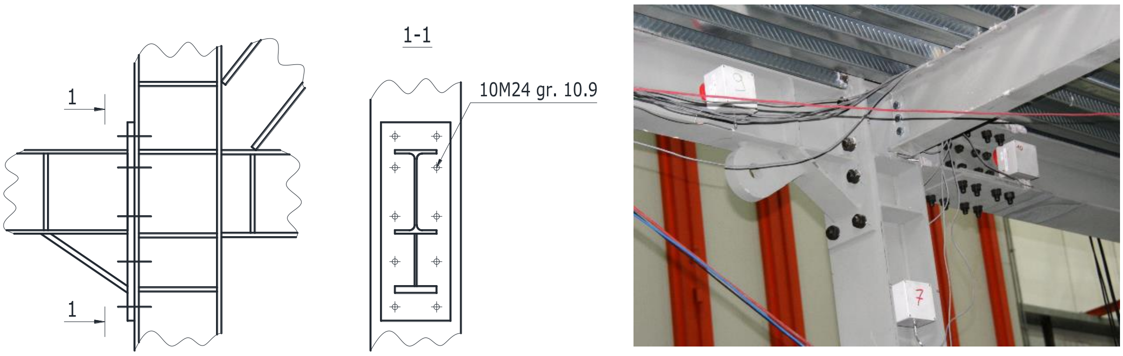

Figure 8.14: Beam to column connection

For the bolted links to be replaceable, the flush end plate connection (Figure 8.15) was designed to remain in the elastic range (considering an elastic distribution of the internal bolt rows forces). Contact surfaces were class B (blasted with shot or grit with zinc paint), providing a coefficient of friction of at least 0.4 and bolts should be preloaded.

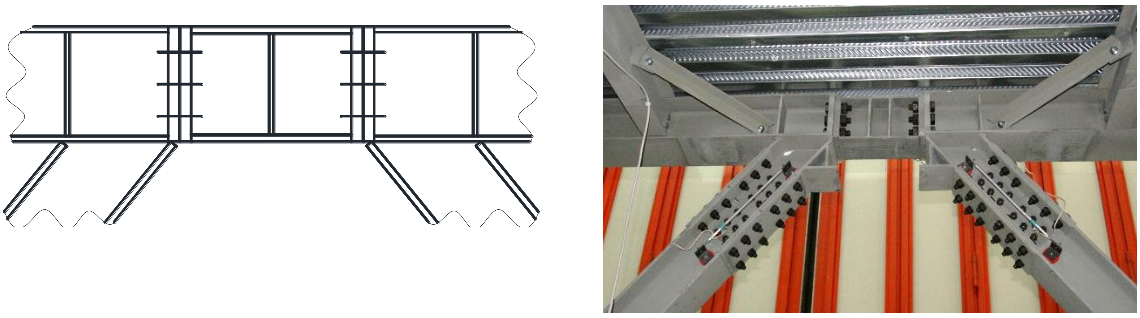

Figure 8.15: Link flush end plate connection

Table 8.8 summarizes the results from verification checks.

Table 8.8: Link flush end-plate connection

Story	End-plate	Bolts	Design efforts		Resistance	
			Shear force	Bending moment	Shear force	Bending moment
1	250x200x25	6 M27 10.9	688.62	137.72	931.73	166.35
2	250x200x25	6 M27 10.9	688.62	137.72	931.73	166.35
3	250x200x25	6 M27 10.9	344.30	68.86	931.73	166.35

8.9 REFERENCES

1. Ioan A., Stratan A., Dubina D., Poljansek M., Molina F. J., Taucer F., Pegon P., Sabau G., Experimental validation of re-centring eccentrically braced frames with removable links, Engineering Structures 113 (2016) 335–346;
2. Dubina D., Stratan A., Chesoan (Ioan) A., “Design Recommendations for Dual Moment - Eccentric Braced Frames with Replaceable Links”, EUROSTEEL 2017, September 13–15, 2017, Copenhagen, Denmark (in print);

3. Dubina D., Stratan A., Chesoan (Ioan) A., Design of steel dual frames with replaceable bolted links eccentric bracing systems, 1st EU-Sino Workshop on Earthquake-resistance of Steel Structures, Shanghai, China, October 27, 2016;
4. Stratan A., Chesoan (Ioan) A., Dubina D., Design criteria and modelling of re-centring dual eccentrically braced frames, COMPDYN 2017, 6th ECCOMAS Thematic Conference on Computational Methods in Structural Dynamics and Earthquake Engineering, M. Papadrakakis, M. Fragiadakis (eds.), Rhodes Island, Greece, 15–17 June 2017;
5. EN1991-1-1, Eurocode 1, Actions on structures - Part 1-1: General actions Densities, self-weight, imposed loads for buildings, CEN, European Committee for Standardization, 2002;
6. EN1998-1-1, Eurocode 8: Design of structures for earthquake resistance – Part 1-1: General rules, seismic actions and rules for buildings. Brussels: Comitee Europeen de Normalisation (CEN); 2003.
7. SeismoSoft, SeismoStruct v6.5 - A computer program for static and dynamic nonlinear analysis of framed structures, www.seismosoft.com;
8. EN1993-1-1. Eurocode 3: Design of steel structures - Part 1-1: General rules and rules for buildings. Brussels: Comitee Europeen de Normalisation (CEN); 2003.
9. NEHRP (2003). NEHRP Recommended provisions for new buildings and other struc-tures (FEMA 450). Part 1: Provisions and Part 2: Commentary. Building Seismic Safety Council, National Institute of Building Sciences, Washington, D.C.;
10. P100-1/2013 (2013). Seismic design code – Part 1: Rules for buildings;
11. Stratan A., Dinu F., Dubina D., "Replacement of bolted links in dual eccentrically braced frames", 14th European Conference on Earthquake Engineering, August 30 – September 3, 2010, Ohrid, Republic of Macedonia;
12. SAP2000, CSI, Computers and Structures Inc., www.csiberkeley.com
13. A. Ioan, A. Stratan, D. Dubina, M. D'Aniello and R. Landolfo, "Seismic performance and re-centring capability of dual eccentrically braced frames with replaceable links", 8th International Conference on Behavior of Steel Structures in Seismic Areas Shanghai, China, July 1-3, 2015;
14. Stratan, A., Ioan, A., Dubina, D. 2012. Re-centring capability of dual eccentrically braced frames with removable bolted links. STESSA 2012 (Behaviour of Steel Structures in Seismic Areas) Conference, 9-11 January 2012, Santiago, Chile, pp. 723-728;
15. Ioan, A., Stratan, A., Dubina, D. 2012. Evaluation of restoring capacity of dual steel EBFs with removable links. The 8th International PhD & DLA Symposium, 29-30 October, 2012, Pecs, Hungary.

9 REPLACEABLE SHEAR PANELS

9.1 GENERAL

9.1.1 Introduction

This case study refers to the seismic design of new low-rise steel office buildings. It aims at demonstration of implementation of the frames with replaceable shear panels. The case study elaborated refers to conceptual design, modelling and analysis by linear response spectrum analysis methods (RSA), detailed design of main dissipative and non-dissipative members and basic structural detailing of replaceable shear panels.

9.1.2 Description of building

9.1.2.1 Geometry and general assumptions

The case study deals with a four-storey frame building with three 8m bays in both directions. The gravity frames are composed of beams and columns, located at each structural axis. The shear panels are the main horizontal load resisting systems, located in the middle of each facade as shown in Figure 9.1. Additional vertical elements (stanchions) are needed in order to border the shear panel. The height of the story is considered 4 m.

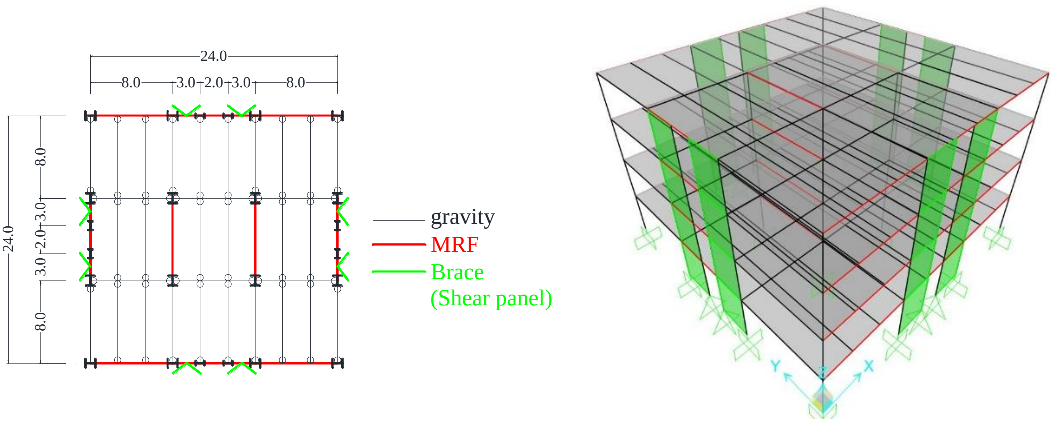

Figure 9.1: Floor plan and elevation

Hot rolled HEB profiles for columns and IPE profiles for beams are used for all gravity frames. Composite action with the concrete slab is not considered. The shear panels are loaded primarily with shear forces resulting from the seismic action (or wind load) and the rest of the frame columns carry the gravity loads.
The shear panels had lower steel grade (S235) than the rest of the structural members (S355). The beams production was not considered to be fully controlled,

so that the properties of the beam material had to comply with EN1993-1-1 [1] recommendations with γ_{ov} =1.25.

Table 9.1 includes the gravity and seismic loads taken into account. The gravity loads were applied as uniform distributed loads on the secondary beams. The dead load takes into account the composite slab and steel sheeting, resulting a value of 2.75 kN/m^2. There were considered some superimposed loads from services, ceilings and raised floors of 0.7 for intermediate floors and 1 for last floor, respectively. A 4.0 kN/m was taken into account for perimeter walls. The live load takes into account de destination of the buildings (offices - class B) and movable partition walls, resulting a value of 3.8 kN/m2.

Type 1-C spectrum [2] (Figure 9.2a) was selected for design considering a high seismicity case, having a peak ground accelerations of 0.3 and a high ductility class structure (Figure 9.2b). Because no recommendation for reduction factor, q, is given in EN1998 [2], and based on previews research [3], [4] a value of 5 was taken into consideration.

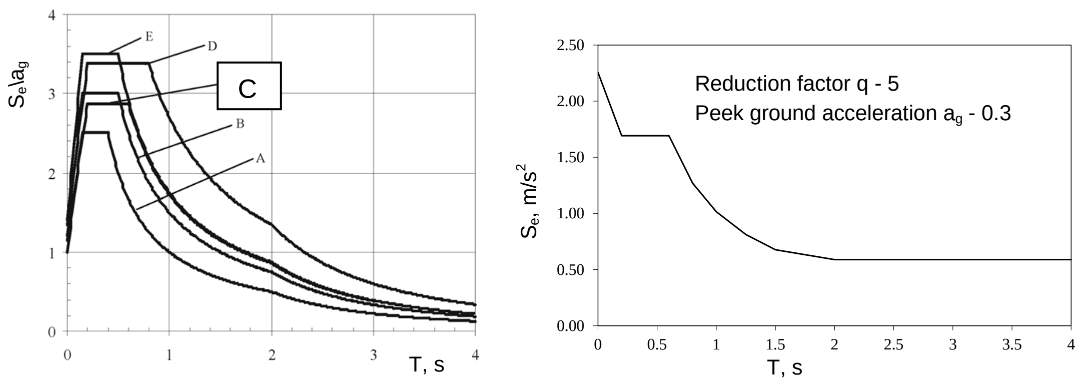

a) Type 1 elastic response spectra b) Design spectrum

Figure 9.2: Response spectrum [2]

Table 9.1: Loads and actions

Vertical loads	
Dead loads (composite slab + steel sheeting)	2.75 kN/m^2
Superimposed loads (Services, ceiling, raised floor)	0.7 kN/m^2 - intermediate floors 1.0 kN/m^2 – last floor
Perimeter walls	4.0 kN/m
Live loads – (office cl. B +movable partition)	3.00+0.800=3.8 kN/m^2
Seismic load	
Elastic response spectra	Type 1
Peak ground acceleration	a_g=0.3g
Importance class II	γ_I = 1.0 (Ordinary buildings)
Ground type	C (T_B = 0.2 s, T_C = 0.60 s)
Proposed behaviour factor q (DCH)	5
Damping ratio	5%
Seismic combination coefficient for the quasi-permanent value of variable actions	ψ_2=0.30

For preliminary design, in order to determine the size of the panels, horizontal and vertical boundary elements (HBE and VBE), the shear panels are replaced with tension only diagonals (further denoted as equivalent braces) (Figure 9.3). The structure is then designed according to [1], [2], [5] and [6].

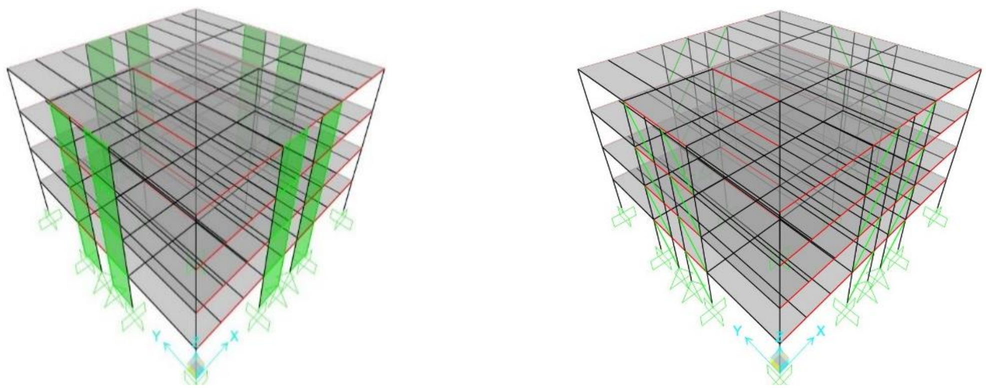

a) Frame with shear panels b) Equivalent frame

Figure 9.3: Preliminary design

9.1.2.2 Modelling for linear elastic analyses

The modelling of the building was performed with the finite element software SAP2000 [7]. The structural model is a linear-elastic 3D model with beam elements (Figure 9.4). Rigid diaphragms were assigned at each level to account for the effect of reinforced concrete slabs. The structural masses were taken into account from loads.

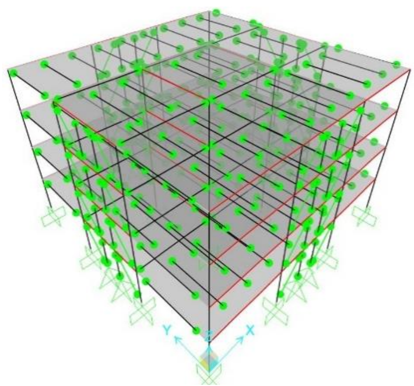

Figure 9.4: Modelling of 4 story structure for liner analysis.

On transversal direction (X), the lateral load resisting system is located in the exterior frames. In this frames, all joints between gravity floor beams and columns are considered rigid with exception of the stanchions which are double pinned. For interior frames, all joints between gravity floor beams and columns are considered pinned.

On Y direction the lateral load resisting system is, also, located in the exterior frames, but in this case just the beam-to-column joints in the braced span are rigid, while the MRF joints are pinned. For the interior frames, only the interior spans have rigid beam-to-column joints, while the rest are pinned.
The elements simulating the equivalent braces are defined through constant RHS-shape section and joined to the frame by simple pin connections. Diaphragm action of floor and roof concrete decks is simulated by diaphragm constraint.
The current case study was developed by centreline-to-centreline (CL-to-CL) model. It is quick and easy to be defined, since the axis geometry of the frame is known at the beginning of the design process.

9.1.3 Persistent design situation

As the shear panels are not designed to account for gravitational loads, the moment resisting frames were designed at ultimate and serviceability limit state under persistent design situation.

9.1.3.1 Ultimate Limit State

MRFs were designed from fundamental design load combination without taking into account the shear panels, see Eq. (9.1). Figure 9.5 presents the resulted structural elements.

$$\sum_{j>1} 1.35.G_{k,j} + \sum_{i>1} 1.5.Q_{k,i} \qquad \text{Eq. (9.1)}$$

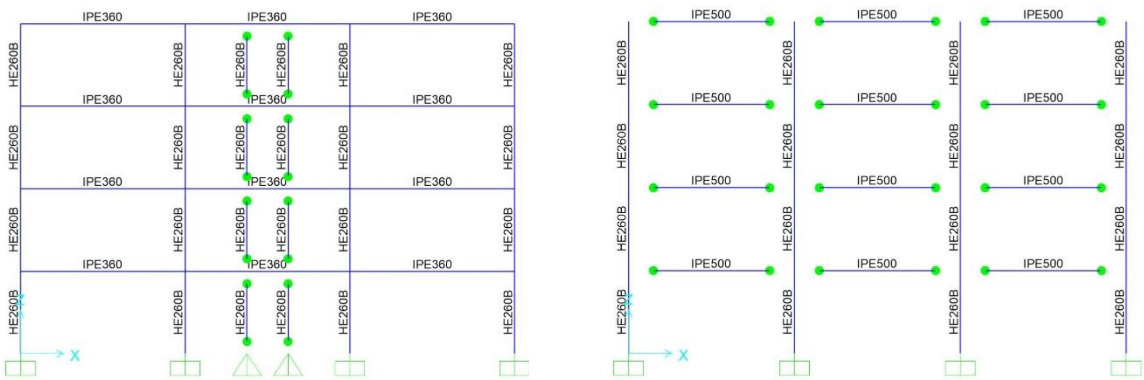

a) Transversal exterior frames (x axis) b) Transversal interior frames (x axis)

Figure 9.5: 4 story gravity frames (continues)

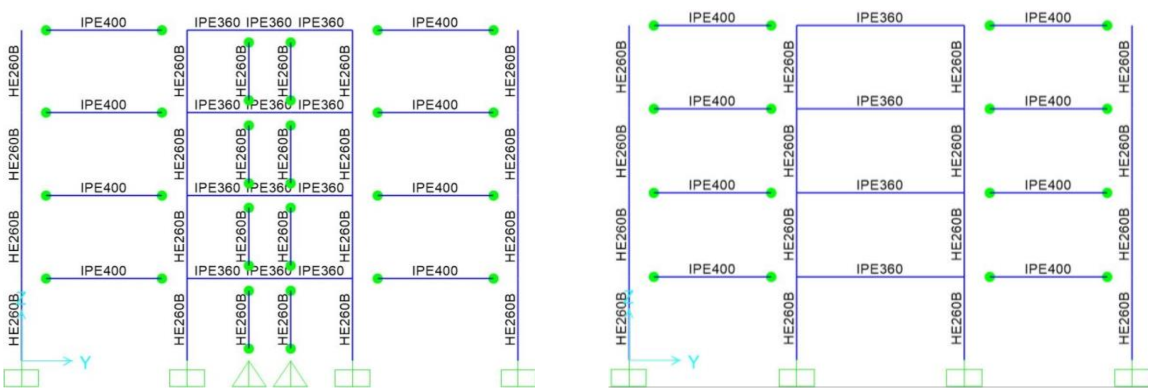

c) Longitudinal exterior frames (y axis) d) Longitudinal interior frames (y axis)

Figure 9.6: 4 story gravity frames (continued)

9.1.3.2 Serviceability Limit State

Beams deflections were checked from fundamental load combination and found to be less than the limit taken into account, *L*/250, see Table 9.2

Table 9.2: Beam deflection

Frame	Beam	Max. deflection	L/250
Transv. ext.	IPE360	17.7	32
Transv. int.	IPE500	20.5	
Long. ext.	IPE400	20.0	
Long. int.	IPE400	21.8	
Secondary beams	IPE360	30.8	

9.1.4 Response spectrum analysis

Multi-modal response spectrum analysis was performed and the results are summarized in Table 9.3, presenting the modes (Figure 9.7) that activated more than 90% of the mass.

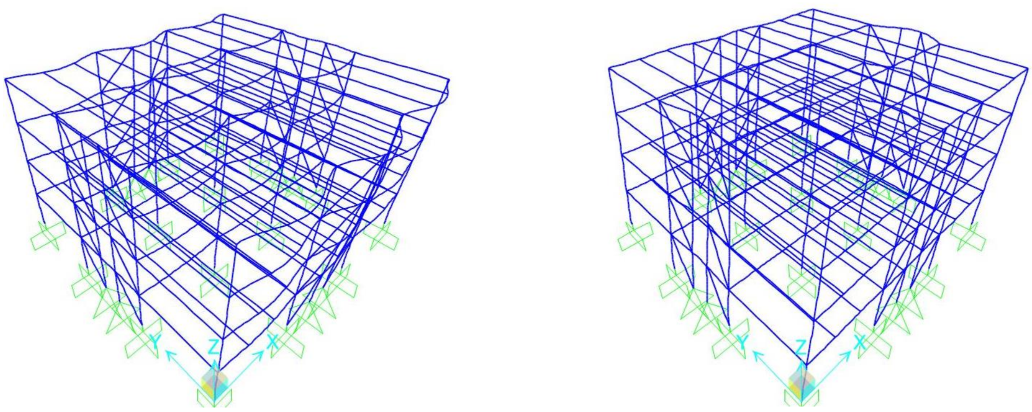

a) Mode 1 – translation on Y b) Mode 2 – translation on X

Figure 9.7: 1st and 2nd modes of vibration

Table 9.3: Participating mass ratio

Mode No	Eigen Period (s)	Participating mass in direction X (%)	Participating mass in direction Y (%)
1	1.18	-	75.6
2	0.97	81.4	-
3	0.83	-	5.4
8	0.73	-	5.2
10	0.69	-	2.6
23	0.39	-	3.7
24	0.317	11.7	-
Sum of participating masses		**93.1**	**92.5**

9.1.5 Global imperfections and 2nd order effects

Global imperfections of H_i*=17.09 KN* were considered in the structural analysis, according to EN1993-1-1 [1], through equivalent lateral forces, from combination 1.35·G + 1.5·Q. These forces were computed based on total gravitational loads and initial global imperfection ϕ, level by level, and considered in every load combination further on.

Second order effects were not accounted for in design because the inter-story drift sensitivity coefficient θ, computed according to EN1998-1-1 [2], found to be 0.0743 smaller than 0.1.

9.1.6 Seismic design

9.1.6.1 Ultimate Limit State - Dissipative elements design

The equivalent braces and shear panel boundary beams were designed to resist the forces of the most unfavourable seismic combination. The resulted equivalent brace areas are presented in Table 9.4. In order to satisfy a homogeneous dissipative behaviour, the 25% limit between the maximum overstrength Ω_{max} and the minimum value Ω_{min}, was ensured (Table 9.5).

Table 9.4: Equivalent brace areas

Story	A_{brace} [mm^2]
1,2	2250
3	2100
4	1450

Table 9.5: Homogeneity of equivalent braces

Element	Ω_{min}	Ω_{max}	Homogeneity
Brace	1.27	1.69	25%
MRF beam	2.16	2.5	15%

Additionally, the minimum moments of inertia, $I_{b,req}$, about an axis taken perpendicular to the plane of the web (Eq. (9.2)), of shear panels boundary beams was checked [6] (see Table 9.6).

$$0.0031 \cdot \frac{\Delta t_w \cdot L^4}{L} h \qquad \text{Eq. (9.2)}$$

Table 9.6: Checking of shear panels boundary beam

Story	t_w	Beam	$I_{b,req}$	I_b
1,2	1.1	IPE 360	4.4E+06	1.6E+08
3	1.0	IPE 360	1.9E+07	1.6E+08
4	0.7	IPE 360	4.3E+07	1.6E+08

9.1.6.2 Ultimate Limit State – Non-dissipative element design

The non-dissipative elements, columns and stanchions, where checked with the most unfavourable seismic combination, to ensure that the failure of the shear panels occurs first.

Additionally, minimum moments of inertia, $\mathbf{I_{c,req}}$, about an axis taken perpendicular to the plane of the web, was checked [6] (see Table 9.7).

$$0.003 \cdot t_w \cdot \frac{h^4}{L} \qquad \text{Eq. (9.3)}$$

Table 9.7: Checking of shear panels boundary columns

Story	Columns	I_c	$I_{c,req}$
1,2	HE 320 B	3.1E+08	2.9E+08
3	HE 300 B	2.5E+08	2.5E+08
4	HE 280 B	1.9E+08	1.9E+08

9.1.6.3 Limitation of inter-story drift

Considering that the building has ductile non-structural elements the inter-story drift is limited to 0.0075, in accordance with EN 1998-1 [2]. The inter-story drifts (Table 9.8) were computed with Eq. (9.4) using story displacements taken from Sap2000 [7] from the combination of loads given in Eq. (9.5):

$$(d_{e,top} - d_{e,bottom}) / h < 0.0075 \qquad \text{Eq. (9.4)}$$

$$1 \cdot G + \nu \cdot q \cdot E \qquad \text{Eq. (9.5)}$$

Where ν =0.5 is a reduction factor on the design displacements due to the importance class of the building (ordinary buildings), q=5 is the behaviour factor, h=4 is the story height, $d_{e,top}$ and $d_{e,bottom}$ are top and bottom displacement of considered story.

Table 9.8: Beam deflection

Frame	Inter-story drift
Transv. ext.	0.0058
Transv. int.	0.0059
Long. ext.	0.0058
Long. int.	0.00585

9.1.6.4 Shear panels

After design, the equivalent braces are converted into shear panels having the thickness, t_w (Table 9.9), calculated with the Eq. (9.6).

$$t_w = \frac{2 \cdot A_{brace} \cdot \Omega \ \sin\phi}{L \cdot \sin 2\alpha} \qquad \text{Eq. (9.6)}$$

Where:

θ is angle between the vertical and the longitudinal axis of the equivalent brace;
L is the distance between VBE centrelines;
α is the angle of inclination of the tension field in the shear panels, taken as 40°;
Ω is the system overstrength factor.

Table 9.9: Shear panels

Story	Panel thickness, t_w, mm	
1	1.1	1.1
2	1.1	1.1
3	1.0	1.0
4	0.7	0.7

The result of design process is show in Figure 9.8.

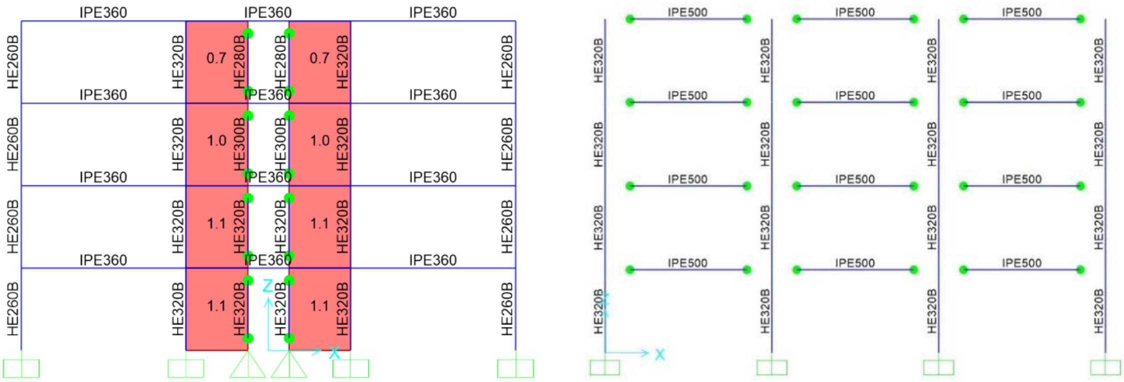

a) Transversal exterior frames (x axis) b) Transversal interior frames (x axis)

Figure 9.8: 4 story structure (continues)

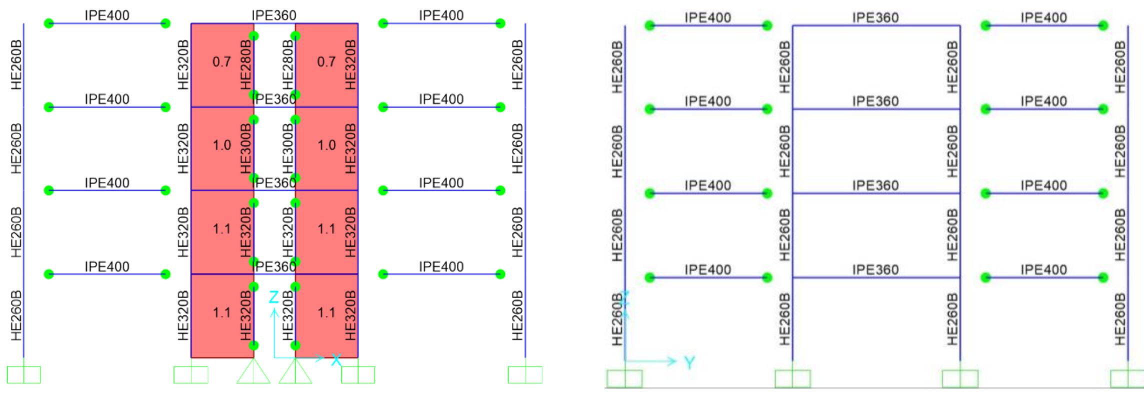

c) Longitudinal exterior frames (y axis) d) Longitudinal interior frames (y axis)

Figure 9.8: 4 story structure (continued)

9.1.6.5 *Dual configurations*

The duality of the structures was checked, in both directions, by verifying that the MRFs is be able to resist at least 25% of the total seismic force. Some adjustments were needed for the structural elements. Figure 9.9 presents the final section for the structural elements.

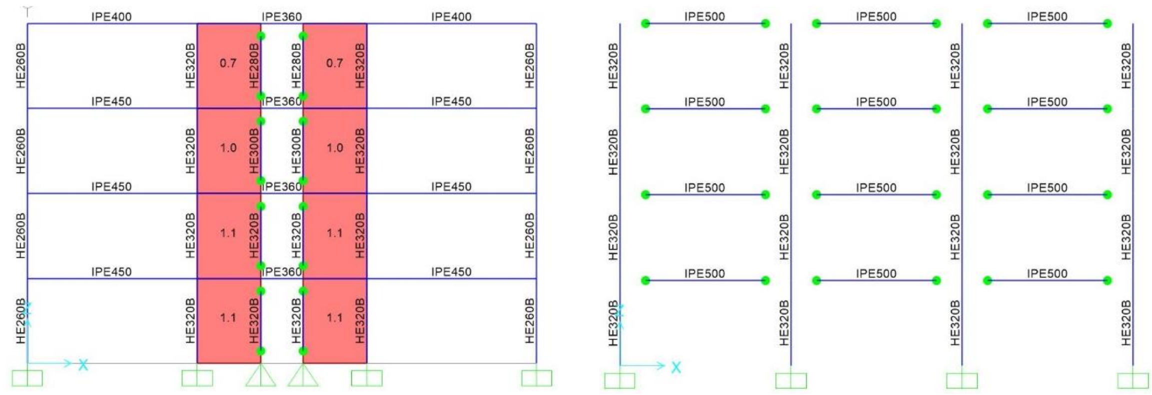

a) Transversal exterior frames (x axis) b) Transversal interior frames (x axis)

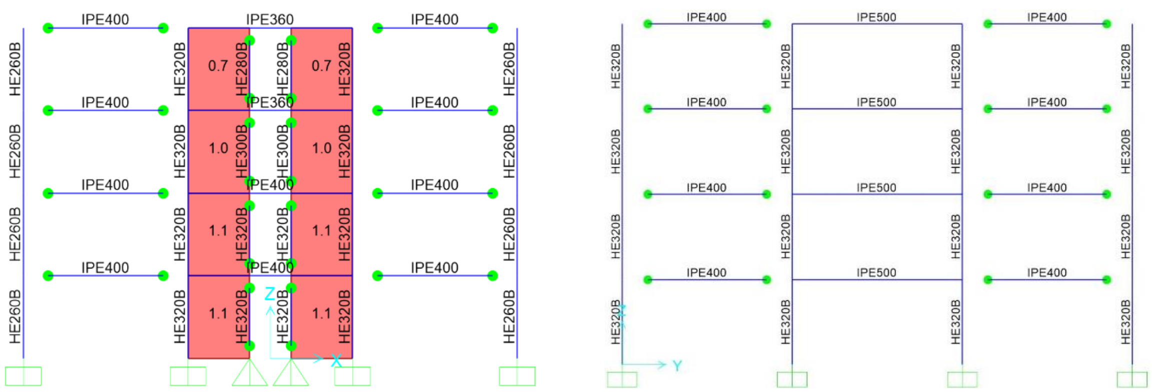

c) Longitudinal exterior frames (y axis) d) Longitudinal interior frames (y axis)

Figure 9.9: Dual 4 story structure

9.1.6.6 Weak beam-strong column

The "weak beam-strong column" condition was checked and found to comply with recommendation given in EN 1998-1-1 [2].

$$\sum M_{Rc} \geq 1.3 \sum M_{Rb} \qquad \text{Eq. (9.7)}$$

Where: ΣM_{Rc} is the sum of upper and lower columns moment resistance and ΣM_{Rb} is the moment resistance of the MRF beam.

9.1.7 Re-centring verification

In order to verify the re-centring capacity of the structure it is recommended to use detailed nonlinear static analysis. 2 types on analysis can be performed:

- push-over analysis where the structure is loaded till failure, calculate the target displacement corresponding to ultimate limit state and check the plastic mechanism at ULS if the damage is isolated in the dissipative members;
- load laterally the structure till ULS, unload it and remove the dissipative members in order to see if the structure recovers its initial position.

9.2 STRUCTURAL DETAILING

In the following are presented the structural detailing of the structure connections (Figure 9.10) and the shear panel corner detail.

The MRF beam-to-column connection was designed using extended end plate with hunch and M20 10.9 class bolts (Figure 9.11a). The shear panel main beam-to-column connection was designed using extended end plate and M20 10.9 class bolts (Figure 9.11b). Stanchion-to-main beam connections were designed using flush end plates and M20 10.9 class bolts (Figure 9.11c). Bottom horizontal boundary element to column connection was done using flush end plate M20 10.9 class bolts (Figure 9.11d). The connection between shear panel and boundary elements were designed using 6 mm welded fin plates to the boundary elements and slip-resistant M12 8.8 class bolts (for the bottom shear panel were needed 17 bolts in vertical direction and 14 in horizontal direction) (Figure 8.11e). The bearing capacity of the bolts was also checked and found that it is needed an additional 3 mm strengthening plate on the bolted are of the shear panels (Figure 8.11e).

All pinned beam to column connection were designed using welded gusset plate on the connecting element and bolts.

The tests carried out at UPT ([3] and [4]) have proven that bolted connections in shear and bearing (category C) between the shear panel and boundary elements, realized by fit bolts, exhibit satisfactory fatigue behaviour, provide enough overstrength and allow the removal of the damaged shear panel after the re-centring of the building.

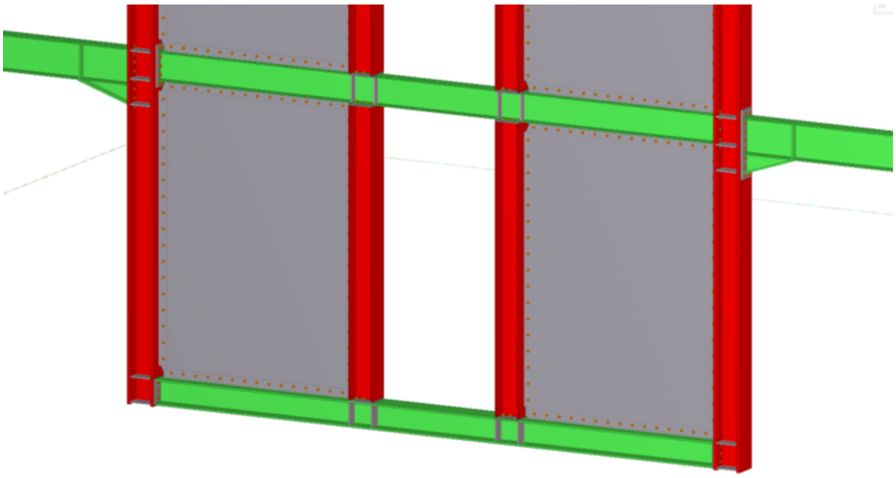

Figure 9.10: Overview of joints

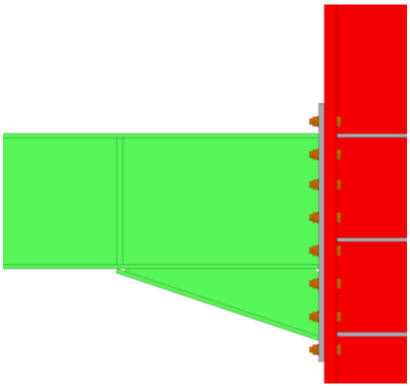

a) MRF beam-to-column connection

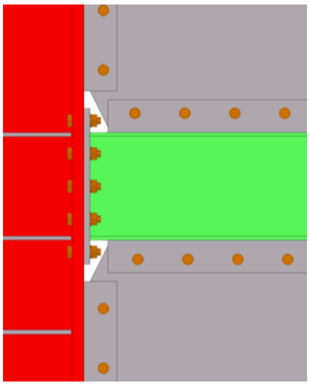

b) Shear panel beam-to-column connection

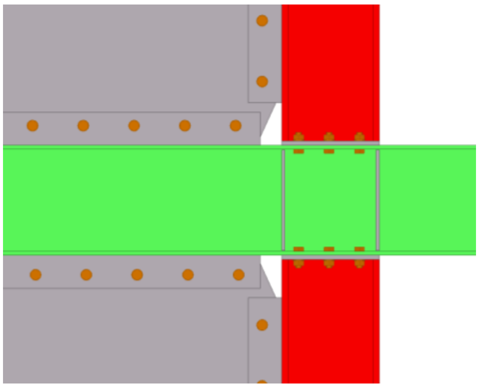

c) Stanchion-to-beam connection

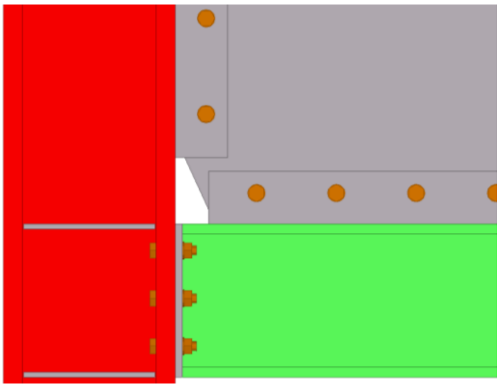

d) Bottom horizontal boundary element to column connection

Figure 9.11: Overview of joints (continues)

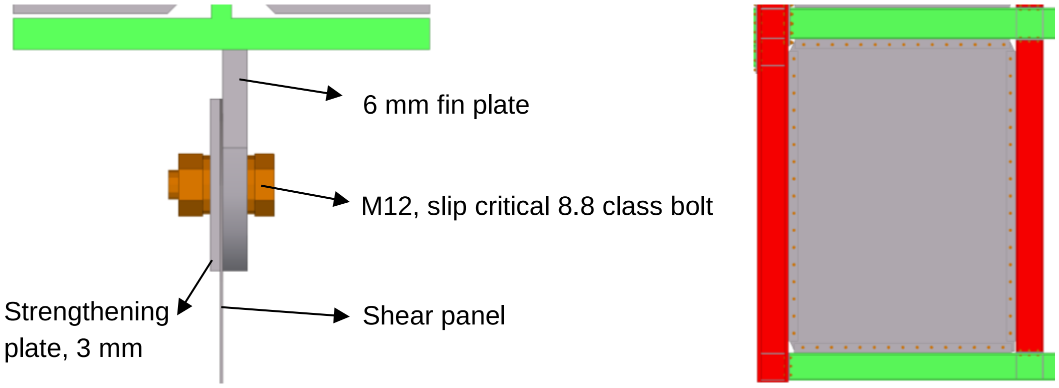

d) Shear panel to boundary element connection

Figure 9.11: Overview of joints (continued)

The presented corner detail of the shear panels has proven to have satisfactory behaviour during experimental tests (Figure 9.12a), even if, from 2% top drift (black dot in Figure 9.12c), crack started to develop (Figure 9.12b).

a) Corner detail

b) Fracture of panel

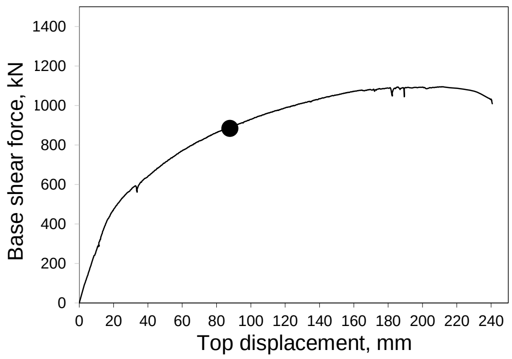

c) Capacity curve

Figure 9.12: Experimental test on frame with rigid connection

9.3 CONCLUSIONS

From the presented case-study it can be observed that for such a low raised structure with the given dimensions (span, bay, height), the resulted shear panels are very thin. Very thin shear panels, even theoretically, are able to provide the necessary stiffness and strength. Problems might appear for manipulation and installation of such panels. So, we can appreciate that for lower rise buildings (< 4 stories) this solution will not be effective.

9.4 BIBLIOGRAPHIC REFERENCES

[1] EN1993-1-1. Eurocode 3: Design of steel structures - Part 1-1: General rules and rules for buildings. Brussels: Comitee Europeen de Normalisation (CEN); 2003.

[2] EN1998-1-1, Eurocode 8: Design of structures for earthquake resistance – Part 1-1: General rules, seismic actions and rules for buildings. Brussels: Comitee Europeen de Normalisation (CEN); 2003.

[3] Dubina D., Dinu F. Experimental evaluation of dual frame structures with thin-walled steel panels. Thin-Walled Structures 2013; 78:57-69.

[4] Neagu C. Multi-story building frames stiffened with dissipative shear wall: PHD Thesis; Ed. Politehnica; University Politehnica Timisoara; Romania, 2011.

[5] EN 1993-1-8: Eurocode 3: Design of steel structures. Part 1-8: Design of joints. Brussels: Comité Européen de Normalisation (CEN); 2004.

[6] AISC 341-10. Seismic provisions for structural steel buildings; American Institute for Steel Construction: 2010.

[7] SAP2000. CSI: Computers and Structures Inc., www.csiberkeley.com.

10 CBF-MB

10.1 GENERAL

10.1.1 Introduction

This case study refers to the seismic design of new two-storey steel office buildings. It aims at demonstration of implementation of the Concentrically Braced Frames with Modified Braces (CBF-MB). The case study elaborated refers to conceptual design, modelling and analysis by linear response spectrum analysis methods (RSA), detailed design of main dissipative and non-dissipative members and basic structural detailing of CBF-MB.

10.1.2 Description of building

10.1.2.1 Geometry and general assumptions

The case study deals with a two-storey frame building with three 8m bays in both directions. The gravity frames are composed of beams and columns, located at each structural axis. Nominally pinned beam-to-column joints and pinned column bases are assumed. The CBF-MBs are the main horizontal load resisting systems, located in the middle of each facade as shown in Figure 10.1.

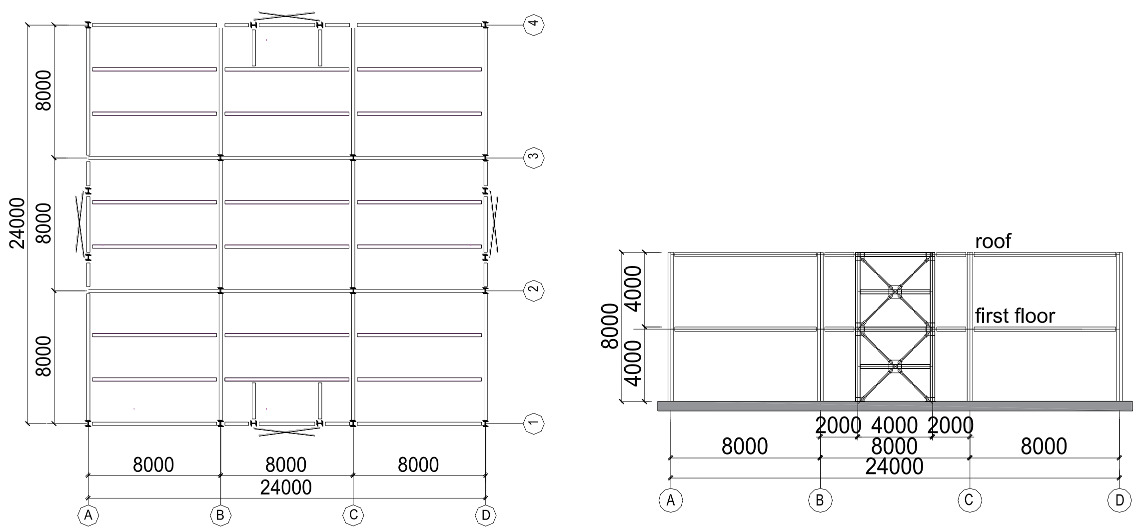

Figure 10.1: Floor plan and elevation

Hot rolled HEA profiles for columns and IPE profiles [2] for floor beams are used for all gravity frames. Both floor slabs (first floor and roof) are designed with steel beams and concrete deck. Composite action with the concrete slab is not considered. However, dowels connecting main and secondary beams to the concrete deck are used to provide structural integration and floor diaphragm action. Diaphragms are assumed rigid, thus neglecting membrane (in-plane) deformations.
Each CBF-MB consists of two columns, floor beams, splitting beams and braces. It is integrated in the centre of each middle bay. In this way columns of the CBF are loaded primarily with axial forces resulting from the seismic action (or wind load) and the rest of the frame columns carry the gravity loads.

10.1.2.2 Materials

Steel grade S235 is used for the design of modified braces (dissipative elements)
The adopted steel grade for CBF columns is S355. CBF-MB floor beams and splitting beams are designed with steel grade S275.
Gravity frame is designed by conventional approach and steel grade S275 is used. Floor slabs are designed by Hi-Bond metal decking used for formwork only, concrete C25/30 and reinforcing steel B500B are assumed.

10.1.2.3 Loads and load combinations

Table 10.1 summarizes the adopted gravity loads and seismic action parameters. Top floor loads are adopted as for non-occupied roof. It is assumed that snow load intensity is less than the imposed roof load and the altitude of construction site is below 1000 meters. Consequently, the snow load is excluded from the seismic design situation.

Table 10.1: Loads and actions (continues)

Vertical loads	
Concrete and metal deck self-weight	2.75 kN/m^2
Utilities, ceiling, floor or roof finishing: – First floors – Roof	 0.70 kN/m^2 1.00 kN/m^2
Facades: Tributary facade height (4 m for first storey and 4 m for roof including parapet wall).	0.60 kN/m^2
Partitions, only at first floor	0.80 kN/m^2
Imposed loads 1st floor (category B): Imposed loads roof (category H):	3.00 kN/m^2 0.75 kN/m^2

Table 10.1: Loads and actions (continued)

Seismic action	
Design response spectrum for elastic analysis	Type 1
Reference peak ground acceleration	$a_{g,R} = 0.30g$
Importance class II (Ordinary building)	$\gamma_I = 1.0$
Ground type	B ($T_B = 0.15$ s, $T_C = 0.50$ s)
Behaviour factor q	5.0
Damping ratio	5%
Factors for storey occupancy	$\varphi = 0.80$
Seismic combination coefficient	
First floor	$\psi_2 = 0.30$, $\psi_E = 0.24$
Roof	$\psi_2 = 0.00$, $\psi_E = 0.00$

The seismic masses are calculated according to Eq. (10.1) and presented in Table 10.2.

$$\sum_{j>1} G_{k,j} + \sum_{i>1} \psi_{E,i} . Q_{k,i} \qquad \text{Eq. (10.1)}$$

Table 10.2: Seismic masses

Seismic mass floor 1 = 315.4 t	
Concrete and metal deck self-weight – ($G_{k1,1}$)	2.75x24.0x24.0/9.81 = 161.5 t
Utilities, ceiling, floor finishing – ($G_{k2,1}$)	0.70x24.0x24.0/9.81 = 41.1 t
Facades – ($G_{k3,1}$)	0.60x4.0x4.0x24.0/9.81 = 23.5 t
Partitions – ($G_{k4,1}$)	0.80x24.0x24.0/9.81 = 47.0 t
Imposed loads – ($Q_{k,1}$). Ψ_E	3.0x24.0x24.0x0.24/9.81= 42.3 t
Seismic mass roof = 243.7 t	
Concrete and metal deck self-weight – ($G_{k1,2}$)	2.75x24.0x24.0/9.81 = 161.5 t
Utilities, ceiling, floor finishing – ($G_{k2,2}$)	1.00x24.0x24.0/9.81 = 58.7 t
Facades – ($G_{k3,2}$)	0.60x4.0x4.0x24.0/9.81 = 23.5 t
Imposed loads – ($Q_{k,2}$). Ψ_E	0.75x24.0x24.0x0.0/9.81= 0.0 t
Steel skeleton seismic mass = 61.3 t	

Seismic masses for the building are summarized in Table 10.3.

Table 10.3: Seismic masses per floor

Floor 1 mass = 315.4 t	Roof mass = 243.7 t	Skeleton mass = 61.3 t
Total seismic mass = 620.4 t		

10.2 BASIC AND NON-SEISMIC DESIGN

10.2.1 Preliminary selection of modified braces

The modified braces provide the primary source of stiffness and dissipation capacity for the CBF-MB system so their design differs from the ordinary brace design. Initially brace shape and first-estimation cross sections need to be chosen. The unexperienced user should expect that some iterations would have to be done. The cross-sections to be defined are illustrated in Figure 10.2: Definition of the cross-sections within modified brace member and the choice of their recommended lengths is demonstrated in Table 10.4. The recommendations of [5, 6] have been followed.

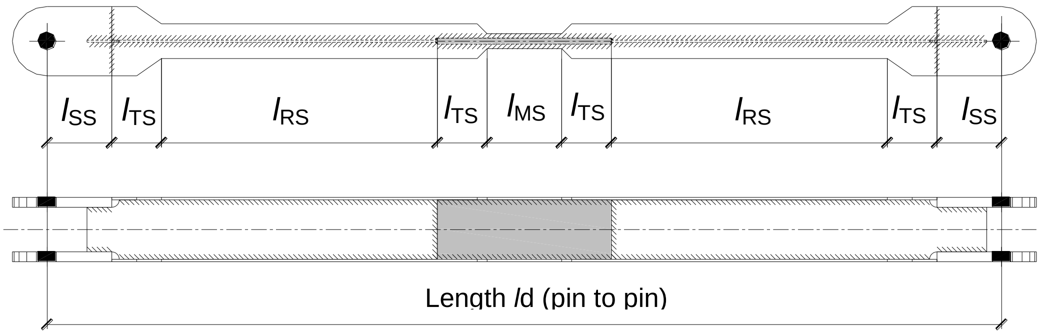

Figure 10.2: Definition of the cross-sections within modified brace member

Table 10.4: Choice of specific lengths in modified braces

Specific length (mm)	Recommendations according to [5], [6]	A particular value in this example (mm)
l	NA	5656
l_d	$(0.375 - 0.40)l$	2150
l_{MS}	$l_{MS} = (0.067 \div 0.085)l_d$	180
l_{TS}	~ 100	100
l_{SS}	Preference of designer	130
l_{RS}	$l_{RS} \approx (0.3)l_d$	655

Where:

l is the system length of the diagonal,

l_d is the pin to pin length of the brace,

l_{MS} is the length of the modified section,

l_{TS} is the length of the transition section,
l_{SS} is the length of the strong section,
l_{RS} is the length of the reduced section,
MS, RS, SS and TS are abbreviations for modified section, reduced section, strong section and transition section respectively.
As stated in [5] and [6], some relations between the area and section modulus of reduced section and modified section should be achieved to ensure that yielding in tension and flexural plastic strains due to buckling occurs in different zones along the modified brace length. The preliminary adjustment of the brace flange and web geometry is demonstrated in Table 10.5. The MB cross sections will be described by abbreviations for example F110.8W150.6-M180.46-T20 that should be interpreted as explained below.

- For reduced section: F (flange) 110.8 width 110 mm, thickness 8 mm; W (web) 150.6 width 150 mm, thickness 6 mm;
- For modified section: M (modified section) 180.46 length 180 mm, flange width 46 mm – T20 (web thickness of MS) 20 mm.

Table 10.5: Choice of Area and Section modulus in modified braces

Storey	Abbreviation of the MB	Recommendations according to [5], [6]	Value adopted in the particular example
1 st storey	F110.8W150.6-M180.46-T20	$A_{MS}/A_{RS} \geq 1.4$	A_{MS} = 37.4 cm^2
			A_{RS} = 26.6 cm^2
			$A_{MS}/A_{RS} = 1.41$
		$W_{pl,RS}/W_{pl,MS} \geq 2.0$	W_{MS} = 23.5 cm^3
			W_{RS} = 49.8 cm^3
			$W_{pl,RS}/W_{pl,MS} = 2.12$
2 nd storey	F90.5W120.5-M180.42-T14	$A_{MS}/A_{RS} \geq 1.4$	A_{MS} = 21.0 cm^2
			A_{RS} = 15.0 cm^2
			$A_{MS}/A_{RS} = 1.40$
		$W_{pl,RS}/W_{pl,MS} \geq 2.0$	W_{MS} = 10.3 cm^3
			W_{RS} = 21.0 cm^3
			$W_{pl,RS}/W_{pl,MS} = 2.04$

Where:
A_{MS} is the modified section area,
A_{RS} is the reduced section area.
$W_{pl,RS}$ is the reduced section plastic modulus,

$W_{pl,MS}$ is the modified section plastic modulus.

10.2.2 Preliminary check of brace slenderness

Since there is modified section inserted in the mid-length, then the real buckling length $l_{cr} = \mu . l_d$ will be longer than l_d. The effective length l_{cr} may be obtained by FE elastic buckling analysis or by Eq. (10.2).

$$\mu = l_{cr} / l_d = 0.88 K_L^{(0.033)} . K_I^{(0.1\ln(K_L) - 0.36)} \qquad \text{Eq. (10.2)}$$

Where:

$K_L = L_{RS} / L_{MS}$ is section length ratio,

$K_I = I_{MS} / I_{RS}$ is inertia moment ratio,

I_{MS} is moment of inertia of modified section,

I_{RS} is moment of inertia of reduced section,

μ is parameter that modifies the geometric brace length l_d to buckling length l_{cr}. .

Hereafter Eq. (10.2) is used and the results are presented in Table 10.6. According to [1] braces of CBFs with X-configuration must have non-dimensional slenderness in the range of $1.3 \leq \bar{\lambda}_{eff} \leq 2.0$. The effective slenderness is defined by Eq. (10.3).

$$\lambda_{eff} = \mu . l_d / i_{RS} \qquad \text{Eq. (10.3)}$$

where i_{RS} is the minor radius of gyration of the reduced section.

Table 10.6: Modified braces slenderness

Storey	Modified Brace	K_L	K_I	μ	L_{cr} (m)	λ_{eff}	$\bar{\lambda}_{eff}$
1	F110.8W150.6-M180.46-T20	3.639	0.1180	1.504	3.234	125.1	1.332
2	F90.5W120.5-M180.42-T14	3.639	0.1465	1.431	3.077	152.7	1.626

10.2.3 Simulation

The structural linear elastic model was formed according to the rules given in [5, 6] by the software SAP 2000 [8]. All gravity columns are modelled as continuous and pin-connected to the bases. All joints between gravity floor beams and columns are nominally pinned as well.

CBF-MB members are designed and modelled as follows. CBF-MB columns are continuous. The joints between splitting beams and columns are assumed to be rigid and full strength so they are modelled as continuous while the joints between beams and CBF-MB columns are assumed nominally pinned. The elements simulating the modified braces are defined through constant H-shape section with characteristics of the reduced section and joined to the frame by simple pin connections. CBF-MB column bases were designed and detailed as pinned which is considered the most practical approach for this type of system. The elastic analysis requires a tension-only diagonal model [1]. Diaphragm action of floor and roof concrete decks is simulated by diaphragm constraint.

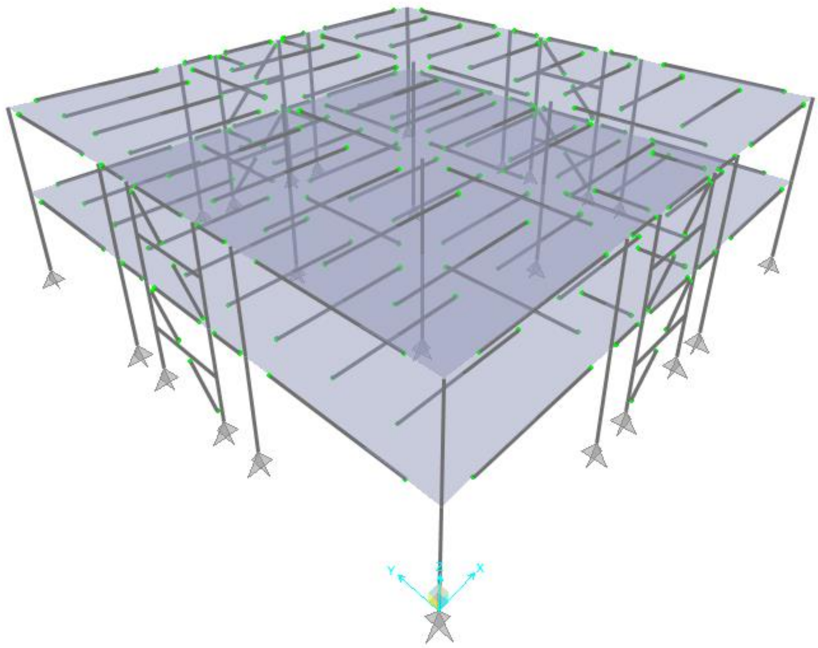

Figure 10.3: FE three-dimensional model

The current case study was developed by centreline-to-centreline (CL-to-CL) model. It is quick and easy to be defined, since the axis geometry of the frame is known at the beginning of the design process.

10.2.4 Design for static combinations

Distinctive feature of the structural configuration demonstrated in this case study is the fact that the proposed seismic resistant system (CBF-MB) is arranged so as to be released from gravity loads, excluding its self-weight and small tributary dead and imposed loads. It is easy to be checked that the seismic design situation governs the design of CBF-MB system, therefore wind combination will not be considered hereafter.

10.2.4.1 Ultimate limit state results

The ultimate limit state load combination that governs the gravity members design is calculated according to Eq. (10.4).

$$\sum_{j>1} 1.35.G_{k,j} + \sum_{i>1} 1.5.Q_{k,i} \qquad \text{Eq. (10.4)}$$

10.2.4.2 Member design

The results from the member design are presented in Table 10.7.

Table 10.7: Verification of gravity members

Member	Section	Steel grade	NEd (kN)	My,Ed (kNm)	Mz,Ed (kNm)	Ratio
Secondary roof beam	IPE300	S275	-	130	-	0.791
Main roof beam	HEA340	S275	-	363	-	0.776
Secondary floor beam	IPE360	S275	-	230	-	0.861
Main floor beam	HEA400	S275	-	606	-	0.937
Internal column	HEA240	S275	-1141	-	-	0.836
External column	HEA200	S275	-520	-5	1	0.693

10.2.4.3 Serviceability limit state checks

Table 10.8: Verification of member's deflection

Member	Section	Deflection	type	Adopted limit
Secondary roof beam	IPE300	1/230	roof	1/200
Main roof beam	HEA340	1/261	roof	1/200
Secondary floor beam	IPE360	1/255	floor	1/250
Main floor beam	HEA400	1/256	floor	1/250

10.3 SEISMIC ANALYSIS

10.3.1 Seismic design situation

The building is recognized as regular in plan and in height. Theoretically the centre of masses and the centre of rigidity coincide. In order to account for uncertainties in the location of masses and for the rotational component of the seismic motion, additional accidental mass eccentricity (§4.3.3.3.3 [1]) with value of 1200 mm (5% of 24000 mm) was introduced in both directions. The mass eccentricity effects were taken into account by defining two static load cases Mx and My, simulating rotation. In order to account for the torsional effects, the storey seismic forces in both main directions were calculated based on the lateral force method (§4.3.3.2 [1]). It was done by introducing quake load pattern, floor diaphragm constraints and eccentricity of 5% in SAP 2000 [8]. The final seismic design situation accounting for accidental torsional effects was derived by Eq. (10.5) as recommended by P. Fajfar [7].

$$E = SRSS\,(Ex \pm Mx, Ey \pm My) \qquad \text{Eq. (10.5)}$$

where:

Ex and *Ey* are results of analysis without accidental torsion by applying RSA in X and Y direction, respectively;

Mx and *My* are accidental torsional effects of applied storey seismic force with eccentricity of 5% in X and Y direction, respectively;

SRSS is square root of sum of squares combination.

The global rotational effect was estimated as about 6% amplification of the seismic effects (internal forces and displacements).

The seismic combination that governs the CBF-MB braces design is calculated according to Eq. (10.6).

$$\sum_{j=1}^{4} G_{k,j} + E + 0.3Q_{k,i} \qquad \text{Eq. (10.6)}$$

where:

$G_{k,j}$ are the gravity load effects in seismic design situation;

E is the effect of the seismic action including accidental torsional effects;

$Q_{k,1}$ is the first floor imposed load effects in seismic design situation;

10.3.2 Response Spectrum Analysis

Multi-modal RSA was performed. The first and the second natural modes of vibrations are presented on Figure 10.4. They are dominantly translational. The third mode of vibration is shown on Figure 10.5 and it is rotational. The results from the analysis are summarized in Table 10.9. The first and the second modes activate less than 90% of the total mass. Although the building is only two-storey, 36 modes of vibration had to be included in the modal analysis to activate at least 90% of the seismic mass. It might be addressed to the fact that automatic check of the beams and columns was performed, which requires more nodes in the slab for more realistic simulation of the load transfer. Finally, it demands inclusion of more modes of vibration.

Table 10.9: Participating mass ratio and periods

Mode No	Eigen Period (s)	Participating mass in direction X (%)	Participating mass in direction Y (%)
1	0.6278	87.9	-
2	0.6277	-	87.9
3	0.384	-	-
31	0.245	12.0	-
36	0.239	-	11.9
Sum of participating masses		99.90	99.80

According to [1] when $T_C \leq T$ the spectrum acceleration has to be greater or equal to the lower bound. Since the first mode dominates the response, the check may be done by Eq. (10.7):

$$S_d(T) = \frac{V_{tot}}{P_{tot}} \geq \beta . a_g \,, \qquad \text{Eq. (10.7)}$$

where V_{tot} is the total base shear from the response spectrum analysis, P_{tot} is the total vertical load, corresponding to the seismic design situation and $\beta = 0.2$ is the lower bound factor for the horizontal design spectrum. The check proves that there is no need to increase the base shear (Table 10.10).

Table 10.10: Check of the lower bound for the horizontal design spectrum

V_{tot} (kN)	P_{tot} (kN)	V_{tot} / P_{tot}	βa_g
807.6	6186.4	0.131	0.060

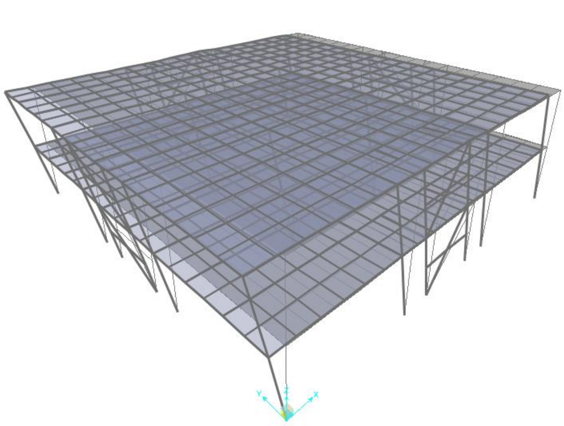

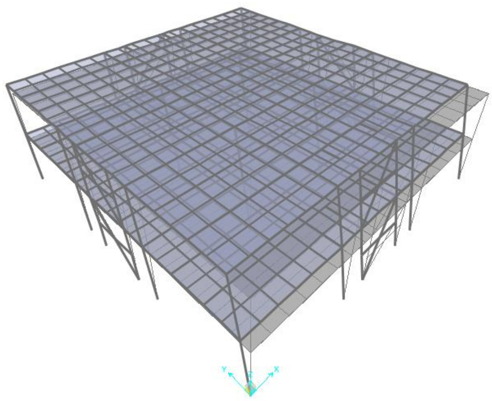

Figure 10.4: First and second mode of free vibrations, $T_1 = 0.62768$ s, $T_2 = 0.62767$ s

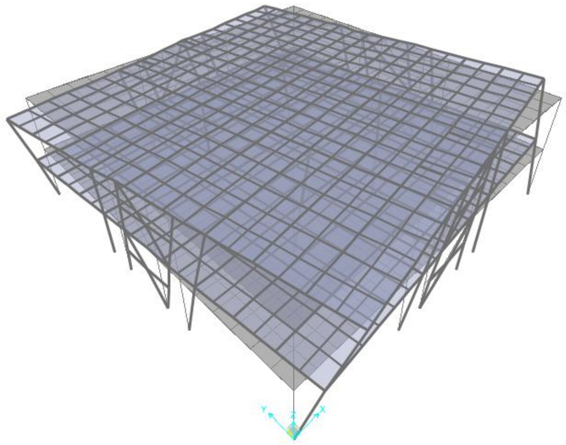

Figure 10.5: Third mode of free vibrations, $T_3 = 0.384$ s

10.4 DETAILED DESIGN

10.4.1 Damage limitation – limitation of interstorey drift

Assuming that the building has ductile non-structural elements the verification is:

$$d_r.\nu \leq 0.0075h = 0.0075.4000 = 30.0\,\text{mm}, \qquad \text{Eq. (10.8)}$$

Where $v = 0.5$ is the reduction factor according to §4.4.3.2 (1) of [1], h is the story height and d_r is the design interstorey drift. Table 10.11 includes the results from the analysis for each of the stories.

Table 10.11: Limitation of interstorey drift

Storey	**1**	**2**
$d_{e,top}$ (mm)	9.3	19.3
$d_{e,bottom}$ (mm)	0.0	9.3
$d_r = (d_{e,top} - d_{e,\,bottom})\,q$ (mm)	46.5	50.0
$d_r\,v$	23.25 < 30.0	25.0 < 30.0

10.4.2 Second order effects

The sensitivity to second order (P–Δ) effects is estimated by the interstorey drift sensitivity coefficient θ given by Eq. (10.9), where P_{tot} and V_{tot} are the total gravity load at and above the storey considered in the seismic design situation and total seismic storey shear, respectively, at the storey under consideration. The calculated values of θ are listed in Table 10.12.

$$\theta = P_{tot} d_r / V_{tot} h \quad \text{Eq. (10.9)}$$

Table 10.12: 2nd order effects

Storey	**1**	**2**
$d_r = (d_{e,top} - d_{e,\ bottom})\ q$ (mm)	46.5	50.0
P_{tot} / V_{tot}	6186 / 807.6	2665 / 506
h (mm)	4000	4000
θ	0.089 < 0.10	0.066 < 0.10

The values of θ for both storeys are less than 0.1, therefore second-order effects may be neglected.

10.4.3 Final verification of dissipative members

The non-dimensional slenderness of the brace $\bar{\lambda}_{eff}$ should be limited to $1.3 \le \bar{\lambda}_{eff} \le 2.0$ as stated in §6.7.3 (1) of [1]. The yield resistance $N_{pl,Rd}$ of the modified brace should fulfill §6.7.3 (5) of [1] and should be obtained by Eq. (10.10). According to §6.7.3 (8) of [1] the maximum and minimum overstrength Ω should not differ more than 25% providing homogeneous dissipative behaviour of the diagonals. Since the initial brace cross-sections are not changed after the verifications in sections 9.4.1 and 9.4.2, the normalized slenderness is not changed and the valid results are shown in Table 10.6. The rest verifications are presented in Table 10.13.

$$N_{pl,Rd} = A_{RS}.f_y / \gamma_{M0} \quad \text{Eq. (10.10)}$$

Table 10.13: Verification of braces and check for homogeneous dissipative behaviour

Storey	Brace cross section	A_{RS} (cm^2)	N_{Ed} (kN)	$N_{pl,Rd}$ (kN)	$\Omega = \frac{N_{pl,Rd}}{N_{Ed}}$	$\frac{\max \Omega}{\min \Omega} < 1.25$
1	F110.8W150.6-M180.46-T20	26.6	580	595.3	1.026	1.02
2	F90.5W120.5-M180.42-T14	15.0	332	335.7	1.011	

10.4.4 Transitions stage

The splitting beam should be designed as per the recommendations of [5, 6]. The transition stage ("just before buckling" stage) is introduced because it causes additional bending moments and axial forces (load case UNB) that occur within the storey H-frame – Figure 10.6. That internal effect is to be accounted for into design. It is simulated in the model for elastic analysis by introducing unbalanced forces integrally in all two stories simultaneously.

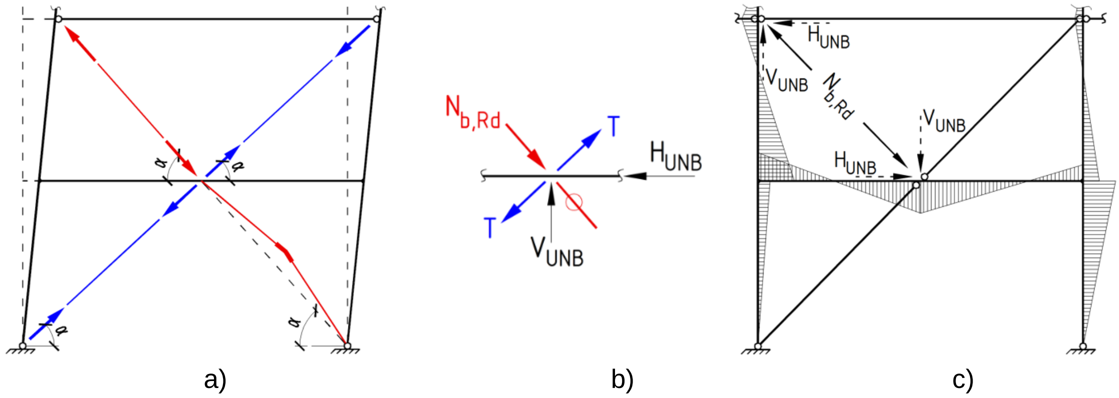

Figure 10.6: a) Transition stage ("just before buckling"); b) Unbalanced forces; c) Internal moments (M_{UNB}) resulting from the unbalanced forces (load case UNB)

The unbalanced forces are calculated based on Eq. (10.11), Eq. (10.12), Eq. (10.13) and the results are presented in
Table 10.14.

$$V_{UNB} = N_{b,Rd}.\sin\alpha \qquad \text{Eq. (10.11)}$$

$$H_{UNB} = N_{b,Rd}.\cos\alpha \qquad \text{Eq. (10.12)}$$

$$N_{b,Rd} = \chi.A_{RS}.f_y/\gamma_{M1} \qquad \text{Eq. (10.13)}$$

Table 10.14: Unbalanced forces in splitting beams

Storey	Brace cross sections	A_{RS} (cm^2)	Buckling curve	χ	$N_{b,Rd}$ (kN)	V_{UNB} (kN)	H_{UNB} (kN)
1	F110.8W150.6-M180.46-T20	26.6	"c"	0.376	223.8	158.3	158.3
2	F90.5W120.5-M180.42-T14	15.0	"c"	0.276	92.7	65.5	65.5

10.4.5 Capacity design of non-dissipative members

CBF-MB columns shall be verified to resist design forces obtained from Eq. (10.14) to Eq. (10.16). The results for column verifications are presented in Table 10.15.

$$N_{col,Ed} = N_{Ed,G} + 1.1\gamma_{OV}\Omega_{\min}\rho(N_E + N_{UNB}) \quad \text{Eq. (10.14)}$$

$$M_{col,Ed} = M_{Ed,G} + 1.1\gamma_{OV}\Omega_{\min}\rho(M_E + M_{UNB}) \quad \text{Eq. (10.15)}$$

$$V_{col,Ed} = V_{Ed,G} + 1.1\gamma_{OV}\Omega_{\min}\rho(V_E + V_{UNB}) \quad \text{Eq. (10.16)}$$

Where:
γ_{ov}=1.25 is the material overstrength factor according to §6.2 (3) of [1],
Ω_{MIN} *=1.011* as per Table 10.13,
ρ = 1.15 is factor accounting for the available overstrength of the system, when DCH is adopted (see [6]).

Table 10.15: CBF columns verification

Storey	Column cross-section / Material	$N_{col,Ed}$	$M_{col,Ed}$	Utilization factor
1	*HEB 260 / S355*	-1191	184.9	0.830
2	*HEB 260 / S355*	-417	97.6	0.377

Splitting beams shall be verified to resist design forces obtained from Eq. (10.17) to Eq. (10.19). The results for splitting beams verifications are presented in Table 10.16.

$$N_{sb,Ed} = N_{Ed,G} + 1.1\gamma_{OV}\Omega_{\min}\rho(N_E + N_{UNB}) \quad \text{Eq. (10.17)}$$

$$M_{sb,Ed} = M_{Ed,G} + 1.1\gamma_{OV}\Omega_{\min}\rho(M_E + M_{UNB}) \quad \text{Eq. (10.18)}$$

$$V_{sb,Ed} = V_{Ed,G} + 1.1\gamma_{OV}\Omega_{\min}\rho(V_E + V_{UNB}) \quad \text{Eq. (10.19)}$$

Table 10.16: Splitting beam verification

Storey	Splitting beam cross-section / Material	$N_{sb,Ed}$	$M_{sb,Ed}$	Utilization factor	$\bar{\lambda}_{LT}$
1	*HEA 240 / S275*	-175.8	150.1	0.937	0.36
2	*HEA 240 / S275*	-88	92.4	0.566	0.36

Floor beams shall be verified to resist design forces obtained from Eq. (10.20) to Eq. (10.22). The results are presented in Table 10.17.

$$N_{b,Ed} = N_{Ed,G} + 1.1\gamma_{OV}\Omega_{\min}\rho(N_E + N_{UNB}) \quad \text{Eq. (10.20)}$$

$$M_{b,Ed} = M_{Ed,G} + 1.1\gamma_{OV}\Omega_{\min}\rho(M_E + M_{UNB}) \quad \text{Eq. (10.21)}$$

$$V_{b,Ed} = V_{Ed,G} + 1.1\gamma_{OV}\Omega_{\min}\rho(V_E + V_{UNB}) \quad \text{Eq. (10.22)}$$

Table 10.17: Floor beam verification

Storey	Floor beam cross-section / Material	$N_{\mathrm{b,Ed}}$[3]	$M_{\mathrm{b,Ed}}$	Utilization factor
1	*HEA 240 / S275*	-666	42	0.685
2	*HEA 240 / S275*	-375	32	0.428

The splitting beam shall be designed so that avoiding lateral-torsional buckling by satisfying Eq. (10.23). Results are presented in Table 10.16.

$$\bar{\lambda}_{LT} \leq 0.40 \quad \text{Eq. (10.23)}$$

The cross sections of splitting beam and columns shall be chosen to satisfy Eq. (10.24) in accordance with §4.4.2.3 (4) of [1].

$$2.M_{Rc} \geq 1.3M_{Rb}, \quad \text{Eq. (10.24)}$$

In that particular case it is obvious that Eq. (10.24) is fulfilled.

10.5 STRUCTURAL DETAILING

After fulfilment of all checks in §9.4 the modified diagonals may be detailed. Their final design is presented in Figure 10.7 and Figure 10.8.

[3] It is recommended that axial beam force is calculated based on the diagonal plastic resistance in tension, additionally corrected by $1.1\gamma_{OV}\rho$. The axial force from the 3D model is non-realistic since the floor diaphragm constraint was implemented.

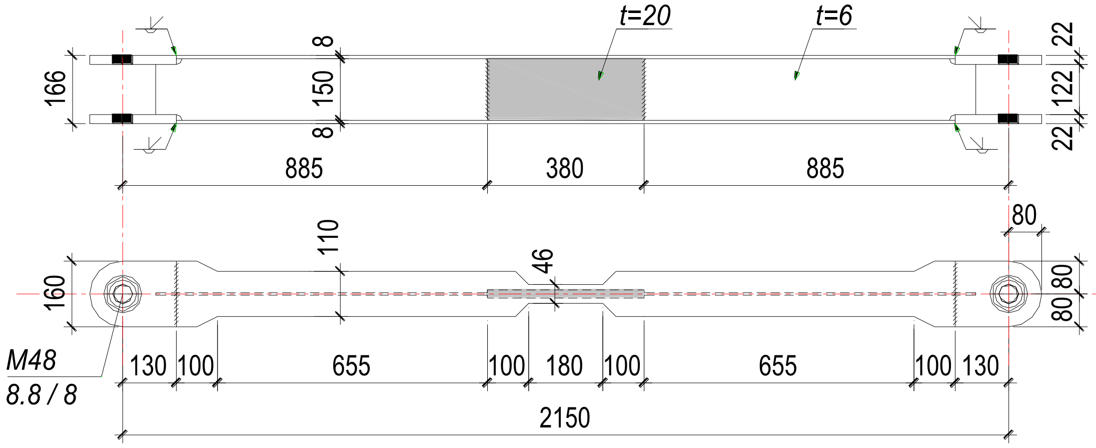

Figure 10.7: Overview of modified brace member at the first storey

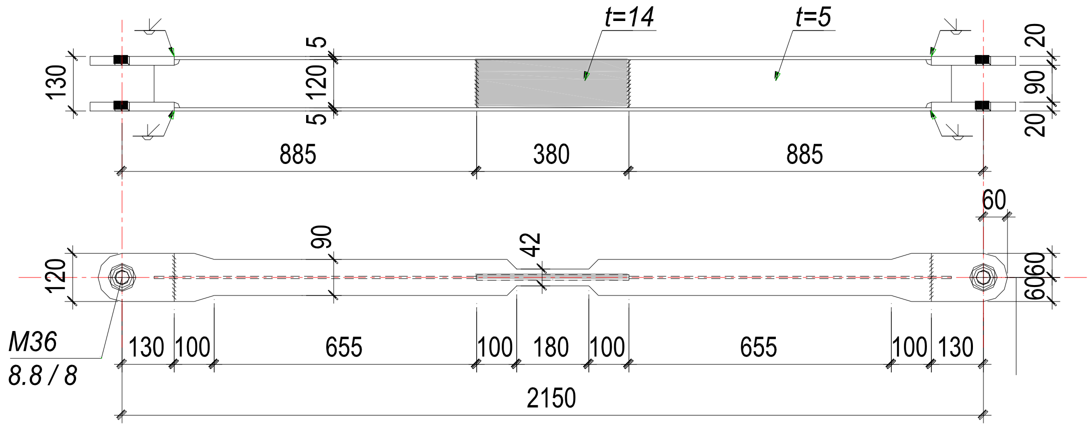

Figure 10.8: Overview of modified brace member at the second storey

The connection between modified braces and the gusset plate should be designed by bolts. The tests carried out [9] have proven that bolted connections in shear and bearing (category A), realized by fit bolts, exhibit satisfactory fatigue behaviour and provide enough overstrength, therefore, in the context of §6.5.5 (6) of [1], are recommended to be used for CBF-MBs. Their dimensioning should fulfil §6.5.5 (3) and (5) of [1].

Table 10.18 summarizes the results from verification checks. It is worth noting that the design force for bolted connection should be obtained by Eq. (10.25). The factor ρ that accounts for the available overstrength of the system is not included since the mentioned overstrength is generated apart from the brace and it will not affect the connection.

Table 10.18: Bolted connection design

Storey	$N_{pl,Rd}$ (kN)	$N_{con,Ed}$ (kN)	Bolt diameter /grade	Plate thickness (mm) / steel grade	Bolt shear resistance (kN)	Plate bearing resistance (kN)	Utilization factor
1	595.3	818.5	M48 / 8.8	22 / S235	1389	912	0.897
2	335.7	461.6	M36 / 8.8	20 / S235	781	622	0.742

$$N_{con,Ed} = 1.1\gamma_{OV} N_{pl,Rd} = 1.375 N_{pl,Rd} \quad \text{Eq. (10.25)}$$

The braces are connected to the gusset plate by means of fit bolts. In order to provide some erection tolerances, the connection between the gusset plate and the column are designed by full penetration field welds. The final design of the joints between the braces and the floor beam and the braces and column bases are illustrated in Figure 10.9.

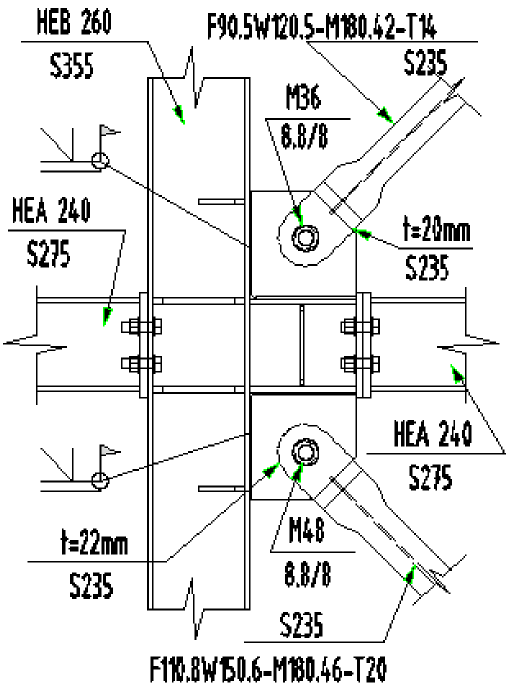

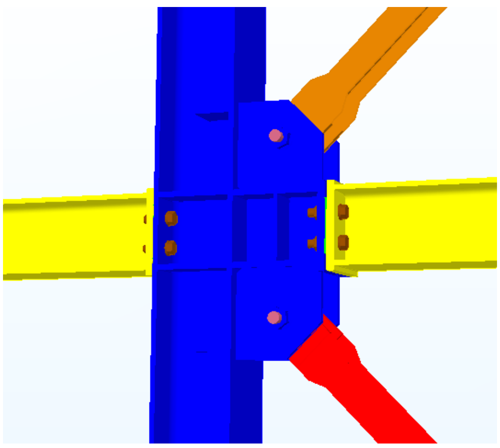

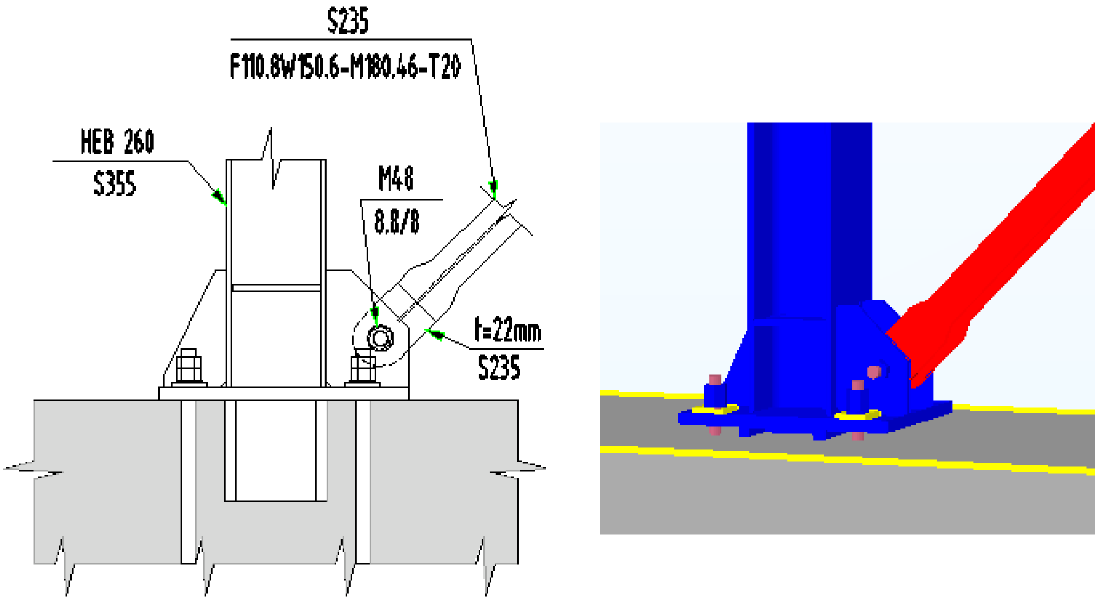

Figure 10.9: Overview of CBF-MB joints

10.6 REFERENCES

[1] Eurocode 8: Design of structures for earthquake resistance - Part 1: General rules, seismic actions and rules for buildings; EN 1998-1:2004.

[2] Hot rolled products of structural steels – Part 2: Technical delivery conditions for non-alloy structural steels; EN 10025-2:2001.

[3] EN1993-1-1, Eurocode 3: Design of steel structures - Part 1-1: General rules and rules for buildings. Brussels: Comitee Europeen de Normalisation (CEN); 2005.

[4] EN1993-1-8, Eurocode 3: Design of steel structures - Part 1-8: Design of Joints. Brussels: Comitee Europeen de Normalisation (CEN); 2005.

[5] Georgiev Tzv., Zhelev D., Raycheva L., Rangelov N.," INNOSEIS - Valorization of innovative anti-seismic devices", WORK PACKAGE 1 – DELIVERABLE 1.1, Volume with information brochures for 12 innovative devices in English, European Commission Research Programme of the Research Fund for Coal and Steel, (Article in Press).

[6] Georgiev Tzv., Rangelov N., Raycheva L., Raykov St., INNOSEIS - Valorization of innovative anti-seismic devices", WORK PACKAGE 3 – DELIVERABLE 3.2, Volume with pre-normative design guidelines for innovative devices, European Commission Research Programme of the Research Fund for Coal and Steel, (Article in Press).

[7] Fajfar P., Kreslin M., "Modelling and Analysis, Chapter 4 of EC8-1", EUROCODE 8 Background and Applications, Dissemination of information for training – Lisbon, 10-11 February 2011.

[8] SAP2000, CSI, Computers and Structures Inc., www.csiberkeley.com.

[9] Tzvetan Georgiev, „Improvement of X-CBF hysteresis behaviour by introduction of MCS", 8th Hellenic National Conference on Steel Structures, Tripoli, Greece, 2-4 October 2014, page 75.

11 SSCD

11.1 GENERAL

11.1.1 Introduction

This case study refers to the seismic design of a new industrial steel building. The building is characterized by the presence of large silos supported by a two storeys braced frame. This chapter aims at demonstrating the design of structures with Steel Self-Centering Devices (SSCDs) placed as bracing elements.

The first part of this documents (Chapter 11.1) describes the geometry and characteristics of the building assumed as case study. Then the second part (Chapter 11.2) presents the global design approach and the application to the case study of buildings equipped with SSCDs, included the dimensioning of the single elements constituting the SSCD.

11.1.2 Description of building

11.1.2.1 Geometry and general assumptions

The case study (see Figure 11.1) is characterized by a large mass placed at high altitude and a concentrically braced supporting structure, where the bracing are realized with SSCDs. The case study has the function of filtering the gasses coming from the steelwork and can be ideally divided into the supporting structure, the silos containing the filtered material and the roof.

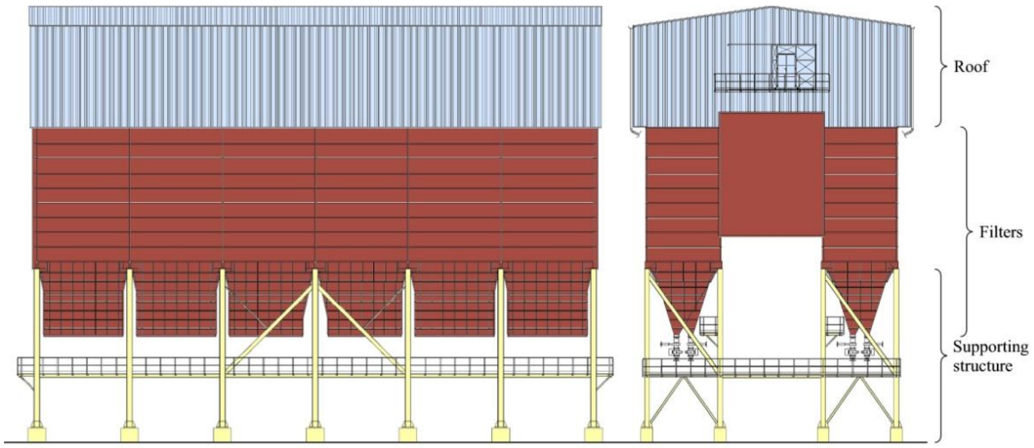

Figure 11.1 Front (left) and lateral side (right) views of the case study

The building has a regular plan, with overall dimensions 37.80 m x 16.94 m and total height 29.64m. The supporting structure, with a total height of about 10.80 m, has six bays in the longitudinal direction and three in the transversal one. The silos are realized with thin (4 mm) walls stiffened with a close series of horizontal UPN and vertical HEA profiles. The total mass of the silo (23700 kN), considering the structural elements and the infill material, represents the 86% of the total mass (27650 kN).

11.1.3 Materials

Steel grade S275 is used for the design of the gravity frame (non-dissipative elements). Different materials are adopted for the several elements of the SSCD:

- the Skeleton elements (external carter, internal sliding frame, end plates and the piston) are realized with S355 grade steel.
- the Dissipative Elements are realized with a particular high ductility/low yield strength steel, whose main mechanical characteristics are: ε_{max} (maximum elongation capacity) >20%; f_{ym} (average yield strength)= 240 N/mm^2 [1].
- The Pretension Elements are realized with aramid tendons characterized by an elastic modulus E_{PTE} of 83000 MPa and a yield strength f_{yPTE} of 3600 MPa [2].

11.1.3.1 Loads and load combinations

Table 11.1 summarizes the adopted gravity loads and seismic action parameters. The action of the wind is neglected, considering that it is not combined with the seismic action, whose value is several times greater due to the large mass of the building.

Table 11.1 Loads and actions

Vertical loads	
Roof self weight External cladding	0.30 kN/m^2 0.30 kN/m^2
Imposed loads 1st floor of the supporting structure: Imposed loads roof:	0.50 kN/m^2 0.50 kN/m^2
Dust self weight	2.69 kN/m^3
Seismic action	
Design response spectrum	Type 1
Reference peak ground acceleration	$a_{g,R}$ = 0.30g
Importance class II (Ordinary building)	γ_I = 1.0
Ground type	B (S=1.2, T_B = 0.15 s, T_C = 0.50 s, T_D = 2.0 s)
Damping ratio	5%

The seismic masses are calculated according to Eq. (11.1).

$$\sum_{j>1} G_{k,j} + \sum_{i>1} \psi_{E,i} . Q_{k,i} \qquad \text{Eq. (11.1)}$$

11.2 DESIGN APPROACH

11.2.1 General design approach

The design procedure proposed hereafter is based on the Capacity Spectrum Method (CSM) proposed by ATC-40 [3]. In fact, this method is able to take into account the dissipative capacity associated to hysteretic shapes different from the classic "elasto-plastic".

The main difficult, indeed, in the design of a structure equipped with SSCDs with respect to traditional elasto-plastic hysteretic device, is the peculiar shape of the hysteretic loops, governed by the re-centering factor β, see Figure 11.2.

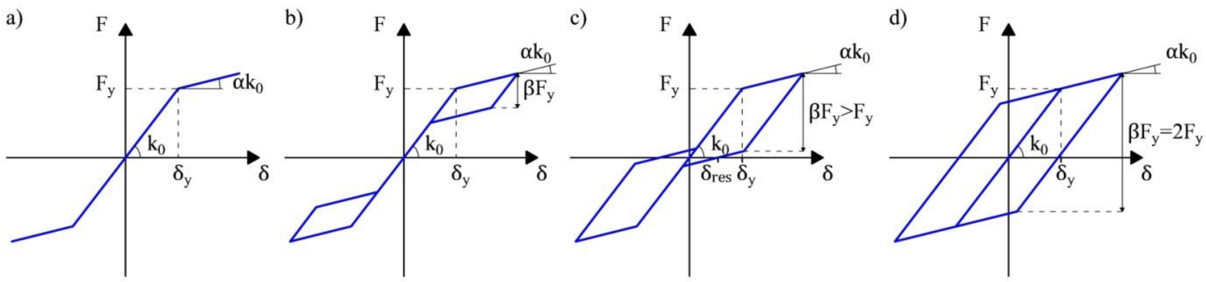

Figure 11.2 Idealized flag-shaped hysteretic curve: a) β = 0 (no dissipation), b) 0 < β < 1; c) 1<β< 2; and d) β = 2

The procedure for the design of the case study equipped with SSCDs can be resumed in the following steps:

1. Individuation of the frames where the SSCDs can be introduced. This choice is influenced on several factors such as architectural or functionality issues, etc.
2. Determination of the initial stiffness and yielding force of the SSCDs.
3. Assessment of the performances of the designed structure assuming a re-centering factor β = 1 through the capacity spectrum method.
4. Case A): If the checks are satisfied, the characteristics of the SSCDs can be optimized (reducing β, in order to guarantee a better re-centering capacity, reducing the number of SSCDs, etc.).
   Case B): If the checks are not verified, the re-centering factor β or the number of the SSCDs shall be increased until the performances are considered satisfactory.

<u>Step 1. Individuation of the frames where the SSCDs can be introduced</u>

The choice of the SSCDs position is usually made on the base of the structural configuration and functionality issue (especially for industrial buildings). For the case study, the disposition of the bracings is resumed in Figure 11.3, reproducing the typical configuration of similar industrial buildings. Within this document, only the design of SSCDs on the longitudinal (X) direction will be carried out. The design of the devices in the transversal (Y) direction follows the same approach.

a)

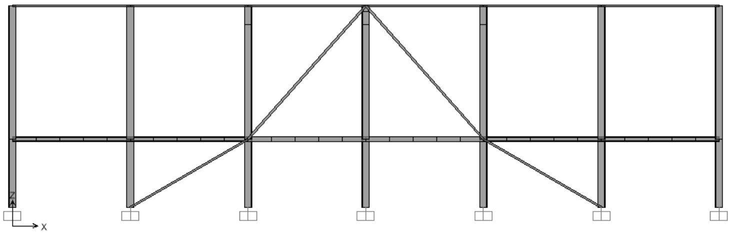

b)

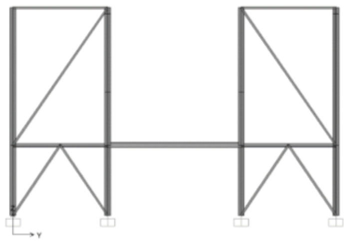

Figure 11.3 Disposition of the SSCDs in the a) longitudinal, X, and b) transversal, Y, directions.

Step 2. Determination of the initial stiffness and yielding force of the SSCDs.

The primary objective of the SSCDs is to assure the required safety level to the whole structure and to limit, as much as possible, the damage to the gravity structure and to the content of the building in order to avoid collapses and the interruption of activities. With reference to Figure 11.2, the SSCD characteristics to be defined are:

- the initial stiffness, k_0;
- the yielding force, F_y;
- the post-elastic stiffness, k_h;
- the re-centering factor, β.

For the considered device, the parameters are not completely independent one from the other, e.g. the post elastic stiffness mainly depends on the pre-tensioning cables stiffness that influence also the initial stiffness and the yielding force.
Considering the primary goal of protecting the gravity structure and its content (including eventual human lives) and also considering that, until now, no reliable design method for the retrofitting adopting self-centering devices such as the

SSCD exists, three main issues or "limitations" were considered during the dimensioning of the SSCDs:

1. The SSCDs should not transmit actions greater than the capacity of the steel members of the frame in which the device is inserted (avoiding so the buckling or yielding of the beams and columns).
2. The interstorey drifts should be compatible with the SSCD maximum elongation capacity.
3. The whole gravity structure and the non-structural elements should be protected thus avoiding heavy damage related to the excessive horizontal displacements.

The limitation "1" can be quantified evaluating the axial, shear or flexural resistance of the elements connected to the SSCDs and the maximum force transmitted by the SSCDs themselves should be lower than such resistance. The limitation "2" depends on the geometrical and mechanical characteristics of the SSCDs adopted in the retrofit. The limitation "3" depends on the desired degree of protection of the gravity structure and of non-structural elements.
These three limitations can be so represented as a force (limitation 1) and displacement (limitations 2 and 3) constraints. Figure 11.4a schematically represents such limitations in a Force-Displacement plane, where it is arbitrarily assumed that the limitation 2 is more strict that the limitation 3. The configuration of the SSCDs characteristics that respect these limitation are theoretically infinite, considering that the parameter k_0, k_h and F_y are, to certain degree, independent, as schematically shown in Figure 11.4b. .

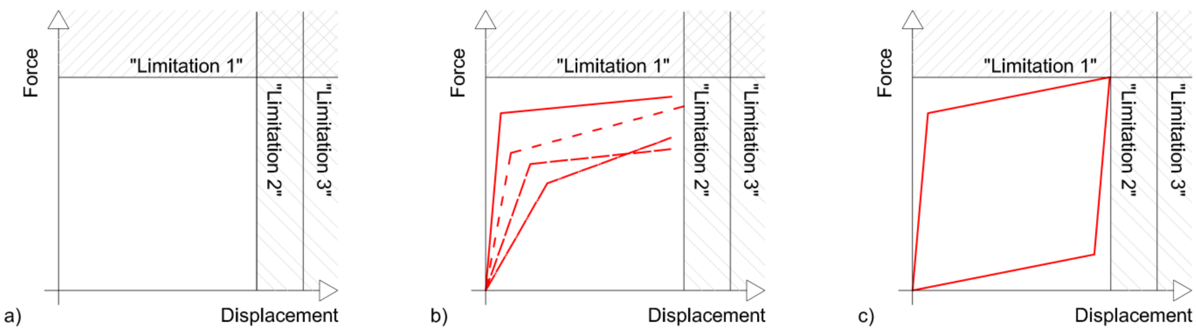

Figure 11.4 Representation, on the force-displacement plane, of the a) design limitations, b) of the possible monotonic SSCD behaviors and c) the assumed force displacement curve of SSCDs for the reference configuration

<u>Step 3. Assessment of the performances of the designed structure assuming a re-centering factor β = 1 through the capacity spectrum method</u>

Once the hysteretic behavior of all the SSCDs is defined (see Step 2), the assessment of the global behavior shall be carried out adopting the Capacity Spectrum method (see the next paragraph).

<u>Step4. Evaluation of the structural performance and eventual re-design</u>

In the case which the assessment carried out in Step 3 shows an ample structural capacity, meaning that the SSCDs characteristics can be optimized, a re-design can be carried out.
The first option is to reduce the β factor, maintaining all the other parameters. In this way only the dissipative capacity and the re-centering capability are affected (the former reduced and the latter increased) and the calculation is straight-forward.
In the case in which also for low values of β (around 0.4 - 0.5) the assessment checks are satisfied, the possibility of reducing the SSCDs number or modifying the characteristics of each SSCD can be taken into account.

Capacity Spectrum Method

The Capacity Spectrum Method is based on the determination of the performance point of the building, representing the intersection between the capacity spectrum of the system (elaborated through the execution of pushover analysis) and the seismic demand represented in an acceleration/displacement plane (acceleration displacement response spectra - ADRS) and opportunely reduced to take into consideration dissipation of energy. The performance point represents the condition in which the seismic capacity of the building is estimated to be equivalent to the seismic demand.
In order to shift the traditional response spectrum (in terms of spectral acceleration S_a vs. period T) into the ADRS plane and to evaluate the spectral displacement S_{di} (being T_i the period of the building) the following relationship can be used:

$$S_{di} = \frac{T_i^2}{4\pi^2} \cdot S_{ai} g \qquad \text{Eq. (11.2)}$$

In order to convert the capacity curve of the system in the capacity spectrum, a punctual transformation is needed. Each single point (F_b – base shear vs. d_c – displacement of the control point) is translated into a (S_{di}, S_{ai}) point through the following equations:

$$S_{di} = \frac{d_c}{FP_1 \times \phi_{1,c}} \quad \text{and} \quad S_{ai} = \frac{F_b}{W} \cdot \frac{1}{\alpha_1} \qquad \text{Eq. (11.3)}$$

Being α_1 and FP_1 the modal mass coefficient and the participating factor for the first vibration mode, while $\phi_{1,c}$ is the amplitude of the control point for the first vibration mode. After the representation of the two diagrams in the same ADRS plane, a preliminary performance point (d_{pi}, a_{pi}) is selected on the base of the equivalent displacement approach.

A bilinear representation of the capacity curve can be used, with the first branch characterized by the same slope of the elastic branch of the capacity curve and the second branch defined in order to have the energy dissipation equivalence (Figure 11.5a).

The Spectral Reduction (*SR*) factors shall be then evaluated (Figure 11.5b): the dissipation of seismic energy of the structure in the post-elastic field can be considered as the combination of two parts, a viscous part and an hysteretic part. The hysteretic part is related to the internal area of executed cycles when the maximum base shear is obtained as a function of the displacement d_c.

The hysteretic dissipation can be represented with its equivalent viscous dissipation through the adoption of literature expressions. The equivalent viscous dissipation β_{eq} associated to the maximum displacement d_{pi} can be evaluated according to:

$$S_{di} = \frac{d_c}{FP_1 \times \phi_{1,c}} \quad \text{and} \quad S_{ai} = \frac{F_b}{W} \cdot \frac{1}{\alpha_1} \qquad \text{Eq. (11.4)}$$

$$\beta_{eq} = \beta_0 + 0.05 \quad \text{where} \quad \beta_0 = \frac{1}{4\pi} \frac{E_D}{E_{S0}} \qquad \text{Eq. (11.5)}$$

In which β_0 is the hysteretic dissipation represented as viscous and 0.05 represents the 5% intrinsic viscous dissipation of the structure (constant), E_D is the dissipated energy per cycle and E_{S0} is the maximum energy deformation associated to the same cycle.

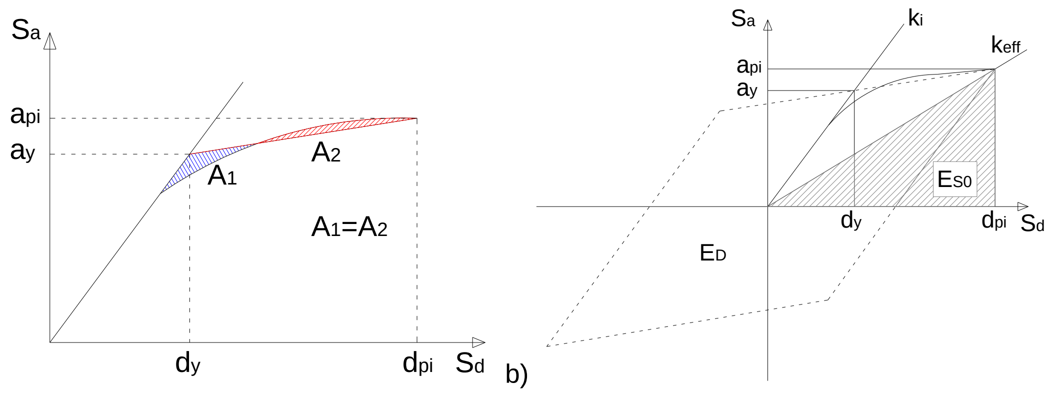

Figure 11.5: a) Bilinear representation for CSM, b) scheme for the evaluation of the spectral reduction factor.

The spectral reduction factors, necessary to evaluate the 5% reduced factor, can be then evaluated according to the following expressions for the reduction of the acceleration and displacement spectra, respectively in the constant acceleration and velocity ranges. Notice that in building code or guidelines such as ATC-40 [3], no spectrum reduction factors are suggested in the constant displacement range. However, this type of structures rarely have periods that fall into constant displacement range. The control of the intersection between the demand and the capacity spectra present in correspondence of point (d_{pi}; a_{pi}) shall be executed (at least controlling if the intersection displacement d_i is within the confidence range $0.95 \cdot d_{pi} \leq d_i \leq 1.05 \cdot d_{pi}$). If there is not intersection between demand and capacity spectra in the confidence interval, a new point (d_{pi}; a_{pi}) shall be selected and the procedure executed again. If the intersection is allowable, the point (d_{pi}; a_{pi}) represents the effective "performance point" (d_p; a_p) where d_p represents the maximum displacement demand attainable.

$$SR_A = \frac{3.21 - 0.68\ln(\beta_{eff})}{2.12} \quad \text{and} \quad SR_V = \frac{2.31 - 0.41\ln(\beta_{eff})}{1.65} \qquad \text{Eq. (11.6)}$$

11.2.2 Application to the case study

The design of the case study (Figure 11.6) equipped with the SSCDs is carried out, only on the longitudinal (X) direction, in the following steps:

- Pre-dimensioning of all the beams considering only static (non-seismic) loads;
- Application of the iterative procedure described in paragraph 11.2.1
- Design of the columns and eventual re-design of the beams involved in the resisting mechanism to seismic actions.

The first and last of such steps involves the traditional checks usually carried out in steel structure, while the application of the procedure described in paragraph 11.2.1 deserves more attention.

Step 1. Pre-dimensioning of all the beams

All the beams of the first storeys are pre-dimensioning considering only vertical static loads. The sections used are HE220A for the beams in transverse direction and HE280A for the longitudinal ones.

Step 2. Determination of the initial stiffness and yielding force of the SSCDs (q=1)

The scheme adopted for the design is resumed in Figure 11.7: all the beams and columns are supposed to be perfectly hinged to the columns. In the reality, columns are hinged at the base and to the silos. However, by considering a perfect hinge in each intersection, the design of the SSCDs can be carried out considering a statically determinate resisting mechanism in which the elements are subjected mainly to axial forces. In this scheme, the stress resultants in the element do not depend on the section features of members. Moreover, the top of the structure, characterized by industrial equipment, has not been taken into account in the pre-dimensioning and just the supporting structure is designed.
These assumptions make the design simpler. In fact, the forces in the SSCDs structure, due to seismic actions, can be estimated by manual calculations.

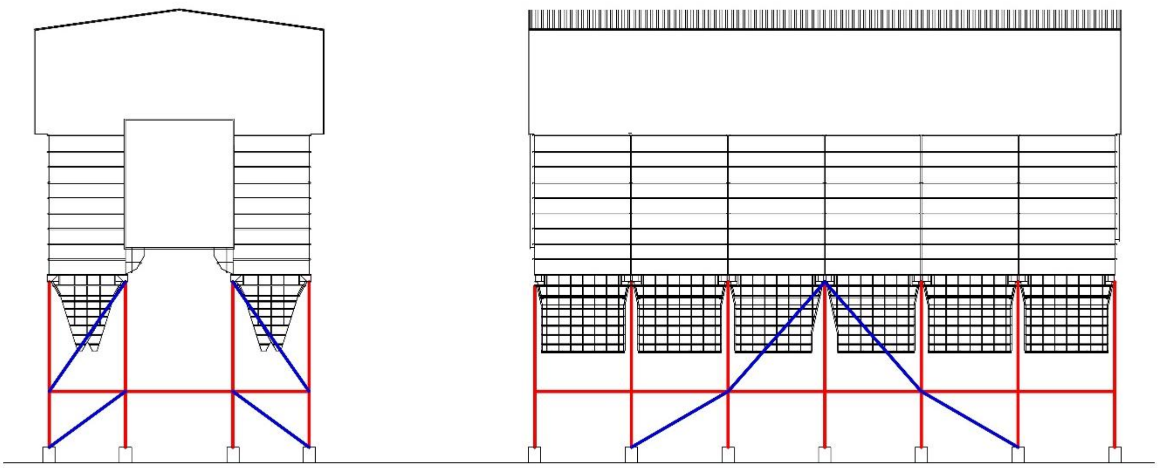

Figure 11.6: Transversal (left) and longitudinal (right) direction of the case study building

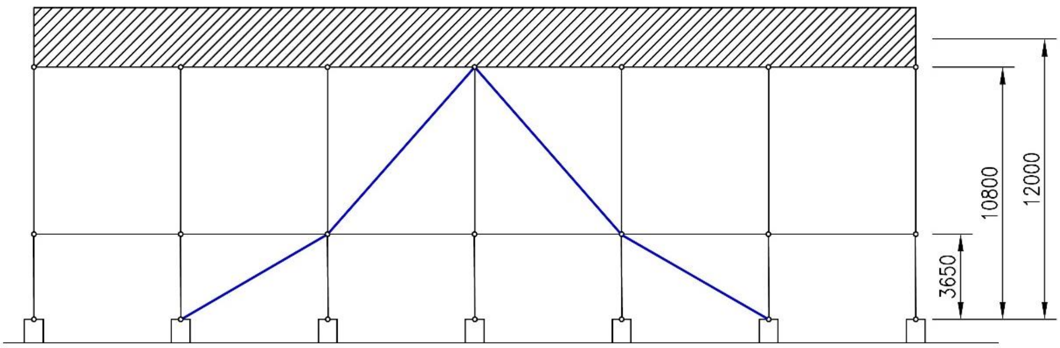

Figure 11.7: Schemes adopted for the design (dimensions are in mm)

The SSCDs are designed by considering the resulting base shear and the maximum deformation of the devices. The base shear is derived from the seismic weight of the structure and the maximum spectral acceleration, corresponding to the constant acceleration range. The response spectrum, related to the ultimate limit state, should be reduced by a suitable behaviour factor q in order to account the over-strength and ductility of the system while designing the structure in the linear range. However, behaviour factors are not defined for re-centering systems. Thus, it is possible to start the pre-dimensioning considering an elastic behaviour and then repeat the calculations in the end of the procedure described in paragraph 11.2.1.

The case study building has a weight equal to 30000 kN in seismic combination and the maximum acceleration of the response spectrum (Figure 11.8) is equal to 0.9 g. The base shear is thus 27000 kN and, taking into account 8 couples of SSCDs, the shear related to each system is 3375 kN. The maximum forces in the devices can be easily defined on the base of the geometry of the structure.

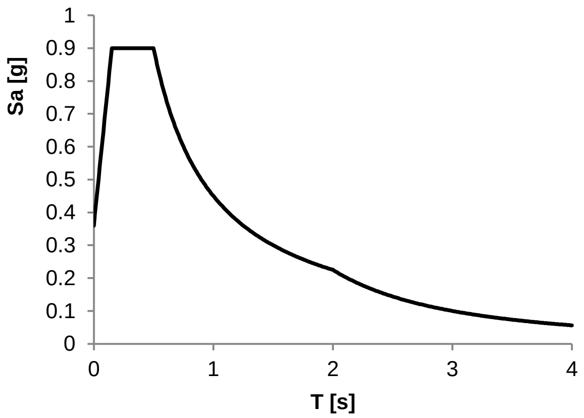

Figure 11.8: Ultimate Limit State response spectrum (Eurocode 8 Type 1 spectrum q=1)

The maximum displacement have to be calculated considering the yielding elongation of the cables, pre-tensioned with a force equal to the 50% of the yielding force, with the following formula:

$$\Delta L_{MAX} = (1 - \rho_{PTE}) \frac{f_{yPTE}}{E_{PTE}} L_{PTE} \qquad \text{Eq. (11.7)}$$

Where:
L_{PTE} = 0.8 L_{SSCD} is the cable length;
ρ_{PTES}= 0.50 is the cable pre-tensioning factor;
f_{yPTE} = 3600 MPa is the cable tensile strength;
E_{PTE} = 83000 MPa is the cable tensile modulus.

Starting to the maximum force and displacement, the others characteristics of the SSCD behaviour are defined in function of the following parameters:

- Cables diameter (considering Kevlar-29 cables [2], tensile modulus 83000 MPa, tensile strength 3600 MPa, tensile elongation 4.0%), which affects:
  - The post-elastic stiffness, corresponding to the cables elastic stiffness;
  - The yielding force, provide by the yielding force of the dissipative elements and by the total cables pre-tensioning force. This condition only occurs when the yield of the dissipative elements occurs at the same time as the overload of the pre-tensioning force in the cables is reached. Although this condition is difficult to verify, we can consider this simplification for an immediate dimensioning of the elements.
- Dissipative elements area and material, which affect the yielding force, as previously mentioned.

To ensure the re-centering of the system, the total pre-tensioning force of the cables has to be higher than the total yielding force of the dissipative elements. Otherwise, the cables cannot cause recenter the system, yielding back in compression the dissipative elements when the external load drops to zero. Thus, the SSCD yielding force has to be lower than two times the total pre-tensioning cables force.

This latter limitation, combined with the maximum force in the device, leads to the pre-dimensioning of the cables. Then, once the SSCD behaviour has been defined (Figure 11.9), the area and material of the dissipative elements can be chosen to provide the requested SSCD yielding force.

In this procedure, the SSCD initial stiffness is defined “a priori” because it mainly depends on the characteristic of the carter and others non-dissipative elements.

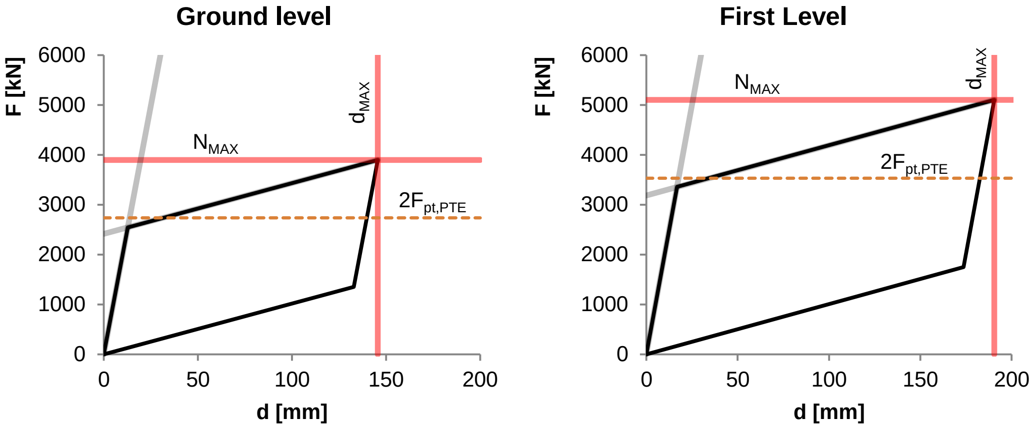

	$N_{MAX,SSCD}$ [kN]	D_{PTE} [mm]	n_{PTE}	$\Delta L_{MAX,SSCD}$ [mm]	$F_{y,PTE}$ [kN]	$F_{pt,PTE}$ [kN]	A_{DE} [mm²]	n_{DE}	$F_{y,DE}$ [kN]	$d_{y,SSCD}$ [mm]	$F_{y,SSCD}$ [kN]	$K_{0,SSCD}$ [kN/mm]	$K_{h,SSCD}$ [kN/mm]
Ground Level	3901	22	2	146	2736	1368	368	8	1178	13	2546	200	10
First Level	5105	25	2	191	3533	1766	497	8	1591	17	3358	200	10

Figure 11.9: Definition of the SSCDs behaviour parameters

<u>Step 3. Assessment of the performances of the designed structure assuming a re-centering factor β = 1 through the capacity spectrum method</u>

Once the hysteretic behavior of all the SSCDs is defined, the assessment of the global behavior shall be carried out adopting the Capacity Spectrum method. The first requirement is the definition of the global pushover curve (Figure 11.10), starting to the SSCDs behavior.

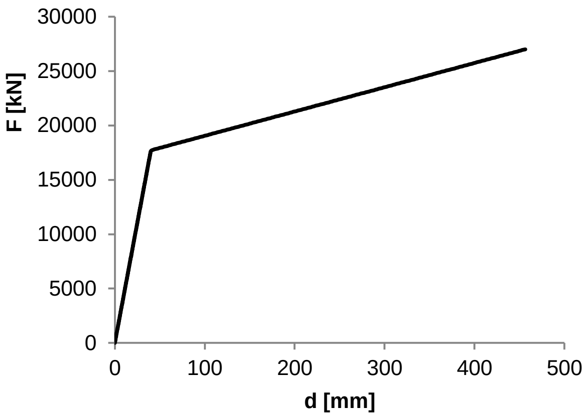

Figure 11.10: Pushover curve of the structure (q=1)

The equivalent viscous dissipation β_{eq} associated to the maximum displacement d_{pi} can be now evaluated, according to the following formulas:

$$\beta_{eq} = \beta_0 + 0.05 \text{ where } \beta_0 = \frac{1}{4\pi}\frac{E_D}{E_{S0}} \quad \text{Eq. (11.8)}$$

In which β_0 is the hysteretic dissipation represented as viscous and 0.05 represents the 5% intrinsic viscous dissipation of the structure (constant), E_D is the dissipated energy per cycle and E_{S0} is the maximum energy deformation associated to the same cycle. Considering the SSCD behaviour with a re-centering factor equal to 1 (see Figure 11.11), the energy components for each device are defined with the following formulas:

$$E_D = 2\cdot\left(F_Y\cdot\delta_u - F_u\cdot\delta_y\right) \text{ and } E_{S,0} = \frac{F_u\cdot\delta_u}{2} \quad \text{Eq. (11.9)}$$

$$\beta eq = \beta_0 + 0.05 = \frac{1}{4\pi}\frac{E_D}{E_{S0}} + 0.05 = 0.23 \quad \text{Eq. (11.10)}$$

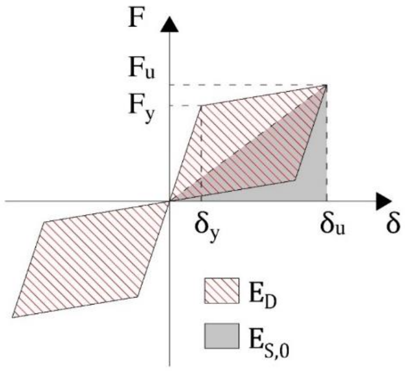

Figure 11.11: Energy components of a Re-centering system with β equal to 1

The reduction factors are calculated with previously defined formulas:

$$SR_A = \frac{3.21 - 0.68\ln(\beta_{eq})}{2.12} = 1.984 \quad \text{Eq. (11.11)}$$

$$SR_V = \frac{2.31 - 0.41\ln(\beta_{eq})}{1.65} = 1.764 \quad \text{Eq. (11.12)}$$

In Figure 11.12 is represented the comparison between pushover curve and reduced response spectrum.

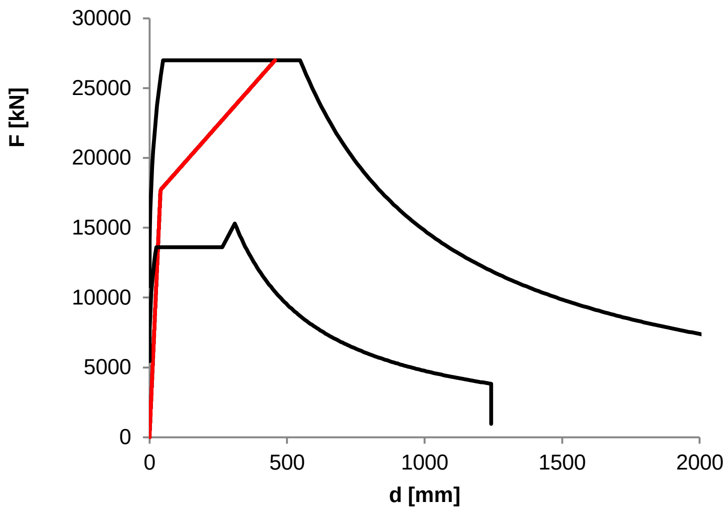

Figure 11.12: Comparison between pushover curve and ADRS reduced response spectrum

Considering the results, the devices have been redesigned through the Step 2 by using a reduction factor RF of 2.

Step 2-bis. Determination of the initial stiffness and yielding force of the SSCDs (RF =2)

The maximum acceleration of the response spectrum, considering a behaviour factor equal to two is 0.9 g. The base shear is thus 13500 kN and the shear associated with each system is 1687.5 kN. The maximum displacements are no subject to change. The new behaviours are represented in Figure 11.13

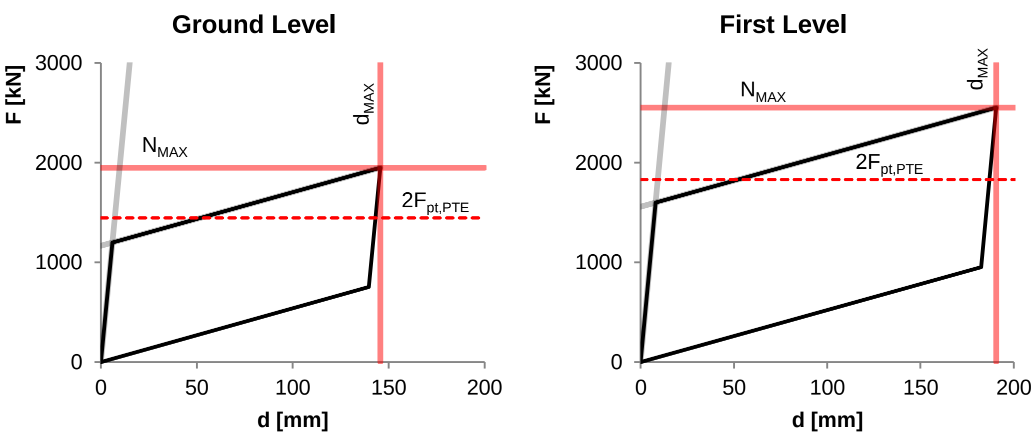

	$N_{MAX,SSCD}$	D_{PTE}	n_{PTE}	$\Delta L_{MAX,SSCD}$	$F_{y,PTE}$	$F_{pt,PTE}$	A_{DE}	n_{DE}	$F_{y,DE}$	$d_{y,SSCD}$	$F_{y,SSCD}$	$K_{0,SSCD}$	$K_{h,SSCD}$
	[kN]	[mm]		[mm]	[kN]	[kN]	[mm²]		[kN]	[mm]	[kN]	[kN/mm]	[kN/mm]
Ground Level	1950	16	2	146	1447	723	148	8	474	6	1198	200	5.4
First Level	2553	18	2	191	1831	916	214	8	685	8	1601	200	5.2

Figure 11.13: Definition of the SSCDs behaviour: a) ground level, b) first level (RF =2)

<u>Step 3-bis. Assessment of the performances of the designed structure assuming a re-centering factor β = 1 through the capacity spectrum method</u>

The new pushover curve is represented in Figure 11.14.

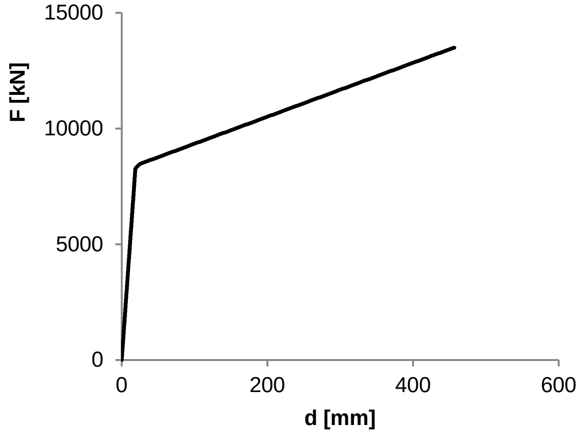

Figure 11.14: Pushover curve of the structure (RF=2)

The equivalent viscous dissipation β_{eq} associated to the maximum displacement d_{pi} can be now re-evaluated:

$$\beta eq = \beta_0 + 0.05 = \frac{1}{4\pi}\frac{E_D}{E_{S0}} + 0.05 = 0.235 \quad \text{Eq. (11.13)}$$

The reduction factors are re-calculated with previously defined formulas:

$$SR_A = \frac{3.21 - 0.68\ln(\beta_{eq})}{2.12} = 1.979 \quad \text{Eq. (11.14)}$$

$$SR_V = \frac{2.31 - 0.41\ln(\beta_{eq})}{1.65} = 1.760 \quad \text{Eq. (11.15)}$$

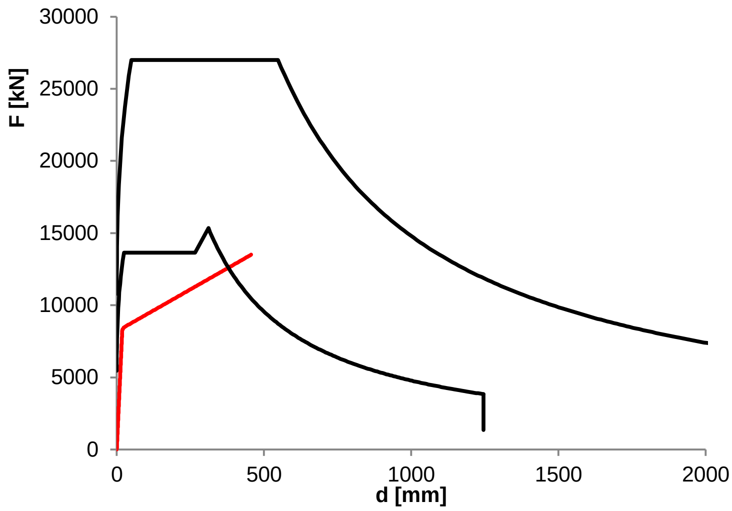

Figure 11.15: New comparison between pushover curve and the reduced response spectrum

Figure 11.15 shows the comparison between the new pushover curve and the new reduced response spectrum.

Considering the satisfying comparison, the devices characteristics are not re-valuated. The performance point has been found in an additional step by reducing the maximum displacement from 457 to 386 mm and then re-calculating the reduction factors:

$$\beta eq = \beta_0 + 0.05 = \frac{1}{4\pi}\frac{E_D}{E_{S0}} + 0.05 = 0.232 \quad \text{Eq. (11.16)}$$

$$SR_A = \frac{3.21 - 0.68\ln(\beta_{eq})}{2.12} = 1.982 \quad \text{Eq. (11.17)}$$

$$SR_V = \frac{2.31 - 0.41\ln(\beta_{eq})}{1.65} = 1.763 \quad \text{Eq. (11.18)}$$

Due to an homogeneity reduction of the two energy components involved in the equivalent viscous dissipation, in case of reduction of the maximum displacement, the new reduction factors are very close to the previously calculated. In Figure 11.16 is represented the new reduced response spectrum with the obtained Performance Point.

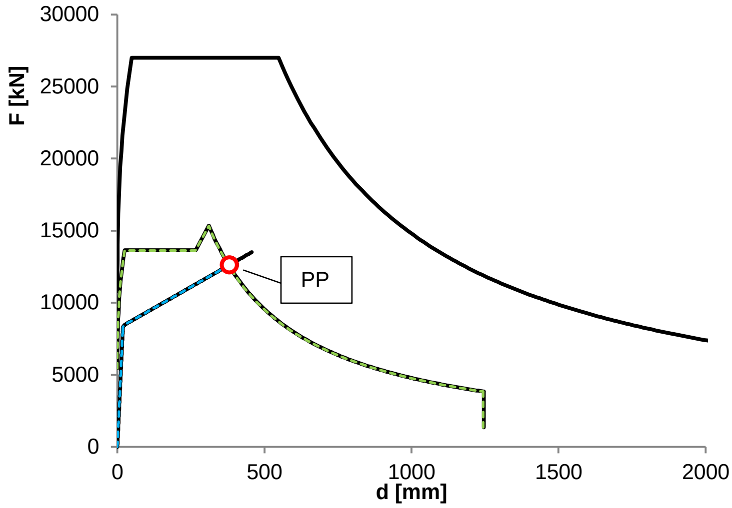

Maximum Displacement **386 mm**

Maximum Base Shear **12680 kN**

Figure 11.16: Performance Point definition

Step 4. Design of the columns and assessment of the beams involved in the resisting mechanism to seismic actions.

Taking into account the performance point, columns are designed and assessed for axial loads. The forces are calculated by combining the effects of gravity loads with those of the seismic action incremented by the material and geometric over-strength factors of the ductile elements. Axial forces, in compression, are calculated with the usual following formula:

$$N_{Ed} = N_{Ed,G} + 1.1 \cdot \gamma_{ov} \cdot \Omega \cdot N_{Ed,E} \qquad \text{Eq. (11.19)}$$

where for Ω a value of 1 can be assumed.

The verification in compression, considering buckling phenomena, has led to HE280B section for the columns.

Step 5. Design of the SSCDs connections

The design of the connections is performed with the following formula, suggested by Eurocode 8, part 1 (EN 1998-1:2013 paragraph 6.5.5):

$$R_d \geq 1.1 \cdot \gamma_{ov} \cdot N_{MAX} \qquad \text{Eq. (11.20)}$$

where the over-strength coefficient, of the connected SSCDs, γ_{ov} is equal to 1.25.

Finally, in Figure 11.17 and 11.18, are reported respectively a general view of the longitudinal designed frames and the details of the designed connections.

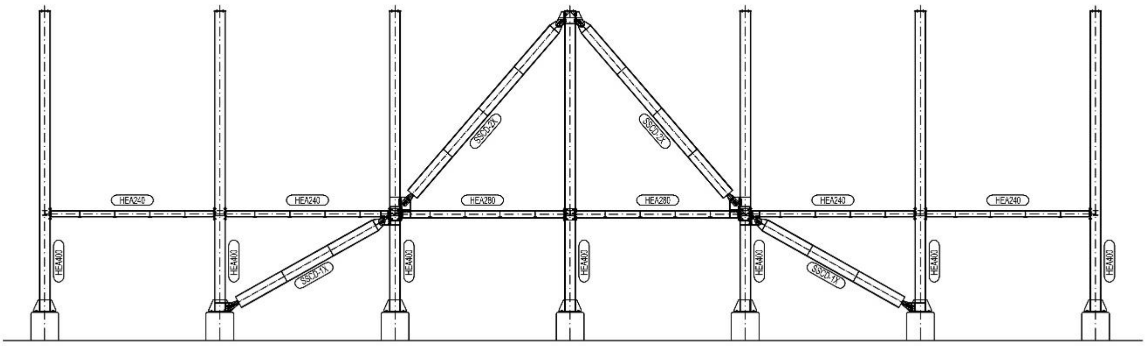

Figure 11.17: Longitudinal view of the designed supporting structure

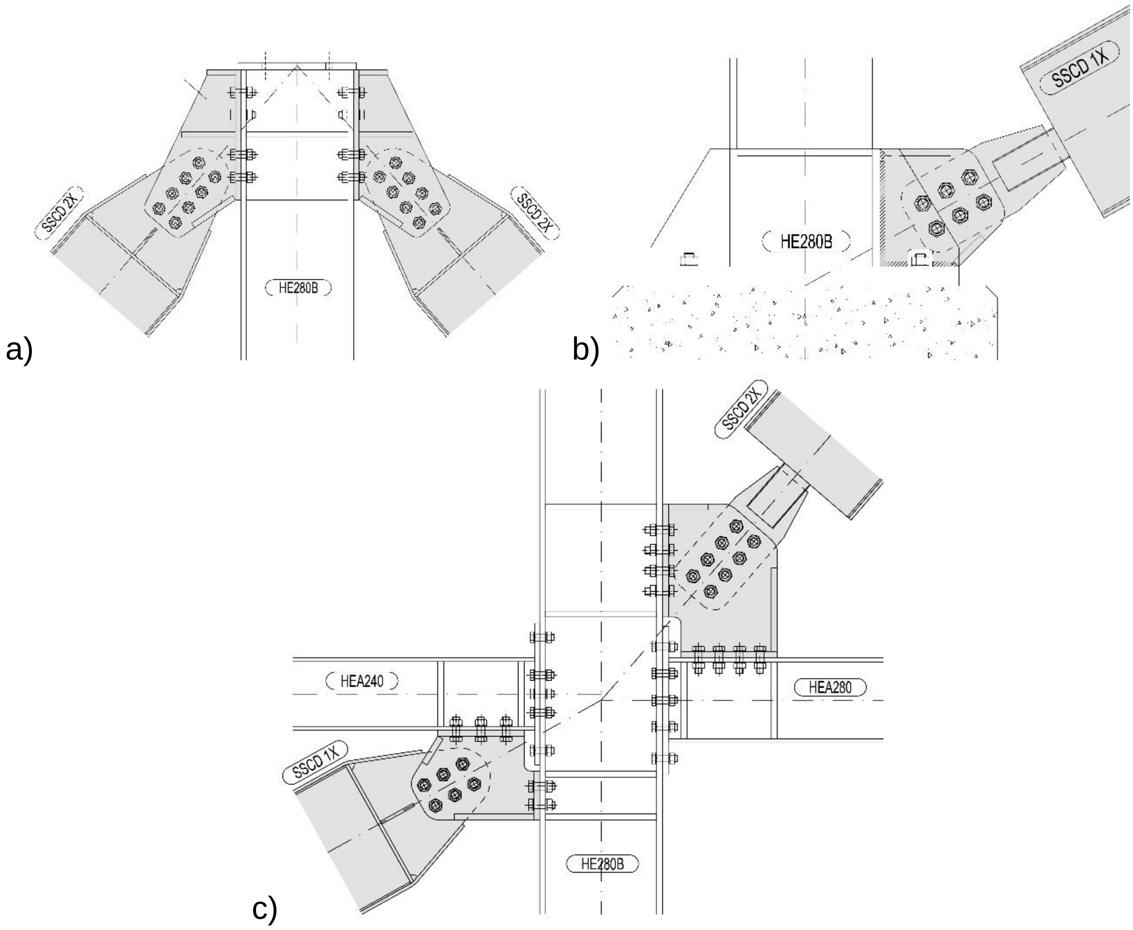

Figure 11.18: SSCDs connections: a) top of the column, b) base of the column and c) first storey

11.3 REFERENCES

[1] Braconi, A., Morelli, F., Salvatore, W., (2012), "Development, design and experimental validation of a steel self-centering device (SSCD) for seismic protection of buildings". Bulletin of Earthquake Engineering, 10 (6), 1915 – 1941.

[2] Christopoulos C., Tremblay R., Kim H.-J., Lacerte M., (2008), "Self-Centering Energy Dissipative Bracing System for the Seismic Resistance of Structures: Development and

Validation", Journal of Structural Engineering 134 (2008) 96–107. doi:10.1061/(ASCE)0733-9445(2008)134:1(96).

[3] ATC-40 Seismic Evaluation and Retrofit of Concrete Buildings Volume 1 by APPLIED TECHNOLOGY COUNCIL 555 Twin Dolphin Drive, Suite 550 Redwood City, California 94065

12 TRSH

12.1 INTRODUCTION

In the present study, a specific design procedure for the implementation of TRiangular Shaped Hysteretic (TRSH) devices in “V-bracing” systems of multi-story steel structures is proposed and applied to a low-rise (2 storeys) case-study building located in a moderate seismic area (PGA=0.20g). In particular, since TRSH elements are categorized as anti-seismic devices, the EN 1993-1 (CEN, 2005-1) and EN 1998-1 (CEN, 2005-2) performance requirements are slightly modified in order to accomplish also EN 15129 (CEN, 2009) provisions. Moreover, the identified solution, thanks to an optimized layout of the TRSH devices, is shown to ensure a complete protection of the case-study structure during the seismic excitation.

12.2 DESIGN RULES

The philosophy behind the proposed design procedure aims at pursuing two main goals: (1) during the seismic excitation, the main structure (beams and columns) remain in the elastic range; (2) yielding and dissipation mechanisms occur only in TRSH elements (that are easily replaceable).

12.2.1 General

The design methodology, described in the following, is based on the provisions of EN 1993-1 (CEN, 2005-1), EN 1998-1 (CEN, 2005-2), and EN 15129 (CEN, 2009). In particular, some clauses of EN 1998-1-1 are appropriately rearranged to cover also the provisions given in EN 15129.

The proposed procedure consists of two steps: (1) a preliminary structural layout is defined by means of a simple analytical calculation, i.e. equivalent lateral loads method; (2) a linear multimodal response spectrum analysis is carried out in order to assess the suitability of the proposed structural layout against the EN 1998-1 performance requirements (the final solution is usually identified iteratively). Two different approaches can be adopted for the second step:

1. multimodal response spectrum analysis with consideration of the elastic stiffness k_1 of the TRSH devices and an appropriate q-factor;
2. multimodal response spectrum analysis with consideration of the equivalent stiffness k_{eff} of the TRSH devices with an appropriate q-factor.

In the following the structural design taken into account the first approach is shown.
It is worth noting that for a more accurate design, the EN 15129 strongly recommends to perform nonlinear time-history analyses, when the equivalent damping ratio related to hysteretic energy dissipation is higher than 15 %.

12.2.2 Preliminary Design

Assuming that the gravitational loads at Ultimate Limit States (ULS) combination $(1.3G_1 + 1.5G_2 + 1.5Q)$ are entrusted to the main frame (beams and columns), at each story level of the building, the TRSH bracing system is preliminary designed in order to withstand alone the overall lateral seismic load. In this regard, according to EN 1998-1 (§ 4.3.3.2.2 - 4.3.3.2.3, CEN, 2005-2), a rough approximation of the lateral seismic load (inertia force) acting at the i-th floor level F_i can be obtained from a simple analytical calculation (equivalent lateral loads method):

$$F_i = F_b \cdot \frac{z_i \cdot m_i}{\sum z_j \cdot m_j} \qquad \text{Eq. (12.1)}$$

where:

$F_b = S_a(T_1) \cdot m \cdot \lambda$	seismic base-shear;
$S_a(T_1) = (\frac{1}{q}) \cdot S_{ae}(T_1)$	inelastic spectrum;
$S_{ae}(T_1)$	reference elastic spectrum;
$q = 3.0$	assumed behavior factor;
$T_1 = C_t \cdot H^{3/4}$	fundamental period of the building.

Once known the inertia forces F_i, the shear load acting at the base of column elements at each story level $F_{b,i}$ can be calculated (sum of inertia forces at upper story levels) and the TRSH device shall be designed in order to accomplish the following verification:

$$F_{Rd,t,i} = n_i \cdot F_{y,t,i} \geq \gamma_x \cdot \gamma_b \cdot F_{b,i} \qquad \text{Eq. (12.2)}$$

where $F_{Rd,t,i} = n_i \cdot F_{y,t,i}$ is the design resisting force of the TRSH device (being $F_{y,t,i}$, and n_i respectively the yielding force, and the number of triangular elements composing the device). $\gamma_x = 1.2$ is the reliability factor and $\gamma_b = 1.1$ is the partial factor for the device acc. to EN 15129 (CEN, 2009).
In case of a frame with V bracings, it is worth noting that both tension and compression diagonals shall be taken into account and element cross-sections should be chosen in order to fulfill the following checks:

$$N_{Ed,b,i} = \frac{F_{b,i} \cdot cos\alpha}{2} \leq 0.5 \cdot N_{Rd,b,i} \qquad \text{Eq. (12.3)}$$

$$\lambda_{b,i} = \sqrt{A_{b,i} \cdot f_y / N_{cr,b,i}} \leq 2.0 \qquad \text{Eq. (12.4)}$$

where $N_{Ed,b,i}$ is the axial action effect; $N_{Rd,b,i}$, $N_{cr,b,i}$ are respectively the design axial resisting force and the critical bucking load of brace elements; $\lambda_{b,i}$ is the a-dimensional slenderness of the same (2.0 is the limit for "V bracing systems" according to EN 1993-1 (CEN, 2005-1).

12.2.3 Design for linear elastic analysis

12.2.3.1 Multi-modal response spectrum analysis

In the current state of the art, a building with a TRSH bracing system may be simulated with linear-elastic elements with appropriate lateral stiffness (for the calculation of elastic stiffness of TRSH devices see the relevant Information Brochure-INNOSEIS, 2017). Both dissipative and non-dissipative structural elements shall be verified with reference to the seismic load combination ($G_1 + G_2 + \psi Q + E$). In this regard, the conventional method for the calculation of internal forces due to the seismic action (E) is Multi-Modal Response Spectrum Analysis, where the number of vibration modes considered in each direction is such that the sum of the effective mass is at least equal to 85% of the total mass and there are no modes with mass participating > 5%. The design spectrum shall be defined with a maximum behavior factor equal q =3.0, which was obtained from preliminary Pushover analyses (see the Information Brochure-INNOSEIS, 2017).

12.2.3.2 Limitation of interstory drift

Limitation of interstory drift ensures the protection of non-structural elements under seismic loading and consists a basic criterion for the design of TRSH devices. It provides an estimation of the damage for different performance levels and defines the distribution of stiffness within the structure and eventually the size and type of the cross sections applied on the system.

Assuming that the building has ductile non-structural elements the following verification relevant of the maximum interstorey d_r shall be fullfilled:

$$d_r \cdot \mathrm{v} \leq 0.0075 \cdot \mathrm{h} \qquad \text{Eq. (12.5)}$$

where *v =0.5* is a reduction factor on the design displacements due to the importance class of the building (ordinary buildings) and *h* is the story height.

In linear analysis the displacements induced by the design seismic action d_s shall be calculated on the basis of the elastic deformations d_e of the structural system through the expression:

$$d_s = q \cdot d_e \qquad \text{Eq. (12.6)}$$

In case the capacity ratios of the dissipative elements (Ω) are low, the calculation of the design interstory drift based on d_s is conservative and a therefore reduction factor (q_Ω) equal to the capacity ratio of the devices may be employed as follows:

$$d_s = q \cdot q_\Omega \cdot d_e \qquad \text{Eq. (12.7)}$$

The design interstory drift d_r is defined as the difference of the average lateral displacements at the top and bottom of the story under consideration. Depending on the type of the non-structural elements (brittle materials, ductile or not connected) and the importance class of the building, the design interstory drift d_r is compared to the corresponding values of the Code. The optimal design is achieved when the maximum interstory drifts of the structure are close to the limit values. Since the horizontal displacements are multiplied by the behavior factor the limitation of interstory drift does not depend on it.

12.2.3.3 *Second order effects*

The possible influence of 2nd order effects shall be controlled by the limitation of the interstory drift sensitivity coefficient θ below the limit values of the Code. Coefficient θ is calculated as:

$$\theta = \frac{P_{tot} \cdot d_r}{V_{tot} \cdot h_{story}} \qquad \text{Eq. (12.8)}$$

where P_{tot} is the total gravity load at and above the considered story, V_{tot} is the seismic story shear, d_r is the interstorey drift, and h_{story} is the interstorey height.

Alternatively, the interstory drift sensitivity coefficient θ may be calculated more accurately by a linear buckling analysis through the factor α_{cr}, the factor by which the design loading would have to be increased to cause elastic instability in a global mode. The analysis is carried out under conditions of the constant gravity loads of the seismic combination (1,0·G+0,3·φ·Q) and produces the buckling modes. The modes that move the building at x and y directions are chosen and the correspondent α_{cr} values are calculated as follows:

$$\alpha_{cr} = \frac{1}{\theta} = \frac{F_{cr}}{F_{Ed}} \qquad \text{Eq. (12.9)}$$

where F_{cr} is the elastic critical buckling load for global instability mode based on initial elastic stiffnesses and F_{Ed} is the design loading for the seismic combination.
To take into consideration the inelastic displacements of the building, α_{cr} shall be divided by the q factor. The values of θ in this case are:

$$\theta = \frac{q}{\alpha_{cr}} \qquad \text{Eq. (12.10)}$$

The relevant EN1993-1 (CEN, 2005-1) provisions require for buildings that the interstory drift sensitivity coefficient is limited to $\theta \leq 0.1$, if second order effects are ignored. If $0.1 < \theta < 0.2$, second-order effects may approximately be taken into account by multiplying the relevant seismic action effects by a factor equal to $1/(1 - \theta)$. If $0.2 < \theta < 0.3$ a more accurate second order analysis applies. In any case it shall be $\theta < 0.3$.

12.2.3.4 Dissipative elements (TRSH devices)

At each generic i-th story level it shall be verified that the seismic action $F_{Ed,i}$, taking into account $\gamma_x = 1.2$ as reliability factor and $\gamma_b = 1.1$ as partial safety factor for TRSH devices, does not exceed its design resistance $F_{Rd,t,i}$ (see EN 15129, section 4.1.2):

$$F_{Rd,t,i} = n_i \cdot F_{y,t,i} \geq \gamma_b \cdot \gamma_x \cdot F_{Ed,i} \qquad \text{Eq. (12.11)}$$

Moreover, to achieve an uniform dissipative behavior at each storey level, it should be checked that the maximum over-strength ratio Ω of TRSH elements over the entire structure do not differ from the minimum value Ω more than 25%:

$$\frac{max\Omega_i}{min\Omega_i} \leq 1.25 \qquad \text{Eq. (12.12)}$$

where $\Omega_i = (n_i \cdot F_{y,t,i})/F_{Ed,i}$.
In all above checks, in safety favour, upper and lower bound design properties of TRSH devices (provided by the manufacturer) should be considered.

12.2.3.5 Non-dissipative elements

In order to ensure that the yielding occurs only in the TRSH elements, non-dissipative structural members (beams, columns and braces) shall be capacity designed for increased values of internal forces compared to the ones derived from the analyses with the most unfavourable seismic combination:

$$\begin{cases} N_{Rd} \geq N_{Ed,G} + 1{,}1 \cdot \gamma_{ov} \cdot \Omega \cdot N_{Ed,E} \\ M_{Rd} \geq M_{Ed,G} + 1{,}1 \cdot \gamma_{ov} \cdot \Omega \cdot M_{Ed,E} \\ V_{Rd} \geq V_{Ed,G} + 1{,}1 \cdot \gamma_{ov} \cdot \Omega \cdot V_{Ed,E} \end{cases} \quad \text{Eq. (12.13)}$$

where:

- N_{Rd} (M_{Rd}, V_{Rd}) is the axial (bending or shear accordingly) design resistance of the structural element;
- $N_{Ed,G}$ ($M_{Ed,G}$, $V_{Ed,G}$) is the axial (bending or shear accordingly) force acting on the structural element due to the non-seismic actions;
- $N_{Ed,E}$ ($M_{Ed,E}$, $V_{Ed,E}$) is the axial (bending or shear accordingly) force acting on the structural element due to the design seismic action;
- γ_{ov} is the overstrength factor ($\gamma_{ov} = 1{,}25$ for steel S355);
- $\Omega = \min(N_{Rd,i}/N_{Ed,E,i})$ over all the bracing diagonals.

12.3 LOW-RISE CASE-STUDY BUILDING

Equations, element properties, design recommendations, critical checks and proposed behaviour factor (q-factor), included in the Information Brochure (INNOSEIS, 2017)), are verified hereafter through numerical analyses on a 3D low-rise case-studies building equipped with TRSH devices. Both dissipative and non-dissipative elements of the resisting frame are preliminary designed with a simplified analytical procedure (equivalent lateral loads method, see Section 2.2). Eventually a multi-modal response spectrum analysis is carried out and relevant results are verified by means of structural checks prescribed in EN1998 (see Section 2.3) in to in order to assess the suitability of the proposed structural design (the final solution is usually defined iteratively). All numerical analyses are carried out by means of the commercial software SAP2000 v.19 (CSI, 2016).

12.3.1 Description of the building frame

12.3.1.1 Geometry

Both front-view and planar geometries of the considered case-study frame are represented in Figure 12.1.

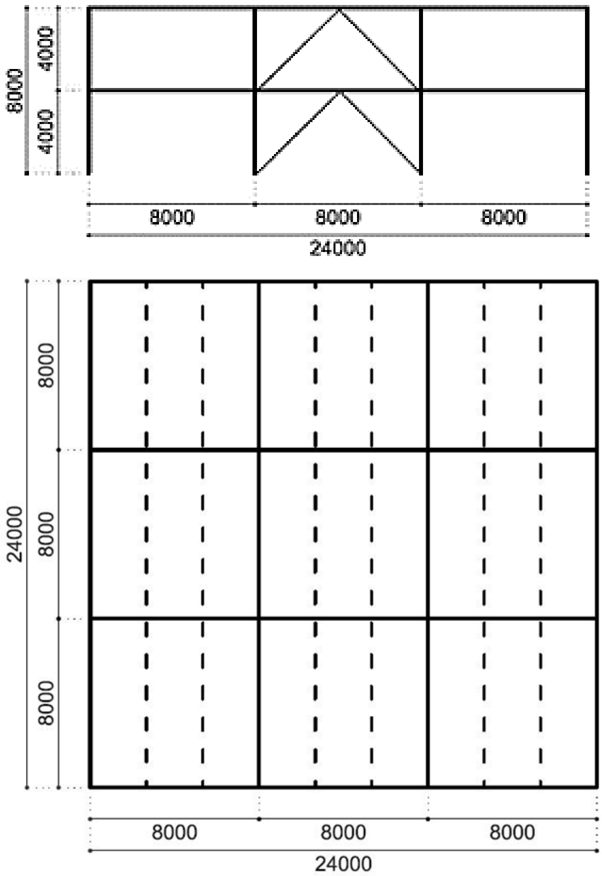

Figure 12.1: Front (up) and planar (down) geometry views of the case-studies building frame, all dimension in [mm]

3.1.2 Load analysis

The following Dead Loads (G) have been assumed in structural calculations:

- steel self-weight: 78.5 kN/m³;
- composite slab: $g_{2,c} = 2.75\,kN/m^2$ (concrete self-weight 25.0 kN/m³, steel sheeting height 73 mm, thickness 1 mm, slab thickness 150 mm, equivalent uniform slab thickness 110 mm);
- services, ceilings, raised floors: $g_{2,if} = 0.70\,kN/m^2$ for intermediate floors, $g_{2,tf} = 1.00\,kN/m^2$ for top floor;
- perimeter walls ($1.00\,kN/m^2$): $g_{2,per} = 4.00\,kN/m$.

Live Loads (q) have been estimated as:

- offices (class B): $q = 3.00\,kN/m^2$
- movable partitions ($\leq 2.00\,kN/m^2$): $q_{add} = 0.80\,kN/m^2$
- total live load: $q_{add} = 3.80\,kN/m^2$
- coeff. for seismic combinations: $\psi_2 = 0.60$
- roof accessible and snow load neglected.

Seismic Loads (E) have been defined through the EN1998 reference elastic spectrum assuming:

- importance factor: $\gamma_I = 1.0$;
- peak ground acceleration: $a_{gR} = 0.20g$;
- ground Type B, Type 1 spectrum: $S = 1.2$, $T_B = 0.15s$, $T_C = 0.50s$, $T_D = 2.00s$;
- vertical ground acceleration not accounted for.

12.3.2 Preliminary design

The non-dissipative elements of the resisting frame (beams and columns) are preliminary designed in order to withstand ($N_{Rd} \geq N_{Ed}$, $V_{Rd} \geq V_{Ed}$, and $M_{Rd} \geq M_{Ed}$) alone the gravitational loads at Ultimate Limit States (ULS) combination ($1.3G_1 + 1.5G_2 + 1.5Q$). The columns are supposed completely restrained at the base while beams are hinged to the columns. The resulting beams and columns cross-sections are reported in Table 12.1.

Table 12.1: Beam and column cross-section at each storey level

Storey Level	**Column**	**Beam**	**Steel**
1	HEB 240	IPE 450	S 355
2	HEB 240	IPE 450	S 355

The TRSH dissipative bracing system is then preliminary designed according to the procedure described in Section 11.2.2. Assuming a behaviour factor $q = 3.0$ (see Information Brochure-INNOSEIS, 2017), the base-shear $F_b(T_1)$ is calculated as:

$$T_1 = C_t \cdot H^{\frac{3}{4}} = 0.36s \quad \text{Eq. (12.14)}$$

$$S_a(T_1) = S_{ae}(T_1)/q = 0.20g \quad \text{Eq. (12.15)}$$

$$F_b(T_1) = m_{tot} \cdot \lambda \cdot S_a(T_1) = 1388.5kN \quad \text{Eq. (12.16)}$$

Resulting inertia F_i ($F_i = F_b \cdot (z_i \cdot m_i)/(\sum z_j \cdot m_j)$) and shear $F_{b,i}$ forces on column elements at each storey level are reported in Table 12.2.

Table 12.2: Mass and inertia force distribution at each storey level

Storey Level	$\boldsymbol{m_i}$ **[kg]**	$\boldsymbol{F_i}$ **[kN]**	$\boldsymbol{F_{b,i}}$ **[kN]**	$\boldsymbol{\gamma_x \cdot \gamma_b \cdot F_{b,i}}$ **[kN]**
1	354000	462.8	1388.5	1832.9
2	354000	925.7	925.7	1221.9

The TRSH devices to be installed at the i-th storey level are chosen among real devices prototypes experimentally tested within the European LESSLOSS project (LESSLOSS, 2007). Lower and upper bound design properties of the TRSH have to be provided by the device manufacturer and then the number of triangular plates n_i can be determined as:

$$n_i = \frac{\gamma_x \cdot \gamma_b \cdot F_{b,i}}{F_{y,LBDP,t,i}} \quad \text{Eq. (12.17)}$$

where $F_{y,LBDP,t,i}$ is the lower bound design property of the yielding force $\boldsymbol{F_{y,t,i}}$ of the single dissipative element, $\gamma_x = 1.2$ is the reliability factor and $\gamma_b = 1.1$ the partial factor for the TRSH device.
Resulting design parameters of TRSH devices at each story level are reported in Table 12.3 (note that two TRSH devices are installed at each storey level – one along each horizontal direction).

Table 12.3: Layout of TRSH devices at each storey level

Storey Level	**TRSH type**	$\boldsymbol{F_{y,t,i}}$ **[kN]**	$\boldsymbol{F_{u,t,i}}$ **[kN]**	$\boldsymbol{k_{el,i}}$ **[kN/m]**	$\boldsymbol{n}$ **[-]**	$\boldsymbol{F_{y,t,i}}$ **[kN]**	$\boldsymbol{F_{u,t,i}}$ **[kN]**	$\boldsymbol{k_{el,i}}$ **[kN/m]**
1	TR250(7)-S355J2	50	59	5000	2x19	2x950	2x1121	2x97500
2	TR250(7)-S355J2	50	59	5000	2x13	2x650	2x767	2x65000

Moreover, the cross-section of brace-elements are chosen in order to fulfil the requirements related to both axial resistance and non-dimensional slenderness (see Section 11.2.2). Relevant design parameters are reported in Table 12.4 (note that two bracing systems are installed at each storey level – one along each horizontal direction).

Table 12.4: Bracing elements cross-sections at each storey level

Storey Level	**cross section**	$\boldsymbol{N_{Ed,i}}$ **[kN]**	$\boldsymbol{N_{Rd,i}}$ **[kN]**	$\boldsymbol{l_0}$ **[m]**	$\boldsymbol{N_{cr,i}}$ **[kN]**	$\boldsymbol{\lambda_{b,i}}$ **[-]**
1	2x(2UPN300)	490.9	2x(2x3795)	5.26	2x(2x943.5)	2.0
2	2x(2UPN300)	327.3	2x(2x3795)	5.26	2x(2x943.5)	2.0

The structural layout resulting from the preliminary design is represented in Figure 12.2. In the next section, the same solution is shown to fulfill all EN 1998-1 performance requirements.

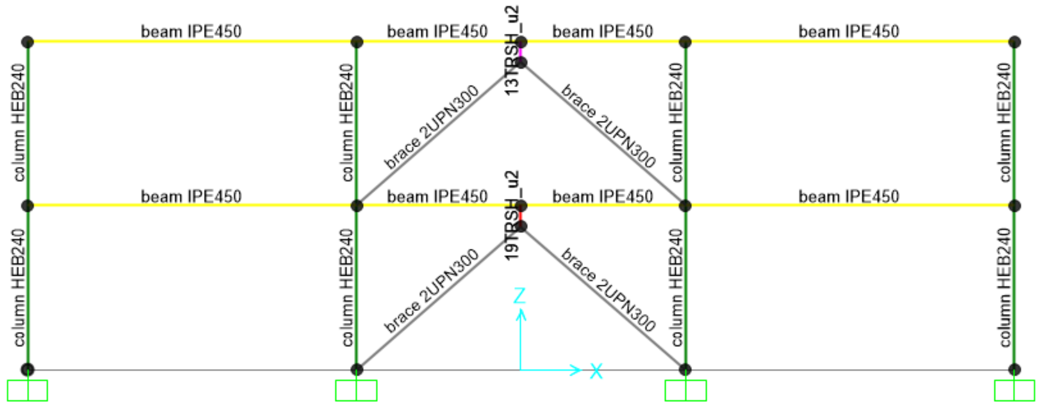

Figure 12.2: Structural layout resulting from the preliminary design

12.3.3 Linear elastic analysis

A linear elastic analysis is carried out in accordance with the EN 1998-1-1 provisions (CEN, 2005-2) described in Section 11.2.3. In particular, both dissipative and non-dissipative structural elements are verified with reference to the seismic load combination ($G_1 + G_2 + \psi Q + E$).

12.3.3.1 Multi-modal response spectrum analysis

A multi-modal response spectrum analysis has been performed taking into account inertia seismic loads relevant to the first mode shapes (Figure 12.3) that jointly activate at least the 90% of the total mass of the building along both horizontal directions.

Mode 1 *Mode 2*

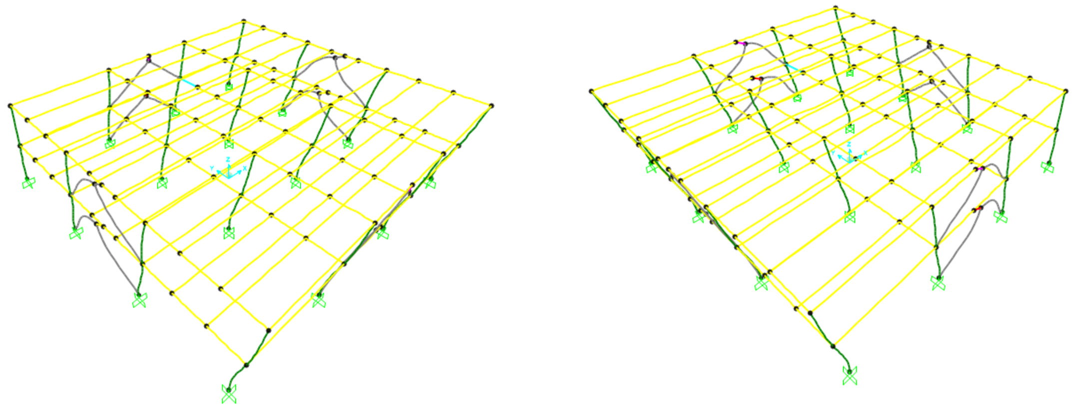

Figure 12.3: Mode shapes considered in response-spectrum analysis (continues)

Mode 3

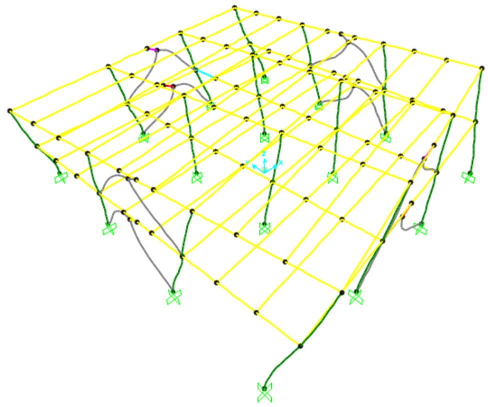

Mode 4

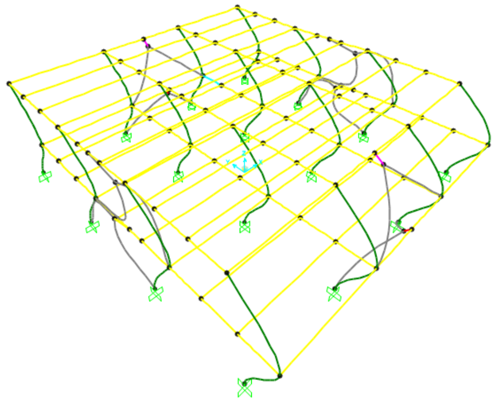

Mode 5

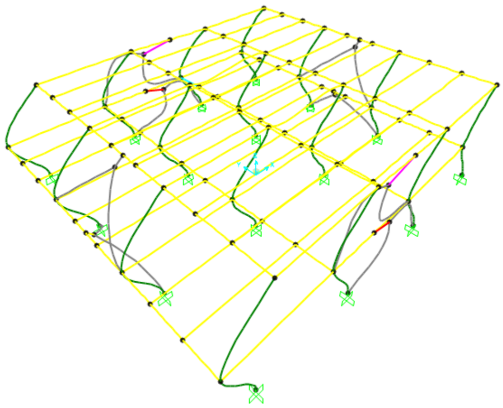

Figure 12.3: Mode shapes considered in response-spectrum analysis (continued)

Relevant modal parameters are summarized in Table 12.5. It is worth noting that the CQC rule has been used to combine modal results while the SRSS rule for the directional combination (seismic spectrum loads are simultaneously applied along both horizontal directions).

Table 12.5: Periods and participating mass ratios of considered mode shapes

Mode n°	**Period [s]**	**Part. mass X [%]**	**Part. mass Y [%]**	**Sum X [%]**	**Sum Y [%]**
1	0.70	0	0.90	0	0.90
2	0.65	0.89	0	0.89	0.90
3	0.48	0	0	0.89	0.90
4	0.28	0	0.09	0.89	0.99
5	0.24	0.10	0	0.99	0.99

12.3.3.2 Limitation of interstory drift

Assuming that the building is equipped with ductile non-structural elements, the following limitation of the maximum interstory drift d_r has been verified (see Section 11.2.3):

$$d_r \cdot \mathrm{v} \leq 0.0075 \cdot \mathrm{h} = 30\mathrm{mm} \qquad \text{Eq. (12.18)}$$

As witnessed by results reported in Table 12.6, this requirement is fulfilled at each storey level.

Table 12.6: Results of interstory drift verifications at each storey level

Storey level	$d_{e,top,X}$ [mm]	$d_{e,top,Y}$ [mm]	$d_{e,bottom,X}$ [mm]	$d_{e,bottom,Y}$ [mm]	$d_r = q \cdot \lvert d_{e,top} - d_{e,bottom} \rvert$ [mm]	$d_r \cdot \mathrm{v}$ [mm]
1	9	11	0	0	34	17.0
2	18	21	9	11	40	20.0

12.3.3.3 Verification of second order effects

The possible influence of 2nd order effects has been controlled by the limitation of the interstory drift sensitivity coefficient θ below the limit values of the Code (see Section 11.2.3):

$$\theta = \frac{P_{tot} \cdot d_r}{V_{tot} \cdot h_{story}} \qquad \text{Eq. (12.19)}$$

Since $\theta < 0.1$ at each storey level, second order effects can be neglected (Table 12.7).

Table 12.7: Results of 2nd order effects verification at each storey level

Storey level	P_{tot} [kN]	d_r [mm]	V_{tot} [kN]	h_{story} [mm]	θ [-]
1	6946	34	1195	4000	0.049
2	3473	40	1270	4000	0.027

12.3.3.4 Verification of dissipative elements

It has been verified that, along both horizontal directions, the maximum seismic action ($\gamma_x \cdot \gamma_b \cdot F_{Ed,i}$) on the TRSH devices has not exceeded the design resistance $F_{Rd,t,i}$ of the element (see Section 11.2.3):

$$F_{Rd,t,i} = n_i \cdot F_{y,t,i} \geq \gamma_x \cdot \gamma_b \cdot F_{Ed,i} \qquad \text{Eq. (12.20)}$$

This requirement is fulfilled at each storey level as witnessed by results reported in Table 12.8

Table 12.8: Resistance verification of TRSH elements at each storey level

Storey level	**TRSH type**	$\boldsymbol{n}$ **[-]**	$\boldsymbol{n \cdot F_{y,t,i}}$ **dir. X [kN]**	$\boldsymbol{n \cdot F_{y,t,i}}$ **dir. X [kN]**	$\boldsymbol{\gamma_x \cdot \gamma_b \cdot F_{Ed,i}}$ **dir. X [kN]**	$\boldsymbol{\gamma_x \cdot \gamma_b \cdot F_{Ed,i}}$ **dir. Y [kN]**
1	TR250(7)-S355J2	2x19	2x950	2x950	2x506	2x621
2	TR250(7)-S355J2	2x13	2x650	2x650	2x415	2x464

Moreover, to achieve a uniform dissipative behavior among all storey levels, the following requirement related to the distribution of the over-strength ratios Ω of the TRSH elements over the entire structure has been verified (see Section 11.2.3):

$$\frac{max\Omega_i}{min\Omega_i} \leq 1.25 \qquad \text{Eq. (12.21)}$$

where $\Omega_i = (n_i \cdot F_{y,t,i})/(\gamma_x \cdot \gamma_b \cdot F_{Ed,i})$.
This requirement is fulfilled as witnessed by relevant results reported in Table 12.9

Table 12.9: TRSH devices over-strength factor verification

Storey level	$\boldsymbol{\Omega_i}$ **dir. X [-]**	$\boldsymbol{\Omega_i}$ **dir. Y [-]**	$\boldsymbol{max(\Omega_i)/min(\Omega_i)}$ **dir. X [-]**	$\boldsymbol{max(\Omega_i)/min(\Omega_i)}$ **dir. Y [-]**
1	1.88	1.53	1.19	1.09
2	1.57	1.40		

12.3.3.5 Verification of non-dissipative elements

In order to ensure that the yielding occurs only in TRSH devices, non-dissipative structural members (beams, columns, and braces) have been verified according to capacity design requirements (see Section 11.2.3):

$$\begin{cases} N_{Rd} \geq N_{Ed,G} + 1{,}1 \cdot \gamma_{ov} \cdot \Omega \cdot N_{Ed,E} \\ M_{Rd} \geq M_{Ed,G} + 1{,}1 \cdot \gamma_{ov} \cdot \Omega \cdot M_{Ed,E} \\ V_{Rd} \geq V_{Ed,G} + 1{,}1 \cdot \gamma_{ov} \cdot \Omega \cdot V_{Ed,E} \end{cases} \qquad \text{Eq. (12.22)}$$

Results relevant to elements under maximum axial load, shear load and bending moment are respectively reported from Table 12.10 to
Table 12.12.

Table 12.10: Verification of non-dissipative element under max axial load

Element Type	N_{Rd} [kN]	$N_{Ed,G} + 1,1 \cdot \gamma_{ov} \cdot \Omega \cdot N_{Ed,E}$ [kN]
column - HEB240	3421.0	771.5
beam – IPE450	-	-
brace – 2UPN300	3795.0	329.9

Table 12.11: Verification of non-dissipative element under max shear load

Element Type	$V_{Rd,X}$ [kN]	$V_{Rd,Y}$ [kN]	$V_{Rd,Z}$ [kN]	$V_{Ed,G} + 1,1 \cdot \gamma_{ov} \cdot \Omega \cdot V_{Ed,E}$ [kN]		
				dir. X	dir. Y	dir. Z
column - HEB240	1520.0	619.3	-	32.8	5.9	-
beam – IPE450	-	-	1034.0	-	-	141.6
brace – 2UPN300	-	-	-	-	-	-

Table 12.12: Verification of non-dissipative el. under max. bend. moment

Element Type	$M_{Rd,X}$ [kN]	$M_{Rd,Y}$ [kN]	$M_{Rd,Z}$ [kN]	$M_{Ed,G} + 1,1 \cdot \gamma_{ov} \cdot \Omega \cdot M_{Ed,E}$ [kN]		
				dir. X	dir. Y	dir. Z
column - HEB240	339.8	160.8	-	57.9	30.6	-
beam – IPE450	-	-	549.3	-	-	353.7
brace – 2UPN300	-	-	-	-	-	-

12.4 CONCLUSIONS

In the present study, a specific design procedure for the implementation of TRSH devices in “V-bracing” systems of steel structures is proposed and applied to a 3D case-study low-rise (2 storeys) building located in a moderate seismic area (PGA=0.20g). The preliminary design of the resisting frame is defined by means of a simple analytical procedure (equivalent lateral loads method) and then the proposed structural layout is assessed in a multi-modal response spectrum analysis. The final solution, usually obtained iteratively adjusting the preliminary design, is shown to widely fulfil all the requirements relevant to both dissipative and non-dissipative structural elements provided by EC8-1 (CEN, 2005-2).
Since based on simple calculations, the proposed method can be easily adopted by practitioners; however, for a more accurate design, EN 15129 strongly

recommends to perform nonlinear time-history analyses when the equivalent damping ratio related to hysteretic energy dissipation is higher than 15 %.

12.5 REFERENCES

[1] CEN (Comitee Europeen de Normalisation). *EN 15129: Anti-seismic devices*, Brussels, 2009.

[2] CEN (Comitee Europeen de Normalisation). EN1993-1-1, *Eurocode 3: Design of steel structures - Part 1-1: General rules and rules for buildings*. Brussels, 2005(1).

[3] CEN (Comitee Europeen de Normalisation). *EN1998-1-1, Eurocode 8: Design of structures for earthquake resistance – Part 1-1: General rules, seismic actions and rules for buildings*. Brussels, 2005(2).

[4] CSI (Computer & Structures, INC). *SAP2000 – Reference Manual*. California, Berkeley, 2016.

[5] FEMA (Federal Emergency Management Agency). *FEMA-P695: Quantification of building seismic performance factors*. Washington, 2009.

[6] INNOSEIS XX/2017. *Information Brochure - TRSH device*. 2017.

[7] LESSLOSS 2007/03. *Innovative Anti-Seismic Systems Users Manual*. Available online at http://elsa.jrc.ec.europa.eu/events.php?id=4#reports.

[7] Setti P. *A method to compute the behaviour factor for construction in seismic zones*. Costruzioni Metalliche. Vol. 37(3), p. 128–139, 1985.

12.6 ANNEX A: Q-FACTOR ESTIMATION

In the present Annex two different methods for the estimation of the q-factor resp. behaviour factor, the “FEMA 695” and the “Ballio-Setti”, are applied to the considered case-study building.

Obtained q-factors differ from one another on the basis of the considered horizontal direction of the resisting frame (small discrepancies) and on the adopted calculation method (wider discrepancies). In general, the “FEMA 695” method seems to provide too conservative values with respect to the “Ballio-Setti” ones. Due to these uncertainties, further investigations will be conducted in future research developments. In the meanwhile, a safe-side value $q = 3.0$ is recommended to be adopted in structural calculations.

12.6.1 “FEMA 695” method

The “FEMA 695 method” (FEMA, 2009) consist of a series of provisions that allow to estimate the behaviour factor q of a structure by means of a non-linear static analysis (Pushover). The calculation method is represented in Figure 12.4.

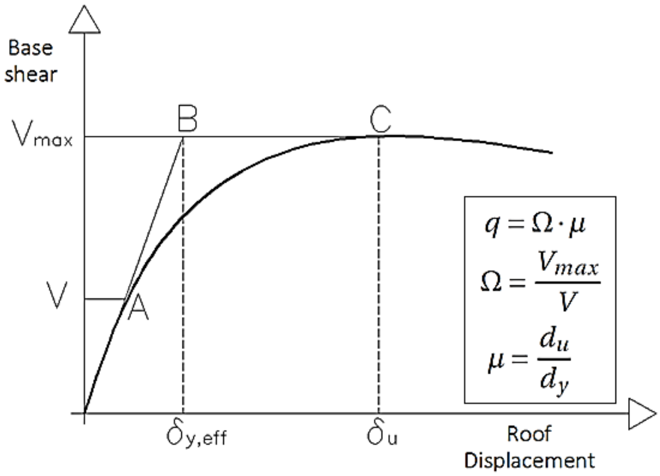

Figure 12.4: Behaviour factor q calculation method according to FEMA 695

With regard to the considered case-study building, the structural model used for elastic analysis is extended to include the response of structural elements beyond the elastic state and estimate expected plastic mechanisms and the distribution of damage. Link elements with a bilinear behavior in the horizontal shear direction are used to model the TRSH devices. Fiber hinges with coupled axial and bending plastic behaviors are introduced at the base of columns while other structural members (beams) are modelled as linear. Mechanical properties of TRSH elements are calculated according to the analytical models described in the Information Brochure (INNOSEIS, 2017). Since quasi-static analyses are carried out, the hysteresis of TRSH elements is neglected in the behavior-diagram (Figure 12.5). On the contrary, the failure of the element due to the exceedance of the ultimate displacement is accounted for.

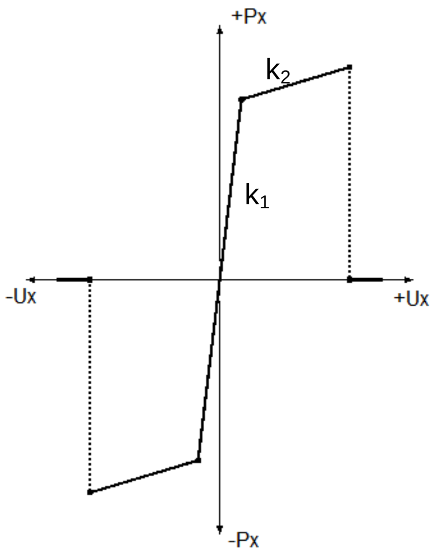

Figure 12.5: Qualitative force-displacement diagram used for TRSH elements in Pushover analyses

A Static Pushover analysis (SPO) along both horizontal directions has been performed considering the modal distribution of lateral loads. Relevant capacity curves are represented in Figure 12.6.

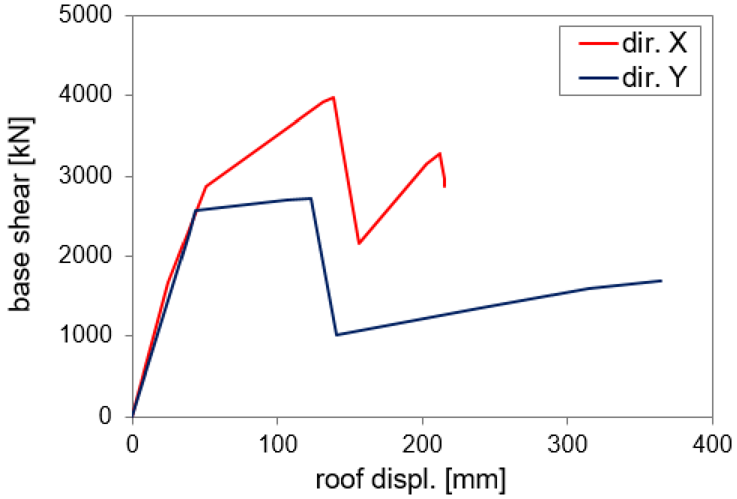

Figure 12.6: Capacity curves relevant to X and Y horizontal directions

Due to the asymmetric mechanical behaviour of column cross-sections, behaviour factors q obtained from the pushover analysis along both horizontal directions are slightly different (Table 12.13).

Table 12.13: Behaviour factors q along both horizontal directions

Direction	V_{max} **[kN]**	V **[kN]**	Ω **[-]**	d_u **[mm]**	$d_{y,eff}$ **[mm]**	μ **[-]**	q **[-]**
X	3983	2863	1,39	138	50	2,76	3,84
Y	2713	2577	1,05	123	44	2,80	2,94

12.6.2 "Ballio-Setti" method

The "Ballio-Setti" method (Setti, 1985) is a procedure that allows to quantify the behaviour factor q of a structure based on the results of Incremental Dynamic Analyses (IDA). Indeed, it consists in performing several non-linear dynamic analyses and obtaining the maximum response of the structure during each time-history. A certain number of ground motion time histories is usually selected and then multiplied by a scaling factor λ in order to reach step-by-step increasing values of a certain Intensity Measure (IM). For each analysis (given a ground motion and a fixed value of λ), the response of a multi-storey structure is synthetically quantified by means of a damage measure (DM) that is usually represented by the peak displacement of the top storey or the maximum interstory drift.

According to the "Ballio-Setti" mehod the behaviour factor is quantified as:

$$q = \frac{\lambda_u}{\lambda_y} \qquad \text{Eq. (12.23)}$$

where, with regard to the considered case-study building, the relevant terms have been set as:

λ_u : scaling factor corresponding to the first failure among all TRSH devices;
λ_y : scaling factor corresponding to the first yielding among all TRSH devices.

Moreover, IDA have been conducted with the following assumptions:

- nonlinearities of both TRSH and column elements modelled by means of the same methods adopted for pushover analyses;
- seven independent ground motion natural records compatible with the reference elastic spectrum (Figure 12.7) have been selected;
- the selected records have been applied separately along each horizontal direction of the resisting frame;
- the following Intensity Measure (IM) has been considered to compute the scaling factors (λ) reported in Table 12.14 and Table 12.15:

$$IM = AvgSa(T_{Ri}) = \left(\prod_{i=1}^{n} S_a(T_{Ri})\right)^{1/n} \qquad \text{Eq. (12.24)}$$

where T_{Ri} have been selected as linearly spaced within a range $[T_2; 1.5T_1]$ (being T_1 the fundamental period and T_2 the period relevant to second bending mode of the structure).

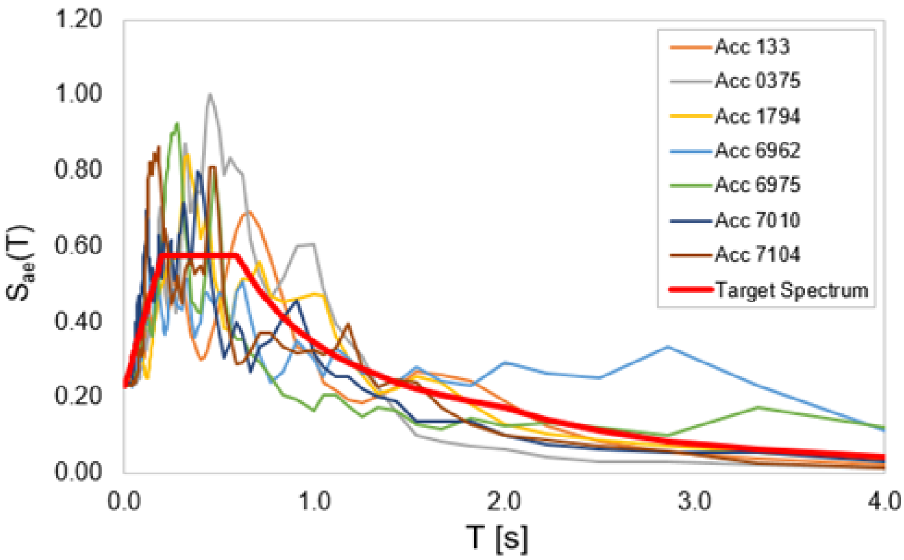

Figure 12.7: Ground motion natural records selected for IDA analyses

Table 12.14: Adopted scaling factor for IDA analyses along X horizontal direction

	$IM = AvgSa(T_{Ri})$									
SF	**0,10**	**0,20**	**0,30**	**0,40**	**0,50**	**0,60**	**0,70**	**0,80**	**0,90**	**1,00**
λ_1	0.22	0.45	0.67	0.89	1.12	1.34	1.56	1.79	2.01	2.23
λ_2	0.14	0.28	0.42	0.56	0.70	0.84	0.98	1.12	1.26	1.40
λ_3	0.17	0.33	0.50	0.67	0.83	1.00	1.17	1.33	1.50	1.66
λ_4	0.24	0.48	0.73	0.97	1.21	1.45	1.70	1.94	2.18	2.42
λ_5	0.20	0.40	0.60	0.80	1.00	1.20	1.40	1.60	1.80	2.00
λ_6	0.19	0.39	0.58	0.77	0.97	1.16	1.35	1.55	1.74	1.94
λ_7	0.21	0.42	0.62	0.83	1.04	1.25	1.46	1.66	1.87	2.08

Table 12.15: Adopted scaling factor for IDA analyses along Y horizontal direction

	$IM = AvgSa(T_{Ri})$									
SF	**0,10**	**0,20**	**0,30**	**0,40**	**0,50**	**0,60**	**0,70**	**0,80**	**0,90**	**1,00**
λ_1	0.20	0.39	0.59	0.79	0.99	1.18	1.38	1.58	1.78	1.97
λ_2	0.17	0.33	0.50	0.66	0.83	1.00	1.16	1.33	1.50	1.66
λ_3	0.17	0.35	0.52	0.69	0.86	1.04	1.21	1.38	1.56	1.73
λ_4	0.16	0.33	0.49	0.66	0.82	0.99	1.15	1.31	1.48	1.64
λ_5	0.17	0.35	0.52	0.70	0.87	1.04	1.22	1.39	1.57	1.74
λ_6	0.22	0.45	0.67	0.89	1.11	1.34	1.56	1.78	2.01	2.23
λ_7	0.17	0.34	0.51	0.67	0.84	1.01	1.18	1.35	1.52	1.69

The maximum interstorey drift (θ_{max}) has been selected as Damage Measure (DM) to represent the IDA curves obtained along X (Figure 12.8) and Y (Figure 12.9) horizontal directions. Relevant q factors (mean values) are quite different and are reported in Table 12.16.

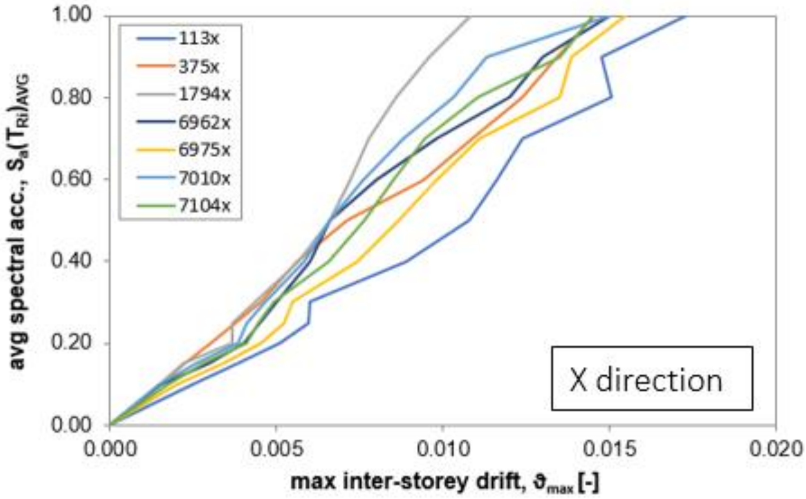

Figure 12.8: IDA curves along the X horizontal direction of the resisting frame

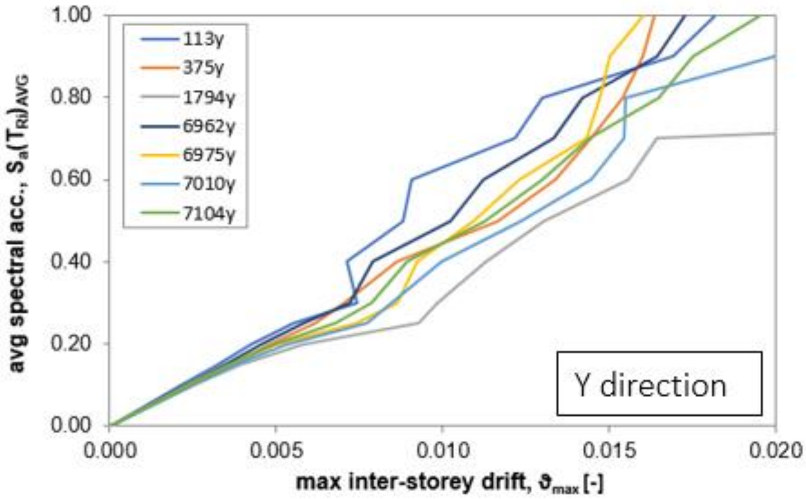

Figure 12.9: IDA curves along the Y horizontal direction of the resisting frame

Table 12.16: Behaviour factors q along both horizontal directions

Direction	λ_u [-]	λ_y [-]	q [-]
X	1.97	0.29	6.70
Y	1.58	0.27	5.82

13 MSSH

13.1 LIMIT OF APPLICABILITY

MSSH device, in its current configuration, represents an effective solution to achieve high damping levels in mid and high-rise steel buildings.

On the contrary, since characterized by a substantially large elastic deformations before experiencing the plastic field, its application in low-rise buildings do not produce the same benefits (reduction of seismic inertia forces) for the structure. Indeed, low-rise steel buildings, since usually characterized by a low fundamental period and a high lateral stiffness, during the seismic excitation are subjected to rather small interstorey drifts that debar the hysteresis of the devices and hence the dissipation of the seismic energy.

Thus this document does not include a specific design of MSSH applied to the 2-storey case-study building. Furthermore, in order to fill this gap, a wide experimental and numerical investigation is currently undergoing at MAURER SE with the aim to develop new MSSH prototypes with lower elastic deformations and higher ductility levels.